THE USE OF GOLD AND SILVER CYANIDES IN THE PREPARATION OF SUPRAMOLECULAR COORDINATION COMPLEXES

by

Carolyn J. Shorrock
B. Sc., Trinity Western University, 2001

THESIS SUBMITTED IN PARTIAL FULFILLMENT OF
THE REQUIREMENTS FOR THE DEGREE OF

MASTER OF SCIENCE

in the Department
of
Chemistry

SIMON FRASER UNIVERSITY
August 2003

APPROVAL

Name: Carolyn J. Shorrock

Degree: M.Sc.

Title of Thesis: The use of Gold and Silver Cyanides in the Preparation of Supramolecular Coordination Complexes.

Examining Committee:

Chair: Dr. G.R. Agnes, Associate Professor

Dr. D.B. Leznoff, Assistant Professor, Senior Supervisor

Dr. G.W. Leach, Associate Professor, Committee Member

Dr. R.H. Hill, Professor, Committee Member

Dr. N.R.Branda, Associate Professor, Internal Examiner

Date Approved: Aug 8/03

PARTIAL COPYRIGHT LICENCE

I hereby grant to Simon Fraser University the right to lend my thesis, project or extended essay (the title of which is shown below) to users of the Simon Fraser University Library, and to make partial or single copies only for such users or in response to a request from the library of any other university, or other educational institution, on its own behalf or for one of its users. I further agree that permission for multiple copying of this work for scholarly purposes may be granted by me or the Dean of Graduate Studies. It is understood that copying or publication of this work for financial gain shall not be allowed without my written permission.

Title of Thesis/Project/Extended Essay:

THE USE OF GOLD AND SILVER CYANIDES IN THE PREPARATION OF SUPRAMOLECULAR COORDINATION COMPLEXES.

Author:

_____
(signature)

_____
(name)

Aug 11/03
(date)

Several other studies are briefly discussed, including the use of tetrahedral cyanometallates of both Ag(I) and Cu(I). The reactions suggest complex equilibria, resulting in stable complexes of $[Cu_x(CN)_y]^{n-}$ and $[Ni(CN)_4]^{2-}$. Possible applications are also examined, such as the use of Au(I) cyanometallates to increase the dimensionality of polymers with Fe(II) spin-transition complexes.

To my parents, Mike and Thyiela Maschek,
my brother Kurt, and
my patient and loving husband Chris.

"Wisdom is, and starts with, the humility to accept the fact that you don't have all the right answers, and the courage to learn to ask the right questions."

Anonymous

ACKNOWLEDGEMENTS

I wish to express my sincere thanks to Dr. Danny Leznoff for his guidance, wisdom, patience and most of all, his infectious enthusiasm.

To my fellow group members: thank you for your friendship, suggestions and support. I would like to especially thank Garry Mund, for all the help he has given me these past few years. Thank you to all the undergraduate students who have worked with me: Howie Jong, Peter Kim, Heidi Lefebvre and Angela Chekaluk. Your hard work was greatly appreciated.

I would also like to express my gratitude to Dr. Ray Batchelor and Dr. Fred Einstein for teaching me everything I know about X-ray diffraction and solving crystal structures. The countless hours you've spent explaining and assisting me with structures has been so very much appreciated. Mr. Miki K. Yang is also gratefully acknowledged for completing all the C, H, N analyses, as well as Dr. Ian Gay for performing porosity studies.

I could not have completed my program without the support, care and encouragement that was provided by my family, Mike, Thyiela and Kurt Maschek, and my husband, Chris Shorrock.

To those who have inspired and encouraged me to continue learning about science, I also express my thanks and appreciation. To Mr. Don Dupuis and Mr. Dieter Stamm, I thank you for teaching me to love science from an early age. To Dr. Craig Montgomery, I thank you for guiding me through my undergraduate years, introducing me to research and being such a wonderful role-model and inspiration to me.

The generous financial support from NSERC and Simon Fraser University is also gratefully acknowledged.

Table Of Contents

LIST OF TABLES

LIST OF FIGURES

LIST OF ABBREVIATIONS

Å	Angstrom
Anal	analysis
a_o	Bohr radius
AO	atomic orbital
au	atomic unit
bipy	2,2′-bipyridine
bpe	bispyridylethylene
bpm	2,2′-bipyrimidine
br	broad
Bu	butyl
C	Celsius
C	Curie constant
c	speed of light
calcd	calculated
cm	centimeter
coe	cyclooctene
cyclen	1,4,7,10-tetraazacyclododecane
D	zero field splitting parameter
deeda	N,N-diethylethylenediamine
deg	degree(s)
dien	diethylenetriamine
dimphen	2,9-dimethyl-1,10-phenanthroline
dmaep	2-(2-dimethylaminoethyl)pyridine
dmeda	N,N-dimethylethylenediamine
dmbpy	4,4′-dimethyl-2,2′-bipyridine
dppe	1,2-bis(diphenylphospino)ethane
e	electron
EA	elemental analysis
eaep	2-(2-ethylaminoethyl)pyridine
en	ethylenediamine
equiv	equivalent(s)

fac	facial
g	Landé g factor
$\hbar$	Plank constant ÷ 2π
H	Hamiltonian
H	external magnetic field
HS	high spin
imH	imidazole
IR	infrared
J	magnetic coupling parameter
k	Boltzmann constant
K	Kelvin
kJ	kilojoule
L	ligand
LS	low spin
m	mass
m_s	spin quantum number
mg	milligram
mL	milliliter
medpt	bis(3-aminopropyl)methylamine
mepy	4-picoline
mmol	millimole
mol	mole
M	metal
Me	methyl (CH_3)
MO	molecular orbital
mol	mole
n	number of moles
N_A	Avogadro's number
oop	out of plane
Ortep	Oak Ridge Thermal Ellipsoid Plot Program
phen	1,10-phenanthroline
pyz	pyrazine
s	strong
S	total spin quantum number

SQUID	super conducting quantum interference device
T_c	critical temperature
teeda	N,N,N′,N′-tetraethylethylenediamine
tn	1,3-diaminopropane
TM	transition metal
tmeda	N,N,N′,N′-tetramethylethylenediamine
tmpd	N,N,N′,N′-tetramethyl-o-phenylenediamine
tren	tris(2-aminoethyl)amine
vw	very weak
w	weak
Z	nuclear charge
zfs	zero field splitting
1-D	one dimensional
2-D	two dimensional
2miz	2-methylimidazole
3-D	three dimensional
β	Bohr magneton
ε_o	permittivity of a vacuum
φ	Cu–O–Cu angle
θ	Weiss constant
ν	frequency
χ_M	molar magnetic susceptibility
°	degree

CHAPTER 1

INTRODUCTION

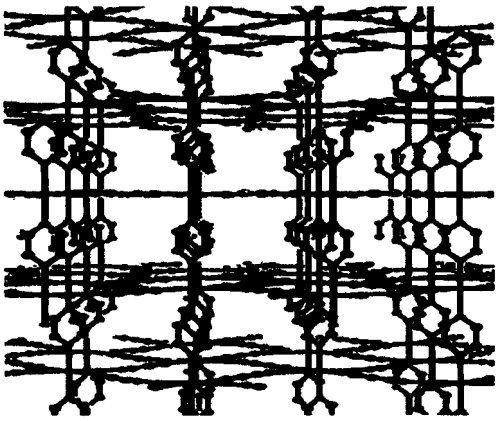

1.1 SUPRAMOLECULAR CHEMISTRY AND BUILDING DIMENSIONALITY

1.1.1 Introduction to Supramolecular Chemistry

Supramolecular chemistry has been defined as "the chemistry of molecular assemblies and of the intermolecular bond" by one of its leading proponents, Jean-Marie Lehn [1,2]. In the past several decades, it has become one of the fastest growing areas of experimental chemistry and has since been casually defined as "the chemistry beyond the molecule" [3]. The boundaries of what is and is not classified as supramolecular chemistry, however, remain relatively blurred. In general, all supramolecular fields involve some attempt to rationally predict and/or design systems that will aggregate via non-covalent interactions. A variety of strategies exist for aggregating building blocks. These strategies generally involve using interactions, such as combinations of ion/dipole–ion/dipole interactions, hydrogen bonding, cation–π interactions, π–π stacking and others [3].

Of specific interest to this thesis is the field of supramolecular coordination chemistry, involving the multi-dimensional assembly of repeating metal (M) and ligand (L) building

blocks where the "interactions" employed to aggregate units are strong metal–ligand (M–L) coordinate bonds [3]. It has been suggested that, by the nature of the building blocks and interactions between them, this field of supramolecular chemistry is quite predictable and controllable [3]. A wide variety of structures and systems can be developed using ligands as spacers, combined with ligands as directional (or capping) agents and metals with predictable coordination numbers and geometries. This method is often referred to as the directional-bonding approach as it uses M–L bonding to direct the structures formed [4]. To do this, directional ligands are coordinated to the metal centre before the introduction of the linking ligand, thereby gaining control over the potential outcome by controlling the number and often orientation of "open" coordination sites. Some examples of the use of the directional-bonding approach are displayed in Figure 1.1.

1.1.2 Increasing Dimensionality

Controllably increasing dimensionality of supramolecular systems is of importance with respect to the generation of functional materials [4-9]. This interest results from the potential of high-dimensionality systems to produce useful magnetic [10-12], nonlinear optical [13-15], conducting [16-19] or porous [20-22] properties.

Many of the methods used to aggregate building blocks can also be used to increase dimensionality, such as hydrogen bonding and π–π stacking. Hydrogen bonding is a dipole–dipole interaction whereby a hydrogen atom that is covalently bound to an electronegative atom interacts with another dipole [3]. The strength of these interactions can range between 4 – 120 kJ/mol and the strength of the interactions can be related to the distance between the donor (H atom) and acceptor [3]. Generally, a donor–acceptor distance of 1.2 – 1.5 Å would be considered strong, where as a distance of 2.2 – 3.2 would be considered quite weak [3]. It is often, however, difficult to accurately state this distance due to the difficulty associated with finding hydrogen atoms from X-ray diffraction data, and thus distances are often expressed as between the electronegative atom (to which the hydrogen atom is bound) and the acceptor atom. Stacking interactions between π systems occur between aromatic rings and are generally considerably weaker (0 – 50 kJ/mol) [3]. These π interactions often serve to influence packing arrangements in supramolecular systems.

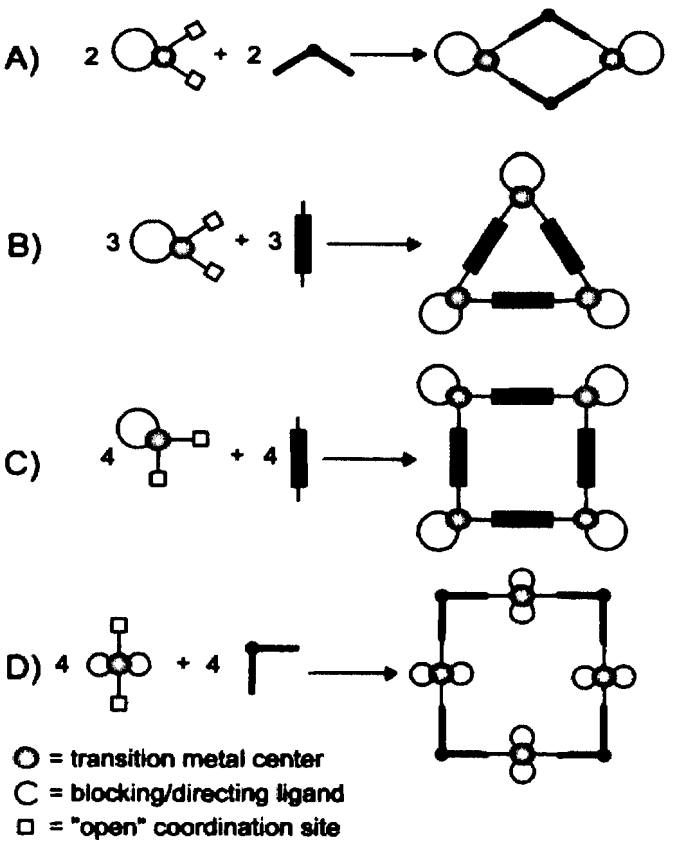

Figure 1.1 – Supramolecular systems constructed by the directional-bonding approach [4].*

1.1.3 Goals and Scope of This Thesis

Another much less investigated approach to increasing dimensionality is that of metal–metal bonding. For the purposes of this thesis, two types of metal–metal bonding will be discussed: bonding between d^{10} metal centres (Au(I) and Ag(I)), and bonding between d^8 metal centres (Au(III)).

The terms "metallophilicity" and "aurophilicity" were originally coined by Schmidbauer in 1989, in response to the growing number of examples of this metal–metal bonding (specifically, Au(I)–Au(I) bonding) that could not be explained by conventional concepts of chemical bonding [23-28]. This bonding is considered to be intermediate between conventional covalent/ionic bonding and van der Waals interactions [28]. It is now

---

* Mirkin, C. A.; Holliday, B. J. *Angew. Chem. Int. Ed.* **2001**, *40*, 2022. Used by permission of Wiley-VCH.

recognized as a widespread phenomenon of great relevance [29] and recent surveys have found hundreds of publications on the topic [28]! The energy contributions associated with aurophilic interactions have been found to be in the range of 6 – 12 kcal/mole (20 – 50 kJ/mol), as determined by variable temperature NMR solution studies [30-39]. Other lighter coinage metals (silver and copper) have also been shown to exhibit such intramolecular metal–metal interactions, although to a lesser extent than gold(I). The theoretical evidence, based on a combination of ab initio calculations, semi-empirical calculations and density functional calculations, has suggested that the interactions between d^{10} metal centres originate from correlation effects and are strengthened by relativistic effects [40-48]. A detailed explanation of such effects can be found in Appendix 1.

The first computational study of d^8–d^8 interactions was done in 1995 using ab initio methods and a variety of Pt(II) and Rh(I) compounds [43,49]. Because of the large crystal-field splitting, d^8 ions can be considered, in a sense, closed-shell atoms like d^{10} and can thus be involved in similar interactions [50]. In fact, numerous interactions between d^{10} and d^8 ions have been reported [50]. Further discussion of these interactions and influences is found in Chapter 3.

The concept of metallophilicity has begun to be recognized as a useful method for the design of homometallic supramolecular structures [9,28,51,52]. If these metals, capable of such metallophilic interactions, are built into a supramolecular building block capable of coordinate bonding, the potential for higher dimensionality supramolecular structures is increased. The use of the cyanometallates $[Ag(CN)_2]^-$ and $[Au(CN)_4]^-$ as building blocks thus combines the capability of metal-metal bonding with the coordination capability (to a secondary metal centre) of the cyanide moiety. This provides a method with which to build heterobimetallic coordination polymers, as has been observed by the Leznoff research group to be the case for the $[Au(CN)_2]^-$ moiety as a building block [53-55].

The primary focus of this thesis is to examine the trends associated with the use of Ag(I) and Au(III) cyanometallate building blocks in the formation of supramolecular coordination polymers. The desire to is be able to build a database of resulting complexes and the factors influencing their formation, such that with a known metal/ligand set and reaction condition the outcome of coupling with one of the building blocks will be predictable.

1.2 AN OVERVIEW OF THE BUILDING BLOCKS

1.2.1 Transition Metal Cyanide Complexes

The use of transition metal cyanide complexes in supramolecular coordination chemistry dates back to 1704 with the discovery of Prussian Blue [56]. Since this discovery, the vast diversity and availability of transition metal cyanide complexes has rendered them popular choices for a variety of applications. This popularity has resulted in a large number of excellent reviews on cyanometallate structures, reactivity and properties [57-66], including the very useful book by Sharpe [67], which summarizes much of the earlier literature. This section, therefore, will simply address the aspects of these reviews that relate directly to the research focus of this thesis.

Cyanometallates of transition metals are very stable [56] and very few ligands are capable of displacing cyanide under mild conditions [68]. The cyanide ligand is unique due to its ability to act as both a σ donor and π acceptor, combined with its ambidentate nature and negative charge [56]. The discussion of σ donor vs. π acceptor abilities of the CN^- ligand becomes crucial in the discussion of infrared spectral trends. As compared to free cyanide (in solution), which exhibits a $\nu(C\equiv N)$ stretch at 2080 cm^{-1} [69], there is a frequency shift when cyanide acts as a ligand (in the case of M–CN). This shift depends on whether the bonding is primarily L→M σ bonding or M→L π bonding [56]. In the case of σ bonding, the electrons are removed from a σ MO of the CN^- ligand, which is weakly antibonding with respect to the C≡N bond, and thus the frequency of the $\nu(C\equiv N)$ stretch increases. If the bonding is strongly influenced by π back-bonding from the metal (as is the case with lower oxidation state transition metals), electrons are added to the $2p\pi^*$ antibonding orbital of the CN^- and thus the frequency decreases. A more detailed analysis of $\nu(C\equiv N)$ stretching frequencies is discussed in the characterization section (1.3.3) of this introduction.

Transition metal cyanide anions (cyanometallates) exist with coordination numbers anywhere from two to eight [56]. Cyanometallates of Au(I) and Ag(I) exist as linear, two-coordinate $[M(CN)_2]^-$ complexes [70,71], whereas the d^8 metal containing cyanometallates favor square planar geometry, such as is observed with $[M(CN)_4]^{2-}$ (M = Ni(II), Pd(II), Pt(II)) [72,73] and $[Au(CN)_4]^-$ [74].

Discussion thus far has been focused on a terminal binding mode of the CN^- ligand (as depicted in Figure 1.2(a)). Various other bridging modes (Figure 1.2(b-f)) have also

been observed for the cyanide ligand [56]. The binary (or bridging) binding mode of Figure 1.2(b) is undoubtedly the most common, and will be the focus of this thesis. Note that in the bridging mode, significant deviation from linearity of the M–C≡N angle has been observed, whereas this is not the case in terminal binding modes of the cyanide ligand [56].

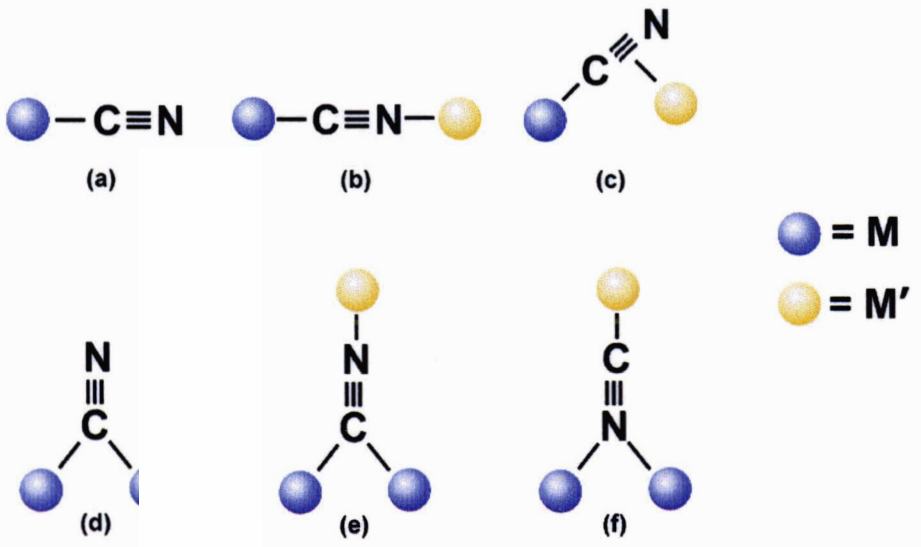

Figure 1.2 – Observed binding modes for the cyanide ligand.

1.2.2 Cyanometallates in Supramolecular Chemistry

Using cyanometallates to build M–CN–M′ type polymers and multi-dimensional systems has been rigorously explored, with most of the focus being on octahedral and square planar cyanometallates [75-88]. The ability of the cyanide ligand to strongly bridge two different or similar metal centres makes the cyanometallate ion an excellent design element in supramolecular coordination systems. To better control such systems, the directional-bonding approach is often used, employing capping ligands on the M′ centre, such that the resulting complexes adopt the general formula $L_wM'_x[M(CN)_y]_z$. As could be envisioned, there is an enormous range of resulting compositions and shapes that could result, with only a limited number that have yet been realized [88].

The use of linear cyanometallates as building blocks has received comparatively less attention, although the Leznoff research group has put considerable effort into examining

$[Au(CN)_2]^-$ for use as a building block for supramolecular coordination complexes [53-55]. Other groups have also contributed to this field and a variety of other heterobimetallic supramolecular coordination systems have been reported [81,89-95] that show similar conclusions and trends. Studies have also been done on a Ni(II)–Au(I) cyano-bridged polymer using electrospray mass spectroscopy, indicating that the aggregation into supramolecular systems is not simply a solid-state phenomenon [96]. Bimetallic systems have been constructed without ligands [97,98] and with non-transition metal atoms such as Gd(III) [99]. Monometallic systems with Au(I), cyanides and organic moieties show cyanide bridging and Au–Au interactions as well [100-102].

In light of the success of aurophilic interactions, investigations have begun using the similar dicyanoargentate complex $[Ag(CN)_2]^-$ as a building block, particularly by the group of Černák and Chomič [87,103-109] as well as by a variety of other groups. The use of $[Ag(CN)_2]^-$ as a building block will be examined in greater detail in Chapter 2 of this thesis.

The Leznoff group also works with the neutral moiety $Hg(CN)_2$, which has resulted in some recent publications indicating that this unit can also be used as a building block to form heterobimetallic coordination polymers [110,111].

1.2.3 Gold

For the first half of the twentieth century, knowledge of gold chemistry was quite limited, but since the second World War, there has been a steady increase of the quantity and quality of research and reviews that have been produced owing to the emergence of applications in modern technologies [28,112-114]. Some of the most active aspects of gold chemistry include the areas of organometallic gold chemistry, bioinorganic and medicinal chemistry, and synthesis and properties of gold clusters [114]. Gold can be found in oxidation states of –1, 0, 1, 2, 3 and 5 [114] although gold(I) and gold(III) complexes are the most common [115]. Gold(I) can form linear, trigonal planar or tetrahedral complexes, though it has a much stronger tendency towards linear coordination complexes [115]. Gold(III) forms primarily square planar complexes, but some complexes of higher coordination numbers are known [114]. Being a relatively soft metal, both gold(I) and gold(III) form strong complexes with sulfur, carbon and phosphorous donor ligands. Stable complexes with nitrogen and oxygen donors as well as halides are also known, especially with Au(III) [114].

Many interesting properties of gold can be attributed to relativistic effects (as detailed in Appendix 1). Gold has an unusually clear preference not only for short and strong bonds (suggesting smaller atomic/ionic radius and high electronegativity) but also for small coordination numbers [28,116]. Also, the ability of gold(I) to associate into dimers, oligomers and even multidimensional polymers via gold–gold contacts is partially attributed to the effect of relativity.

The range of Au–Au distances associated with aurophilic interactions is approximately 2.7 Å to 3.9 Å [116], which includes the distance between gold atoms in the metal and approaches, or even overlaps the range of distances for single bonds of Au^{2+} [28,117]. Generally, metallophilic interactions are identified by means of X-ray diffraction studies such that a M–M distance below the sum of the van der Waals radii is considered to be real [118]. This becomes somewhat controversial, however, as the van der Waals radii are often determined by halving the distance of a homoatomic nonbonding interaction and this distance varies a great deal in different compounds [43]. As such, for the purposes of this thesis, where possible, comparisons with literature examples of these interactions will be used such that the basis for defining an interaction will depend on the general consensus amongst researchers in the field (for example, most experts consider a distance of 3.6 Å to be the upper limit for aurophilic interactions [30]). In cases where this consensus does not yet exist, identification will be based upon the interaction being significantly less than the sum of the van der Waals radii as determined by Bondi (from molar volumes) [119].

1.2.4 Silver

Unlike the plethora of oxidation states available for gold, silver exists primarily in the oxidation state of zero or one, though less stable complexes are known containing Ag(II) and Ag(III) [120]. Like Au(I), Ag(I) is quite soft and tends to form stable complexes with P-donors, S-donors, N-donors and halides [120]. Like gold, silver chemistry has been shown to be important in biological and medicinal chemistry, but is better known for its applicational uses in technology such as the photographic industry [120].

The effects of relativity on silver are less pronounced than gold and as a result, Au(I) has actually been found to be smaller than Ag(I), despite the higher atomic number and the previously published radius predictions [121]. The validity of the metal-metal interactions between Ag(I) centres (argentophilic interactions) have been disputed in the

past, but recently have been accepted due to the emergence of ligand-unsupported interactions [122]. These interactions are discussed in more detail in Chapter 2.

1.3 GENERAL TECHNIQUES

1.3.1 Preparation and Choice of Ligands

With only a few exceptions, reactions to form heterobimetallic coordination complexes with cyanometallates are extremely simple and the ease of preparation has made this field appealing to many chemists. In general, a stock solution of the ligand is added to a transition metal salt dissolved in an appropriate solvent. A color change is usually observed, indicating that the ligand has bound to the transition metal centre. A solution of the cyanometallate is then added to the $[TM(ligand)]^{n+}$ solution. Many reactions produce an immediate precipitate, which is filtered, washed, dried and characterized by a variety of methods (as described in Section 1.3.3). In cases where an immediate precipitate is not formed, the solution is allowed to slowly evaporate until a product can be isolated from solution. Figure 1.3 illustrates the general reaction technique used throughout this thesis. After general characterization is complete, crystals are required in order to obtain accurate structural parameters. Various crystallization methods are detailed in Section 1.3.2.

In general, the ligands used in the reactions serve to limit the number of open coordination sites on the transition metal used. For stability, chelating amines are chosen, as the nitrogen donor is an excellent choice for most transition metals and the chelating effect further increases the strength of coordination to the metal. Also, many amine ligands are available (and are inexpensive), thus varying the basicity and bulk of the ligands is easily done and the effects of these factors are discussed throughout this thesis. One or two equivalents of the ligand are generally used, depending on the number of open coordination sites desired. Figure 1.4 depicts the ligands used throughout this thesis.

1.3.2 Crystallization Techniques

Depending on the reaction, several crystallization techniques may be employed. In cases where an immediate precipitate forms upon reaction, crystals of the same composition (as determined by infrared and/or elemental analysis characterization) are

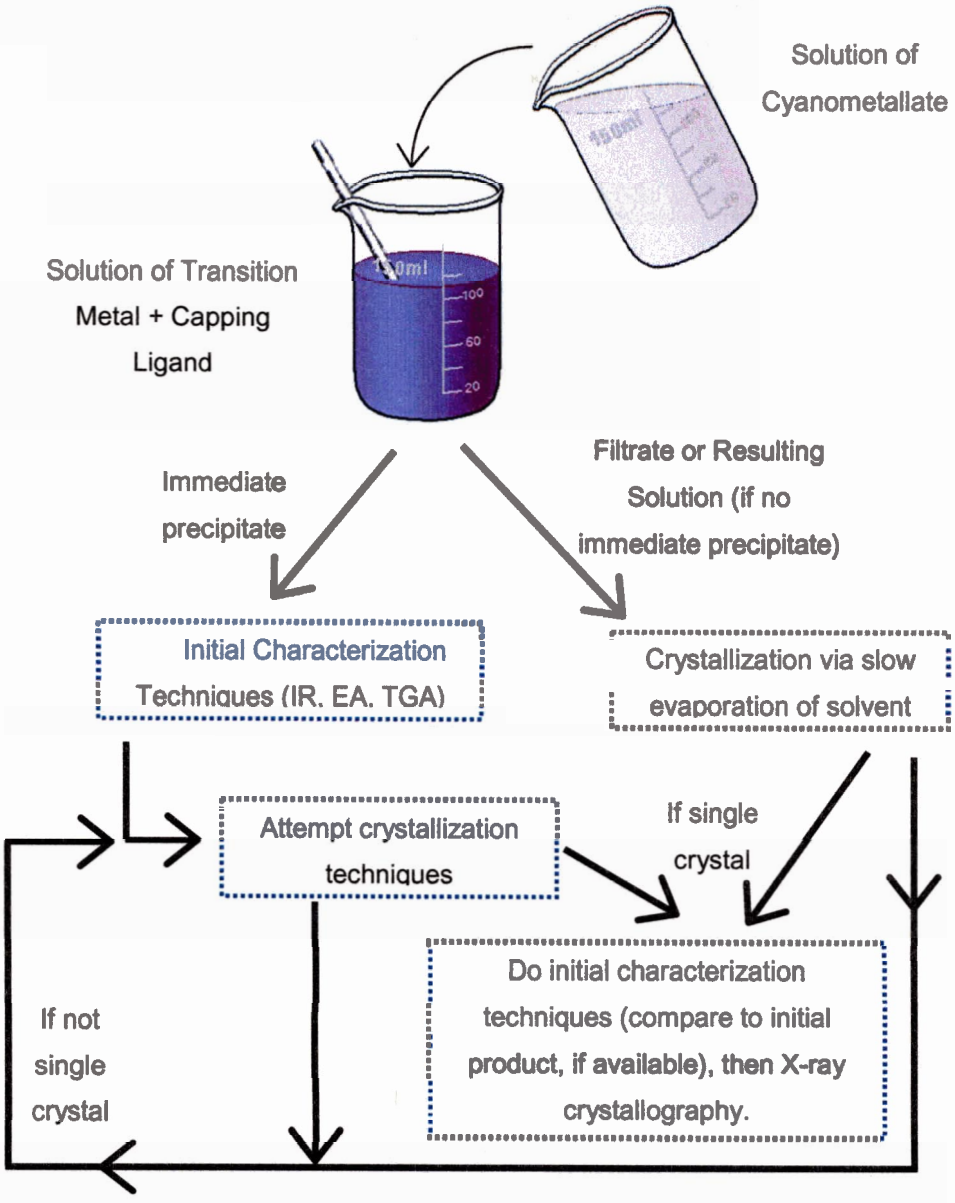

Figure 1.3 – General preparation technique for heterobimetallic coordination polymers using cyanometallate building blocks.

sometimes deposited from the filtrate solution if it is left undisturbed and/or cooled over several days or weeks. Often, this process requires slow evaporation of solvent. In cases where this process is unsuccessful, slow diffusion of the two reagent solutions (TM/ligand and cyanometallate solutions) is attempted. This is accomplished either with

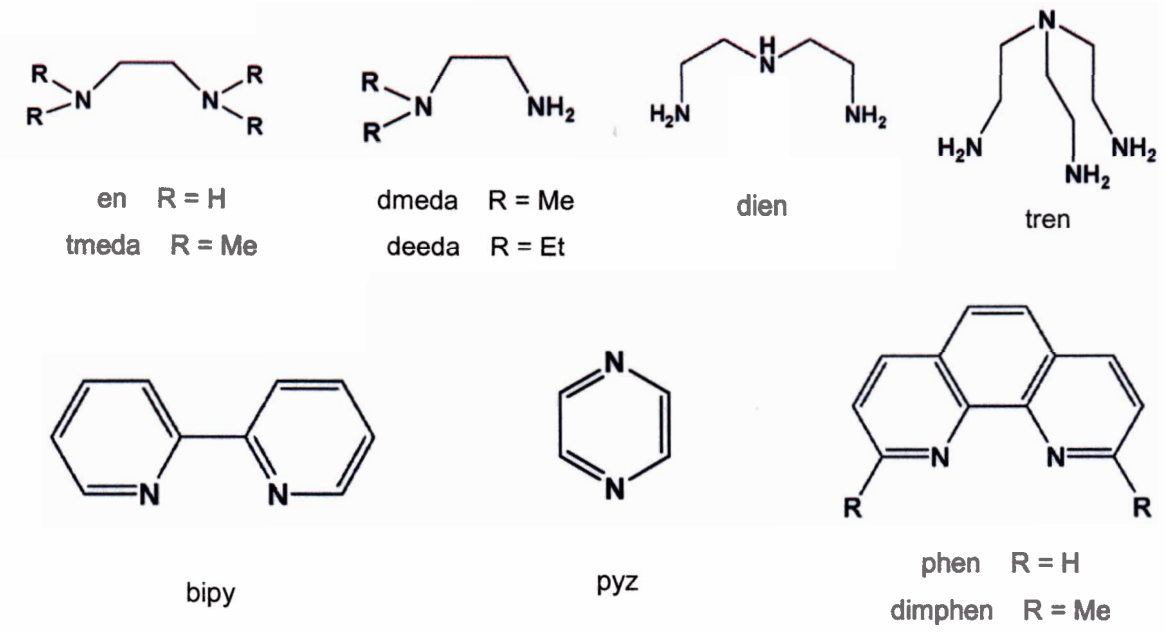

Figure 1.4 – Capping ligands for transition metals.

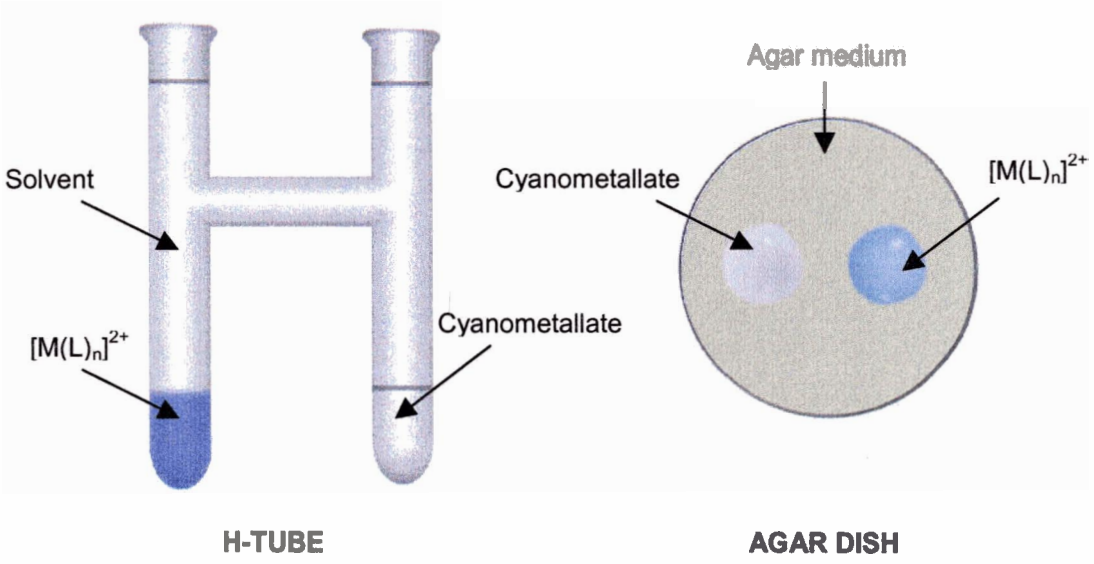

Figure 1.5 – Crystallization techniques.

the use of an H-shaped tube or an agar dish, as depicted in Figure 1.5. In the case of an H-tube the concentrated reactant solutions slowly diffuse through the solvent and crystals are formed either in the tubes or in the glass bridge. The crystals are extracted

either with a pipette or by removing the solutions, breaking the tube and removing them manually. Because only one single crystal is required for X-ray diffraction studies, yield is not necessarily a priority. In rare cases, the resulting crystals are of different composition as compared to the immediate precipitate product, due to the formation of thermodynamic rather than kinetic products. These cases are discussed individually, as necessary throughout the thesis.

Other methods of crystallization, less often utilized in this thesis but nonetheless important in the field, include slow inter-diffusion of the two reagent solutions in a single tube, layering a solution of the product with another solvent in which it is less soluble (such as ethanol) [123] or use of a solubilizing, volatile ligand such as ammonia [124]. In the latter case, using a ligand that slowly evaporates results in the slow formation of the resulting product as the excess ligand evaporates [87].

1.3.3 Characterization Methods

1.3.3.1 Initial Characterization: Infrared and Elemental Analyses

Generally, the first characterization performed on a product is infrared spectroscopy (IR). For cyanometallates, IR is a valuable tool with which to gain an understanding of the binding mode of the cyanide group as it can provide a means of distinguishing between terminal (non-bridging) and bridging modes of the cyanides [125].

When a cyanometallate bridges to another metal centre the $\nu(C\equiv N)$ stretches shift from their non-bridging values. The non-bridging cyanide stretches of each cyanometallate have been determined and are listed in their respective chapters throughout this thesis. In most instances an increase in the frequency of the stretch is observed as the cyanide bridges in the M–CN–M′ mode [56]. This increase is attributed primarily to the effect of the lone pair of the N atom, which is antibonding with respect to cyanide triple bond [126-128]. There are, however, instances where the shift will occur towards lower frequencies. This has been attributed to an increase in π-back bonding from the metal to the carbon and to π-back bonding through the M′–N bond, both weakening the C≡N bond [56]. If the trends counter-balance each other the $\nu(C\equiv N)$ stretches do not change significantly. Also, if the bridging is elongated (as is the case with binding to Jahn-Teller distorted sites), changes in the frequency may be undetectable.

If the IR spectrum suggests that there is cyanometallate in the product, a quantitative elemental analysis (EA) is generally obtained. From the results the percentage of carbon, nitrogen and hydrogen can be calculated and compared to the expected product percentages, giving useful information as to the product composition.

1.3.3.2 X-Ray Crystallography

If a suitable crystal is obtained via one of the crystallization methods, X-ray crystallography is performed. X-ray crystallography is undoubtedly the most useful characterization and provides the most conclusive evidence towards the structure of the resulting product, but is often complicated by the inability to form suitable single crystals. Also, there are some minor deficiencies in the characterization – namely the inability to accurately determine the location of hydrogen atoms. This is due to the fact that hydrogen atoms have very little electron density and thus have very weak X-ray diffraction, as diffraction is proportional to Z^2 [129]. For similar reasons, it is also quite common to have difficulty differentiating between atoms of close nuclear charge (such as carbon and nitrogen).

1.3.3.3 Thermogravimetric Analysis

Depending on the system, thermogravimetric analysis (TGA) may also be done. This becomes especially useful in determining the nature of water in the structure, as well as the overall stability of the compound. For the former, if water is simply included in the crystal lattice of the structure (unbound), it will be lost (as identified by an appropriate percent weight decrease) at temperatures slightly above 100°C, whereas metal-coordinated water will be lost at a significantly higher temperature. In the absence of a crystal structure, this gives valuable information about the resulting complex and also helps confirm quantities of co-crystallized water in systems with an X-ray structure. The thermal stability of the product also gives an indication of the strength of the bonds in the coordination complex.

1.3.3.4 Magnetic Properties

If the X-ray structure shows promising magnetic pathways, magnetic data is obtained using a SQUID magnetometer. A brief tutorial on magnetism is outlined below in Section 1.4.

1.4 AN INTRODUCTION TO MAGNETISM

Magnetism is generated by the motion of charged particles. In transition metals, the overall magnetism is due to both the intrinsic spin of unpaired electrons and the orbital motion of electrons [130]. A compound in an external magnetic field will produce a magnetization, **M**, due to the alignment of its magnetic dipoles. Magnetic data can be obtained from a SQUID (Superconducting QUantum Interference Device) magnetometer, which measures the total magnetization (hence a bulk property) of the sample. The magnetic susceptibility per mole can then be defined as follows:

$$\chi_M = \mathbf{M}/(H \times n) \qquad \text{(Equation 1.1)}$$

where H is the external magnetic field and n is the number of moles in the sample. A paramagnetic compound (containing unpaired electrons) is characterized by large, positive χ values [130].

Modeling of magnetic susceptibility vs. temperature is based on the idea that the distribution of unpaired electron population into the energy levels of a system (as governed by the Boltzmann distribution) defines the susceptibility at any given temperature, as each energy level has a different magnetic moment (that can be calculated). In the simplest case, with a system with only one unpaired electron (S = 1/2), an external field will cause splitting of the Kramer's doublet containing the two quantum levels (m_s = +1/2 and m_s = –1/2) into two separate non-degenerate states [130]. This splitting is known as Zeeman splitting (Figure 1.6).

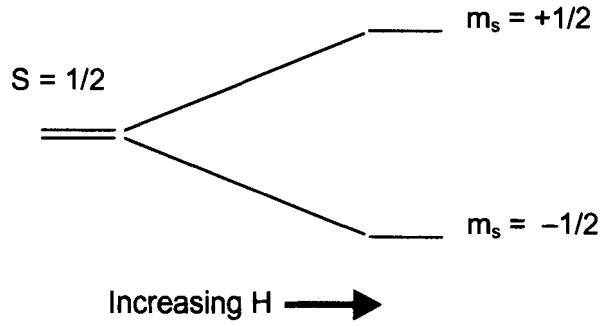

Figure 1.6 – Zeeman splitting of a S = 1/2 Kramer's doublet.

If it is assumed that the thermal energy (kT, where k = Boltzmann constant) is greater than this splitting effect, the equations for the spin angular momentum of the electron and the Boltzmann distribution yield the following expression:

$$\chi_M = \mathbf{C}/T \qquad \text{where } \mathbf{C} = N_A g^2 \beta^2 / 4k \qquad \text{(Equation 1.2)}$$

The above equation, where **C** = Curie constant, N_A = Avogadro's number, β = the Bohr magneton of the electron and g is the Landé factor (a proportionality constant equal to approximately 2.0 for an electron in an isotropic field with no orbital angular momentum) is known as the Curie Law (where **C** is defined for an S = 1/2 system) and predicts that the product $\chi_M T$ will be temperature independent in the absence of magnetic interactions.

When data is obtained from a SQUID magnetometer through a temperature range, the resulting information can thus be analyzed for the presence of magnetic interactions by plotting the $\chi_M T$ product against temperature. In its general form, the Curie Law is proportional to the total spin quantum number (S) (Equation 1.3).

$$\chi_m T = 0.5[S(S+1)] \qquad \text{(Equation 1.3)}$$

The above equation is only valid if there are no magnetic interactions (i.e. a magnetically dilute system where only one isolated magnetic centre is being considered), the magnetism is spin-only, there are no thermally accessible excited states and external fields and temperatures are moderate [131]. If there are magnetic interactions between magnetic centres, another parameter (θ = the Weiss constant) is required, and the Curie-Weiss Law (Equation 1.4) is used.

$$\chi_{para} = C/(T-\theta) \qquad \text{(Equation 1.4)}$$

The above equation is empirically observed and results from the addition of a perturbation to the Zeeman splitting energy diagram [131]. Experimentally, if χT is plotted against T, it becomes clear whether magnetic interactions exist (Figure 1.7a).. A plot of $1/\chi$ vs T will yield the exact θ value (from the x-intercept, Figure 1.7b). A positive

θ value indicates ferromagnetic interactions (parallel spin alignment), whereas a negative θ value indicates antiferromagnetic interactions (antiparallel spin alignment).

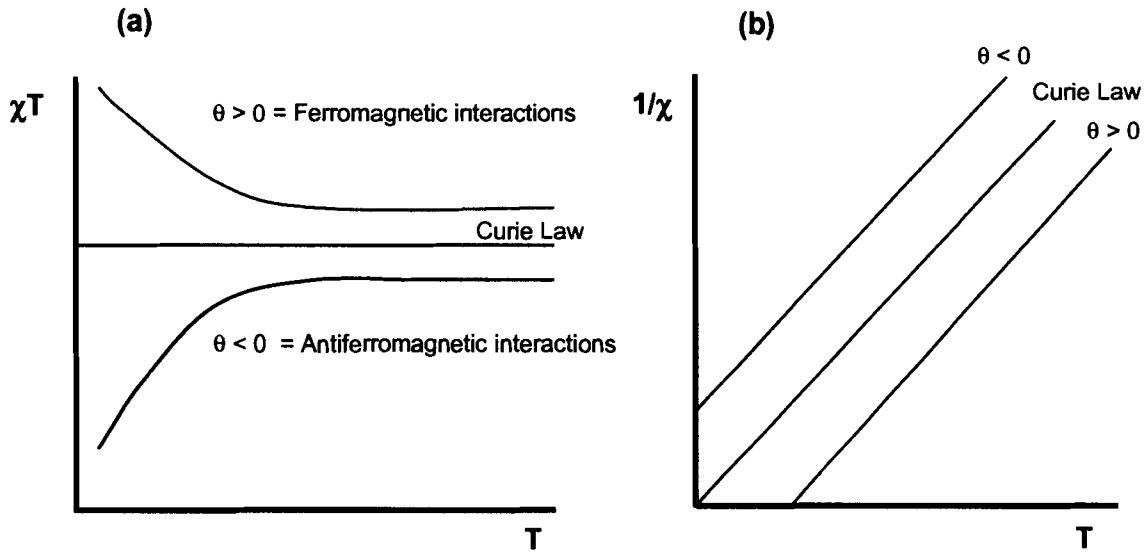

Figure 1.7 – (a) χT vs. T and (b) $1/\chi$ vs. T graphs depicting magnetic interaction possibilities.

The Curie-Weiss Law does not account for a variety of factors such as orbital angular momentum, spin-orbit coupling, anisotropy, crystal field effects, etc. that would affect the observed magnetism [130,131]. A variety of different models have been proposed to further quantify the magnetic interactions of various specific systems and will be used to model the experimentally observed magnetism of many systems in this thesis. The above Curie-Weiss Law (Equation 1.4) and the mathematical models do not, however, account for how the magnetic interactions are mediated or the origin of the magnetic interactions [130,131].

The basis of most magnetic models originate from the more general equation for the treatment of magnetic behavior that was proposed by Van Vleck, whereby the equation predicts the magnetic susceptibility vs. temperature with the possible presence of all orbital contributions to magnetism, second-order effects, magnetic interactions and excited state mixing [132]. The basic task of the development of magnetochemistry models is the deduction of the appropriate energy level diagram, the calculation of the magnetic moment for each level, and the application of the Van Vleck equation to these energy levels.

For example, if a compound has a total spin quantum number higher than 1/2, the crystal field effect may result in a splitting of its Zeeman energy levels in the absence of a magnetic field [131]. This phenomenon is referred to as zero-field splitting and results in anisotropy of magnetic properties such that χ has a perpendicular and parallel component (as related to the applied magnetic field). The case of zero-field splitting in a Ni(II) centre (S = 1) is depicted in Figure 1.8. Depending on the ground state, D may be positive (lowest m_s state is the ground state) or negative (higher m_s state is the ground state).

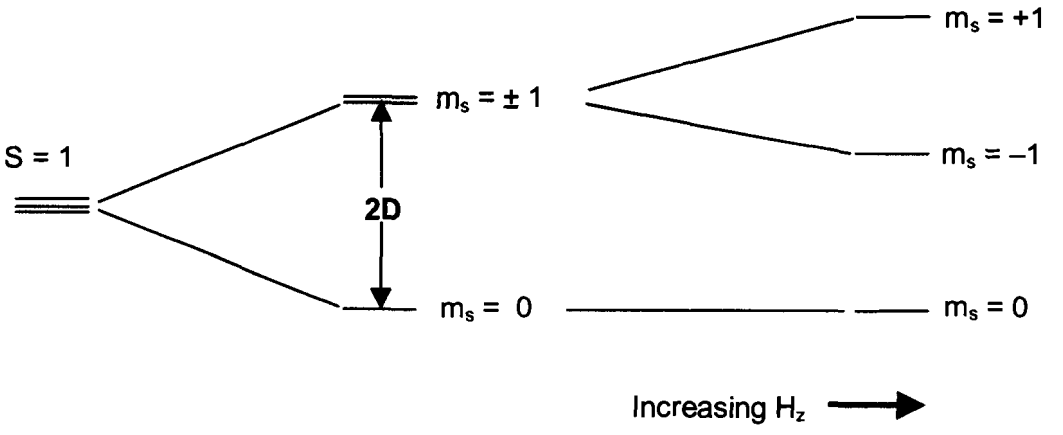

Figure 1.8 – Zero-field splitting energy diagram of an S = 1 metal centre.

If the above energy levels are introduced into the Van Vleck formula, the equations for the parallel magnetic susceptibility ($\chi_{parallel}$) and the perpendicular magnetic susceptibility (χ_{perp}) are as follows [131]:

$$\chi_{parallel} = \frac{2Ng_z^2\beta^2}{kT} \frac{\exp(-D/kT)}{1 + 2\exp(-D/kT)} \qquad \text{(Equation 1.5)}$$

$$\chi_{perp} = \frac{2Ng_x^2\beta^2}{D} \frac{1 - \exp(-D/kT)}{1 + 2\exp(-D/kT)} \qquad \text{(Equation 1.6)}$$

The observed χ (when using powder samples) is actually the weighted average of these equations, as follows [130]:

$$\chi_{av} = \frac{\chi_{parallel} + 2\chi_{perp}}{3} \qquad \text{(Equation 1.7)}$$

The χT product with the average χ value will always decrease at lower temperatures where this zero-field splitting is most prominent. It is thus often difficult to differentiate between weak antiferromagnetic interactions and zero-field splitting as they occur simultaneously. An average D value for a Ni(II) system ranges from 0.5 to 6 cm^{-1} [130].

In another example, consider a case involving multiple paramagnetic centres that interact in a homometallic dimer system of S = 1/2 centres (e.g. a Cu(II) dimer) if the two centres are magnetically interacting through a bridge the spin quantum numbers of S_A = S_B = 1/2 are no longer applicable and the more appropriate interpretation of the system is S = 0 (antiferromagnetic interaction) and S = 1 (ferromagnetic interaction). The relavent energy diagram is displayed in Figure 1.9.

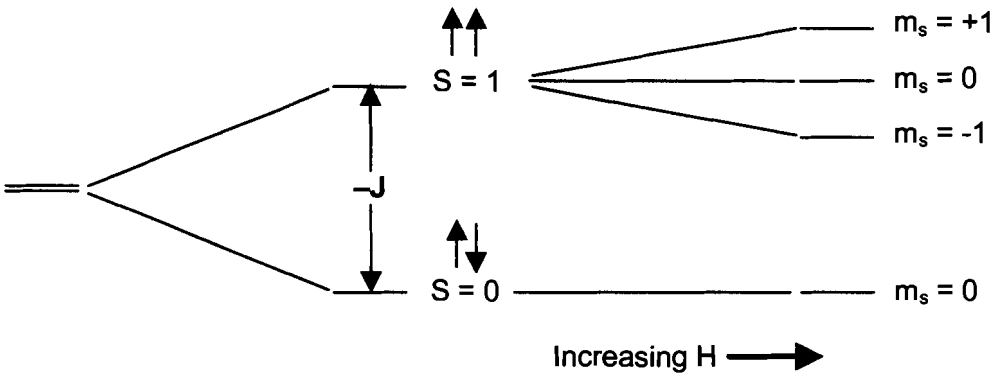

Figure 1.9 – Energy level diagram for a homodinuclear S = 1/2 complex.

In the above diagram J represents the interaction parameter or "coupling" of the two states. If J is negative, the lowest spin state (S = 0) is the ground state and the system is antiferromagnetically coupled. If J is positive, the higher spin state (S = 1) is the ground state and the system is ferromagnetically coupled. Ferromagnetic coupling is observed much less frequently than antiferromagnetic coupling and tends to be stronger, such that for J = |x|, a positive value will impact the χT value at higher temperatures than will a negative value [131]. If J > |200| cm^{-1} the χT will be impacted at room temperature (hence the system is strongly coupled), where as J values below approximately |20| cm^{-1} will only impact χT at lower temperatures (<50 K) [131]. Above that temperature, the χT will approximately follow the Curie Law. To obtain the above energy diagram, the Hamiltonian of $\mathbf{H} = -2JS_AS_B$ must be solved. This Hamiltonian is known as the Heisenberg Hamiltonian and requires that the assumption be made that the coupling in the system is isotropic. If orbital contributions, zero-field splitting and intermolecular

coupling are ignored, the following equation results from the application of the Van Vleck equation to the above energy level diagram and is known as the Bleaney-Bowers equation [131,133]:

$$\chi_M = \frac{2Ng^2\beta^2}{kT} \frac{1}{3 + \exp(-J/kT)} \qquad \text{(Equation 1.8)}$$

For most Cu(II) dimers, the g value ranges from 2.0 to 2.3 [130].

Extending the system to a 1-D uniform chain of antiferromagnetically interacting S = 1/2 centres, the assumption of isotropic coupling is also made. Assuming that the J value between closest neighbors is the same, and is significantly larger than J values between next nearest neighbors, the Bonner-Fisher model can be applied [131]. This model is an extrapolation from a model of a ring of S = 1/2 centres, whereby results have been fitted by the following numerical expression [134-136]:

$$\chi_M = \frac{Ng^2\beta^2}{kT} \frac{0.25 + 0.074975x + 0.075235x^2}{1.0 + 0.9931x + 0.172135x^2 + 0.757825x^3} \qquad \text{(Equation 1.9)}$$

(where $x = |J|/kT$)

Various other models for magnetic interactions have also been developed, but generally follow the same methodology as described above. Additional parameters and models are discussed as required throughout this thesis.

1.5 RESEARCH OBJECTIVES

The general purpose of this thesis is to examine the use of cyanometallates in the preparation of supramolecular coordination polymers. Specifically, the use of the Ag(I) cyanometallate ($[Ag(CN)_2]^-$) as a building block in systems similar to those containing the $[Au(CN)_2]^-$ building block is examined in order to facilitate comparisons between the cyanometallates. Also, the potential of the Au(III) cyanometallate ($[Au(CN)_4]^-$) moiety, which has never before been used as a building block, is examined. Simultaneously, attention is given to the various other factors influencing the formation of the coordination complexes, including the effect of ligand size and basicity, solvent and other interactions (such as hydrogen bonding). All of the resulting factors and trends are

of interest because they aid in the development of a predictable approach to designing 3-D systems and the often-debated concept of crystal engineering.

Also of interest are the resulting magnetic properties of the supramolecular systems, thus paramagnetic transition metals are used as the secondary metal. Because multidimensional systems often exhibit cooperative magnetic behavior (ferromagnetic, antiferromagnetic coupling and ordering, etc.), the use of cyanometallates as building blocks for magnetic applications (and other applications) is of interest.

CHAPTER 2

THE USE OF ARGENTOPHILICITY TO INCREASE DIMENSIONALITY

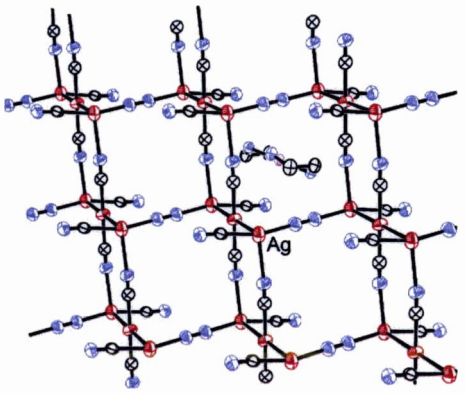

2.1 INTRODUCTION

2.1.1 Previous $[Au(CN)_2]^-$ Results

As detailed in Chapter 1, much work has been done to successfully demonstrate that aurophilic interactions between Au(I) atoms are viable design elements which can be used to increase dimensionality [53-55,81,89-102]. Of particular interest amongst these examples are systems that use $[Au(CN)_2]^-$ to bridge paramagnetic transition metals and further increase dimensionality via such aurophilic interactions [53-55,89,90]. These examples not only display the usefulness of the Au–Au interactions as a tool with which to increase dimensionality, but indicate that thermal stability can be increased and magnetic interactions can be mediated by the $[Au(CN)_2]^-$ unit.

2.1.2 Aurophilic vs. Argentophilic Interactions

In a similar fashion, silver–silver (argentophilic) interactions could, in principle, impart the desired control of supramolecular structure and dimensionality. These argentophilic interactions have been reported and calculated, however, to be weaker than gold–gold interactions [53,93,137]. This is perhaps not surprising, as such metallophilic

interactions are thought to be strengthened by relativistic effects [40-48] which would be less significant in Ag(I) as compared to Au(I). As a result, for the lighter congeners of the coinage metals there has been much debate over the legitimacy of the often ligand-supported [138-146] observed d^{10}-d^{10} interactions. Recent reports of ligand-unsupported systems displaying Ag(I)–Ag(I) interactions [104,122,147-150] have led to the general acceptance of "argentophilicity" as a valid and significant interaction.

2.1.3 The Use of $[Ag(CN)_2]^-$ in Coordination Polymers

Silver cyanides are very well studied, as (like with Au(I)) cyanidation has been an important method for the extraction of silver from silver ores [120]. In aqueous solutions with excess cyanide, a complex equilibria of $[Ag(CN)_2]^-$, $[Ag(CN)_3]^{2-}$ and $[Ag(CN)_4]^{3-}$ has been identified [151] and further studies regarding these equilibria have been published [152,153]. The crystal data for both the sodium salt [154] and the potassium salt [71], of $[Ag(CN)_2]^-$ have been published. Both show the $[Ag(CN)_2]^-$ unit as a linear moiety.

The $[Ag(CN)_2]^-$ unit has only recently been employed in the literature as a building block for coordination polymers [84,94,104,106-109,155-162]. These studies have shown that bridging cyano-coordination of the unit results in coordination polymers and the dimensionality of these polymers is often increased via ligand-unsupported argentophilic interactions. A summary of the coordination polymers that exhibit argentophilic interactions is found in Table 2.1.

2.1.4 Research Objectives

In an effort to facilitate comparisons between gold(I) and silver(I), this chapter is focused on the reactions of a the same series of M(II)-amine complex cations as those used in previously reported $[Au(CN)_2]^-$ studies [53-55] with $K[Ag(CN)_2]$. The dimensionality of the resulting compounds is of interest, as are the methods by which this dimensionality is achieved.

Table 2.1 – Coordination Polymers Containing $[Ag(CN)_2]^-$ and Argentophilic Interactions

Formula	Dimensionality	Ag – Ag Distance	Reference
$[Cd(pyz)Ag_2(CN)_3Ag(CN)_2]$	3-D	3.14 Å	[84]
$Eu[Ag(CN)_2]_3 \bullet 3H_2O$	3-D	3.34 Å	[94]
$[Zn(en)_2Ag(CN)_2][Ag(CN)_2]$	1-D	3.22 Å	[104]
$[Cu(bipy)_2Ag(CN)_2][Ag(CN)_2]$	2-D	2.99 – 3.04 Å	[106]
$[Cu(en)_2Ag(CN)_2][Ag(CN)_2]$	2-D	3.16 Å	[108]
$[Ni(tn)_2\{Ag(CN)_2\}_2]$	1-D	3.26 Å	[109]
$[Cu(tn)_2Ag(CN)_2][Ag(CN)_2]$	1-D	3.23 – 3.42 Å	[109]
$[Cd(imH)_5Ag(CN)_2][Ag(CN)_2]$	3-D	3.08 Å	[160]
$[Cd(Mepy)_2\{Ag(CN)_2\}_2] \bullet Mepy$	3-D	3.08 Å	[159]
$[Cd(Mepy)_4Ag_2(CN)_3][Ag(CN)_2]$	3-D	2.99 Å	[159]
$[Ni(en)_2Ag_2(CN)_3][Ag(CN)_2]$	3-D	3.32 Å	[162]
$[Ni(cyclen)Ag(CN)_2][Ag(CN)_2]$	1-D	3.03 – 3.04 Å	[161]

Other ligand abbreviations:

cyclen = 1,4,7,10-tetraazacyclododecane
mepy = 4-picoline
tn = 1,3-diaminopropane
imH = imidazole

2.2 RESULTS AND ANALYSES*

2.2.1 Synthesis and Structure

A summary of crystallographic data and refinement details for all structures in this chapter are collected in Appendix 2, and the coordinates are collected in Appendix 3.

2.2.1.1 $[Cu(en)_2][Ag_2(CN)_3][Ag(CN)_2]$ (2.1)

The reaction of an aqueous solution containing 1 equivalent of $Cu(ClO_4)_2 \bullet 6H_2O$ and 2 equivalents of en with an aqueous solution of 2 equivalents of $KAg(CN)_2$ produced an immediate precipitate which was filtered, washed and air-dried. This precipitate was characterized by IR and elemental analysis, the details of which are found in Section 2.5. Crystals with an identical IR and EA as the powder precipitate were formed upon slow

* Reproduced in part with permission from C. J. Shorrock, B.-Y. Xue, P. B. Kim, R. J. Batchelor, B. O. Patrick and D. B. Leznoff, *Inorganic Chemistry*, **2002**, *41*, 6743-6753, Copyright 2002, American Chemical Society.

diffusion of an aqueous solution of 1 equivalent of $[Cu(en)_2]^{2+}$ and 2 equivalents of $[Ag(CN)_2]^-$ in an H-shaped tube. The X-ray crystal structure of $[Cu(en)_2][Ag_2(CN)_3][Ag(CN)_2]$ (**2.1**) is depicted in Figures 2.1 and 2.2, with the corresponding bond lengths and angles collected in Table 2.2. The X-ray crystal structure of **2.1** reveals a 1-D zig-zag chain of $[Ag_2(CN)_3]^-$ and $[Ag(CN)_2]^-$ units connected via argentophilic interactions (Fig. 2.1). The Ag(1)–Ag(2) bond length is 3.102(1) Å, which is significantly lower than 3.44 Å, the sum of the van der Waals radii of two Ag(I) centres [119]. This argentophilic interaction can be compared to the 2.889 Å distance of the Ag–Ag bonds in metallic silver and many silver(I) oxides [163]. The $[Ag(CN)_2]^-$ and $[Ag_2(CN)_3]^-$ fragments are oriented nearly orthogonally with respect to each other (C(21)–Ag(2)–Ag(1)–C(11)′ = 81.7°), as has been observed in other $[Ag(CN)_2]^-$ and $[Ag_2(CN)_3]^-$ systems [104,106,108,109,150,161].

Cyano-N(11)–Ag(2) interactions connect these 1-D zig-zag chains into a 2-D array (Fig. 2.2). The Ag(2)–N(11)″ bond distance of 2.572(3) Å is well below the sum of the van der Waals radii (3.27 Å) [119] and within the range of other Ag–N bonds (2.085 – 2.979 Å) reported in the literature [164-176]. The $[Ag_2(CN)_3]^-$ unit is distorted from linearity (C(21)–Ag(2)–C/N(20) = 163.59(13)°) due to the Ag–N interaction. There have been very few studies where the binding of silver atoms by the nitrogen atoms of $[Ag(CN)_2]^-$ units has been observed [162,175,176]. Furthermore, this is only the second reported structure where an $[Ag(CN)_2]^-$ nitrogen generates a strong Ag–N interaction in a non-linear fashion (N(11)″–Ag(2)–C/N(20) = 96.06(11)°). The first, recently reported structure with such an interaction was $[Ni(en)_2Ag_2(CN)_3][Ag(CN)_2]$, which showed similar non-linearity (N–Ag–C/N = 95.2(2)°) and a slightly stronger interaction (Ag–N = 2.415(4) Å) [162].

The $[Cu(en)_2]^{2+}$ cation is not strongly coordinated to the 2-D array (Fig. 2.1). There are, however, weak interactions (Cu(1)–N(21) = 2.657(3) Å) between the copper(II) centre and the free cyano(N) atoms of the $[Ag_2(CN)_3]^-$ units.

There are significant differences between the structure of **2.1** and the previously reported structure of $[Cu(en)_2Ag(CN)_2][Ag(CN)_2]$ [108]. This complex, containing no $[Ag_2(CN)_3]^-$ units, forms a 1-D chain of $[Cu(en)_2]^{2+}$ and bridging $[Ag(CN)_2]^-$ units with a Cu–N bond of 2.569(4) Å, a stronger interaction than observed in **2.1**. In $[Cu(en)_2Ag(CN)_2][Ag(CN)_2]$, the Ag–Ag interaction between the bridging $[Ag(CN)_2]^-$ and the free $[Ag(CN)_2]^-$ is 3.1580(5) Å, creating a 2-D array. This argentophilic interaction is

slightly weaker than that observed in **2.1**. Finally, $[Cu(en)_2Ag(CN)_2][Ag(CN)_2]$ displays no Ag–N interactions.

Table 2.2 – Selected Bond Lengths (Å) and Angles (deg) for $[Cu(en)_2][Ag_2(CN)_3][Ag(CN)_2]$ (**2.1**)

Selected Atoms	Bond Length	Selected Atoms	Bond Length
Ag(1) – C(11)	2.046(3)	Ag(2) – C(21)	2.071(4)
Ag(2) – C/N(20)	2.085(4)	C/N(20) – C/N(20)′[a]	1.129(8)
N(11) – C(11)	1.125(4)	N(21) – C(21)	1.110(6)
Cu(1) – N(1)	1.998(3)	Cu(1) – N(4)	2.0162(21)
Ag(1) – Ag(2)	3.102(1)	Ag(2) – N(11)′	2.572(3)
Selected Atoms	**Angle**	**Selected Atoms**	**Angle**
C(21) – Ag(2) – C/N(20)	163.59(13)	C/N(20)′ – C/N(20) – Ag(2)	178.3(3)
N(1) – Cu(1) – N(4)	84.50(11)	N(11)″ – Ag(2) – C/N(20)	96.06(11)

[a]Symmetry transformations: ′ ≡ –x, 1 – y, –z; ″ ≡ 1 – x, –y, –z.

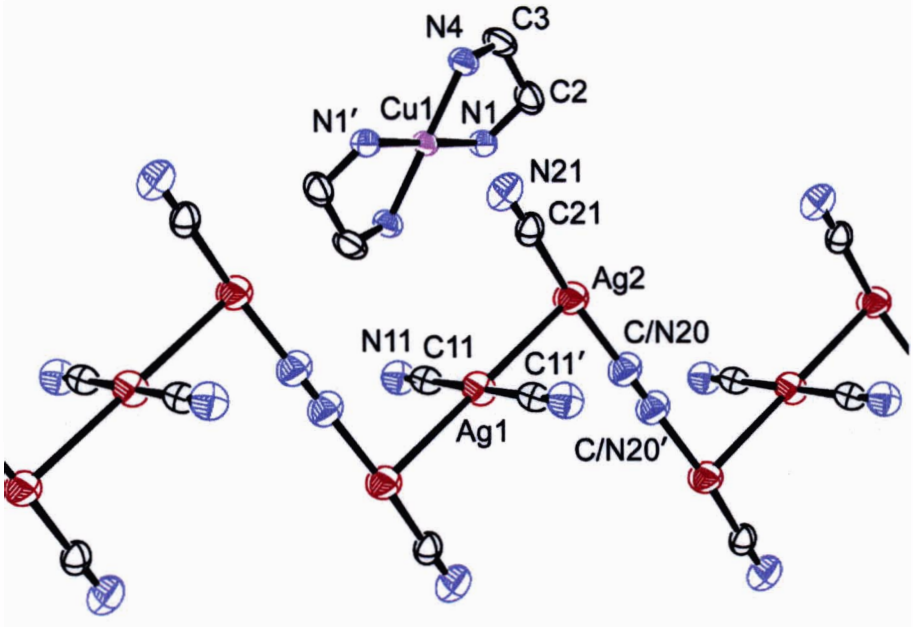

Figure 2.1 – Extended structure of $[Cu(en)_2][Ag_2(CN)_3][Ag(CN)_2]$ (**2.1**) showing only the 1-D chain.

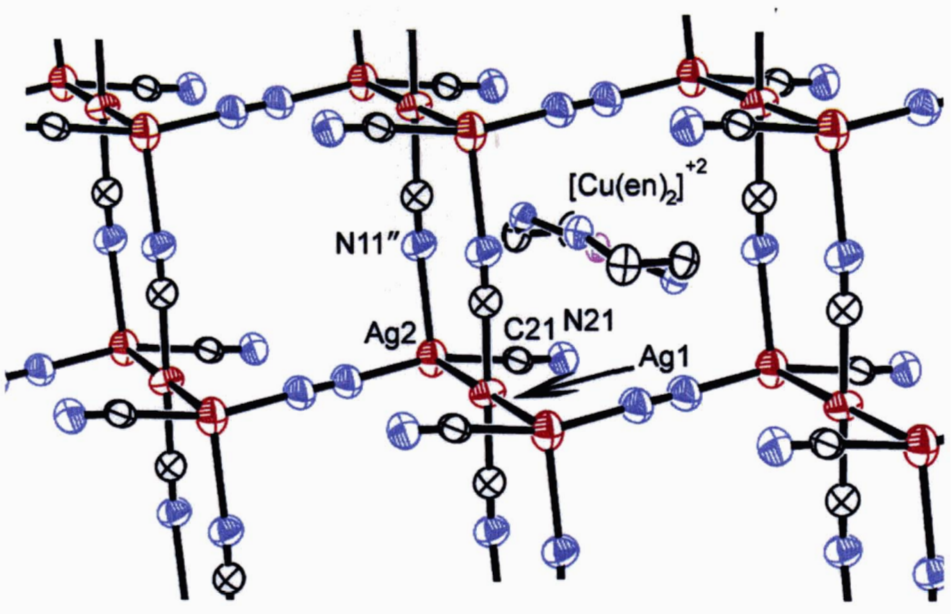

Figure 2.2 – Extended structure of $[Cu(en)_2][Ag_2(CN)_3][Ag(CN)_2]$ (**2.1**) showing the 2-D network propagated by Ag–N interactions. Only one $[Cu(en)_2]^{2+}$ cation is shown for clarity.

For all of the $[Ag(CN)_2]^-$ complexes, the IR spectra are very valuable in understanding the structure based on the different possible environments of the cyanide moieties. The νCN bands in the IR spectra of each complex, as well as related systems, are collected in Table 2.3 for comparison.

The IR spectrum of **2.1** shows νCN bands of 2156, 2140 and 2118 cm^{-1}. As compared to the νCN band of $KAg(CN)_2$ of 2139 cm^{-1} [152] the observed 2140 cm^{-1} can be attributed to the non-bridging $[Ag(CN)_2]^-$ anion. As has been discussed earlier, a shift from this value to higher frequencies suggests the bridging of the cyanide moiety, and thus the 2156 cm^{-1} band can be attributed to the bridging $[Ag(CN)_2]^-$ moieties as observed in the crystal structure. Similar assignments for the νCN bands of proceeding complexes are compiled in Table 2.3. The final νCN band of **2.1** occurs at a much lower frequency (2118 cm^{-1}) and has been assigned to the central cyanide of the $[Ag_2(CN)_3]^-$ moiety, as will be discussed further in Section 2.3.

Table 2.3 – Comparison of Cyanide (νCN) Absorptions (cm^{-1}) for Complexes **2.1–2.6** and Related Systems*

Complex	νCN Absorption(s) (by type)			
	Ag-***CN*** or Au-***CN***	Ag-***CN***-M or Au-***CN***-M	Ag-***CN***-Ag	Other
$KAg(CN)_2$ [152]	2139			
$[Cu(en)_2][Ag_2(CN)_3][Ag(CN)_2]$ (**2.1**)	2140	2156	2118	
$[Cu(en)_2Ag(CN)_2][Ag(CN)_2]$ [104]	2136 (broad)			
$[Cu(dien)Ag(CN)_2]_2[Ag_2(CN)_3][Ag(CN)_2]$ (**2.2**)	2141, 2134	2166, 2156	2119	
$[Ni(en)_2Ag_2(CN)_3][Ag(CN)_2]$ (**2.3**)		2159, 2140	2123	
$[Ni(en)_2Ag(CN)_2][Ag(CN)_2]$ [104]	2136	2152		
$[Ni(en)][Ni(CN)_4]\bullet 2.5H_2O$ (**2.4**)				2164
$K_2[Ni(CN)_4]$ [67]				2170
$[Ni(tren)Ag(CN)_2][Ag(CN)_2]$ (**2.5**)	2139	2174		
$[Ni(tren)Au(CN)_2][Au(CN)_2]$ [96]	2144	2179		
$[Cu(en)Cu(CN)_2Ag(CN)_2]$ (**2.6**)		2151, 2141		2127
$K[Cu(CN)_2]$ [67]				2115 ± 5

* Values determined from the maximum of the absorption peak. A representative spectrum is shown for **2.2** in Figure 2.5. IR spectrometer resolution = 2 cm^{-1}, all spectra were done as KBr pellets.

2.2.1.2 $[Cu(dien)Ag(CN)_2]_2[Ag_2(CN)_3][Ag(CN)_2]$ (2.2)

In a similar fashion to the synthesis of **2.1**, the reaction of a solution containing 1 equivalent of $[Cu(dien)]^{2+}$ with a solution containing 2 equivalents of $[Ag(CN)_2]^-$ produced an immediate precipitate of $[Cu(dien)Ag(CN)_2]_2[Ag_2(CN)_3][Ag(CN)_2]$ (**2.2**). The filtrate solution yielded crystals of **2.2** (with an identical IR spectrum to the initial precipitate). The X-ray crystal structure of **2.2** is depicted in Figures 2.3 and 2.4, with the corresponding bond lengths and angles collected in Table 2.4. The X-ray structure of **2.2** shows that the $[Cu(dien)]^{2+}$ cations are each connected to two $[Ag(CN)_2]^-$ units, thus each copper(II) is five-coordinate (Fig. 2.3). The copper centre adopts a distorted square pyramidal coordination such that one $[Ag(CN)_2]^-$ moiety is coordinated equatorially (Cu(1)–N(11) = 1.984(5) Å), one is coordinated apically (Cu(1)–N(12)′ = 2.166(5) Å) and the final three equatorial sites are occupied by the dien ligand. The

apical Cu–N bond is slightly shorter as compared with previously reported distorted square pyramidal copper complexes (Cu–N apical = 2.2-2.7 Å) [106,108,109,177-179]. The $[Ag(CN)_2]^-$ fragments bridge apical/equatorial sites between $[Cu(dien)]^{2+}$ cations to form a 1-D zig-zag chain (Fig. 2.3).

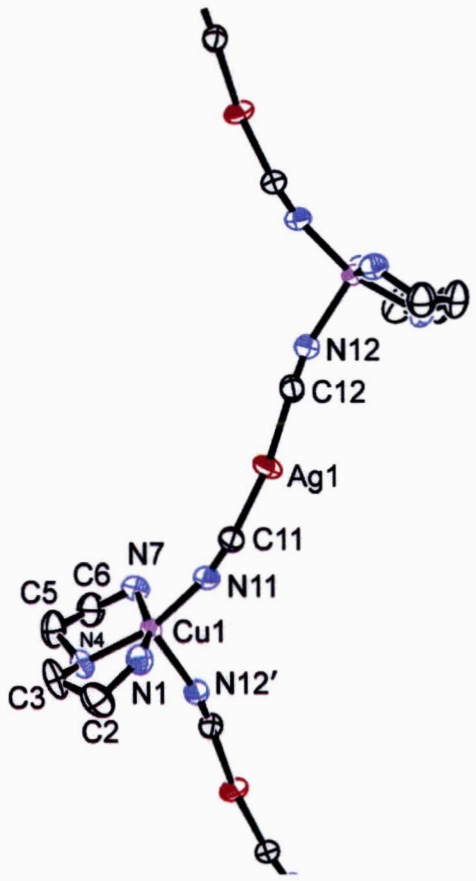

Figure 2.3 – Extended structure of $[Cu(dien)Ag(CN)_2]_2[Ag_2(CN)_3][Ag(CN)_2]$ (**2.2**) showing only the 1-D chain.

Zig-zag chains of alternating $[M(ligand)]^{2+}$ and $[M(CN)_2]^-$ units have been observed for both $[Au(CN)_2]^-$ and $[Ag(CN)_2]^-$ complexes [53,161]. Unlike **2.2**, the dicyanoaurate analogue, $Cu(dien)[Au(CN)_2]_2$, does not display such chains [53]. Instead, $[Au(CN)_2]^-$ moieties are coordinated to $[Cu(dien)]^{2+}$ cations at one end only, leaving the other cyano(N) atom free. The resulting molecular $Cu(dien)[Au(CN)_2]_2$ units are then connected through Au–Au interactions.

Table 2.4 – Selected Bond Lengths (Å) and Angles (deg) for $[Cu(dien)Ag(CN)_2]_2[Ag_2(CN)_3][Ag(CN)_2]$ (**2.2**)

Selected Atoms	Bond Length	Selected Atoms	Bond Length
Cu(1) – N(1)	2.008(5)	Cu(1) – N(4)	2.016(4)
Cu(1) – N(7)	2.011(5)	Cu(1) – N(12)′[a]	2.166(5)
Cu(1) – N(11)	1.984(5)	Ag(1) – C(12)	2.068(6)
Ag(1) – C(11)	2.050(6)	Ag(2) – C/N(22)	2.064(5)
Ag(2) – C(21)	2.041(7)	Ag(3) – C(31)	2.066(7)
C/N(22) – C/N(22)″	1.139(9)	Ag(1) – Ag(3)	3.2889(5)
Ag(1) – Ag(2)	3.1718(8)		
Selected Atoms	**Angle**	**Selected Atoms**	**Angle**
N(12)′ – Cu(1) – N(11)	101.95(18)	N(12)′ – Cu(1) – N(7)	98.46(18)
N(12)′ – Cu(1) – N(4)	93.95(19)	N(12)′ – Cu(1) – N(1)	100.51(19)
N(7) – Cu(1) – N(4)	83.74(19)	N(7) – Cu(1) – N(11)	90.81(19)
N(4) – Cu(1) – N(11)	163.8(2)	N(4) – Cu(1) – N(1)	83.85(19)
N(7) – Cu(1) – N(1)	157.96(19)	N(11) – Cu(1) – N(1)	96.13(19)
Ag(2) – Ag(1) – C(11)	69.58(16)	Ag(3) – Ag(1) – C(11)	116.62(16)
Ag(2) – Ag(1) – C(12)	103.06(16)	Ag(3) – Ag(1) – C(12)	72.13(16)
C(11) – Ag(1) – C(12)	169.3(2)	Ag(2) – Ag(1) – Ag(3)	103.742(17)
Ag(1) – Ag(2) – C/N(22)	78.16(16)	Ag(1) – Ag(2) – C(21)	101.21(17)
C/N(22) – Ag(2) – C(21)	172.0(2)	Ag(1) – Ag(3) – C(31)	67.87(18)

[a]Symm try transformations: ′ ≡ –x+1/2, y–1/2, –z+1/2; ″ ≡ 1–x, 1–y, –z.

The chains in **2.2** are crosslinked via Ag(1)–Ag(2) interactions of 3.1718(8) Å to $[Ag_2(CN)_3]^-$ units, thus creating a 2-D array in the (101) plane (Fig. 2.4). A distortion from linearity is observed for both the $[Ag_2(CN)_3]^-$ units and the $[Ag(CN)_2]^-$ moieties (C(21)–Ag(2)–C/N(22) = 172.0(2)° and C(12)–Ag(1)–C(11) = 169.3(2)°), which could be due to the presence of argentophilic interactions. Such distortions have been recently discussed in $[Au(CN)_2]^-$ dimers [89]. In contrast to **2.1**, $[Ag(CN)_2]^-$ forms an interaction with only one $[Ag_2(CN)_3]^-$ unit in **2.2**.

The 2-D planes are connected into a weakly held 3-D array via further argentophilic interactions of 3.2889(5) Å between silver atoms in the $[Ag(CN)_2]^-$ units of the 2-D array (Ag(1)) and the remaining 1/2 equivalent of free $[Ag(CN)_2]^-$ (Ag(3)) (3-D array not shown). As a result, argentophilic interactions have increased the dimensionality of **2.2**

from one to three and can thus be viewed, like aurophilic interactions, as a tool with which to increase structural dimensionality.

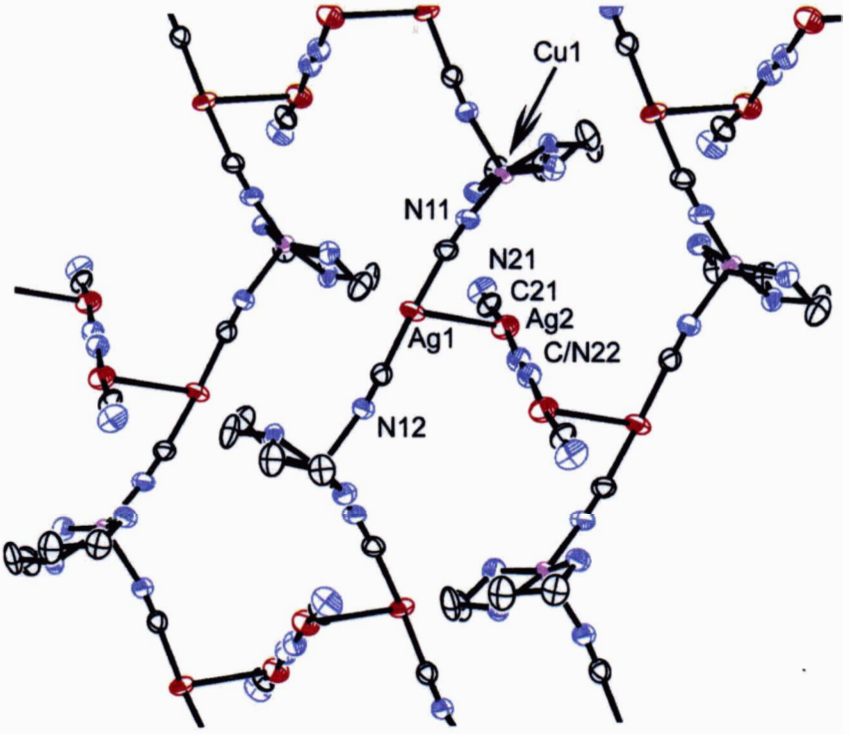

Figure 2.4 – Extended structure of $[Cu(dien)Ag(CN)_2]_2[Ag_2(CN)_3][Ag(CN)_2]$ (**2.2**) showing the 2-D network propagated through argentophilic interactions.

The IR spectrum of **2.2** is depicted in Figure 2.5 as a representative example of the IR spectral data throughout this thesis. The spectrum shows νCN bands of 2166, 2156, 2141, 2134 and 2119 cm^{-1}. As discussed for **2.1**, the bands at higher frequency (2166 and 2156 cm^{-1}) can be attributed to the bridging $[Ag(CN)_2]^-$ anion and the band at 2141 cm^{-1} can be attributed to the non-bridging $[Ag(CN)_2]^-$ anion. The lower νCN bands of **2.2** (2134 and 2119 cm^{-1}) have been assigned (Table 2.3) to the $[Ag_2(CN)_3]^-$ moiety, and will be discussed further in Section 2.3

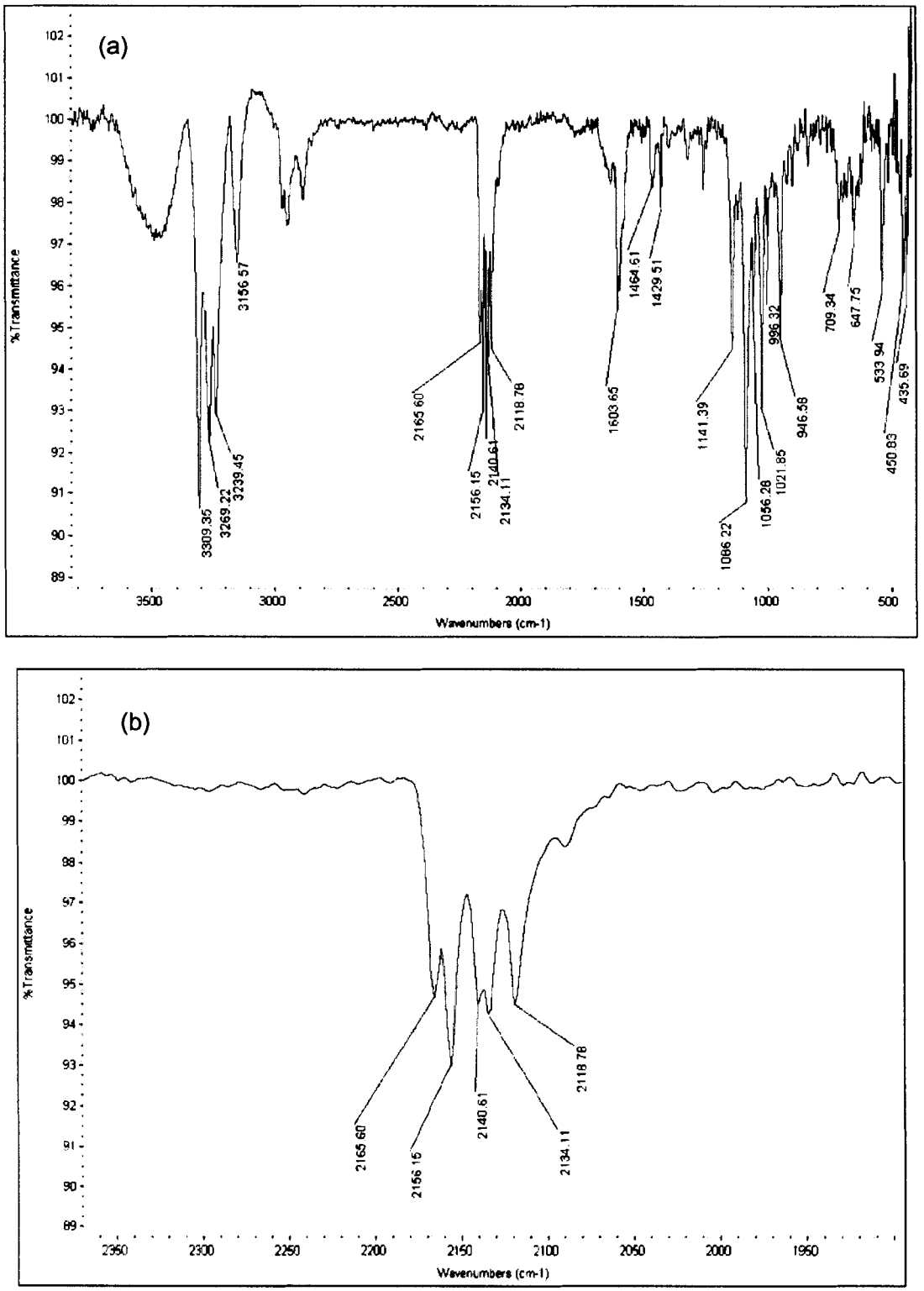

Figure 2.5 – (a) IR spectrum of $[Cu(dien)Ag(CN)_2]_2[Ag_2(CN)_3][Ag(CN)_2]$ (**2.2**).
(b) Magnification of the νCN region of the same spectrum.

2.2.1.3 $[Ni(en)_2Ag_2(CN)_3][Ag(CN)_2]$ (2.3) and its byproduct $[Ni(en)][Ni(CN)_4]\bullet 2.5H_2O$ (2.4)

The reaction to form $[Ni(en)_2Ag_2(CN)_3][Ag(CN)_2]$ (**2.3**) was conducted in a similar manner as the reaction to form **2.1**, however $Ni(NO)_3\bullet 6H_2O$ was used in place of the Cu(II) salt. Crystals of both $[Ni(en)_2Ag_2(CN)_3][Ag(CN)_2]$ (**2.3**) and $[Ni(en)][Ni(CN)_4]\bullet 2.5H_2O$ (**2.4**) were obtained through an H-tube experiment (containing the same ratio of reactants). The X-ray structure of **2.3** was published [162] during the preparation of the manuscript containing this research project, although there was no discussion of the formation of the $[Ni(CN)_4]^{2-}$ by-product (**2.4**). For comparison, the X-ray crystal structure of **2.3** is depicted in Figure 2.6, with the corresponding bond lengths and angles collected in Table 2.5. The crystal structure of **2.3** shows that the $[Ni(en)_2]^{2+}$ units are joined into a 1-D undulating chain by the $[Ag_2(CN)_3]^-$ unit, such that the Ni(II) centre adopts an octahedral geometry. These chains are then connected into a 2-D sheet by the $[Ag(CN)_2]^-$ units, via Ag–N interactions between the N atom of the $[Ag(CN)_2]^-$ unit and the Ag atom of the $[Ag_2(CN)_3]^-$ unit (Ag(1)–N(21)′ = 2.411(4) Å). The Ag–N bond in **2.3** is similar to that observed in **2.1**. The result can be described as an infinite (6,3) net [180], as depicted in Figure 2.6.

Table 2.5 – Selected Bond Lengths (Å) and Angles (deg) for $[Ni(en)_2Ag_2(CN)_3][Ag(CN)_2]$ (**2.3**)

Selected Atoms	Bond Length	Selected Atoms	Bond Length
Ag(1) – C(11)	2.0827(21)	Ag(2) – C(21)	2.057(4)
Ni(1) – N(1)	2.109(3)	Ni(1) – N(4)	2.109(3)
Ni(1) – N(11)	2.0832(18)	Ag(1) – N(21)′[a]	2.411(4)
Selected Atoms	**Angle**	**Selected Atoms**	**Angle**
C(11) – Ag(2) – C/N(12)	148.83(12)	Ag(1) – N(21)′ - C(21)′	162.91(24)
C(11) – Ag(1) – N(21)′	115.52(11)	Ag(1) – C(11) – N(11)	174.13(24)
N(1) – Ni(1) – N(11)	90.40(9)	N(1) – Ni(1) – N(4)	82.05(1)

[a]Symmetry transformation: ′ ≡ 1 – x, 2 – y, 1 – z.

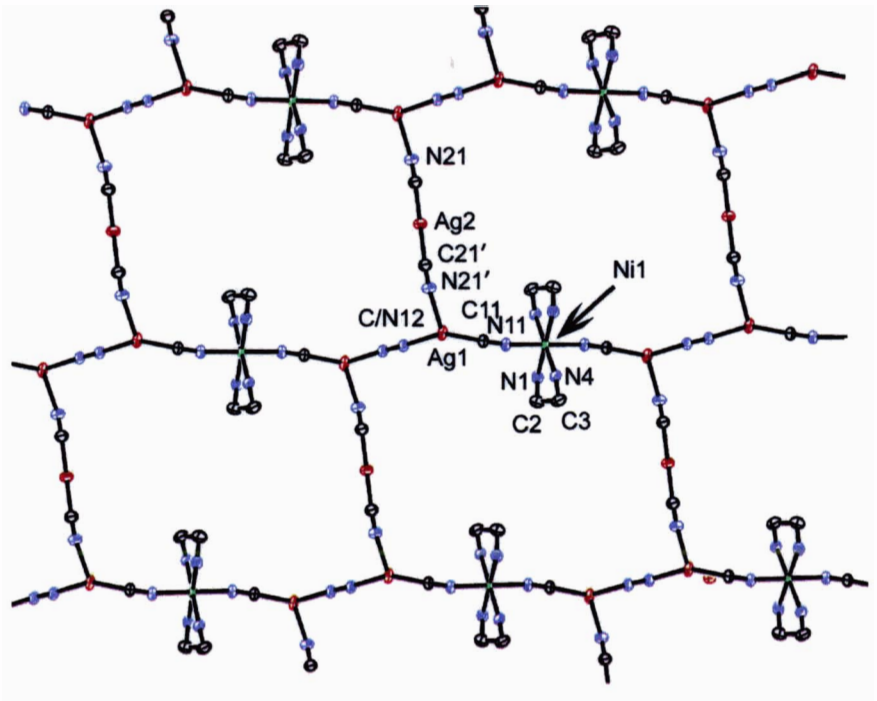

Figure 2.6 – Extended structure of $[Ni(en)_2Ag_2(CN)_3][Ag(CN)_2]$ (**2.3**) showing the 2-D network.

The IR spectrum of **2.3** shows νCN bands at 2159, 2140 and 2123 cm^{-1}. Similar assignments can be made to these bands (Table 2.3) in accordance with the X-ray crystal structure containing a bridging $[Ag(CN)_2]^-$ (2159 cm^{-1}), and an $[Ag_2(CN)_3]^-$ moiety (2140 cm^{-1} and 2120 cm^{-1}).

No discussion has been reported regarding the structural impact of the increased length of the $[Ag_2(CN)_3]^-$ unit as compared to the $[Ag(CN)_2]^-$ building block. The structure of **2.3** can be compared to the previously reported $[Ni(tn)_2][Ag(CN)_2]_2$ (tn = 1,3-diaminopropane) [109]. Even though only one carbon atom has been added to the chelate backbone, in $[Ni(tn)_2][Ag(CN)_2]_2$, 1-D chains of alternating $[M(L)_2]^{2+}$ and $[Ag(CN)_2]^-$ do not form; rather, only a trimetallic molecule of $Ni(tn)_2(\mu\text{-NC-Ag-CN})_2$ is observed [109]. This suggests that the increased length of the $[Ag_2(CN)_3]^-$ unit (approximately 11.6 Å vs. 6.3 Å for the $[Ag(CN)_2]^-$ unit) is sufficient to allow for linear propagation in an axial fashion. This would suggest that the additional length of the building block may be able to offset any steric hindrances to the formation of a chain.

There are also no Ag–N bonds in $[Ni(tn)_2][Ag(CN)_2]_2$ that increase dimensionality (potentially again due to steric hindrances). These comparisons suggest that the incorporation of $[Ag_2(CN)_3]^-$ units can serve to enhance dimensionality, as the increased length may allow for coordination between units that could be sterically hindered if connected by $[Ag(CN)_2]^-$ units.

From the crystals of $[Ni(en)][Ni(CN)_4]\bullet 2.5H_2O$ (**2.4**) that were obtained from the same H-tube experiment that yielded **2.3**, the crystal structure obtained was not suitable for publication due to poor diffraction of the crystal, however the data obtained was sufficient to confirm the identity of the compound, as well as its atomic connectivity. Each octahedral nickel centre is capped by en, and the remaining four sites are occupied by $[Ni(CN)_4]^{2-}$ units, which then bridge to three other nickel centres; related compounds such as $[Cd(en)Ni(CN)_4]$ have been reported [80]. The resulting 3-D structure contains cavities throughout that are filled with 2.5 equivalents of water.

2.2.1.4 [Ni(tren)Ag(CN)$_2$][Ag(CN)$_2$] (2.5)

Following the same method as used for **2.1**, with the use of $Ni(NO_3)_2\bullet 6H_2O$ instead of the Cu(II) salt and 1 equivalent of tren, $[Ni(tren)Ag(CN)_2][Ag(CN)_2]$ (**2.5**) was formed. Crystals were obtained through an H-tube diffusion method. The resulting crystal structure is virtually isostructural with the previously reported gold analogue [96]. The X-ray crystal structure of **2.5** is depicted in Figure 2.7, with the corresponding bond lengths and angles collected in Table 2.6. In both cases, $[Ni(tren)]^{2+}$ cations are linked in a cis fashion by $[M(CN)_2]^-$ units to form a 1-D zig-zag chain in the [010] direction (Fig. 2.7). The Ni(II) adopts an octahedral geometry in both cases. It was observed in $[Ni(tren)Au(CN)_2][Au(CN)_2]$ that the two cyano(N)–Ni distances varied slightly in bond lengths (2.05(2) Å vs 2.12(1) Å) [96] and this was also observed in **2.5** (Ni(1)–N(22)′ = 2.039(3) Å and Ni(1)–N(21) = 2.098(3) Å). The $[M(CN)_2]^-$ moieties in both structures were linear. In $[Ni(tren)Au(CN)_2][Au(CN)_2]$, the gold–gold distances were 3.5963(8) Å and 3.5932(8) Å [96]. In the Ag(I) equivalent (**2.5**), the silver–silver distances are 3.5607(6) Å (Ag(1)–Ag(2)) and 3.7125(6) Å (Ag(2)–Ag(3)). In both cases, these long distances suggest that there are no significant metallophilic interactions present, and both structures remain one-dimensional.

The IR spectrum of **2.5** shows νCN bands consistent with a bridging (2179 cm^{-1}) and non-bridging (2139 cm^{-1}) $[Ag(CN)_2]^-$ unit, as is confirmed by the X-ray structure.

Table 2.6 – Selected Bond Lengths (Å) and Angles (deg) for $[Ni(tren)Ag(CN)_2][Ag(CN)_2]$ (**2.5**)

Selected Atoms	Bond Length	Selected Atoms	Bond Length
Ag(1) – C(11)	2.046(4)	Ag(2) – C(21)	2.046(3)
Ni(1) – N(1)	2.123(3)	Ni(1) – N(4)	2.106(3)
Ni(1) – N(7)	2.093(3)	Ni(1) – N(10)	2.112(3)
Ni(1) – N(21)	2.098(3)	Ni(1) – N(22)′[a]	2.039(3)
Selected Atoms	**Angle**	**Selected Atoms**	**Angle**
C(21) – Ag(2) – C(22)	179.31(15)	N(1) – Ni(1) – N(7)	83.18(11)
N(1) – Ni(1) – N(4)	82.11(12)	N(4) – Ni(1) – N(10)	82.88(12)
N(1) – Ni(1) – N(10)	91.96(12)	Ni(1) – Ni(1) – N(21)	85.93(12)
N(7) – Ni(1) – N(10)	93.58(11)	N(7) – Ni(1) – N(21)	87.59(11)
N(4) – Ni(1) – N(21)	93.59(12)	N(1) – Ni(1) – N(22)′	99.49(13)
N(4) – Ni(1) – N(22)′	172.85(12)	N(7) – Ni(1) – N(22)′	96.03(12)
N(10) – Ni(1) – N(22)′	90.09(12)	N(21) – Ni(1) – N(22)′	93.48(12)
Ni(1) – N(21) – C(21)	174.4(3)	Ni(1) – N(22)′ – C(22)′	170.6(3)

[a]Symmetry transformation: ′ ≡ –x + 1/2, y + 1/2, –z + 3/2.

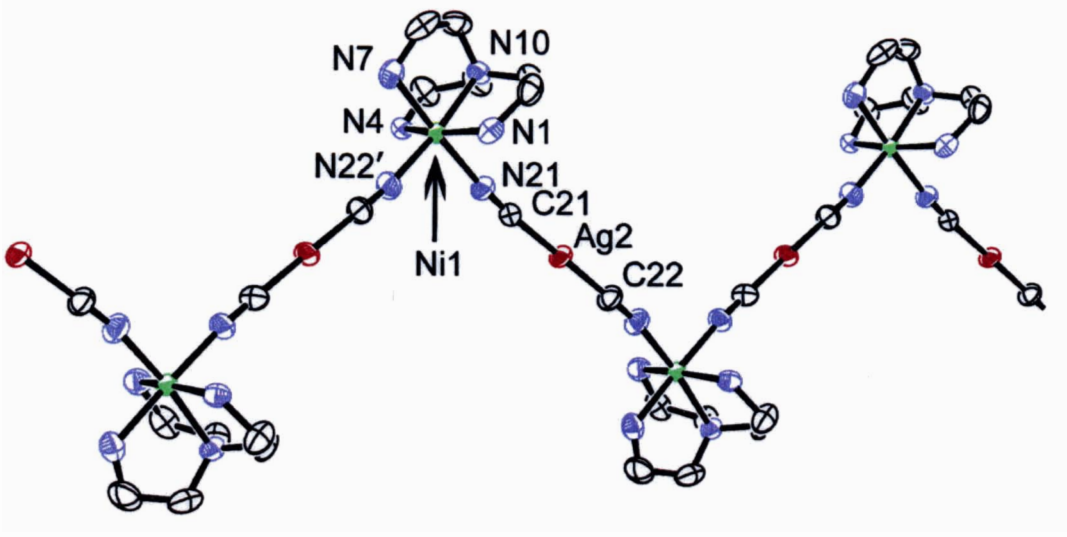

Figure 2.7 – Extended structure of $[Ni(tren)Ag(CN)_2][Ag(CN)_2]$ (**2.5**).

2.2.1.5 $[Cu(en)Cu(CN)_2Ag(CN)_2]$ (2.6)

The reaction of an aqueous solution of $[Cu(en)]^{2+}$ with an aqueous solution of 2 equivalents of $[Ag(CN)_2]^-$ (as described for **2.1**) only produced a pure product of

$[Cu(en)Cu(CN)_2Ag(CN)_2]$ (**2.6**) when done via an H-tube diffusion method; repeated attempts to prepare **2.6** via other methods led to complex mixtures. The X-ray crystal structure of **2.6** is depicted in Figures 2.8 and 2.9, with the corresponding bond lengths and angles collected in Table 2.7. The resulting X-ray structure reveals a five-coordinate, distorted square pyramidal copper(II) centre, with equatorial sites occupied by en (Cu(1)–N(1) = 2.030(2) Å and Cu(1)–N(2) = 2.036(2) Å), and $[Cu(CN)_2]^-$ units (Cu(1)–N(3) = 1.984(2) Å and Cu(1)–N(7) = 1.989(2) Å) and the apical site coordinated by an $[Ag(CN)_2]^-$ moiety (Cu(1)–N(4) = 2.211(2) Å) (Fig. 2.8).

Each $[Cu(CN)_2]^-$ moiety bridges two $[Cu(en)]^{2+}$ cations. This trigonal (C(3)″–Cu(2)–C(7) = 126.1(1)°) Cu(I) centre is three-coordinate by virtue of cyano(N) coordination from an $[Ag(CN)_2]^-$ unit (Cu(2)–N(6) = 1.975(2) Å). This linear Ag(I) fragment then bridges to another $[Cu(en)]^{2+}$ cation. The end result is a coordinately bonded, 2-D array of elongated hexagons (Fig. 2.8), which can be described as an infinite (6,3) net [180]. This (6,3) net is comparable to that seen in **2.3**, but in **2.3**, a 3-D array of these nets results via argentophilic interactions [162].

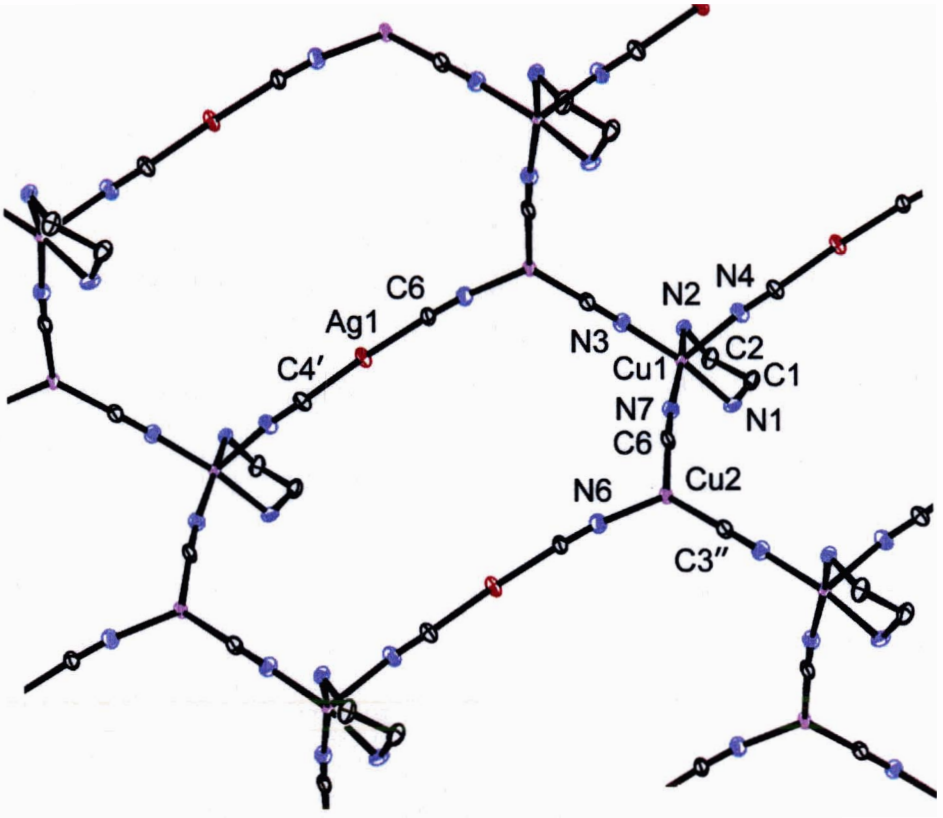

Figure 2.8 – Extended structure of $[Cu(en)Cu(CN)_2Ag(CN)_2]$ (**2.6**) showing only the 2-D net.

Table 2.7 – Selected Bond Lengths (Å) and Angles (deg) for $[Cu(en)Cu(CN)_2Ag(CN)_2]$ (**2.6**)

Selected Atoms	Bond Length	Selected Atoms	Bond Length
Ag(1) – C(4)′[a]	2.062(2)	Ag(1) – C(6)	2.073(2)
Cu(1) – N(1)	2.030(2)	Cu(1) – N(2)	2.036(2)
Cu(1) – N(3)	1.984(2)	Cu(1) – N(4)	2.211(2)
Cu(1) – N(7)	1.989(2)	Cu(2) – N(6)	1.975(2)
Cu(2) – C(3)″	1.923(2)	Cu(2) – C(7)	1.926(2)
Ag(1) – Cu(2)	3.1000(4)		
Selected Atoms	**Angle**	**Selected Atoms**	**Angle**
N(1) – Cu(1) – N(2)	83.48(8)	N(1) – Cu(1) – N(3)	167.82(9)
N(1) – Cu(1) – N(4)	90.82(9)	N(1) – Cu(1) – N(7)	90.21(8)
N(2) – Cu(1) – N(3)	91.33(8)	N(2) – Cu(1) – N(4)	93.92(8)
N(2) – Cu(1) – N(7)	163.13(8)	N(3) – Cu(1) – N(4)	100.56(9)
N(3) – Cu(1) – N(7)	91.70(9)	N(4) – Cu(1) – N(7)	101.83(8)
C(4)′ – Ag(1) – C(6)	175.0(1)	N(6) – Cu(2) – C(3)″	117.5(1)
N(6) – Cu(2) – C(7)	116.35(9)	C(3)″ – Cu(2) – C(7)	126.1(1)

[a]Symmetry transformations: ′ ≡ 1 + x, y, z; ″ ≡ 1/2 + x, 1/2-y, -1/2 + z.

Although the nets in **2.6** do not possess interactions extending them into infinite 3-D networks, the apparent free volume in the structure is filled by a second, interpenetrating (6,3) net (Fig. 2.9). The interpenetration occurs in a parallel fashion, and the layers are connected and stabilized by Cu(2)–Ag(1) interactions of 3.1000(4) Å. This is an unusual example of metallophilic d^{10}-d^{10} interactions between Cu(I) and Ag(I). The only previously reported Cu(I)-Ag(I) interactions are in constrained cluster complexes, with concomitantly smaller Cu(I)–Ag(I) distances (2.67 Å – 3.07 Å) [181-185]. A related structure, $Cu(NH)_3(pyz)Ag_{3-x}Cu_x(CN)_5$, has similar framework and interpenetration, but the Cu(I) and Ag(I) sites are disordered due to partial replacement of Ag(I) for Cu(I) [186]. The metallophilic interactions (2.791(3) Å and 2.641(1) Å) in this case are between adjacent trigonal centres (as opposed to trigonal and linear centres in **2.6**) and are supported by partially bridging CN-ligands, thus accounting for their strength compared with **2.6**. The disorder present in this previously reported structure, however, precludes any further meaningful discussion of metallophilic interactions.

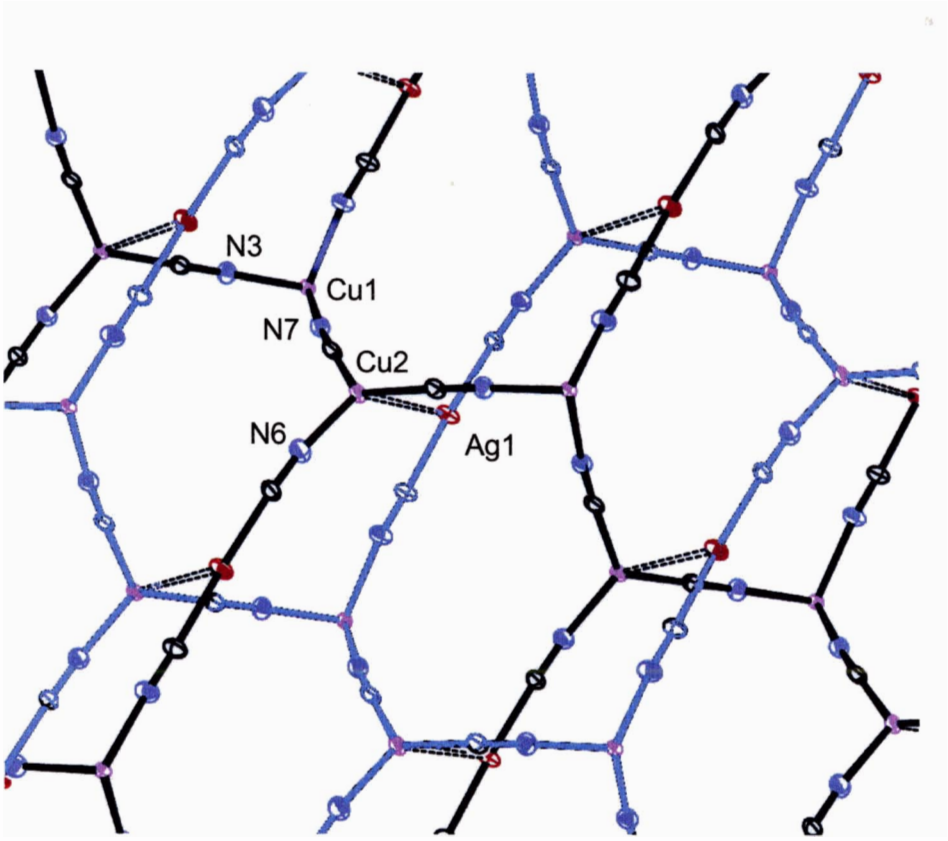

Figure 2.9 – Extended structure of $[Cu(en)Cu(CN)_2Ag(CN)_2]$ (**2.6**) showing two interpenetrating 2-D nets stabilized by Cu-Ag interactions (3.1000(4) Å, dotted lines) (en ligand removed for clarity).

The IR spectrum for **2.6** shows the expected νCN bands associated with bridging $[Ag(CN)_2]^-$ units (2151 and 2141 cm^{-1}). Another band is observed at 2127 cm^{-1}, which can be compared to the value for $KCu(CN)_2$ of 2115 ± 5 cm^{-1} [67], thus likely representing the νCN stretch of the Cu(I) cyanide.

2.2.2 Magnetic Properties

The product of the magnetic susceptibility with temperature, $\chi_M T$, for **2.1** at 300 K was determined to be 0.39 cm^3 K mol^{-1}, consistent with the presence of an S=1/2, Cu(II) centre (as determined from the Curie Law, Equation 1.3). No significant magnetic interactions are expected in this system as the $[Cu(en)_2]^{2+}$ ions are structurally isolated from each other, according to the X-ray structure.

For complexes **2.2** – **2.6**, the temperature (T) dependence of the molar magnetic susceptibilities (χ_M) were measured from 2 to 300 K and the data examined for the presence of magnetic interactions. For $[Cu(dien)Ag(CN)_2]_2[Ag_2(CN)_3][Ag(CN)_2]$ (**2.2**), $\chi_M T$ = 0.47 cm^3 K mol^{-1} at 300 K and is temperature independent until 25 K, at which point $\chi_M T$ drops to0.43 cm^3 K mol^{-1}at 2 K. The lower temperature range $\chi_M T$ values are depicted in Figure 2.10.

The data can be fit to the Curie-Weiss law with θ = –0.17 K, consistent with weak antiferromagnetic coupling between Cu(II) centres. This magnetic interaction is likely mediated by bridging $[Ag(CN)_2]^-$ units, which bridge Cu(II) centres in an apical/equatorial fashion to yield a 1-D coordinately-bonded chain; the distance between Cu(II) centres is 10.541 Å. Using the Bonner-Fisher model for a 1-D Heisenberg chain of S = 1/2 centres [135,136], an exchange coupling constant of J = –0.18 cm^{-1} with g = 2.25 is obtained. Although the diamagnetic Ag(I) ion is mediating magnetic exchange in this system, the long distance between magnetic centres mitigates against strong exchange in this system. Silver(I) ions have been reported to be mediators of magnetic exchange, particularly between organic radical ligands [187,188]. In addition, the observation of antiferromagnetic interactions in this system, as opposed to the ferromagnetic interactions usually observed in apical/equatorial Cu(II)-chain systems [189] can be attributed to the N(12)′–Cu(1)–N(11) bond angle of 101.95(18)° vs. the 90° angle

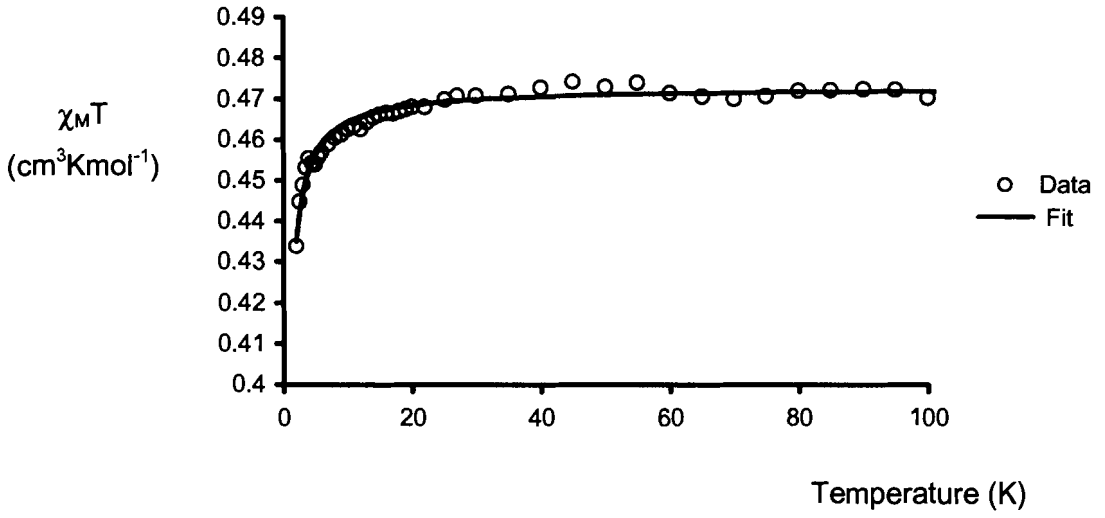

Figure 2.10 – Temperature dependence of the product $\chi_M T$ for **2.2**. The solid line is the fit using the S=1/2, 1-D Heisenberg chain model (see text).

required for the strict orthogonality that generates ferromagnetic coupling; in the related Cu(tmeda)[Au(CN)$_2$]$_2$, a N–Cu–N angle of 89.3(4)° in an axial/equatorial chain yielded a significant ferromagnetic interaction mediated by the Au(I) centres [55].

In [Cu(en)Cu(CN)$_2$Ag(CN)$_2$] (**2.6**), from a magnetic point of view, a similar 1-D coordinately bonded chain of Cu(II) centres is present and is bridged by non-linear [Cu(CN)$_2$]$^-$ units. It is assumed that the Cu(I)–Ag(I) interactions and the chain-crosslinking [Ag(CN)$_2$]$^-$ units do not significantly contribute to the magnetic behavior of **2.6**. In this case, $\chi_M T$ = 0.39 cm^3 K mol^{-1} at 300 K and, starting from 15 K, drops to 0.26 cm^3 K mol^{-1} at 2 K as depicted for the lower temperature values in Figure 2.11.

The data can be fit with the Curie-Weiss law with θ = –0.83 K and the same Bonner-Fisher 1-D chain model applied for **2.2** with J = –0.93 cm^{-1} and g = 2.06. The substantially larger exchange interaction for this Cu(I)-mediated system (vs. **2.2**) can be rationalized by the short Cu–N bond lengths (< 2 Å) that propagate the chain compared to a longer 2.166(5) Å Cu–N(12)′ apical bond length in **2.2**. In addition, the chain-structure of **2.6** has an equatorial/equatorial arrangement, which produces the observed antiferromagnetic exchange [190]. The previously reported magnetic studies involving diamagnetic copper(I) centres have all contained orthogonal magnetic orbitals, therefore the magnetic exchange interactions have been ferromagnetic [187,188,191].

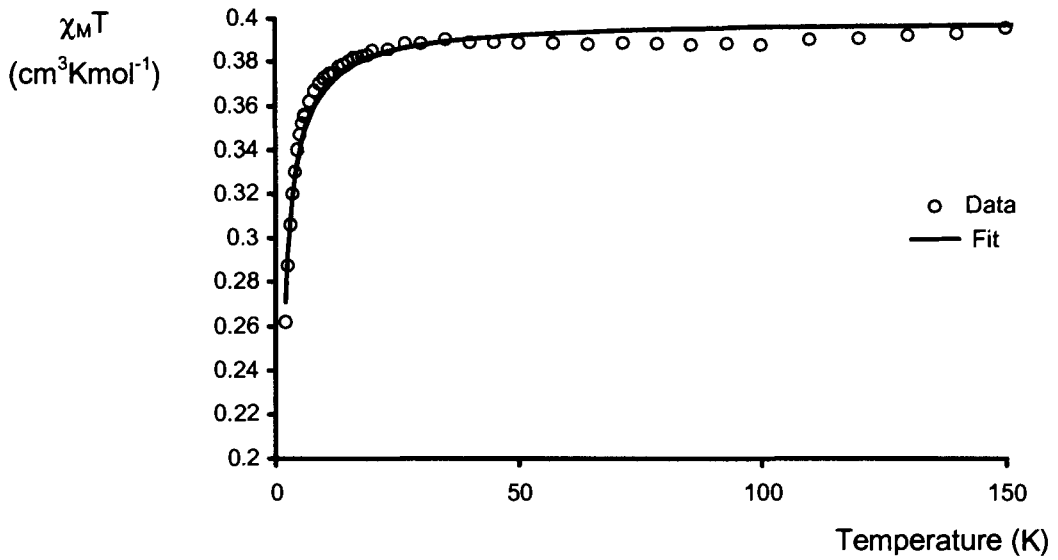

Figure 2.11 – Temperature Dependence of the Product $\chi_M T$ for **2.6**. The solid line is the fit using the S=1/2, 1-D Heisenberg chain model (see text).

The investigation of weak magnetic interactions in the Ni(II) complexes is complicated by the presence of the zero-field splitting (zfs) of octahedral Ni(II) ions. $[Ni(en)_2Ag_2(CN)_3][Ag(CN)_2]$ (**2.3**), which contains an eight-atom $[Ag_2(CN)_3]^-$ bridge between Ni(II) centres, is a good representation of isolated octahedral Ni(II) centres with which to compare to the other Ni(II) structures. For **2.3**, $\chi_M T$ = 1.15 cm^3 K mol^{-1} at 300 K and decreases to 1.00 cm^3 K mol^{-1} at 2 K. The data for **2.4** and **2.5** show the same general trends. The data for **2.3** can be fitted [131] using the zfs parameter as described in Chapter 1, resulting in D = 2.8 cm^{-1} with g = 2.23; these are reasonable values for magnetically dilute S = 1 Ni(II) centres [130].

The magnetic susceptibility data for $[Ni(en)][Ni(CN)_4]\bullet 2.5H_2O$ (**2.4**) can be fitted using the same isolated-Ni(II) model to yield D = 5.0 cm^{-1}. In this procedure, g was fixed at 2.23 to allow for a meaningful comparison of D-values between systems (by limiting the number of parameters); the coordination spheres of **2.3**, **2.4** and **2.5** are very similar, thus this is an acceptable approximation. The significantly larger value of D for **2.4** than that for **2.3** implies that Ni(II)-mediated magnetic interactions are operative in this system. The addition of a molecular-field parameter yields an improved fit for **2.4** but this over-parameterization is inappropriate [131].

Similarly, the variable temperature magnetic susceptibility data for $[Ni(tren)Ag(CN)_2][Ag(CN)_2]$ (**2.5**) can be fit using D = 4.6 cm^{-1} with g = 2.23. Weak antiferromagnetic interactions within the 1-D chain of Ni(II) centres, mediated by $[Ag(CN)_2]^-$ bridges, are indicated by the larger value of D compared to **2.3**; again, the quantification of this weak interaction would be ambiguous. However, in order to compare the relative abilities of Ag(I) and Au(I) to mediate magnetic exchange, the variable temperature magnetic susceptibility for the isostructural $[Ni(tren)Au(CN)_2][Au(CN)_2]$ complex was measured. In this case, using the same methodology, D = 3.1 cm^{-1} with g fixed at 2.23. Based on the reasonable assumption that the D-values for these isostructural compounds should be the same in the absense of any coupling interactions, this results suggests that Ag(I) is a better mediator of magnetic interactions as compared to Au(I).

2.3 DISCUSSION

2.3.1 Effect of Capping Ligand and Transition Metal

An examination of the structural trends displayed in the systems presented here yields an array of conclusions, some of which are consistent with previous $[Au(CN)_2]^-$ work, and some of which display trends specific to using $[Ag(CN)_2]^-$ as a design element for enhancing structural dimensionality in heterometallic systems. As expected, the structures are dependent on both the number of available coordination sites on the metal (increasing available sites by altering the choice of capping ligand increases structural dimensionality) and the metal identity. Thus, $[Ag(CN)_2]^-$ reactions involving M(tren) and M(dien) cations resulted in immediate precipitates of polymeric products, whereas the reaction involving $[Cu(en)_2]^{2+}$, with its Jahn-Teller lengthened axial binding sites, did not. However, the analogous reaction with $[Ni(en)_2]^{2+}$ yielded an immediate polymeric precipitate due to the lack of Jahn-Teller distortion in Ni(II) as compared with copper(II) centres.

2.3.2 Metallophilic Interactions

The influence of argentophilic interactions on the structures of **2.1** and **2.2** is apparent, with Ag–Ag bonds ranging from 3.102(1) to 3.2889(5) Å. An increase in dimensionality from zero to one in $[Cu(en)_2][Ag_2(CN)_3][Ag(CN)_2]$ (**2.1**) is assisted (in conjunction with Ag–N bonds) by Ag–Ag bonds. More significantly, dimensionality is increased from one to three in $[Cu(dien)Ag(CN)_2]_2[Ag_2(CN)_3][Ag(CN)_2]$ (**2.2**) as a sole result of argentophilic interactions. This demonstrates their use as a tool analogous to Au(I)–Au(I) interactions, whereby aurophilic interactions have been shown to increase dimensionality from 1-D to 2-D and from 2-D to 3-D [53]. Similarly, the weak heterometallic Cu(I)–Ag(I) interaction of 3.1000(4) Å in $[Cu(en)Cu(CN)_2Ag(CN)_2]$ (**2.6**) also increases the structural dimensionality from two to three.

2.3.3 Ag – N Interactions

The formation of Ag–N interactions is also an important factor that has an impact on the overall structure of the $[Ag(CN)_2]^-$-containing polymers. In the structures of both $[Cu(en)_2][Ag_2(CN)_3][Ag(CN)_2]$ (**2.1**) and $[Ni(en)_2Ag_2(CN)_3][Ag(CN)_2]$ (**2.3**), interactions between the cyano(N) of the $[Ag(CN)_2]^-$ unit and the Ag of the $[Ag_2(CN)_3]^-$ were found. This is the first instance where the cyano(N) of an $[Ag(CN)_2]^-$ unit associates with

another silver centre. Note that in every case, it is the Ag atoms in an $[Ag_2(CN)_3]^-$ unit that acts as an "acceptor". On this basis, the incorporation of the $[Ag_2(CN)_3]^-$ unit also serves to increase structural dimensionality through Ag–N interactions.

Similar Au–N bonds were not observed in $[Au(CN)_2]^-$ analogues [53-55]. The ability of Ag(I) to form interactions with nitrogen atoms is likely due to the increased propensity of Ag(I) to display coordination numbers greater than two (linear) as compared to Au(I) [113,114,120]. Ag(I) has also been shown to form many complexes with three and even four nitrogen donors [120].

2.3.4 Lability of $[Ag(CN)_2]^-$

Clearly, when compared to the high-yield, straightforward reactions of metal-ligand cations with $KAu(CN)_2$, in which products that reflected the initial stoichiometries and reagents were obtained [53-55], the analogous reactions with $KAg(CN)_2$ are substantially more complex. In most cases, the $[Ag(CN)_2]^-$ unit is not entirely preserved: new anionic units, including $[Ag_2(CN)_3]^-$, $[Ni(CN)_4]^{2-}$ and $[Cu(CN)_2]^-$, are formed and are incorporated into the supramolecular products. The key to explaining this difference in reactivity complexity lies in the lability of $KAg(CN)_2$ relative to $KAu(CN)_2$. The overall formation constant β_2 for $KAu(CN)_2$ is 10^{37}, but is much lower (10^{20}) for $KAg(CN)_2$ [67]. The lability of $KAg(CN)_2$ was first observed in a comparison of the IR absorption studies of aqueous Au(I) and Ag(I) cyanide complexes [152]; this lability was also noted in the reactions of $KAg(CN)_2$ with organometallic cations $[Cp(dppe)Fe]^+$ and $[Cp(PPh_3)_2Ru]^+$, in which Ag-isocyanide coordination was invariably observed [192]. Significantly, a study of $KAg(CN)_2$ solutions in liquid ammonia using Raman spectroscopy suggested the dissociation of $[Ag(CN)_2]^-$ into CN^- and AgCN (Equation 2.1) [153].

$$KAg(CN)_2 \rightleftharpoons KCN + AgCN \qquad \text{(Equation 2.1)}$$

In our systems, a variety of secondary reactions can then occur between these products and the original reactants, resulting in the range of structures observed.

One common secondary reaction pathway is shown in Equation 2.2 - the formation of $[Ag_2(CN)_3]^-$ from the aggregation of *in situ* generated AgCN (Eq. 2.1) with $[Ag(CN)_2]^-$ [153].

$$AgCN + KAg(CN)_2 \rightleftharpoons KAg_2(CN)_3 \qquad \text{(Equation 2.2)}$$

Though this $[Ag_2(CN)_3]^-$ unit has never been isolated for study, it has been identified in several crystal structures [84,159,162,193], and is present in **2.1**, **2.2** and **2.3**. The $[Ag_4(CN)_5]^-$ unit has also been reported (a further extension of the dissociation and aggregation process seen with $[Ag_2(CN)_3]^-$) [194]. It is important to note that coordination polymers containing $[Ag(CN)_2]^-$ that do not incorporate the $[Ag_2(CN)_3]^-$ unit have been isolated [104,106,108,109,150,155-158,160,161,175,195]. It is difficult to compare these diverse systems, as they involve different ligands, use of ammonia for crystal formation, different solvents and different metals. This might suggest that any of these factors may influence the incorporation of $[Ag(CN)_2]^-$ over $[Ag_2(CN)_3]^-$ into crystal structures. In previously reported $[Ag_2(CN)_3]^-$-containing complexes [84,159,193], no attempt has been made to explain the mechanism of formation of this anion. It appears that due to the lability of $[Ag(CN)_2]^-$ in solution, the incorporation of either $[Ag(CN)_2]^-$ or a mix of $[Ag(CN)_2]^-$ and $[Ag_2(CN)_3]^-$ into the final polymer is a result of competition between the two moieties and their associated equilibria. This competition is influenced by the solvent medium, reagent concentrations and the overall stability and solubility of the final product.

2.3.5 Other Reactions of Lability Products

In the presence of $Ni(II)_{aq}$, another secondary reaction from the lability of $KAg(CN)_2$ becomes accessible. The free CN^- liberated via Equation 2.1 can react with $Ni(II)_{aq}$ to yield the $[Ni(CN)_4]^{2-}$ unit. The large β_4 of 10^{30} drives the formation of this well-known cyanometallate building block [67]; its further reaction with available metal-cations accounts for secondary products such as $[Ni(en)][Ni(CN)_4]\bullet 2.5H_2O$ (**2.4**). There is no evidence of formation of $[Ni(CN)_4]^{2-}$ moieties accompanying the synthesis of $Ni(tren)[Ag(CN)_2]_2$ (**2.5**), suggesting that this reaction pathway is impeded by strongly complexing ligands. Many supramolecular assemblies are known that utilize the $[Ni(CN)_4]^{2-}$ unit in direct synthesis [80,105,179,196-198].

Finally, if unligated $Cu(II)_{aq}$ is available, a secondary reaction with CN^- can occur: the reduction of Cu(II) to Cu(I) with the concomitant formation of cyanogen [199]. Further reaction of the Cu(I) with CN^- yields $[Cu(CN)_2]^-$ moieties. This Cu(I) product is another anionic building block that can form supramolecular structures. In conjunction with the available $[Ag(CN)_2]^-$ and remaining $[Cu(en)]^{2+}$, the mixed-valent, heterometallic coordination polymer **2.6**, with linear Ag(I), trigonal Cu(I) and square pyramidal Cu(II) centres is formed. This reaction pathway is not observed when a higher denticity or

concentration of amine ligand is present; amine ligands are known to suppress the reduction of Cu(II) by the CN^- anion [199].

This third alternative pathway, along with the other two secondary reactions already described, illustrates the potential complexity of reactions involving the building block $[Ag(CN)_2]^-$. Other labile cyanometallate building blocks would likely present similar design challenges in supramolecular coordination polymer chemistry.

2.3.6 Infrared Analysis

Many of the IR νCN stretches have been assigned to the various bridging modes of their respective cyanometallate and are displayed in Table 2.3. The higher frequency bridging modes and the non-bridging modes have been previously observed and discussed in the introduction. The observed IR frequencies in **2.1** – **2.6** assist in the expansion of the database of known frequencies (together with the X-ray structures) such that it can be concluded that an IR band in the range between 2141 and 2174 cm^{-1} can be attributed to a transition-metal, N-bound, bridging $[Ag(CN)_2]^-$ unit and an IR band in the range between 2134 and 2141 cm^{-1} can be attributed to a non-bridging terminal cyanide.

The lowest of the observed νCN bands (ranging from 2118 to 2123 cm^{-1} in **2.1**, **2.2** and **2.3**) have not been observed in previous $[Ag(CN)_2]^-$ studies [104,106,108,109,155-158,160]. IR investigations of $[Ag_2(CN)_3]^-$ have not been conducted due to the inability to isolate this complex as a pure solid; the few reported $[Ag_2(CN)_3]^-$ containing coordination polymers did not present IR data [84,159,193]. It is thus suggested that these bands are attributable to the bridging central cyanide moiety in $[Ag_2(CN)_3]$; the shift to a lower frequency relative to $[Ag(CN)_2]^-$ may result from π-back-bonding from each silver atom into this CN bond. Although CN is generally a weak π acceptor, shifts to lower frequencies for bridging cyanides have been reported where the π-back-bonding influence dominates [56].

The terminal cyanides of $[Ag(CN)_2]^-$ and $[Ag_2(CN)_3]^-$ exhibit stretches in the same region and thus their differentiation on this basis is not necessarily possible. This is most noticeable in the IR spectrum of **2.2**, which shows 2 stretches at 2134 and 2137 cm^{-1}. These stretches can not be conclusively assigned to either building block due to their proximity and the lack of deconvolution of the spectrum.

In **2.3**, the only νCN stretching frequency that is unaccounted for is 2140 cm^{-1} - a value that suggests a terminal cyanide, though there is no unbound $[Ag(CN)_2]^-$ present in the

structure. This stretching frequency is thus attributed to the bridging cyanide units of the $[Ag_2(CN)_3]^-$ moieties, which do not bridge in any other observed structure. It is possible that this stretching frequency remains relatively unaltered as compared to the terminal stretching frequencies due to an interplay of shifts to both higher and lower frequencies [56].

2.4 CONCLUSIONS

It has been illustrated that argentophilic interactions, like the previously examined aurophilic interactions, are a valuable tool with which to increase structural dimensionality in supramolecular systems. Furthermore, $[Ag(CN)_2]^-$ can also increase dimensionality through Ag–N interactions, though with minimal control and predictability. As compared to $[Au(CN)_2]^-$, the increased lability of $[Ag(CN)_2]^-$ results in a variety of complex equilibria and the formation of $[Ag_2(CN)_3]^-$, $[Ni(CN)_4]^{2-}$ and $[Cu(CN)_2]^-$.

Many of the complexes exhibit weak antiferromagnetic interactions, indicating that the $[Ag(CN)_2]^-$ moiety is capable of mediating magnetic interactions. The J values suggest that these interactions are quite weak, but not negligible. Comparisons between isostructural Ag(I) and Au(I) complexes have shown that Ag(I) is a more efficient mediator as compared to Au(I).

2.5 EXPERIMENTAL

For these reactions, and all subsequent reactions in proceeding chapters, all manipulations were performed in air using purified solvents. The amine ligands ethylenediamine (en), diethylenetriamine (dien), tris(2-aminoethyl)amine (tren), and all other reagents were obtained from commercial sources and used as received. **CAUTION**: Although we have experienced no difficulties, perchlorate salts are potentially explosive and should only be used in small quantities and handled with care.

For all complexes within this thesis, IR spectra were obtained using a Thermo Nicolet Nexus 670 FT-IR spectrometer. Microanalyses (C, H, N) were performed at Simon Fraser University by Mr. Miki Yang. Variable temperature magnetic susceptibility data were collected using a Quantum Design SQUID MPMS-5S magnetometer working down

to 2 K at 1 T field strength. All data was corrected for TIP, the diamagnetism of the sample holder, and the constituent atoms (by use of Pascal constants) [131].

Unless otherwise indicated, data for all crystal structures described throughout this thesis were collected for each single crystal (mounted on a glass fiber) at room temperature, using the diffractometer control program DIFRAC [200] and an Enraf Nonius CAD4F diffractometer. The programs used for all absorption corrections, data reduction and all structure solutions contained within this thesis were from the *NRCVAX* Crystal Structure System [201]. The structures were refined using CRYSTALS [202]. Diagrams were made using Ortep-3 [203], with 50% ellipsoids. Complex scattering factors for neutral atoms [204] were used in the calculation of structure factors.

The data for the structure of **2.6** was collected at the University of British Columbia (U.B.C.) on a Rigaku/ADSC CCD diffractometer at 198 K. The data was also processed at U.B.C. and corrected for Lorentz and polarization effects, as well for absorption [205]. The structure was solved by heavy-atom methods (PATTY [206]) and expanded using Fourier techniques.

2.5.1 Preparation of $[Cu(en)_2][Ag_2(CN)_3][Ag(CN)_2]$ (2.1)

To a 5 mL aqueous solution of $Cu(ClO_4)_2 \bullet 6H_2O$ (74 mg, 0.2 mmol), a 2 mL aqueous solution of en (stock solution, 0.4 mmol) was added and the resulting solution stirred for 5 minutes. While stirring, a 5 mL aqueous solution of $KAg(CN)_2$ (80 mg, 0.4 mmol) was added drop-wise to this dark purple solution. The purple solution was then evaporated to half volume and then covered and cooled in a refrigerator overnight to yield a purple crystalline solid that was filtered, washed with 2 mL of water and air-dried overnight to give $[Cu(en)_2][Ag_2(CN)_3][Ag(CN)_2]$ (**2.1**). Yield: 45 mg (53%). Anal. Calcd. for $C_9H_{16}N_9Ag_3Cu$: C, 16.96; H, 2.53; N, 19.78. Found: C, 16.78; H, 2.46; N, 19.98. IR (KBr): 2156 (w νCN), 2140 (νCN) and 2118 (s νCN), 1581, 1455, 1317, 1268, 1084, 1026, 975, 696, 520 cm^{-1}. In order to obtain X-ray quality crystals, an H-shaped tube containing an 2 mL aqueous solution of $Cu(ClO_4)_2 \bullet 6H_2O$ (74 g, 0.2 mmol) and en (stock solution, 0.4 mmol) on one side and a 2 mL aqueous solution of $KAg(CN)_2$ (80 mg, 0.4 mmol) on the other side was prepared (as desribed in Chapter 1). Slow diffusion of the two reagents yielded dark purple single crystals of $[Cu(en)_2][Ag_2(CN)_3][Ag(CN)_2]$ (**2.1**) after 2 weeks. Several crystals were extracted with a pipette from the H-tube. The X-ray quality crystals had a comparable IR spectrum to the crystalline powder.

2.5.2 Preparation of $[Cu(dien)]_2[Ag_2(CN)_3][Ag(CN)_2]$ (2.2)

To a 3 mL aqueous solution of $Cu(ClO_4)_2 \bullet 6H_2O$ (140 mg, 0.377 mmol), a 1 mL aqueous solution of dien (stock solution, 0.377 mmol) was added and the resulting solution stirred for 5 minutes. While stirring, a 3 mL aqueous solution of $KAg(CN)_2$ (150 mg, 0.753 mmol) was added drop-wise to this dark blue solution, resulting in an immediate blue precipitate, which was filtered, washed with 2 mL of water and air-dried overnight to give $[Cu(dien)Ag(CN)_2]_2[Ag_2(CN)_3][Ag(CN)_2]$ (**2.2**). Yield: 108 mg. Anal. Calcd. for $C_{17}H_{26}N_{15}Ag_5Cu_2$: C, 18.45; H, 2.37; N, 18.98. Found: C, 18.14; H, 2.31; N, 18.77. IR (KBr): 3309, 3269, 3239, 3157, 2166 (νCN), 2156 (s νCN), 2141 (νCN), 2134 (νCN), 2119 (νCN), 1604, 1464, 1430, 1141, 1086, 1056, 1022, 996, 947, 709, 648, 534, 451, 436 cm^{-1}. The blue filtrate was covered and cooled in a refrigerator to yield X-ray quality crystals of **2.2** after 3 days which were extracted from the solution with a pipette, washed with 1 mL of water and air dried overnight. Yield of crystals: 53 mg (96% total yield). The crystals and powder had comparable IR spectra and elemental analysis.

2.5.3 Preparation of $[Ni(en)_2Ag_2(CN)_3][Ag(CN)_2]$ (2.3)

The powder product of $[Ni(en)_2Ag_2(CN)_3][Ag(CN)_2]$ (**2.3**) was prepared in a similar fashion to that which was recently reported [162]. An improved synthesis and characterization is given here, along with the identified by-product. To a 3 mL aqueous solution of $Ni(NO_3)_2 \bullet 6H_2O$ (110 mg, 0.377 mmol), a 1 mL aqueous solution of en (stock solution, 0.753 mmol) was added and the resulting solution stirred for 5 minutes. While stirring, a 3 mL aqueous solution of $KAg(CN)_2$ (150 mg, 0.753 mmol) was added drop-wise to this purple solution, resulting in an immediate pink/purple precipitate, which was filtered, washed with 2 mL of water and air-dried overnight to give $[Ni(en)_2Ag_2(CN)_3][Ag(CN)_2]$ (**2.3**). Yield: 122 mg (65%). Anal. Calcd. for $C_9H_{16}N_9Ag_3Ni$: C, 17.09; H, 2.55; N, 19.93. Found: C, 17.42; H, 2.56; N, 19.54. IR for **2.3** (KBr): 2159 (w νCN), 2140 (s νCN), 2123 (νCN), 1582, 1462, 1384, 1329, 1276, 1132, 1023, 979, 661, 504 cm^{-1}. To acquire crystals, H-shaped tubes were prepared (as described in Chapter 1) with 1 mL reagent solutions containing half the quantities of each reagent listed above. After several weeks, along with a white precipitate impurity (AgCN, identified via IR analysis), dark pink $[Ni(en)_2Ag_2(CN)_3][Ag(CN)_2]$ (**2.3**) and pale pink $[Ni(en)][Ni(CN)_4] \bullet 2.5H_2O$ (**2.4**) crystals were identified and separated via individual crystal extraction from the H-tube using a pipette. The IR spectrum and elemental analysis for crystals of **2.3** were comparable to the powder data. Anal. Calcd. for **2.4**:

$C_6H_8N_6Ni_2 \bullet 2.5\ H_2O$: C, 22.07; H, 4.00; N, 25.73. Found: C, 21.97; H, 3.48; N, 24.93. IR for **2.4** (KBr): 2164 (s νCN), 1602, 1384, 1097, 1035, 963, 672, 440 cm^{-1}.

2.5.4 Preparation of $[Ni(en)][Ni(CN)_4] \bullet xH_2O$ (2.4)

Although crystals of $[Ni(en)][Ni(CN)_4] \bullet 2.5H_2O$ (**2.4**) were isolated as a side product in the above preparation of **2.3**, rational preparation of **2.4** was also attempted as follows: To a 3 mL aqueous solution of $Ni(NO_3)_2 \bullet 6H_2O$ (29 mg, 0.1 mmol), an aqueous solution of en (stock solution, 0.1 mmol) was added and the resulting solution stirred for 5 minutes. While stirring, a 5 mL aqueous solution of $K_2Ni(CN)_4$ (24 mg, 0.1 mmol) was added drop-wise, resulting in an immediate pale purple precipitate. This solid was filtered, washed with 2 mL of water and air-dried overnight to give $[Ni(en)][Ni(CN)_4] \bullet 1.5H_2O$. Yield: 27 mg (96%). The solid prepared in this fashion had a comparable IR spectrum to the crystals (**2.4**) prepared above, despite having a slightly different amount of co-crystallized water. Anal. Calcd. for $C_6H_8N_6Ni_2 \bullet 1.5\ H_2O$: C, 23.35; H, 3.59; N, 27.24. Found: C, 23.28; H, 4.14: N, 27.25.

2.5.5 Preparation of $[Ni(tren)Ag(CN)_2][Ag(CN)_2]$ (2.5)

To a 3 mL aqueous solution of $Ni(NO_3)_2 \bullet 6H_2O$ (29 mg, 0.1 mmol), a 1 mL solution of tren (stock solution, 0.1 mmol) was added and the resulting solution stirred for 5 minutes. While stirring, a 5 mL aqueous solution of $KAg(CN)_2$ (40 mg, 0.2 mmol) was added drop-wise to this pale purple solution, resulting in an immediate purple precipitate. This solid was filtered, washed with 2 mL of water and air-dried overnight to give $[Ni(tren)Ag(CN)_2][Ag(CN)_2]$ (**2.5**). Yield: 51 mg (98 %). Anal. Calcd. for $C_{10}H_{18}N_8Ag_2Ni$: C, 22.89; H, 3.46; N, 21.35. Found: C, 22.80; H, 3.50; N, 21.17. IR (KBr): 2174 (s νCN), 2139 (s νCN), 1599, 1468, 1348, 1322, 1067, 1023, 993, 977, 882, 532, 468 cm^{-1}. Single crystals of **2.5** were prepared by slow diffusion of 1 mL aqueous solutions of Ni/tren and $KAg(CN)_2$ (both using half the reagent quantities listed above) in an H-shaped tube. The crystals and powder had comparable IR spectra.

2.5.6 Preparation of $[Cu(en)Cu(CN)_2Ag(CN)_2]$ (2.6)

An H-shaped tube containing a 1 mL concentrated aqueous solution of $Cu(ClO_4)_2 \bullet 6H_2O$ (70 mg, 0.188 mmol) and a 1 mL solution of en (concentrated stock solution, 0.188 mmol) on one side and a 1 mL aqueous solution of $KAg(CN)_2$ (75 mg,

0.376 mmol) on the other side was prepared. Slow diffusion of the two reagents into the other yielded X-ray quality, dark purple, single crystals of $[Cu(en)Cu(CN)_2Ag(CN)_2]$ (**2.6**) after 3 weeks. The crystals were extracted from the H-tube by removing the solvent (with a pipette), breaking the glass of the H-tube and scraping the crystals off the glass of the tubes. Crystals were washed with 1 mL of water and air dried overnight. Yield: 19 mg (69%). Anal. Calcd. for $C_6H_8N_6AgCu_2$: C, 18.06; H, 2.02; N, 21.06. Found: C, 18.20; H, 1.98; N, 20.80. IR (KBr): 2151 (νCN), 2141 (νCN), 2127 (νCN), 1578, 1458, 1311, 1275, 1088, 1041, 1009, 970, 873, 658, 515 cm^{-1}.

CHAPTER 3

TETRACYANOAURATE AS A SUPRAMOLECULAR BUILDING BLOCK

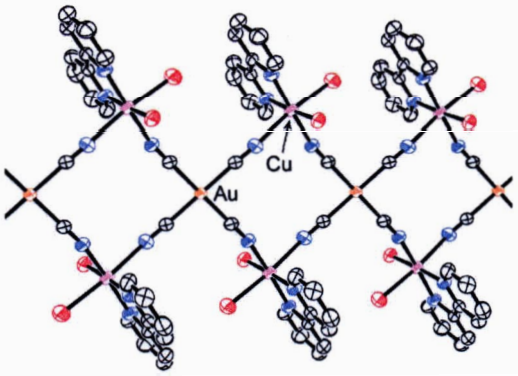

3.1 INTRODUCTION

3.1.1 Square Planar Cyanometallates

Square planar complexes are commonly formed by transition metal ions having a d^8 electron configuration, such as Pt(II), Pd(II) and Ni(II) [56]. Many studies have been done, particularly with $[Pt(CN)_4]^{2-}$ and $[Ni(CN)_4]^{2-}$, indicating their usefulness in building coordination polymers and multidimensional systems [56,80,85,105,124,179,196-198,207-210]. This usefulness stems from the multiple potential bridging modes of a tetracyanometallate with a secondary metal centre, the most common of which are depicted in Figure 3.1. In all reported cases (as shown from crystal structure data), the $[M(CN)_4]^{n+}$ moiety retains its structural integrity with little distortion from the D_{4h} symmetry [80]. In Figure 3.1, the 2-D structure (g) is one sheet of the well-known group of structures known as the Hofmann and Hofmann-type clathrates, the first of which was discovered in 1897 with the crystal structure being solved in 1949 [211-213]. These systems arrange such that the 2-D sheets are parallel, creating cavities that are

occupied by guest molecules and many different classes of these compounds have been defined [56,80].

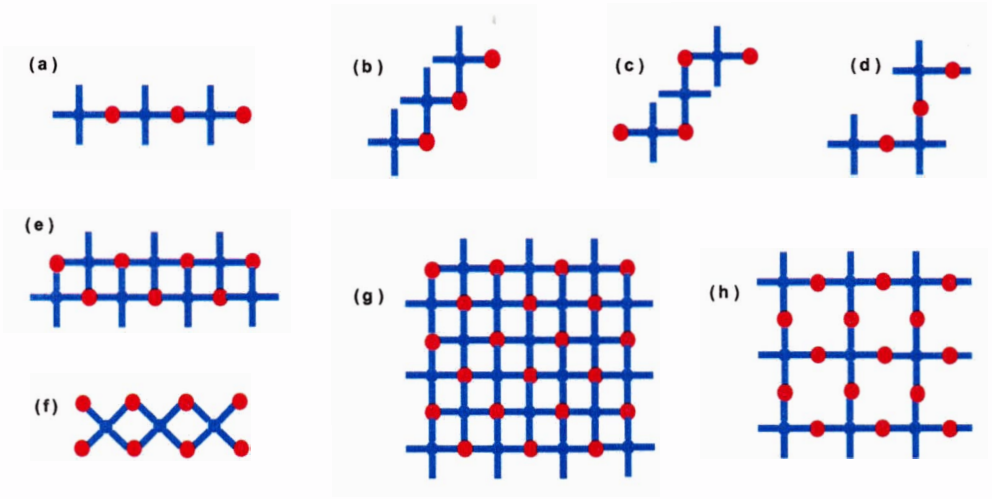

Figure 3.1 - Possible bridging arrangements with $[M(CN)_4]^{n-}$ (blue) and M^{m+} (red): (a) straight 1-D chain; (b) zig-zag 1-D chain; (c) extended zig-zag 1-D chain (cis on M^{m+}); (d) extended zig-zag 1-D chain (trans on M^{m+}); (e) double 1-D chain; (f) criss-cross 1-D chain; (g) 2-D sheet; (h) extended 2-D sheet. [80]*

3.1.2 Au(III) Complexes and Tetracyanoaurate

Au(III) is a soft metal ion and is known to form stable complexes with soft ligands such as thiolates and phosphines [114]. However, compared to Au(I), Au(III) shows a greater propensity to form complexes with harder ligands, such as nitrogen and oxygen donor ligands [114]. Being isoelectronic with Pt(II) (d^8 electronic configuration), Au(III) is always diamagnetic and the vast majority of known complexes are of square planar geometry [214,215]. Five and six coordinate complexes are much less common, adopting square pyramidal and tetragonally distorted octahedral geometries respectively [113].

Tetracyanoaurate, $[Au(CN)_4]^-$, adopts the expected square planar geometry, as determined for both the acid $H[Au(CN)_4]\bullet 2H_2O$ [216] and various salts [74,217]. The potassium salt, as used in this study, can be obtained from Chempur in Germany. It can

---

Reprinted from T. Iwamoto, In *Comprehensive Supramolecular Chemistry*, Vol. 7, J. M. Lehn, J. L. Atwood, J. E. D. Davies, D. D. MacNicol, F. Vogtle, G. T. B. Alberti, Eds.; 643-690, Copyright 1996; with permission from Elsevier.

also be prepared from the Au(I) salt $KAu(CN)_2$, through oxidation by Br_2 and subsequent replacement of bromine with cyanide [218].

3.1.3 Stacking Interactions in Square Planar d^8 Metals

Many square planar complexes with a d^8 electron configuration, particularly those of platinum(II), have been shown to form metal-metal stacking interactions with metal-metal distances as low as 3.1 Å [73,219-222]. Although many different explanations have been explored, the molecular orbital (MO) treatment as first suggested by *Rundle* [223] and later revised by *Miller* [224] has become the most widely accepted [219]. If two d^8 nuclei are considered, the two $5d_{z^2}$ atomic orbitals (AO) of a_{1g} symmetry split to give an antibonding MO of a_{2u} symmetry and a bonding MO of a_{1g} symmetry, as depicted in Figure 3.2(a). A similar situation occurs with the $6p_z$ orbitals, resulting in MOs that also possess a_{2u} and a_{1g} symmetry. Since there are four electrons to be accommodated, the

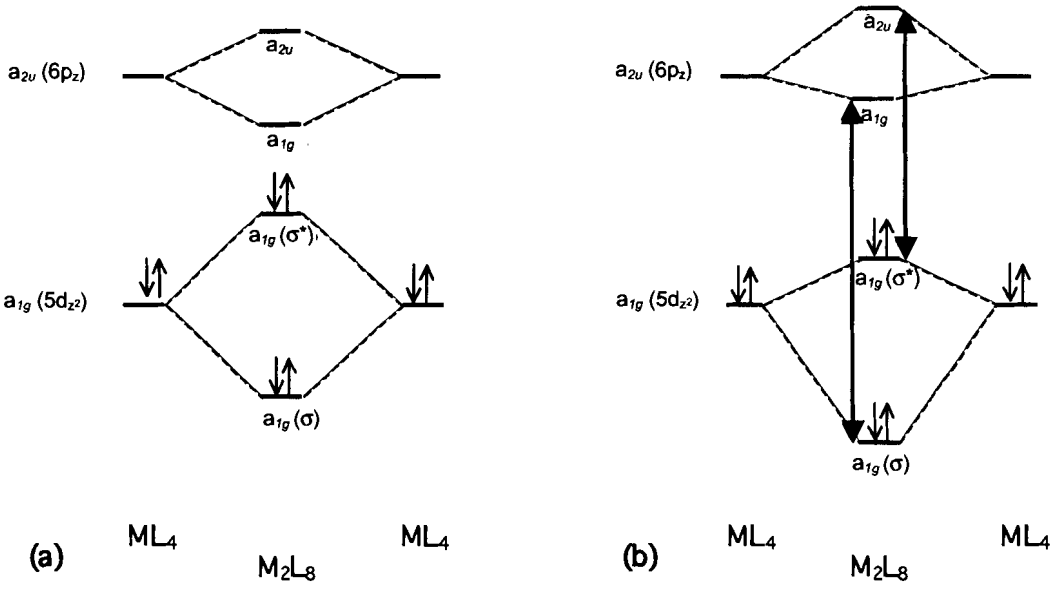

Figure 3.2 – Molecular orbital scheme for a dimer of Pt(II) d^8 square planar molecules (a) without and (b) with interaction between $5d_{z^2}$ and $6p_z$ orbitals. Coloured arrows depict configuration interaction [219]*.

* K. Krogmann, *Angew. Chem. Int. Ed.* **1969**, *8*, 35. Used by permission of Wiley-VCH.

lowest energy bonding and lowest energy anti-bonding MOs are filled, resulting in zero bond order. However, because non-degenerate MOs of the same symmetry are known to energetically "repel" each other as a result of configuration interaction (the extension of simple MO theory to include the effects of excited states) [219,225], the resulting MO diagram (Figure 3.2(b)) shows a decrease in total energy, and thus bonding is favorable.

These d^8-d^8 interactions could also be thought of in a similar fashion to the d^{10}-d^{10} interactions; the d^8-d^8 interactions could be attributed to the energetic proximity of the $5d_{z^2}$ and the $6p_z$ orbitals, which could mix and thus produce the metal-metal interactions. This mixing would occur most prominently in the case of Pt(II) due to relativistic effects. As this reasoning is extended to a chain of nuclei, band theory can be applied, and the result is depicted in Figure 3.3.

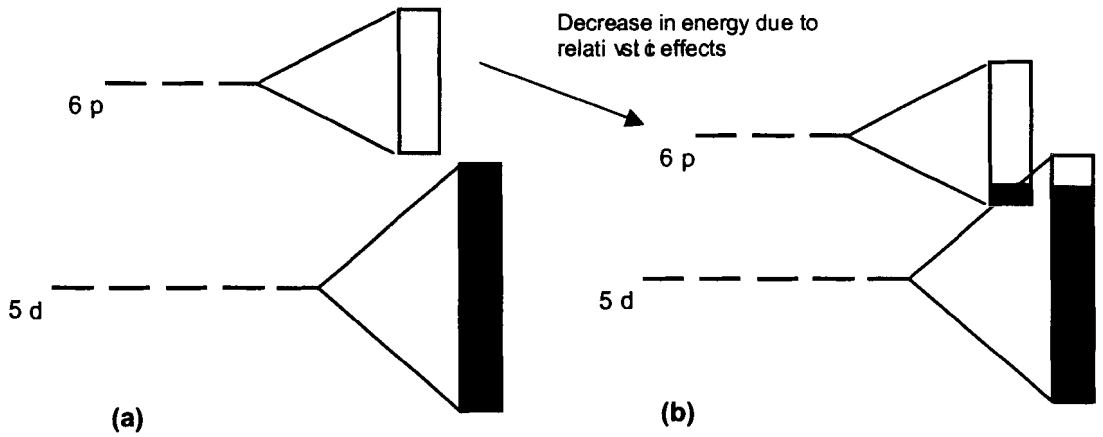

Figure 3.3 - Band structure depiction of (a) no 5d and 6p interaction and (b) 5d and 6p interaction in a chain of Pt(II) stacked square planar complexes.

3.1.4 Research Objectives

Despite the interest in dianionic square planar cyanometallates, the related $[Au(CN)_4]^-$ anion has received no attention in the field of supramolecular coordination chemistry. Both the potential for multiple cyanide coordination and the potential of displaying the aforementioned metal-metal stacking interactions make the $[Au(CN)_4]^-$ moiety an excellent candidate for a building block to form heterobimetallic coordination polymers. The focus of this chapter is thus to examine the ability of tetracyanoaurate to

form coordination polymers and increase dimensionality in systems containing transition metal cations in a similar fashion to the previously examined Au(I) and Ag(I) cyanides.

3.2 RESULTS AND ANALYSES*

3.2.1 Synthesis and Structure

A summary of crystallographic data and refinement details for all structures in this chapter are collected in Appendix 2. The coordinates are listed in Appendix 3.

3.2.1.1 $Ni(en)_2[Au(CN)_4]_2 \bullet H_2O$ (3.1)

The reaction of an aqueous solution of 1 equivalent of $Ni(NO_3)_2 \bullet 6H_2O$ and 2 equivalents of en with an aqueous solution of 2 equivalents of $KAu(CN)_4$ produced no immediate precipitate. If the resulting solution is covered and left undisturbed for 2 months, purple crystals of $Ni(en)_2[Au(CN)_4]_2 \bullet H_2O$ (**3.1**) are deposited from the solution. The X-ray crystal structure of **3.1** is depicted in Figure 3.4, with the corresponding bond lengths and angles collected in Table 3.1. The two $[Au(CN)_4]^-$ anions are bound in a trans-fashion to the octahedral Ni(II) centre (Ni(1)–N(11) = 2.129(5) Å). The slightly distorted octahedral geometry is completed by two mutually trans en ligands. Although the asymmetric unit contains two half-molecules of $Ni(en)_2[Au(CN)_4]_2$ (each sitting on a centre of inversion), the structural parameters are essentially identical for both.

One equivalent of water is also found in the unit cell of the crystal structure. This water serves to weakly connect the $Ni(en)_2[Au(CN)_4]_2$ units into a three dimensional system through hydrogen bonding (O–N distances: 3.206(8) Å, 2.925(8) Å). There are additional hydrogen bonds between many of the amino hydrogen atoms and cyano-nitrogen atoms (N(H)–NC distances: 3.169 Å – 3.323 Å). Due to the length of the hydrogen bonding distances (suggesting weak interactions), the hydrogen bonding is not shown.

---

* Reproduced in part with permission from C. J. Shorrock, H. Jong, R. J. Batchelor and D. B. Leznoff, *Inorganic Chemistry*, **2003**, *42*, 3917-3924. Copyright 2003, American Chemical Society.

Table 3.1 – Selected Bond Lengths (Å) and Angles (deg) for $Ni(en)_2[Au(CN)_4]_2 \bullet H_2O$ (**3.1**)

Selected Atoms	Bond Length	Selected Atoms	Bond Length
Au(1) – C(11)	1.977(6)	Au(1) – C(12)	1.997(6)
Au(1) – C(13)	1.985(6)	Au(1) – C(14)	1.993(6)
Ni(1) – N(11)	2.129(5)	Ni(1) – N(6)	2.099(5)
Ni(1) – N(5)	2.086(5)		
Selected Atoms	**Angle**	**Selected Atoms**	**Angle**
C(11) – Au(1) – C(13)	179.5(2)	N(5) – Ni(1) – N(6)	82.7(2)
N(5) – Ni(1) – N(11)	88.95(19)	N(6) – Ni(1) – N(11)	89.8(2)

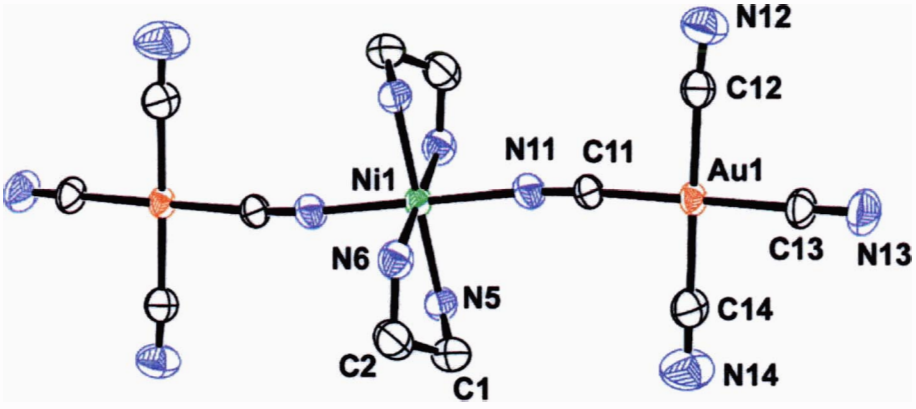

Figure 3.4 – Molecular structure of $Ni(en)_2[Au(CN)_4]_2 \bullet H_2O$ (**3.1**). Water and hydrogen atoms have been omitted for clarity.

The IR spectrum of **3.1** shows νCN stretches at 2214, 2202, 2190 and 2180 cm^{-1}, suggesting a variety of bridging modes as compared to the 2189 cm^{-1} νCN stretch of $KAu(CN)_4$ [67]. The presence of both bridging and non-bridging cyanide moieties in the structure of **3.1** suggests that the earlier description of bridging cyanide νCN bands shifting to higher frequency in the IR holds true for $[Au(CN)_4]^-$ as well (for which no previous IR studies of coordination complexes have been conducted).

3.2.1.2 Cu(dien)$[Au(CN)_4]_2$ (3.2)

Using a similar reaction procedure as used for **3.1**, the reaction of 1 equivalent of $Cu(ClO_4)_2 \bullet H_2O$, 1 equivalent of dien and 2 equivalents of $KAg(CN)_2$ produced crystals of $Cu(dien)[Au(CN)_4]_2$ (**3.2**) after several weeks. The X-ray crystal structure of **3.2** is

depicted in Figures 3.5 and 3.6, with the corresponding bond lengths and angles collected in Table 3.2. The crystal structure indicates that both $[Au(CN)_4]^-$ ions are bound to a Cu(II) centre through cyano-nitrogen atoms. The Cu(II) centre adopts a distorted square pyramidal geometry (Figure 3.5), where one $[Au(CN)_4]^-$ unit is bound to the basal site (Cu(1)–N(11) = 1.977(12) Å) and the other is bound to the elongated apical site (Cu(1)–N(21) = 2.225(13) Å). The remaining three basal sites are occupied by the dien ligand.

Each $Cu(dien)[Au(CN)_4]_2$ complex is connected by weak intermolecular Au(III)–N(cyano) interactions (Au(1)–N(22)′ = 3.002(14) Å), resulting in a 1-D chain (Figure 3.6). This is the first reported Au(III)-N interaction where a nitrogen atom interacts in an apical, intermolecular fashion with a square planar Au(III), making it weakly 5-coordinate. There are also weak hydrogen bonds (not shown) between amino hydrogen atoms and cyano-nitrogen atoms (N(H)-NC distances = 3.106 Å – 3.379 Å).

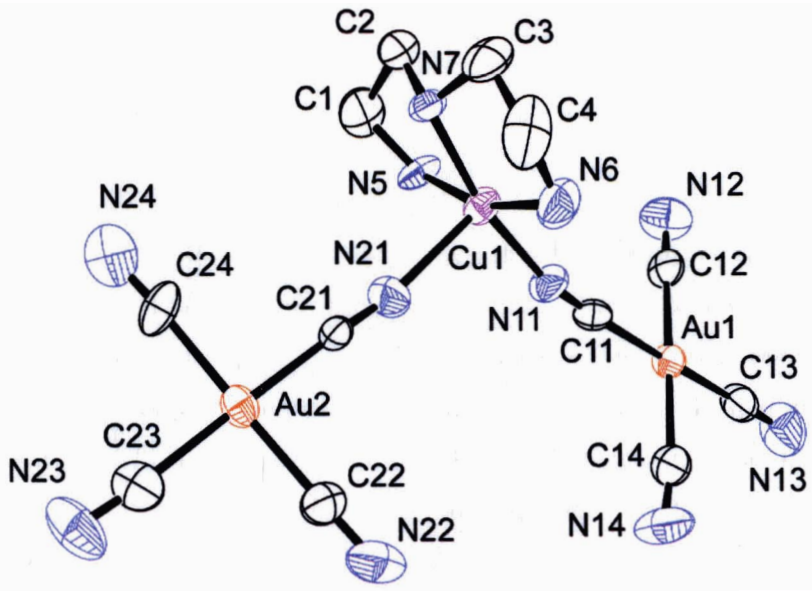

Figure 3.5 – Molecular structure of $Cu(dien)[Au(CN)_4]_2$ (**3.2**). Hydrogen atoms have been omitted for clarity.

The IR of **3.2** shows νCN stretches at 2241 and 2219 cm^{-1}, which can be attributed to the bridging cyano groups, and a stretch at 2189 cm^{-1} which remains unchanged from the νCN of the starting material, suggesting that it originates from non-bridging cyano groups.

Table 3.2 – Selected Bond Lengths (Å) and Angles (deg) for $Cu(dien)[Au(CN)_4]_2$ (**3.2**)

Selected Atoms	Bond Length	Selected Atoms	Bond Length
Au(1) – C(13)	1.973(16)	Au(1) – C(14)	2.011(19)
Au(2) – C(23)	2.025(17)	Au(2) – C(24)	1.953(17)
Cu(1) – N(11)	1.977(12)	Cu(1) – N(21)	2.225(13)
Cu(1) – N(5)	1.994(11)	Cu(1) – N(6)	1.983(14)
Cu(1) – N(7)	1.984(11)	Au(1) – N(22)′[a]	3.002(14)
Selected Atoms	**Angle**	**Selected Atoms**	**Angle**
C(11) – Au(1) – C(13)	179.0(6)	C(21) – Au(2) – C(23)	178.7(6)
N(11) – Cu(1) – N(21)	99.1(5)	N(11) – Cu(1) – N(5)	93.9(5)
N(11) – Cu(1) – N(6)	94.6(6)	N(21) – Cu(1) – N(5)	97.7(5)
N(21) – Cu(1) – N(6)	96.1(5)	N(5) – Cu(1) – N(6)	162.4(6)
N(7) – Cu(1) – N(11)	167.7(5)	N(7) – Cu(1) – N(21)	93.3(5)
N(5) – Cu(1) – N(7)	84.0(5)	N(6) – Cu(1) – N(7)	84.3(5)
Cu(1) – N(11) – C(11)	168.2(12)	Cu(1) – N(21) – C(21)	166.6(13)
Au(1) – N(22)′ – C(22)′	117.65(5)		

[a] Symmetry transformation: ′ x – 1/2, –y + 1/2, z – 1/2.

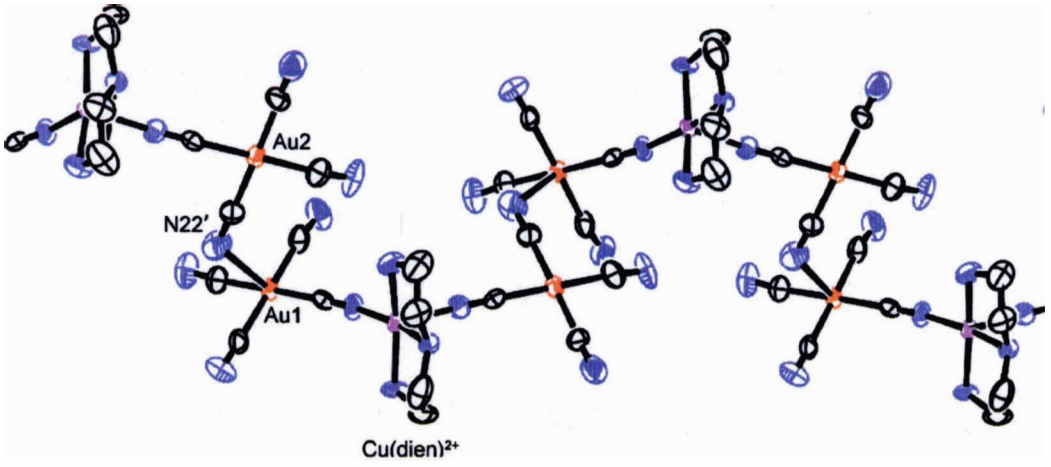

Figure 3.6 – Extended structure of $Cu(dien)[Au(CN)_4]_2$ (**3.2**) showing the 1-D network propagated through Au(III)–N interactions. Hydrogen atoms have been omitted for clarity.

3.2.1.3 $Cu(en)_2[Au(CN)_4]_2$ (3.3)

Using a similar reaction procedure as used for **3.1**, the reaction of 1 equivalent of $[Cu(en)_2]^{2+}$ with 2 equivalents of $[Ag(CN)_2]^-$ produced crystals of $Cu(en)_2[Au(CN)_4]_2$ (**3.3**) after several weeks. The X-ray crystal structure of **3.3** is depicted in Figure 3.7, with the corresponding bond lengths and angles collected in Table 3.3. The crystal structure indicates that the $[Au(CN)_4]^-$ ions are coordinated to the Jahn-Teller distorted axial sites of an octahedral Cu(II) centre (Cu(1)–N(11)′ = 2.548(9) Å). This axial bond length is significantly longer than that seen in the Ni analogue, **3.1**. The axial bond in **3.3** is also further elongated compared to the reported distorted Cu(II) octahedral complexes in the literature (ranging from 2.2 – 2.7 Å) [106,108,109,177-179]. The equatorial sites of the Cu(II) are occupied by the two en ligands.

The crystal structure of **3.3** also displays weak intermolecular Au(III)–N interactions of 3.035(8) Å. These interactions are similar to, but slightly weaker than those observed in **3.2**. A key difference between **3.2** and **3.3** is that in **3.3**, every $[Au(CN)_4]^-$ unit forms two Au–N interactions by acting as a donor via N(12) for one interaction and an acceptor via Au(1) for another, resulting in a 2-D sheet (Figure 3.7). This contrasts with the 1-D chain found in **3.2** (Figure 3.6) that does not propagate in two dimensions because $[Au(CN)_4]^-$ units only participate in one such interaction, *either* through the Au(1) *or* N(22) atoms.

The structure of **3.3** also differs from the analogous Ni(II) compound **3.1**. The Ni analogue does not display Au(III)–N interactions, possibly due to steric hindrances, as the M–N(cyano) bond lengths are significantly shorter in **3.1**. Hydrogen-bonding interactions with the water molecule in **3.1** may also compete with the weak intermolecular Au–N interactions. Weak hydrogen bonding between amino hydrogen atoms and N(cyano) atoms is also present in **3.3** (N(H)-NC distances: 3.121(11) Å – 3.395(12) Å).

The IR spectrum of **3.3** shows two νCN stretches at 2187 cm^{-1} and 2180 cm^{-1}, neither of which would have resulted in the prediction of the observed X-ray structure, which shows cyanide bridging that has been observed (**3.1** and **3.2**) to produce shifts to higher frequencies.

Table 3.3 – Selected Bond Lengths (Å) and Angles (deg) for $Cu(en)_2[Au(CN)_4]_2$ (**3.3**)

Selected Atoms	Bond Length	Selected Atoms	Bond Length
Au(1) – C(11)	1.995(9)	Au(1) – C(12)	1.975(9)
Au(1) – C(13)	1.986(9)	Au(1) – C(14)	1.990(9)
Cu(1) – N(11)′[a]	2.548(9)	Cu(1) – N(3)	2.010(7)
Cu(1) – N(4)	2.015(7)	Au(1) – N(12)″	3.035(8)
Selected Atoms	**Angle**	**Selected Atoms**	**Angle**
C(11) – Au(1) – C(13)	178.6(3)	N(11)′ – Cu(1) – N(3)	93.5(3)
N(11)′ – Cu(1) – N(4)	88.5(3)	N(3) – Cu(1) – N(4)	84.3(3)

[a] Symmetry transformations: ′ ≡ x, y – 1, z; ″ ≡ –x + 1, y – 1/2, –z + 5/2.

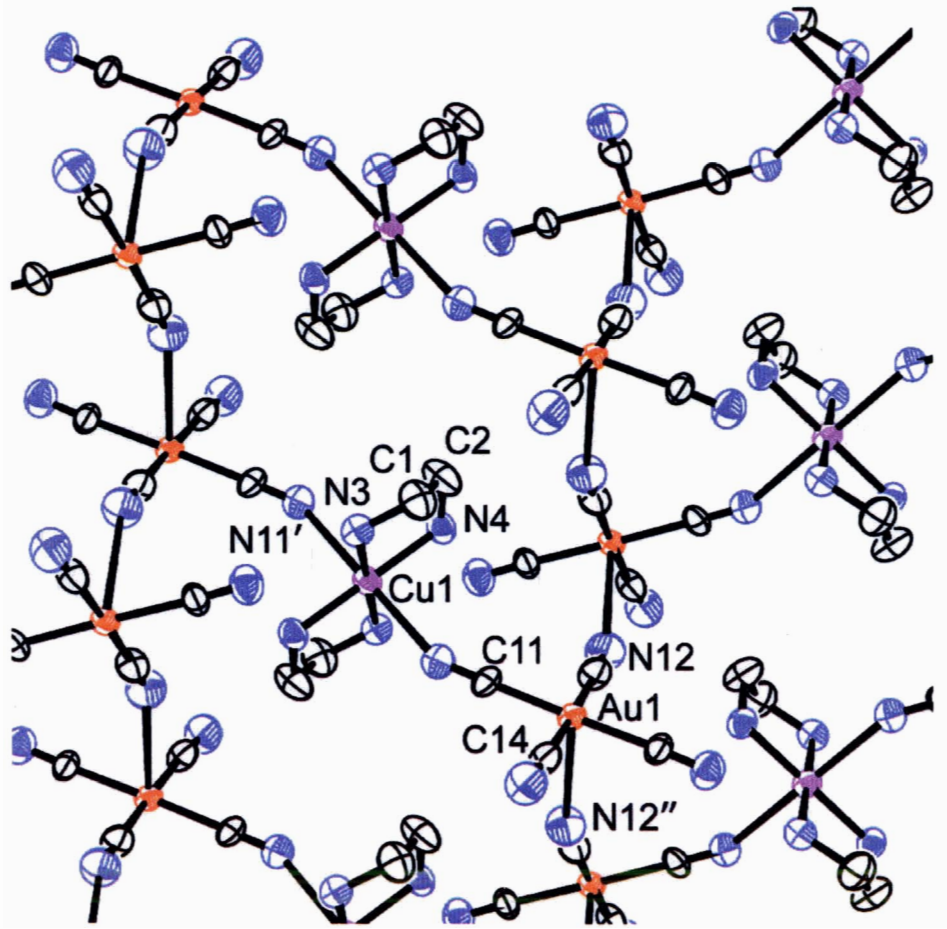

Figure 3.7 – Extended structure of $Cu(en)_2[Au(CN)_4]_2$ (**3.3**). Hydrogen atoms have been omitted for clarity.

3.2.1.4 $[Cu(dmeda)_2Au(CN)_4][Au(CN)_4]$ (3.4)

Using a similar reaction procedure as used for **3.1**, the reaction of 1 equivalent of $Cu(ClO_4)_2 \bullet H_2O$, 2 equivalents of dmeda and 2 equivalents of $KAg(CN)_2$ produced an immediate precipitate of $[Cu(dmeda)_2Au(CN)_4][Au(CN)_4]$ (**3.4**). This is the first instance where the general reaction scheme using 2 equivalents of $[Au(CN)_4]^-$ produces an immediate precipitate. Crystals were obtained from the resulting filtrate solution, left undisturbed for several days. Excellent X-ray quality crystals could also be obtained by performing the reaction with only one equivalent of $[Au(CN)_4]^-$, thus delaying the formation of precipitate. The X-ray crystal structure of **3.4** is depicted in Figures 3.8 and 3.9, with the corresponding bond lengths and angles collected in Table 3.4. The crystal structure reveals a distorted octahedral Cu(II) centre with two equatorially-bound dmeda ligands and elongated N(cyano) axial coordination of $[Au(CN)_4]^-$ (Figure 3.8). This weak coordination (Cu(1)–N(21)′ = 2.724(10) Å) serves to build a 1-D cationic zig-zag chain of alternating $[Cu(dmeda)]^{2+}$ and $[Au(CN)_4]^-$ ions where two cyanides of $[Au(CN)_4]^-$ are coordinated to separate $[Cu(dmeda)]^{2+}$ units in a cis fashion. Despite the weak cyanide ligation, it is chemically significant: an immediate precipitation of the insoluble polymer **3.4** occurs, whereas the previous reactions (not producing cyanometallate-bridged polymeric products) do not immediately precipitate.

The remaining equivalent of $[Au(CN)_4]^-$ is unbound to any Cu centre, but does form Au(III)-N interactions with adjacent free $[Au(CN)_4]^-$ units, generating an anionic 1-D zig-zag chain that runs perpendicular to the $[Cu(dmeda)_2Au(CN)_4]^+$ chain (Figure 3.9). The Au(1)–N(12)″ distance of 2.963(13) is significantly shorter than the Au(III)–N interactions in **3.2** and **3.3**.

The IR of **3.4** shows only one νCN at 2190 cm^{-1}, essentially unshifted from $KAu(CN)_4$.

3.2.1.5 $Ni(dien)[Au(CN)_4]_2$ (3.5)

Using a similar reaction procedure as used for **3.1**, the reaction of 1 equivalent of $[Ni(dien)]^{2+}$ with 2 equivalents of $KAg(CN)_2$ produced crystals of $Ni(dien)[Au(CN)_4]_2$ (**3.5**) after one day. The X-ray crystal structure of **3.5** is depicted in Figures 3.10 and 3.11, with the corresponding bond lengths and angles collected in Table 3.5. Both $[Au(CN)_4]^-$ moieties are coordinated to the Ni centre (N(11)–Ni(1) = 2.127(16) Å and N(21)–Ni(1) = 2.110(15) Å). While one $[Au(CN)_4]^-$ unit is pendant, the other bridges to another Ni

Table 3.4 – Selected Bond Lengths (Å) and Angles (deg) for $[Cu(dmeda)_2Au(CN)_4][Au(CN)_4]$ (**3.4**)

Selected Atoms	Bond Length	Selected Atoms	Bond Length
Au(2) – C(21)	2.007(11)	Au(2) – C(22)	1.958(12)
Cu(1) – N(1)	2.100(8)	Cu(1) – N(2)	1.985(8)
Cu(1) – N(21)′[a]	2.724(10)	Au(1) – C(11)	1.999(10)
Au(1) – C(12)	2.001(15)	Au(1) – C(13)	2.002(13)
Au(1) – N(12)″	2.963(13)		
Selected Atoms	**Angle**	**Selected Atoms**	**Angle**
C(12) – Au(1) – C(13)	175.9(5)	C(21) – Au(2) – C(22)	89.8(5)
Au(1) – C(12) – N(12)	175.1(14)	N(1) – Cu(1) – N(2)	84.6(3)
N(1) – Cu(1) – N(21)′	85.8(3)	N(2) – Cu(1) – N(21)′	86.5(3)

[a] Symmetry transformations: ′ ≡ x – 1/2, -y + 3/2, z; ″ ≡ –x + 1/2, -y + 1/2, z.

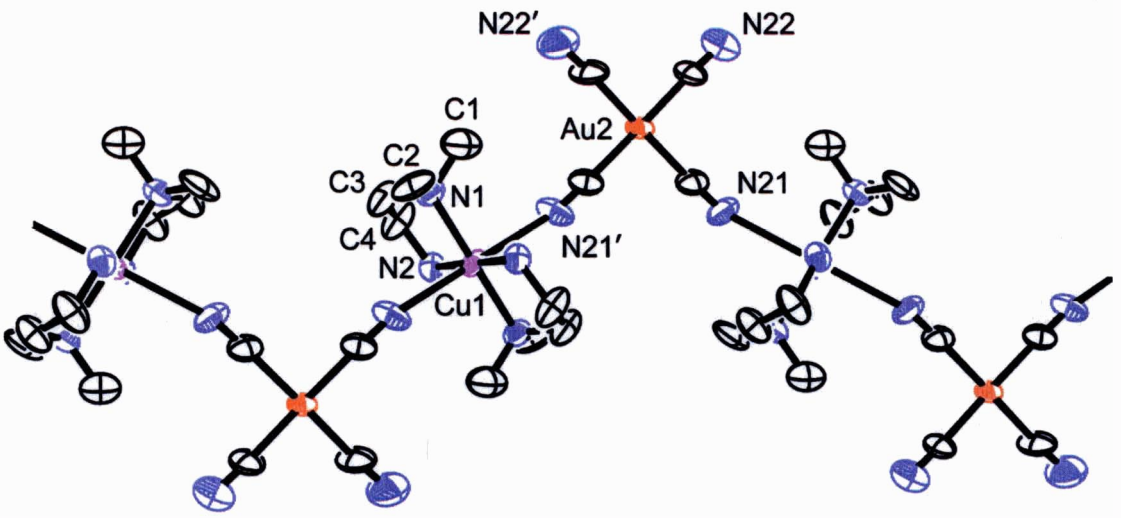

Figure 3.8 – Extended structure of the cation $[Cu(dmeda)_2Au(CN)_4]^+$ in $[Cu(dmeda)_2Au(CN)_4][Au(CN)_4]$ (**3.4**). Hydrogen atoms have been omitted for clarity.

centre (N(14)′–Ni(1) = 2.094(15) Å). The three coordinated cyano(N) atoms adopt a facial (fac) arrangement on the Ni centre. The dien ligand occupies the remaining three sites in a fac arrangement (Ni–N distance range: 2.066 – 2.076 Å), thus the geometry about the Ni centre is slightly distorted octahedral. This produces a bimetallic square

composed of 2 Ni centres and 2 Au centres, as depicted in Figure 3.10. Similar bimetallic squares to that of **3.5**, whereby 2 metals make up the 4 corners of the square and are bridged by cyanide moieties have been reported, though Fe(II) cyanide moieties have been used as the building block [226,227].

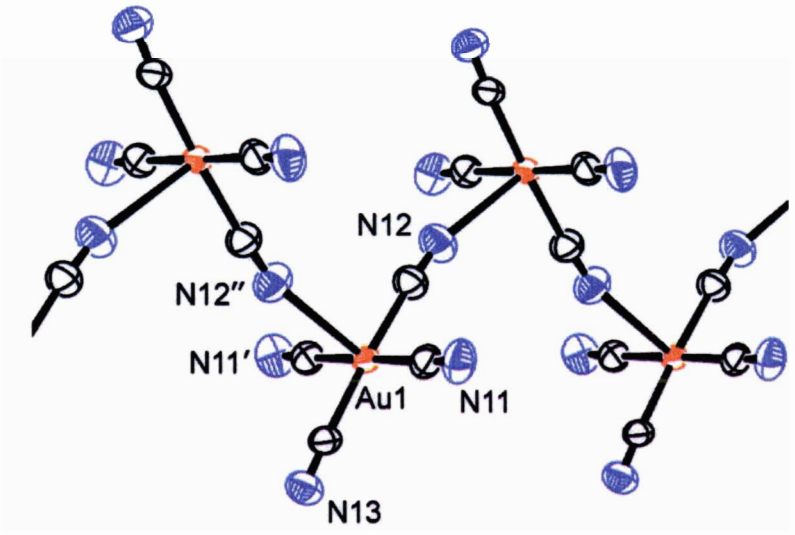

Figure 3.9 – Extended structure of the $[Au(CN)_4]^-$ chain in $[Cu(dmeda)_2Au(CN)_4][Au(CN)_4]$ (**3.4**).

These bimetallic squares in **3.5** are connected to each other through Au–N interactions of 2.961(15) Å between Au(2) (pendant $[Au(CN)_4]^-$ unit) and N(13). A 1-D chain results (Figure 3.11). As compared to complexes **3.2, 3.3** and **3.4**, this Au(III)–N interaction is significantly shorter and thus represents a stronger interaction.

Both diagonal distances (Ni to Ni and Au to Au) within the square of **3.5** are approximately 7.3 Å, suggesting that the structure may be porous, however no N_2 uptake was detected during porosity studies.

The IR spectrum of **3.5** shows several shifted νCN bands at 2236, 2231 and 2199 cm^{-1}, suggesting the variety of bridging modes observed in the crystal structure. An unshifted band at 2187 cm^{-1} is also observed, accounting for the observed non-bridging cyanides of the crystal structure.

Table 3.5 – Selected Bond Lengths (Å) and Angles (deg) for Ni(dien)$[Au(CN)_4]_2$ (**3.5**)

Selected Atoms	Bond Length	Selected Atoms	Bond Length
Au(1) – C(11)	1.981(18)	Au(1) – C(12)	2.013(18)
Au(2) – C(23)	1.97(2)	Au(2) – C(21)	2.03(2)
Ni(1) – N(11)	2.127(16)	Ni(1) – N(21)	2.110(15)
Ni(1) – N(1)	2.068(15)	Ni(1) – N(4)	2.066(13)
Ni(1) – N(7)	2.076(15)	Ni(1) – N(14)′[a]	2.094(15)
Au(2) – N(13)″	2.961(15)		
Selected Atoms	**Angle**	**Selected Atoms**	**Angle**
C(11) – Au(1) – C(14)	90.2(6)	C(21) – Au(2) – C(23)	179.5(6)
N(11) – Ni(1) – N(21)	85.1(6)	N(11) – Ni(1) – N(14)′	91.6(6)
N(11) – Ni(1) – N(1)	88.9(6)	N(1) – Ni(1) – N(4)	82.7(6)
N(1) – Ni(1) – N(7)	97.6(6)	N(4) – Ni(1) – N(7)	81.9(6)
N(4) – Ni(1) – N(21)	95.7(6)	Ni(1)′ – N(14) – C(14)	162.9(14)
Ni(1) – N(11) – C(11)	169.6(15)	Ni(1) – N(21) – C(21)	163.9(15)

[a] Symmetry transformations: ′ ≡ 3 – x, –y, 2 – z; ″ ≡ x, y, z + 1.

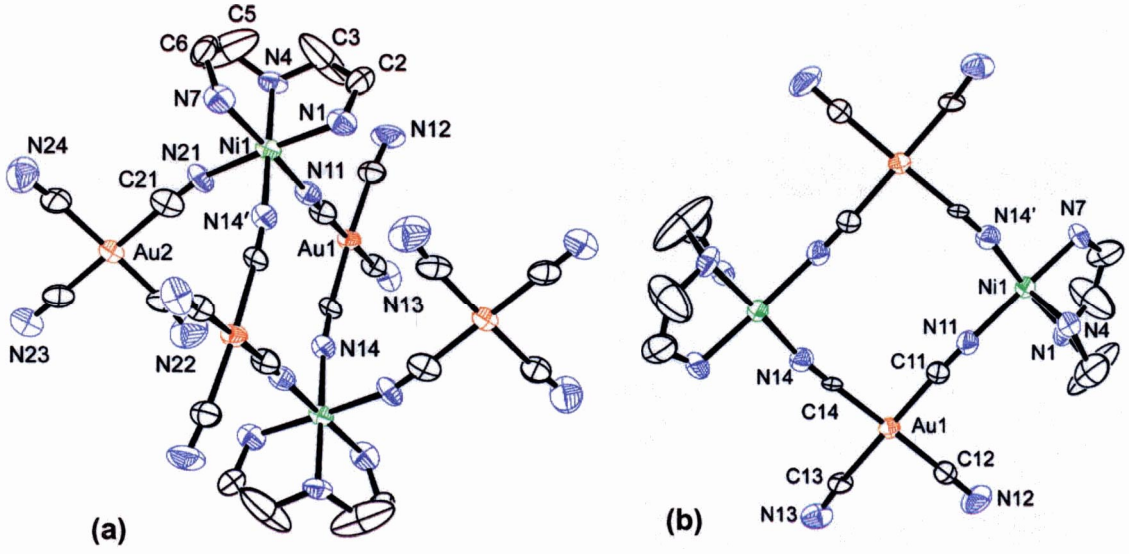

Figure 3.10 – (a) Molecular square structure of Ni(dien)$[Au(CN)_4]_2$ (**3.5**). Hydrogen atoms have been omitted for clarity. (b) Simplification with the pendant $[Au(CN)_4]^-$ omitted.

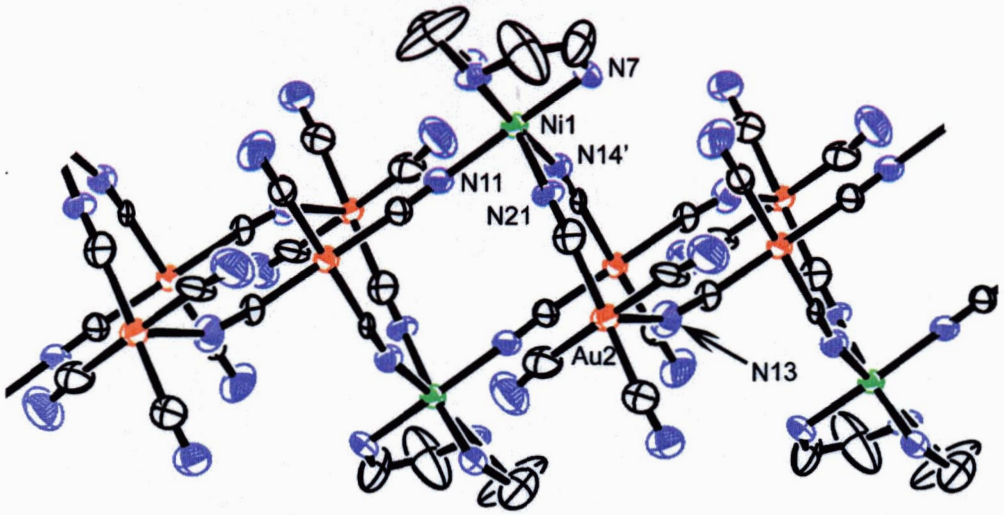

Figure 3.11 – Extended structure of Ni(dien)$[Au(CN)_4]_2$ (**3.5**) showing the 1-D network propagated through Au(III)–N interactions. Hydrogen atoms have been omitted for clarity.

3.2.1.6 $[Cu(bipy)(H_2O)_2(Au(CN)_4)_{0.5}][Au(CN)_4]_{1.5}$ (3.6)

The synthesis of $[Cu(bipy)(H_2O)_2(Au(CN)_4)_{0.5}][Au(CN)_4]_{1.5}$ (**3.6**) requires an excess of copper and the use of small amounts of methanol to fully dissolve the bipy ligand (which is the first ligand used thus far that is a solid). The excess of copper serves to ensure the coordination of only one equivalent of ligand and also to delay the formation of product such that crystals could be formed.

The X-ray crystal structure of **3.6** is depicted in Figure 3.12, with the corresponding bond lengths and angles collected in Table 3.6. The crystal structure shows a 1-D "criss-crossed" chain where one $[Au(CN)_4]^-$ unit is bound to four Cu(II) centres (Figure 3.12). Each Cu(II) centre has two such $[Au(CN)_4]^-$ units bound in a *cis* fashion, resulting in a connectivity to 5 other Cu(II) centres and thus 1-D propagation. The $[Au(CN)_4]^-$ units occupy both an equatorial (Cu(1)–N(12)′ = 1.973(6) Å) and an axial site (Cu(1)–N(11) = 2.359(6) Å) of the distorted octahedral Cu(II) centre. The remaining three equatorial sites on the Cu(II) centre are occupied by the bipy ligand (Cu(1)–N(1) = 1.981(6) Å and Cu(1)–N(2) = 2.001(5) Å) and a bound water molecule (Cu(1)–O(1) = 2.026(5) Å), with the final elongated axial site occupied by the other equivalent of water (Cu(1)–O(2) = 2.475(6) Å).

Table 3.6 – Selected Bond Lengths (Å) and Angles (deg) for $[Cu(bipy)(H_2O)_2(Au(CN)_4)_{0.5}][Au(CN)_4]_{1.5}$ (**3.6**)

Selected Atoms	Bond Length	Selected Atoms	Bond Length
Au(1) – C(11)	1.997(7)	Au(1) – C(12)	1.988(7)
Cu(1) – N(1)	1.981(6)	Cu(1) – N(2)	2.001(5)
Cu(1) – N(11)	2.359(6)	Cu(1) – N(12)′[a]	1.973(6)
Cu(1) – O(1)	2.026(5)	Cu(1) – O(2)	2.475(6)
Selected Atoms	**Angle**	**Selected Atoms**	**Angle**
C(11) – Au(1) – C(12)	91.8(3)	O(1) – Cu(1) – O(2)	91.53(19)
O(1) – Cu(1) – N(1)	95.8(2)	O(2) – Cu(1) – N(1)	91.5(2)
O(1) – Cu(1) – N(2)	176.6(2)	O(2) – Cu(1) – N(2)	86.5(2)
N(1) – Cu(1) – N(2)	81.6(2)	O(1) – Cu(1) – N(11)	84.7(2)
O(2) – Cu(1) – N(11)	174.7(2)	N(1) – Cu(1) – N(11)	92.6(2)
N(2) – Cu(1) – N(11)	97.4(2)	O(1) – Cu(1) – N(12)′	87.8(2)
O(2) – Cu(1) – N(12)′	84.3(2)	N(1) – Cu(1) – N(12)′	174.6(2)
N(2) – Cu(1) – N(12)′	94.7(2)	N(11) – Cu(1) – N(12)′	91.7(2)

[a] Symmetry transformation: ′ ≡ x – 1, y, z.

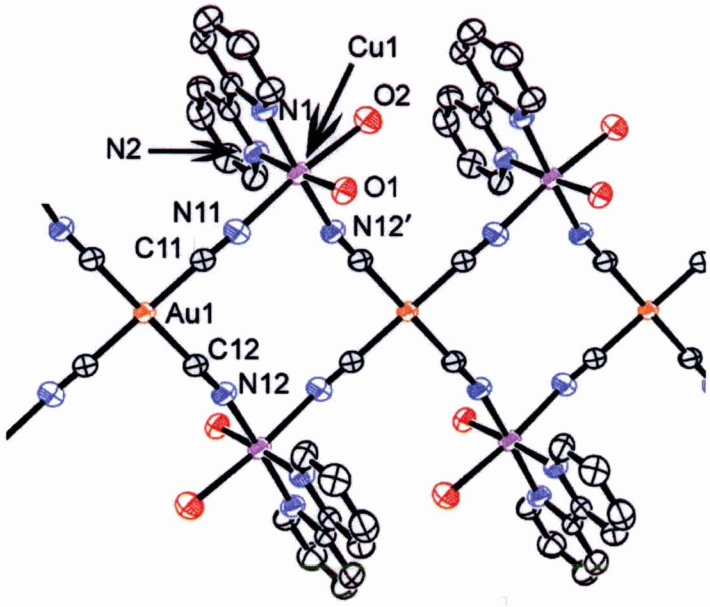

Figure 3.12 – Extended structure of $[Cu(bipy)(H_2O)_2(Au(CN)_4)_{0.5}][Au(CN)_4]_{1.5}$ (**3.6**) showing only the 1-D chain of $[Cu(bipy)(H_2O)_2(Au(CN)_4)_{0.5}]^{1.5+}$. Hydrogen atoms have been omitted for clarity.

The remaining equivalents of $[Au(CN)_4]^-$ form a linear trimeric anionic cluster via a Au(III)–N interaction of 3.052(9) Å, similar to that seen in **3.4** and comparable in length to that seen in **3.2** and **3.3**. However, unlike in **3.4**, the interaction does not propagate.

Both the coordinated water molecules and the bipy ligands serve to increase dimensionality through weak hydrogen bonds and π-interactions respectively. The structure is thus loosely held in a complex three-dimensional array (not shown).

Similar 1-D chains have been observed in a related $[Ni(CN)_4]^{2-}$ complex, $[(Cu_2(medpt)_2Ni(CN)_4)(ClO_4)_2 \bullet 2.5H_2O]$ (medpt = bis(3-aminopropyl)methylamine), whereby $[Ni(CN)_4]^{2-}$ anions coordinate through all 4 cyanides to form a "criss-crossed" 1-D chain of connected square pyramidal Cu(II) cations [198]. The analogous $[Pt(CN)_4]^{2-}$ complex with $[Cu(bipy)]^{2+}$ does not form such "criss-crossed" chains, but instead forms either a discrete supramolecular square via *cis* coordination of two cyanometallates in the case of $[(Cu(bipy)(H_2O)Pt(CN)_4)_2] \bullet 2H_2O$ [228], or an infinite 1-D chain with *trans* cyanide coordination in the case of $Cu(bipy)Pt(CN)_4$ [209]. In both cases, $[Pt(CN)_4]^{2-}$ bridging occurs through only two cyanides, rather than four as seen in **3.6**.

The IR spectrum of **3.6** shows νCN bands of 2203, 2198 and 2187 cm^{-1}, suggesting the observed combination of both bridging and non-bridging cyanide moieties.

3.2.2 Magnetic Properties

For complexes **3.3** – **3.6** the temperature (T) dependence of the molar magnetic susceptibilities (χ_M) was measured from 2 to 300 K, and the data were examined for the presence of magnetic interactions.

The product of the magnetic susceptibility with temperature, $\chi_M T$, for **3.3** at 300 K was determined to be 0.48 cm^3 K mol^{-1}, consistent with the presence of an S = 1/2 Cu(II) centre. According to the X-ray structure, the $Cu(dien)^{2+}$ units in **3.3** are essentially isolated from each other, except for the presence of intermolecular Au(III)–N interactions. This pathway is too long for significant magnetic interactions to occur (and the Cu–N bond is quite long at 2.548(9) Å) thus, as expected, $\chi_M T$ is observed to be virtually temperature independent, exhibiting only a very slight decrease (to 0.46 cm^3 K mol^{-1}) below 25 K.

In both **3.4** and **3.6**, shorter Cu–Cu interaction pathways are present. In $[Cu(dmeda)_2Au(CN)_4][Au(CN)_4]$ (**3.4**), the Cu(II) centres are connected through very elongated (Cu–N = 2.724(10) Å) axial sites in an orthogonal fashion. Poor overlap associated with this long bond effectively severs the pathway for magnetic exchange, as

previously observed [53,54], yielding an essentially temperature independent $\chi_M T$ vs. T graph until 5 K, at which point $\chi_M T$ drops from 0.47 to 0.35 cm^3 K mol^{-1} at 2 K.

For **3.6**, $\chi_M T$ = 0.40 cm^3 K mol^{-1} at 300 K and decreases slightly until 25 K, at which point $\chi_M T$ drops from 0.38 cm^3 K mol^{-1} to 0.29 cm^3 K mol^{-1} at 2 K (Figure 3.13). The data can be fit to the Curie-Weiss law with θ = –0.40 K, consistent with weak antiferromagnetic coupling between the Cu(II) centres. The X-ray structure of $[Cu(bipy)(H_2O)_2(Au(CN)_4)_{0.5}][Au(CN)_4]_{1.5}$ (**3.6**), shows several magnetic exchange pathways between Cu(II) centres that must be considered: each has a through-bond distance of approximately 10 Å. Each Cu(II) centre has 2 linear pathways, one through

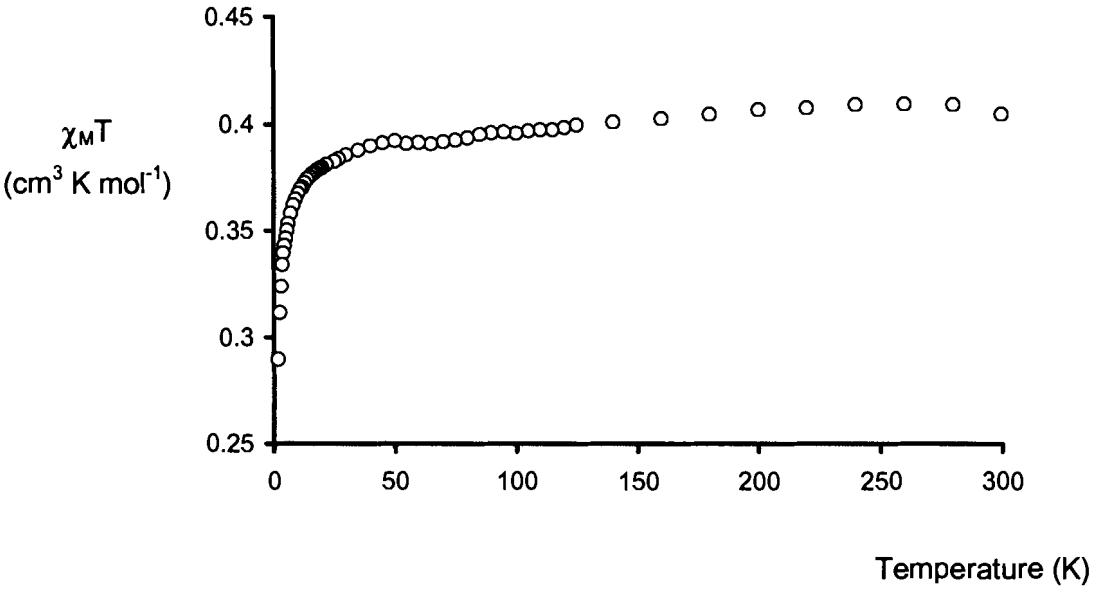

Figure 3.13 – Temperature dependence of the product $\chi_M T$ for **3.6**.

elongated axial/axial bonding (Cu–N(11) = 2.359(6) Å) and one through equatorial/equatorial bonding (Cu–N(12) = 1.973(6) Å). Each Cu(II) centre also has 4 axial/equatorial pathways to another Cu(II) (through a combination of Cu–N(11) and Cu–N(12) bonds). The orthogonal axial/equatorial pathways are known to generate ferromagnetic coupling [189], whereas the equatorial/equatorial and axial/axial pathways generate antiferromagnetic coupling [190]. The observed weak coupling is likely a combination of the antiferromagnetic and ferromagnetic coupling pathways. Of these, the equatorial/equatorial pathway yields the strongest orbital overlap, as all other pathways utilize the elongated Cu–N(11) axial bond of 2.359(6) Å. Due to the

complexity of possible magnetic pathways and the generated weak magnetic interaction, this data was not further analyzed. The result, however, shows that the $[Au(CN)_4]^-$ unit is capable of mediating magnetic interactions between paramagnetic centres, as has been observed with other d^8 cyanometallates [197], as well as previous Au(I) cyanometallate systems [53-55]. Because no isostructural complexes exist, however, comparisons between the ability of Au(III) and each metal (Au(I), Ni(II), Pt(II) or Pd(II)) to mediate these interactions can not be explored at this time.

For **3.5**, $\chi_M T$ = 2.43 cm^3 K mol^{-1} at 300 K per Ni(II) dimer, which is slightly above the expected value of 2.00 cm^3 K mol^{-1} for two independent Ni(II) atoms. The $\chi_M T$ product remains essentially constant (± 0.015 cm^3 K mol^{-1}) until approximately 25 K, at which point it increases from 2.43 cm^3 K mol^{-1} to a maximum of 2.66 cm^3 K mol^{-1} at 4 K (Figure 3.14). The increase is suggestive of weak ferromagnetic interactions between the Ni(II) centres, though the maximum does not correspond to the expected value of 3.0 cm^3 K mol^{-1} for fully ferromagnetically coupled S = 1 centres. This saturation value is not reached because below the 4 K maximum, the $\chi_M T$ value decreases sharply to 2.54 cm^3 K mol^{-1} at 2 K, likely due to zero-field splitting, although possibly due to interdimer antiferromagnetic coupling through the 1-D chain of Au–N interactions.

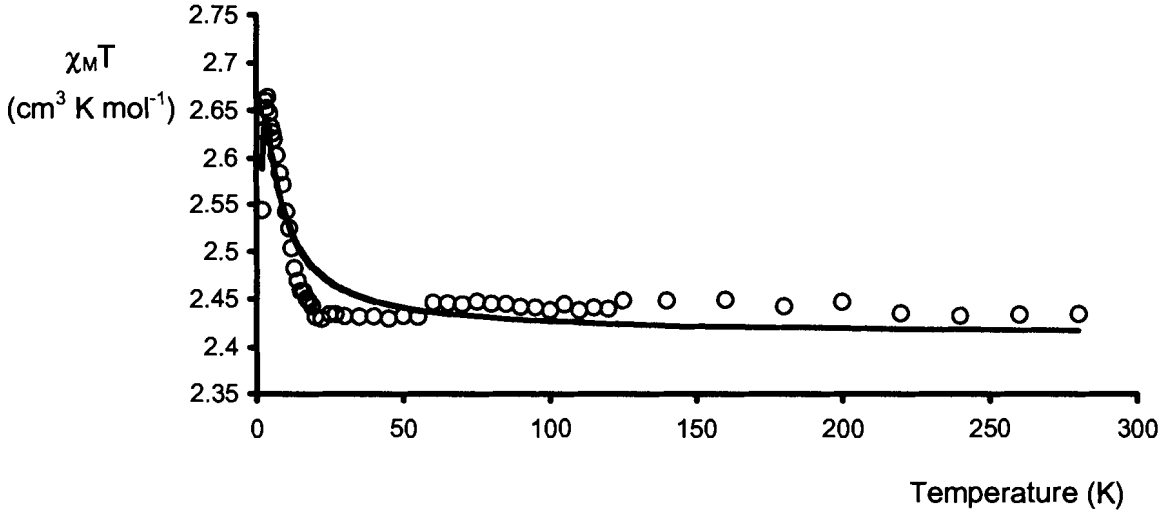

Figure 3.14 – Temperature dependence of the product $\chi_M T$ for **3.5**. The solid line is the fit using the Ginsberg model (see text).

It is expected that, due to the weak nature of the magnetic interaction in **3.5** as compared to the zero-field splitting (as can be deduced from Fig. 3.14), accurate

modeling will require simultaneous consideration of zero-field splitting and antiferromagnetic interactions. The model of Ginsberg, *et al.* incorporates parameters for J, zJ′ (a molecular field approximation to account for weak intermolecular magnetic exchange) and D with the following Hamiltonian [229]:

$$\mathbf{H} = -2JS_1S_2 - D(S_{1z}^2 + S_{2z}^2) - g\beta H(S_1 + S_2) - zJ'S\langle S\rangle \qquad \text{(Equation 3.1)}$$

Using this model, the best fit values of J = 0.49 cm^{-1}, zJ′ = –0.07 cm^{-1}, D = 1.35 cm^{-1} and g = 1.93 were obtained. The fit is depicted by the solid line in Fig. 3.14. Although there is some discrepancy between this model and the observed data between approximately 50 K and 25 K, the reasonable values for the parameters suggest that this provides the most realistic picture of what is occurring magnetically. The difference may be a result of a paramagnetic impurity, but including such a factor into the model will likely result in over-parametization.

3.3 DISCUSSION

3.3.1 Supramolecular Coordination Complexes with $[Au(CN)_4]^-$ and Comparisons to $[Au(CN)_2]^-$ Complexes

Systems **3.1** – **3.6** represent the first examples of cyanide bridging of the $[Au(CN)_4]^-$ unit to a transition metal. Complexes **3.4** and **3.6** are the first examples of $[Au(CN)_4]^-$ based coordination that result in polymer formation via multiple cyanide bridging (2-*cis* and 4) through the anionic building block, both of which form 1-D chains. The $[Au(CN)_4]^-$ based systems are quite different, however, than previously studied $[Au(CN)_2]^-$ based polymers [53-55], as would be expected given the change in oxidation state and geometry (from linear to square planar).

In general, the formation of cyanometallate-containing coordination polymers and their dimensionality depends on the type of capping ligand and number of open coordination sites that exist on the cation [53-55,230]. This dependence, however, does not appear to be a strong factor in $[Au(CN)_4]^-$-based systems. Although **3.1**, **3.2** and **3.3** all have either two or three available coordination sites (hence the possibility for increasing dimensionality via cyanometallate bridging), in all cases the $[Au(CN)_4]^-$ unit coordinates through one cyanide only, resulting in molecular systems (excluding Au(III)–

N or hydrogen bonding interactions). This contrasts with systems such as $[Ni(en)_2Ag_2(CN)_3][Ag(CN)_2]$ [162,230] $[Cu(dien)Ag(CN)_2]_2[Ag_2(CN)_3][Ag(CN)_2]$ [230] and $[Cu(en)_2Au(CN)_2][Au(CN)_2]$ [53], all of which show similar ligand coordination, but show propagation of dimensionality through multiple bridging cyanides (i.e. bridging cyanometallate moieties). This bridging coordination *is* seen in **3.4**, **3.5** and **3.6**, which each contain two or three open coordination sites at the M(II) cation, suggesting that there are more important factors at play. One key factor is likely the decreased basicity of Au(III) vs. Au(I) cyanometallates and $[M(CN)_4]^{2-}$ (where M = M(II)) which would decrease the propensity of the cyanometallate to coordinate to another metal centre. Although the square planar $[Au(CN)_4]^-$ has increased steric bulk as compared to a linear Au(I) cyanometallate, this is likely not causing decreased bridging, as many $[Pt(CN)_4]^{2-}$ and $[Ni(CN)_4]^{2-}$ bridging polymers have been reported (as previously discussed).

3.3.2 Factors Influencing Cyanometallate Bridging of $[Au(CN)_4]^-$

Various bridging modes of the tetracyanoaurate anion are observed in complexes **3.1** – **3.6**, whereby **3.1** – **3.3** show a lack of cyanometallate bridging, **3.4** and **3.5** show cyanometallate bridging through 2 cis-cyanides and **3.6** shows cyanometallate bridging through all four cyanides. This suggests that there are factors influencing the behavior of the $[Au(CN)_4]^-$ moiety.

Decreased basicity of the ligand on the cation may be providing a more optimal bridging environment for the Au(III) anion, as seen in **3.6** where bridging through four cyanides is possible with the use of the bipy ligand. This aromatic ligand is significantly less basic than the other amine ligands used in **3.1** – **3.5** (dien, en and dmeda). Of these structures, those containing en (the most basic of the ligands) only display mono-cyanide coordination of the $[Au(CN)_4]^-$ unit.

In comparing **3.2** and **3.5**, which differ only in the transition metal used, the observation of *cis* cyanide coordination of $[Au(CN)_4]^-$ in the Ni(II) containing system (**3.5**) is likely due to the increased tendency for Cu(II) complexes to be five-coordinate as compared to their Ni(II) counterparts. Because the dien ligand occupies three sites of the metal centre, multiple bridging of the $[Au(CN)_4]^-$ makes the metal centre six-coordinate, as opposed to five-coordinate, as is observed in the Cu(II) complex.

Another consideration is that both the hydrogen bonding and Au(III)–N interactions may be affecting the formation of cyano-coordination to the metal centres. This interplay of intermolecular (hydrogen-bonding) and intramolecular (cyanide coordination)

interactions has been a topic of recent interest. In comparing the discrete square complex of $[Pt(CN)_4Cu(bipy)(H_2O)]_2 \bullet 2H_2O$ to the polymeric 1-D chain of $[Pt(CN)_4Cu(bipy)]$, it has been suggested that the square complex results from the stabilization imparted by hydrogen bonding to the terminal cyanide moieties such that these stabilizing hydrogen-bonds compete with the cyano-coordination and formation of the polymeric form [231]. This has similarly been the suggestion for the differences between $[(CN)_3Pt(\mu\text{-}CN)Cu(NH_3)_4]$ [231] and the Hoffmann clathrate system $[Pt(CN)_4Cu(NH_3)_2]_n \bullet 2nG$ (G = guest molecule) [232]. The former complex, which bridges through only one cyanide of the $[Pt(CN)_4]^{2-}$ unit, contains four NH_3 ligands and an extensive network of intermolecular interactions, whereas the latter PtCu Hoffmann clathrate contains only two NH_3 ligands and bridges through all four cyanides.

3.3.3 Au – N Interactions

Increases in dimensionality through intermolecular Au(III)–N interactions are observed in $[Au(CN)_4]^-$ systems. These are the first reported Au–N interactions whereby a nitrogen atom interacts at the apical site of a square planar Au(III) molecule in an intermolecular fashion (i.e. without the aid of chelation). This interaction serves to increase the dimensionality of heterobimetallic systems (**3.2**, **3.3** and **3.5**) and also generates chains of associated $[Au(CN)_4]^-$ anions (**3.4** and **3.6**). As previously discussed, it is uncommon for Au(III) atoms to display coordination environments other than square planar, although a few higher coordination geometries do exist. In such cases, very elongated apical Au(III)–Ligand bond lengths are observed, such as seen in many examples with Cl in the apical position, where Au–Cl distances range between 2.911(2) Å and 3.223(3) Å [233-236]. A similar interaction has also been observed between Au(III) and oxygen (an atom more comparable in size with nitrogen) where Au–O = 3.010(4) Å [237]. When such interactions are sterically enforced by the presence of a relatively rigid multidentate ligand, such as a chelating amine, the Au–N distances become significantly shorter (2.58(1) – 2.839(5) Å) [238-243]. These examples are considered to be more intramolecular in nature, as they are assisted by the coordination of one part of a multidentate ligand to a square planar site of Au(III). Without literature examples of Au(III)–N intermolecular interactions, it becomes difficult to comment on their strength. It is, however, useful to compare the Au–N interactions distances (2.961(15) to 3.052(9)) to the sum of the van der Waals radii (3.12 – 3.27) [119], which suggests that these interactions are, in fact, quite strong.

Comparisons between similar complexes show that various factors may be influencing the formation of these interactions. This is evident in comparing the similar complexes $M(en)_2[Au(CN)_4]_2$ (**3.1**, M = Ni; **3.3**, M = Cu). In both cases, the $[Au(CN)_4]^-$ unit is coordinated in a trans fashion, but in **3.3** the M–N(cyano) distances are significantly longer (2.548(9) Å) as compared to **3.1** (2.129(5) Å and 2.116(5) Å), due to Jahn-Teller distortion. As a result, the molecular unit of **3.3** is significantly longer than in **3.1**, allowing room for Au(III)–N interactions between molecular units, which does not occur in **3.1**. Although **3.1** has a water molecule within the unit cell, which may interfere with potential interactions, a similar comparison can also be made between the interactions present in **3.3** vs. **3.4**. These complexes differ only in two additional methyl groups on the ligand in **3.4** (dmeda vs. en). There is a difference in coordination lengths between the two systems: the axial Cu–N(cyano) bond length is 2.724(10) Å in **3.4**, compared to 2.548(9) Å in **3.3**. This elongation of the molecular unit in **3.4** may be providing the length required for the $[Au(CN)_4]^-$ unit to further coordinate another Cu(II) centre without steric hindrances, as **3.4** is able to form a cyano-bridged polymer, whereas **3.3** is not. These comparisons suggests that the longer the molecular unit, the stronger the propensity to form additional bridging interactions.

3.3.4 Infrared Analysis

As is the case with other cyanide complexes, the cyanide stretching bands in the infrared spectra are an extremely useful tool in the prediction of the bridging mode(s) of the $[Au(CN)_4]$-based complexes. Observed bands can be compared to the νCN band of $KAu(CN)_4$, which is found at 2189 cm^{-1} [67] (in KBr). Any shift to higher energy values suggests that the $[Au(CN)_4]^-$ is bridging the transition metal via the cyano(N) atom [56]. The IR data of all complexes is presented in Table 3.7, and compared to a summary of actual bridging modes as determined by the crystal structures of each compound.

As seen in the Table 3.7, there is a general consistency between the expected structure, as predicted by the cyanide stretches, and the observed structure from the X-ray analysis. This prediction becomes more ambiguous, however, when Jahn-Teller distortions are present. As observed in **3.3** and **3.4** the presence of these elongated bridging bonds to Cu(II) results in the absence of a higher energy cyanide band in the IR. These distortions are also present in **3.2** and **3.6**, but there are also cyanides that bridge to the non-elongated equatorial positions of the Cu(II), thus producing the higher energy bands. Particularly of interest is **3.4**, which produced an immediate precipitate

despite the elongated bridging mode of the $[Au(CN)_4]^-$ unit and the essentially unchanged νCN frequency.

Together, these results indicate that transition-metal binding to an N(cyano) ligand of $[Au(CN)_4]^-$ in a bridging fashion is often paired with an increase in the frequency of the νCN band to 2199 – 2241 cm^{-1}, although the absence of such a shift does not necessarily mean that the $[Au(CN)_4]^-$ moiety is unbound.

The minimal effect of Au–N interactions on the cyanide stretching frequency is also apparent from the IR spectrum of **3.4**, which shows no shifted bands, despite the presence of these interactions.

Table 3.7 – Comparison of Cyanide (νCN) Absorptions (cm^{-1}) for all Tetracyanoaurate Complexes (**3.1 – 3.6**)*

Complex	Observed νCN Bands (cm^{-1})			Bridging Observed in Crystal Structure
	Suggestive Bridging	Suggestive Non-bridging	Other	
3.1	2214, 2202	2190	2180	Two slightly different bridges*, remaining all non bridging
3.2	2241, 2219	2189		Two bridging (one elongated, one not), one Au-N interaction and remaining all non bridging
3.3		2187	2180	One elongated bridging, one Au-N interaction and remaining all non bridging
3.4		2190		One elongated bridging, one Au-N interaction and remaining all non bridging
3.5	2236, 2231, 2199	2187		Three bridging, one Au-N interaction, remaining non bridging
3.6	2203, 2198	2187		Two bridging (one elongated, one not), one Au-N interaction, remaining non bridging (in trimer)

* Values determined from the maximum of the absorption peak. A representative IR spectrum is found in Figure 2.5. All spectra are done in KBr with resolution of ± 2 cm^{-1}.

3.3.5 Stacking Interactions

No d^8–d^8 stacking interactions were observed in these $[Au(CN)_4]^-$ systems, despite the fact that $[Au(CN)_4]^-$ is isoelectronic and isostructural to $[Pt(CN)_4]^{2-}$. Although this might suggest that there are significant electronic differences between the Au(III) and Pt(II) cyano complexes, the aforementioned PtCu Hofmann clathrate and $[(CN)_3Pt(\mu\text{-}CN)Cu(NH_3)_4]$ complexes suggest that competition from intermolecular interactions and cyano bridging might affect stacking, as the clathrate shows no d^8–d^8 stacking, whereas the latter complex shows Pt–Pt interactions of 3.675 Å [231,232]. The choice of the ancillary ligands used may also exclude the possibility of stacking interactions, as is suggested by the plethora of heterobimetallic systems containing $[M(CN)_4]^{2-}$, where the heteroatom possesses a bulky ligand and no d^8–d^8 stacking interactions are observed [85,207,209,228,244-246]. In contrast, when heterobimetallic systems are formed with small ligands, such as in $[(CN)_3Pt(\mu\text{-}CN)Cu(NH_3)_4]$, strong Pt–Pt stacking is observed (Pt–Pt distance of 3.6751(2) Å) [231].

These observations spurred the examination of heterobimetallic systems of $[Au(CN)_4]^-$ without any ligands. These reactions were done in water, in methanol and in basic media. Crystallization proved very difficult, however, and no publishable results were obtained.

3.4 CONCLUSIONS

The first supramolecular coordination polymers containing $[Au(CN)_4]^-$ have been prepared, indicating that $[Au(CN)_4]^-$ may serve as a useful building block in the preparation of coordination polymers. Through multiple cyanide bridging, it can increase dimensionality of a molecular unit to a 1-D polymer and with the aid of Au(III)–N interactions, $[Au(CN)_4]^-$ can also increase dimensionality up to two dimensions. It was also shown that the $[Au(CN)_4]^-$ unit can mediate both antiferromagnetic and ferromagnetic interactions. Although no metallophilic interactions were observed, the potential to do so has not been disproven and the $[Au(CN)_4]^-$ unit remains a moiety of interest in terms of its ability to increase dimensionality in coordination polymers.

3.5 EXPERIMENTAL

General experimental details were as indicated in Chapter 2, with the addition of the amine ligand N,N-dimethylethylenediamine (dmeda), which was obtained from Aldrich and used as received.

3.5.1 Preparation of $Ni(en)_2[Au(CN)_4]_2 \bullet H_2O$ (3.1)

To a 5 mL aqueous solution of $Ni(NO_3)_2 \bullet 6H_2O$ (32 mg, 0.110 mmol) was added 0.015 mL of neat en (0.2205 mmol) using a microsyringe. The resulting solution was stirred for 5 minutes. While stirring, a 5 mL aqueous solution of $KAu(CN)_4$ (75 mg, 0.220 mmol) was added drop-wise to this pale purple solution. The resulting solution was covered with parafilm and left undisturbed. Over 2 months, pale purple X-ray quality crystals of $Ni(en)_2[Au(CN)_4]_2 \bullet H_2O$ (**3.1**) were deposited from the solution with only a minimal change in solution volume. The crystals were removed from the solution with a pipette, washed with 2 mL of water and air-dried overnight. Yield: 85 mg (98%). Anal. Calcd. for $C_{12}H_{18}N_{12}Au_2NiO$: C, 18.04; H, 2.27; N, 21.04. Found: C, 18.36; H, 2.20; N, 21.19. IR (KBr): 2214 (νCN), 2202 (νCN), 2190 (νCN), 2180 (w, νCN), 1600, 1462, 1384, 1320, 1284, 1272, 1089, 1023, 965, 699, 661, 531, 519, 415 cm^{-1}.

3.5.2 Preparation of $Cu(dien)[Au(CN)_4]_2$ (3.2)

To a 2 mL aqueous solution of $Cu(ClO_4)_2 \bullet 6H_2O$ (30 mg, 0.075 mmol) was added a 1 mL stock solution (0.075 mmol) of dien. The resulting solution was stirred for 5 minutes. While stirring, a 3 mL aqueous solution of $KAu(CN)_4$ (51 mg, 0.150 mmol) was added drop-wise to this dark blue solution. The resulting solution was covered and left undisturbed to yield X-ray quality purple crystals of $Cu(dien)[Au(CN)_4]_2$ (**3.2**) with only a minimal change in solution volume. After 3 weeks, the crystals were removed from the solution with a pipette, washed with 2 mL of water and air-dried overnight. Yield: 47 mg (81%). Anal. Calcd. for $C_{12}H_{13}N_{11}Au_2Cu$: C, 18.75; H, 1.70; N, 20.04. Found: C, 18.58; H, 1.69; N, 19.83. IR (KBr): 2241 (νCN), 2219 (νCN), 2189 (νCN), 1585, 1317, 1142, 1092, 1028, 974, 653, 526, 419 cm^{-1}.

3.5.3 Preparation of $Cu(en)_2[Au(CN)_4]_2$ (3.3)

To a 3 mL aqueous solution of $Cu(ClO_4)_2 \bullet 6H_2O$ (28 mg, 0.075 mmol) was added a 1 mL stock solution (0.150 mmol) of en. The resulting solution was stirred for 5 minutes. While stirring, a 3 mL aqueous solution of $KAu(CN)_4$ (51 mg, 0.150 mmol) was added drop-wise to this purple solution. The resulting solution was covered and left undisturbed to yield X-ray quality purple crystals of $Cu(en)_2[Au(CN)_4]_2$ (**3.3**). After 2 weeks, the crystals were removed from the solution with a pipette, washed with 2 mL of water and air-dried overnight. Yield: 43 mg (84%). Anal. Calcd. for $C_{12}H_{16}N_{12}Au_2Cu$: C, 18.34; H, 2.05; N, 21.39. Found: C, 18.15; H, 2.05; N, 21.22. IR (KBr): 2187 (νCN), 2180 (νCN), 1589, 1462, 1315, 1084, 1037, 973, 702, 533, 413 cm^{-1}.

3.5.4 Preparation of $[Cu(dmeda)_2Au(CN)_4][Au(CN)_4]$ (3.4)

To a 3 mL aqueous solution of $Cu(ClO_4)_2 \bullet 6H_2O$ (41 mg, 0.110 mmol) was added a 2 mL stock solution (0.220 mmol) of dmeda. The resulting solution was stirred for 5 minutes. While stirring, a 3 mL aqueous solution of $KAu(CN)_4$ (75 mg, 0.220 mmol) was added drop-wise to this purple solution. An immediate purple precipitate of $[Cu(dmeda)_2Au(CN)_4][Au(CN)_4]$ (**3.4**) formed. This precipitate was filtered, washed with 5 mL of water and air-dried overnight. The remaining filtrate was left to evaporate slowly, covered in perforated parafilm for 3 days to yield X-ray quality purple crystals of **3.4** upon evaporating approximately 1/8 of the solution. The crystals were removed from the solution with a pipette, washed with 2 mL of water and air-dried overnight. Total yield (powder and crystals): 76 mg (94%). The powder and crystals had identical IR spectra and elemental analyses. Anal. Calcd. for $C_{16}H_{24}N_{12}Au_2Cu$: C, 22.83; H, 2.87; N, 19.96. Found: C, 22.63; H, 2.85; N, 19.78. IR (KBr): 2190 (νCN), 3302, 3245, 3160, 3023, 2986, 2944, 1598, 1478, 1468, 1462, 1444, 1291, 1190, 1151, 1124, 1062, 1033, 1004, 937, 893, 781, 669, 461, 421, 417 cm^{-1}.

3.5.5 Preparation of $Ni(dien)[Au(CN)_4]_2$ (3.5)

To a 5 mL aqueous solution of $Ni(NO_3)_2 \bullet 6H_2O$ (55 mg, 0.189 mmol) was added a 1 mL aqueous stock solution (0.189 mmol) of dien. The resulting solution was stirred for 5 minutes. While stirring, a 5 mL aqueous solution of $KAu(CN)_4$ (128 mg, 0.377 mmol) was added drop-wise to this pale purple solution. The resulting solution was covered and left undisturbed. After one day, 36 mg of pale purple X-ray quality crystals of $Ni(dien)[Au(CN)_4]_2$ (**3.5**) were deposited from the solution with no apparent change in the

volume. The crystals were removed with a pipette, washed with 1 mL of water and air-dried overnight. Left undisturbed and covered with perforated parafilm, more crystals and crystalline powder were deposited from the solution. After 9 weeks, the remaining solution (approximately 1/2 the original volume) was filtered, the precipitate was washed with 2 mL of water and air-dried overnight. Total yield: 77 mg (53%). Anal. Calcd. for $C_{12}H_{13}N_{11}Au_2Ni$: C, 18.87; H, 1.72 ; N, 20.17. Found: C, 18.99; H, 1.71; N, 19.94. IR (KBr): 2236 (νCN), 2231 (νCN), 2199 (νCN), 2187 (νCN), 3353, 3327, 3306, 1611, 1077, 1037, 1006, 981, 660, 567, 431, 423 cm^{-1}.

3.5.6 Preparation of $[Cu(bipy)(H_2O)_2(Au(CN)_4)_{0.5}][Au(CN)_4]_{1.5}$ (3.6)

To a 4 mL aqueous solution of an excess of $Cu(ClO_4)_2 \bullet 6H_2O$ (54 mg, 0.147 mmol) was added a 4 mL methanolic solution of bipy (11 mg, 0.074 mmol). This solution was stirred for 5 minutes. While stirring, a 4 mL aqueous solution of $KAu(CN)_4$ (50 mg, 0.147 mmol) was added drop-wise to this blue solution. The solution was covered and cooled in a refrigerator for 4 days, then left to evaporate slowly (covered with perforated parafilm) at room temperature to yield large X-ray quality crystals of $[Cu(bipy)(H_2O)_2(Au(CN)_4)_{0.5}][Au(CN)_4]_{1.5}$ (**3.6**). After one month, the crystals were extracted from the solution (approximate volume remaining = 1/4) using a pipette, washed with 2 mL of water and air-dried overnight. Yield: 61 mg (97% based on Au). Anal. Calcd. for $C_{18}H_{12}N_{10}Au_2CuO_2$: C, 25.20; H, 1.41; N, 16.33. Found: C, 25.19; H, 1.39; N, 16.25. IR (KBr): 3515, 3277 (broad), 3117, 3091, 3083, 2263 (νCN), 2198 (νCN), 2187 (νCN), 1612, 1605, 1567, 1501, 1475, 1444, 1315, 1254, 1152, 1106, 1037, 777, 731, 650, 531, 430, 415, 405 cm^{-1}.

CHAPTER 4

TETRACYANOAURATE AND HYDROXO-BRIDGED COPPER(II) DIMERS

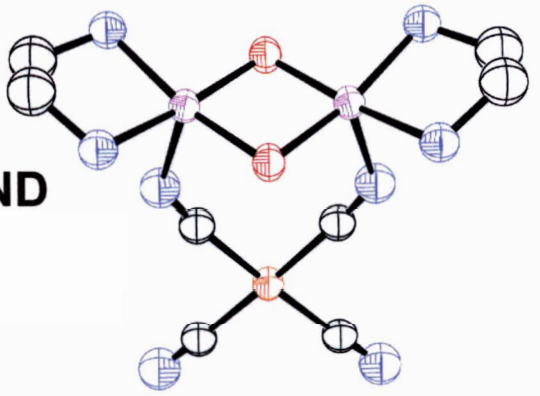

4.1 INTRODUCTION

4.1.1 Magnetostructural Correlations of Copper (II) Dimers

Bridged dinuclear compounds of first-row transition metals have received much attention because of their unique magnetic properties [131,247,248]. Specifically, magnetic properties of copper(II) dimers involving the potential interaction between only one unpaired electron per copper nucleus, have been well documented due to the relative simplicity of modeling [248]. The correlation between various structural parameters and the resulting magnetism (magnetostructural correlations) of such dimers has long been a subject of interest [131,249-251]. The general formula $[CuL(\mu\text{-bridge})]_2^{n+}$ (L = bidentate ligand) can be used for these dimers, and the magnetic properties depend on both the ligand and bridging moiety. Several magnetostructural studies have been done where μ-bridge = chlorine, based on several decades of accumulated structural and magnetic data [252,253]. Other compounds where μ-bridge = alkoxides [254], carboxylates [254], azides [255] and oxides [256,257] as well as cases where the μ-bridge is part of the ligand [258] have also been observed and their

magnetism recorded, but fewer discussions have ensued regarding magneto-correlations [254,259].

4.1.2 Di-μ-Hydroxo Bridged Copper(II) Dimers

The fact that some di-μ-hydroxo bridged copper dimers show antiferromagnetic interactions, whereas others show ferromagnetic interactions was observed decades ago [260]. This phenomenon was observed to be the result of only minor structural changes. With the accumulated evidence of dozens of examples [250,251,255,260-294] many magnetostructural investigations have been explored for these dimeric complexes [248,251,260,262,264-266]. Of particular importance has been the early investigation of Hodgson and Hatfield [262], which suggested that the magnetic interaction parameter (J) was a linear function of the Cu–O–Cu angle (φ) such that $J = -74.53\varphi + 7270$ cm^{-1}. Based on this empirically determined and now widely accepted correlation, it can be concluded that at a Cu–O–Cu angle of greater than 97.55° the overall magnetic behavior of a hydroxo bridged copper dimer should be antiferromagnetic, and ferromagnetic for angles smaller than 97.55°. The range of angles that has been observed (94.5°–104.1°) has correlated to a variety of J values, ranging from large positive values of up to +172 to negative values as low as –509 cm^{-1} [262].

The choice of ligand will obviously affect this angle (via the restraints of the chelate bite angle), as is observed in Table 4.1, showing the parameters and magnetic properties for various hydroxo bridged Cu(II) dimers. Table 4.1 also illustrates that with the same ligand choice, the J value will still vary depending on the counter-ion.

Recently, another parameter has been suggested as influential in the prediction of magnetic properties of di-μ-hydroxo bridged Cu(II) dimers. The influence of the out-of-plane (oop) displacement angle of the hydroxo hydrogen atom has been examined as an explanation to some discrepancies between some experimental J values and those predicted via the Hodgson and Hatfield approach [267-269]. Using this oop angle, it is predicted that if the hydrogen atom remains in the molecular plane (the Cu_2O_2 plane), the magnetism for most hydroxo-bridged Cu(II) dimers will be antiferromagnetic. Conversely, if the oop angle is large (the hydrogen atom is significantly out of the plane), most hydroxo-bridged Cu(II) dimers will be ferromagnetic. Interestingly, the hydroxo-bridged Cu(II) dimers that have small Cu–O–Cu angles tend to show (theoretically and experimentally) large oop angles of the hydrogen atom, suggesting that these two parameters may be correlated [267-269]. Such observations and recent investigations

suggest that the this oop angle contributes to minor fluctuations or perturbations from the previously proposed Cu–O–Cu angle magnetism predictions, primarily for systems where the Cu–O–Cu is between 95° and 99° [267]. However, the difficulties associated with locating the exact position of hydrogen atoms from X-ray data (see Chapter 1) often precludes this discussion, especially in the presence of heavy atoms, such as gold.

Table 4.1 – Summary of Structural and Magnetic Properties of $[CuL(\mu\text{-}OH)]_2^{2+}$ Complexes

Ligand*	Anion	Cu–O–Cu (°)	Cu-Cu (Å)	J (cm^{-1})	Reference(s)
Bipy	NO_3	95.6	2.847	172	[255,260,270]
Bipy	CF_3SO_3	96.9-98.5	2.89-2.92	158, 17	[274]
Dmbpy	CF_3SO_3	94.5		148	[283]
Bipy	C_4O_4	96.4	2.870(1)	145	[273]
Tmpd	ClO_4	no data	no data	130	[262]
Bipy	ClO_4	96.94	2.870	93	[262,282]
Bipy	SO_4	97.0	2.893	49	[263,271,272,275,284,285]
Bipy	PF_6	90.79-105	2.914-3.621	12	[281]
β-Dmaep	ClO_4	98.4	2.938	-2.3	[261,280]
Eaep	ClO_4	98.8 – 99.5	2.917	-130	[276-278]
2miz	ClO_4	100.4	Not available	-175	[286,287]
α-Dmaep	ClO_4	100.4	2.935	-200	[277,279]
Tmeda	**ClO_4**	**102.3**	**2.966**	**-360**	**[262,295]**
Tmeda	**NO_3**	**101.9**	**Not available**	**-367**	**[251,288,289]**
α-Teeda	ClO_4	103.0	2.978(2)	-410	[250,260,290]
Tmeda	**Cl**	**103.2**	**2.98**	**-463**	**[291]**
β-Teeda	ClO_4	104.1	Not available	-469	[251,288,289]
Tmeda	**Br**	**104.1**	**3.000**	**-509**	**[292-294]**

*** Other Ligand Abbreviations:**

Dmaep = 2-(2-dimethylaminoethyl)pyridine

Dmbpy = 4,4′-dimethyl-2,2′-bipyridine

Eaep = 2-(2-ethylaminoethyl)pyridine

Teeda = N,N,N′,N′-tetraethylethylenediamine

Tmpd = N,N,N′,N′-tetramethyl-o-phenylenediamine

2miz = 2-methylimidazole

4.1.3 Previously Examined $[Cu(tmeda)(\mu\text{-}OH)]_2^{2+}$ Dimers and Research Objectives

As illustrated in Table 4.1, there are relatively few $[Cu(tmeda)(\mu\text{-}OH)]_2^{2+}$ dimers and all of them display relatively large Cu–O–Cu angles and thus relatively strong antiferromagnetic interactions [250,251,260,262,288-295]. This contrasts the larger number of studies that have been done on $[Cu(bipy)(\mu\text{-}OH)]_2^{2+}$ complexes, which all display ferromagnetic interactions [255,260,262,263,270-275,281-285].

The use of an anion that coordinates could, potentially, influence the structural parameters to a greater extent as compared to a non-coordinating counter-ion. This has been seen particularly in the case of oxygen-donor coordinating anions, such as ClO_4 systems [261,280], NO_3 [255,282], SO_4 [269] and CF_3SO_3 systems [283]. Thus, the use of the tetracyanoaurate anion, which was shown in Chapter 3 to coordinate to Cu(II) centres, may prove to be an interesting anion in these dimer systems as coordination may alter the structural parameters of the dimer. Furthermore, the potential for increases in dimensionality could also produce further magnetic interaction pathways has been observed in the 1-D chains of Cu(II) dimers, through the use of bridging ligands [296,297], and less commonly through bridging anion coordination [273].

4.2 RESULTS AND ANALYSES

4.2.1 General Synthetic Methods

Two methods have been employed to form the tmeda μ-hydroxo copper dimer complexes, one using a prepared dimer starting material (adapted from literature methods [262]) and the other that employs an *in situ* preparation of the dimer.

Through experience in the laboratory, it was found that the reactions appear to require a basic solution, therefore use of an excess amount of amine ligand or a small amount of added base were often employed as a strategy for increasing purity.

It should also be noted that the increased tendency of complexes with a bulky ligand to form Cu(II) dimers has been previously discussed [298-300], hence this chapter focuses on the use of the tmeda ligand, rather than the variety of capping ligands employed throughout this thesis.

4.2.2 X-Ray Structure Analysis

A summary of crystallographic data and refinement details for all structures in this chapter are collected in Appendix 2, with corresponding coordinates collected in Appendix 3.

4.2.2.1 Structure of the 1-D Chain [{Cu(tmeda)(μ-OH)}$_2$Au(CN)$_4$][Au(CN)$_4$] (4.1).

Various synthetic methods were employed in the preparation of [{Cu(tmeda)(μ-OH)}$_2$Au(CN)$_4$][Au(CN)$_4$] (**4.1**), as discussed in Section 4.5. Crystals of **4.1** were formed by slow evaporation of an ammonium hydroxide solution of [{Cu(tmeda)(μ-OH)}$_2$Au(CN)$_4$][Au(CN)$_4$]. The X-ray crystal structure of **4.1** is depicted in Figures 4.1 and 4.2, with the corresponding bond lengths and angles collected in Table 4.2. The X-ray crystal structure reveals the expected hydroxo-bridged dimer cation, as depicted in Figure 4.1. There are two crystallographically unique half-dimer cations in the asymetric unit, but the structural parameters are essentially identical for both. The square planar geometry about the copper atom is slightly distorted due to the chelating amine (N(1)–Cu(1)–N(2) = 86.6(2)°) and bond distances are all within the expected range (Cu–N range = 2.009(5) – 2.051(5) Å and Cu–O range = 1.930(4) Å – 1.955(4) Å) as compared to previously published Cu(tmeda) hydroxo-bridged dimers [251,262,288,289,291-295], as well as other μ-hydroxo-bridged Cu(II) dimers [250,260,261,263,270-287]. The distance between Cu(II) centres is 2.9041(14) Å, also within the range of 2.870 – 3.000 Å seen in other μ-hydroxo-bridged Cu(II) dimers, and higher than the 2.61 – 2.65 Å range observed for complexes in which direct Cu–Cu bonding is postulated [301-303]. The structural parameters of the dimer are quite similar to the previously observed μ-hydroxo-bridged Cu(tmeda) dimers, with the exception of the Cu–O–Cu angle: The Cu(1)–O(1)–Cu(1)′ angle is 96.24(19)°, whereas the lowest Cu–O–Cu angle reported to date for such dimers is 102.3(4)° [262,295]. This low angle suggests the possibility of ferromagnetic exchange between the paramagnetic Cu(II) centres, as suggested by the Hatfield and Hodgson equation [262]. This angle is particularly low as compared to the same tmeda dimer in the presence of counter-ions such as perchlorate, chloride and bromide, all of which are observed to be strongly antiferromagnetic [250,260,262,290-294]. Note that the data for the location of the hydrogen atoms was not sufficient for refinement of the atoms, and thus the oop angle is unknown.

Table 4.2 – Selected Bond Lengths (Å) and Angles (deg) for $[\{Cu(tmeda)(\mu\text{-}OH)\}_2Au(CN)_4][Au(CN)_4]$ (**4.1**)

Selected Atoms	Bond Length	Selected Atoms	Bond Length
Cu(1) – N(1)	2.023(5)	Cu(1) – N(2)	2.051(5)
Cu(1) – N(11)	2.394(7)	Cu(1) – O(1)	1.947(4)
Cu(1) – Cu(1)′[a]	2.9041(14)	Cu(1) – O(1)′	1.953(4)
Au(1) – C(11)	1.984(7)	Au(1) – C(12)	1.979(9)
Au(3) – C(33)	1.988(8)	Au(3) – C(34)	1.977(7)
Selected Atoms	**Angle**	**Selected Atoms**	**Angle**
Cu(1) – O(1) – Cu(1)′	96.24(19)	N(1) – Cu(1) – N(2)	86.6(2)
N(1) – Cu(1) – N(11)	96.0(2)	N(2) – Cu(1) – N(11)	100.9(2)
N(1) – Cu(1) – O(1)	175.7(2)	N(2) – Cu(1) – O(1)	94.04(19)
N(11) – Cu(1) – O(1)	88.0(3)	O(1) – Cu(1) – O(1)′	83.76(19)
C(11) – N(11) – Cu(1)	148.8(8)	Au(1) – C(11) – N(11)	176.6(7)
C(31) – Au(3) – C(33)	179.4(3)	C(32) – Au(3) – C(34)	178.3(3)

[a] Symmetry transformation: ′ ≡ 1 – x, 2 – y, 1 – z.

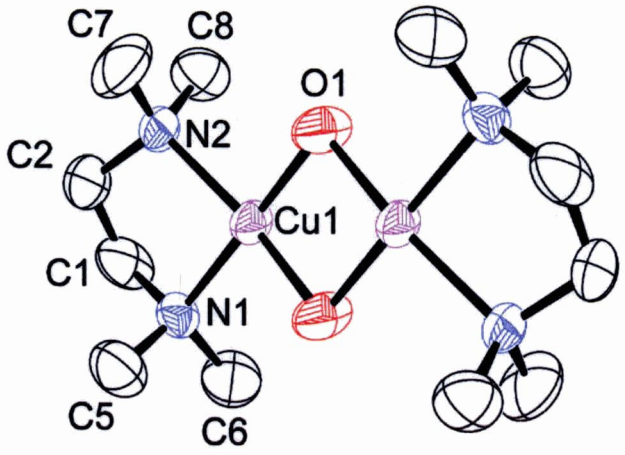

Figure 4.1 – Molecular structure of the $\{Cu(tmeda)(\mu\text{-}OH)\}_2^{2+}$ cation of $[\{Cu(tmeda)(\mu\text{-}OH)\}_2Au(CN)_4][Au(CN)_4]$ (**4.1**). Hydrogen atoms have been omitted for clarity.

The dimer cations are further coordinated by the $[Au(CN)_4]^-$ anion, as seen in Figure 4.2. This anion coordination has only been observed with oxygen donor anions in

hydroxo-bridged Cu(II) dimer complexes [251,255,274,276,278,279]. The Cu(1)–N(11) distance of 2.394(7) Å completes the square pyramidal coordination sphere of the Cu(II) atom.

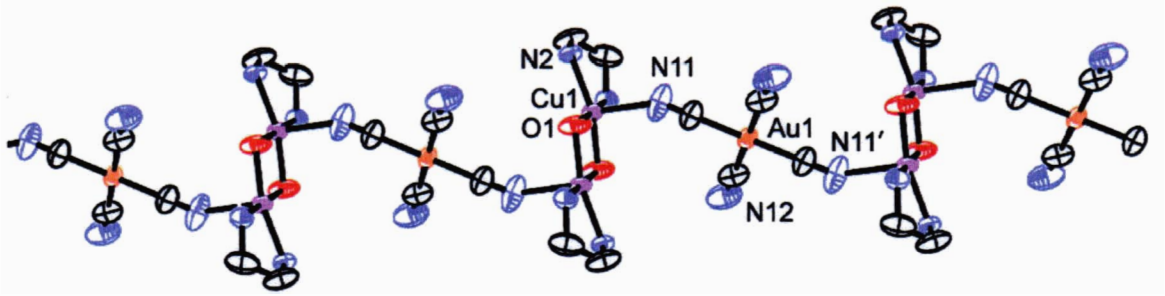

Figure 4.2 – Extended structure of the 1-D chain of $[\{Cu(tmeda)(\mu\text{-}OH)\}_2Au(CN)_4]^+$ cations in **4.1**. Hydrogen atoms and methyl groups have been omitted for clarity.

This coordination results in the formation of a 1-D chain, as depicted in Figure 4.2. There is also one unbound $[Au(CN)_4]^-$ unit (Au(3), not shown). Although 1-D chains of Cu(II) dimers have been observed in the literature [296,297,304], they usually occur through bridging ligands, such as 2,2′-bipyrimidine [296]. The propagation through a bridging anion, as seen in **4.1** is similar to 1-D chain of hydroxo-bridged dimers $[Cu(bipy)(\mu\text{-}OH)]_2(C_4O_4)\bullet 5.5H_2O$ [273] whereby a planar squarate anion coordinates in a trans fashion through oxygen donors to two dimer molecules, thus propagating the chain. **4.1** is also similar to a complex recently reported by the Leznoff group which forms a 1-D chain of $[Cu(bipy)(\mu\text{-}OH)]_2^{2+}$ dimers through a $[\mu\text{-}Cl_2Hg(CN)_2]^{2-}$ unit [111]. In this case, the anion consists of a $Hg(CN)_2$ linear molecule with bridging chlorine atoms coordinated to the Hg atom, thus forming a square planar anionic unit similar to the $[Au(CN)_4]^-$ unit. In the aforementioned case, the chain also propagates through trans coordination of the anionic unit.

4.2.2.2 Structure of the Molecular Isomer $[Cu(tmeda)(\mu\text{-}OH)Au(CN)_4]_2$ (4.2)

Crystals of **4.2** were formed by the slow evaporation of a methanolic solution containing one equivalent of $Cu(ClO_4)_2\bullet 6H_2O$ and 2 equivalents of both tmeda and $K[Au(CN)_4]$. However, despite numerous attempts and many alterations in reaction and crystallization conditions, this reaction could never be repeated to form the same

crystals, hence its preparation is not included in the experimental section. The X-ray crystal structure of **4.2** is depicted in Figure 4.3, with the corresponding bond lengths and angles collected in Table 4.3. The X-ray crystal structure reveals the expected hydroxo-bridged dimer cation, similar to that seen in Figure 4.1 (cation of **4.1**) with only slight differences in bond lengths and angles. As in **4.1**, the $[Au(CN)_4]_2^-$ anion is coordinated to the apical site of the square pyramidal Cu(II) atom (Figure 4.3), though with a slightly longer bond distance (Cu(1)–N(11) = 2.436(6) Å). Unlike in **4.1**, however, this anion does not further coordinate to another cationic dimer unit, and thus the structure is molecular rather than a 1-D chain.

There are significantly more Cu(II) dimer units that show apical coordination of anions without propagation into a 1-D chain. Most, however, consist of apical Cu–O bonds, such as is observed in many bipy hydroxo-bridged dimers with nitrate [255,260,270], sulfate [263,271,272,275,284,285] and triflate [274] anions (whereby Cu–O apical = 2.363 – 2.453 Å). Other Cu(II) dimers also show similar coordination with the above anions (Cu–O apical = 2.56 – 2.72 Å) [278,279]. No such coordination has been observed for tmeda dimers, nor with nitrogen donor anions. Many of the above anion coordinations are also considered to be "semi-coordinated" [305] due to their relatively long bond lengths as compared to other Cu–O apical coordination bonds. The Cu(1)–N(11) bond distance of 2.436(6) Å is shorter than the above Cu–O bond lengths, and within the range of other Cu–N apical bonds of square pyramidal Cu(II) complexes, though slightly longer than the coordination observed in **4.1**.

The Cu(1)–O(1)–Cu(1)′ angle of 98.92(17)° is higher than that observed in **4.1**, and would thus be expected to show antiferromagnetic interactions, as opposed to the predicted ferromagnetic interactions of **4.1**. The hydroxide hydrogen atoms were found from the fourier difference map and refined isotropically, and thus the oop angle could be determined with confidence. The observed oop angle of 47.85° is not likely to alter the predicted antiferromagnetic interactions, as previous calculations have shown that an oop angle of at least 50° is required to change the predicted interactions [267]. Unfortunately, due to synthetic difficulties, magnetic data could not be collected on **4.2** to examine the validity of these predictions.

4.2.2.3 Structure of $[\{Cu(tmeda)(\mu\text{-}OH)\}_2Au(CN)_4][ClO_4]\bullet MeOH$ (4.3)

Crystals of **4.3** were formed by slow evaporation of a methanolic solution containing one equivalent of the preformed dimer $\{Cu(tmeda)(\mu\text{-}OH)\}_2^{2+}$ and one equivalent of $[Au(CN)_4]^-$. The X-ray crystal structure of **4.3** is depicted in Figure 4.4, with the

corresponding bond lengths and angles collected in Table 4.4. The X-ray crystal structure reveals the expected hydroxo-bridged dimer cation (Figure 4.1), with similar Cu–N(amine) and Cu–O bond lengths and angles to the dimers observed in **4.1** and **4.2**.

Table 4.3 – Selected Bond Lengths (Å) and Angles (deg) for the Molecular Isomer $[Cu(tmeda)(\mu\text{-}OH)Au(CN)_4]_2$ (**4.2**)

Selected Atoms	Bond Length	Selected Atoms	Bond Length
Cu(1) – N(1)	2.035(1)	Cu(1) – N(2)	2.059(4)
Cu(1) – O(1)	1.929(4)	Cu(1) – N(11)	2.436(6)
Cu(1) – Cu(1)′[a]	2.937(1)	Cu(1) – O(1)′	1.936(4)
Au(1) – C(11)	1.988(6)	Au(1) – C(12)	1.988(6)
Au(1) – C(13)	1.995(6)	Au(1) – C(14)	1.994(6)
Selected Atoms	**Angle**	**Selected Atoms**	**Angle**
Cu(1) – O(1) – Cu(1)′	98.92(17)	N(1) – Cu(1) – N(2)	86.72(17)
N(1) – Cu(1) – N(11)	93.4(2)	N(2) – Cu(1) – N(11)	96.3(2)
N(1) – Cu(1) – O(1)	174.74(19)	N(2) – Cu(1) – O(1)	95.14(16)
N(11) – Cu(1) – O(1)	91.3(2)	O(1) – Cu(1) – O(1)′	81.08(17)
C(11) – N(11) – Cu(1)	145.0(6)	C(11) – Au(1) – C(13)	178.5(3)

[a]Symmetry transformation: ′ ≡ –x, 1 – y, 1 – z.

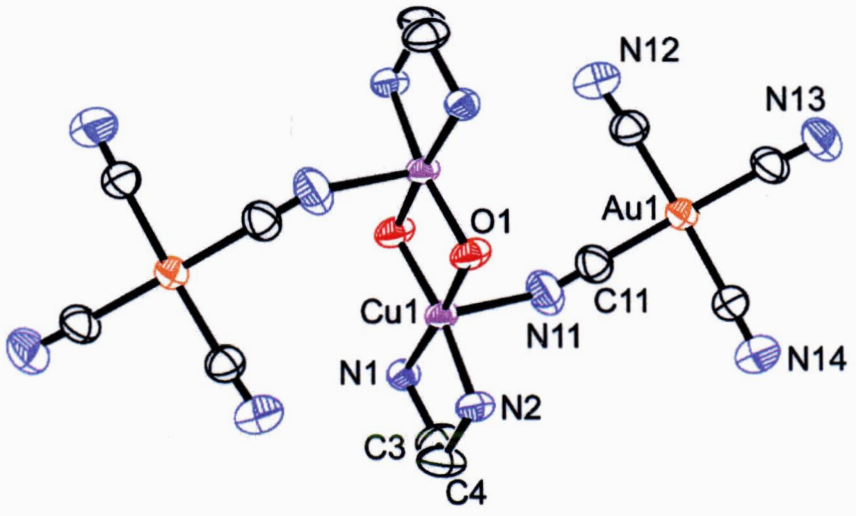

Figure 4.3 – Structure of molecular $[Cu(tmeda)(\mu\text{-}OH)Au(CN)_4]_2$ (**4.2**). Methyl groups and hydrogen atoms have been omitted for clarity.

The Cu(1)–O(1)–Cu(1)′ and Cu(1)–O(2)–Cu(1) angles of 97.9(2)° and 98.8(2)° are most comparable to **4.2** and similarly, weak antiferromagetic interactions are expected. The oop hydrogen atom angle could not be determined, as the hydrogen atoms of the hydroxide bridges could not be found and refined from the Fourier difference map and were thus placed geometrically.

The $[Au(CN)_4]^-$ anion is coordinated through cyano(N) atoms to the Cu(II) centres, as was also observed in **4.1** and **4.2**, thus making the coordination geometry of the Cu(II) atoms square pyramidal. The apical Cu(1)–N(11) distance of 2.462(5) Å is longer than that observed in **4.1** and **4.2**, but still within reasonable boundaries for axially elongated coordination to a Cu(II) centre. Unlike both previous complexes, the anion is bound through two *cis* cyano(N) atoms of the $[Au(CN)_4]^-$ moiety to the two Cu(II) atoms of a single dimer cation, as seen in Figure 4.4. This is a relatively rare form of anion bridging for hydroxo-bridged Cu(II) dimers, but has been observed with a triflate ion in $[Cu(dmbpy)(\mu\text{-}OH)CF_3SO_3]_2$ [283]. In this case, the coordination occurs through an oxygen donor with Cu–O distances of 2.578– 2.666 Å and both triflate anions are bound

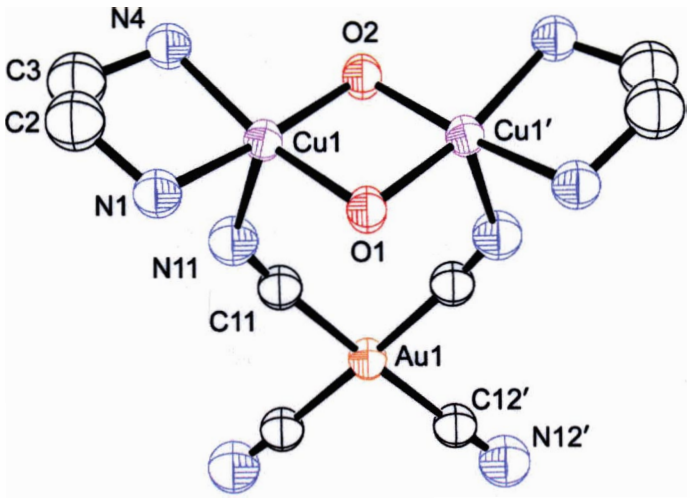

Figure 4.4 – Structure of the cationic moiety $[\{Cu(tmeda)(\mu\text{-}OH)\}_2Au(CN)_4]^+$ in $[\{Cu(tmeda)(\mu\text{-}OH)\}_2Au(CN)_4][ClO_4]\bullet MeOH$ (**4.3**). Methyl groups and hydrogen atoms have been omitted for clarity.

in this fashion to the Cu(II) dimer, resulting in a distorted octahedral Cu(II) geometry. A similar structure results from coordination of the sulfate anion in α-[Cu(dmaep)(μ-OH)SO_4]$_2$ [261]. In **4.3**, only the single $[Au(CN)_4]^-$ anion is bound, while the $[ClO_4]^-$ anion and methanol solvent molecule are both uncoordinated.

Table 4.4 – Selected Bond Lengths (Å) and Angles (deg) for [{Cu(tmeda)(μ-OH)}$_2$Au(CN)$_4$][ClO_4]•MeOH (**4.3**)

Selected Atoms	Bond Length	Selected Atoms	Bond Length
Cu(1) – N(1)	2.029(4)	Cu(1) – N(4)	2.048(4)
Cu(1) – N(11)	2.462(5)	Cu(1) – Cu(1)′[a]	2.9262(12)
Cu(1) – O(1)	1.940(3)	Cu(1) – O(2)	1.928(3)
Au(1) – C(11)	1.993(6)	Au(1) – C(12)	2.005(6)
Selected Atoms	**Angle**	**Selected Atoms**	**Angle**
N(1) – Cu(1) – N(4)	86.03(18)	N(1) – Cu(1) – O(1)	93.79(19)
N(1) – Cu(1) – O(2)	167.0(2)	N(4) – Cu(1) – O(1)	167.0(2)
N(4) – Cu(1) – O(2)	95.93(17)	O(1) – Cu(1) – O(2)	81.48(16)
Cu(1) – O(1) – Cu(1)′	97.9(2)	Cu(1) – O(2) – Cu(1)′	98.8(2)
C(11)′ – Au(1) – C(12)	176.9(2)		

[a] Symmetry transformations: ′ ≡ x, 1/2 – y, z.

4.2.3 Infrared Analysis

The νCN bands of the infrared spectra of complexes **4.1** – **4.3** are much weaker than previously observed $[Au(CN)_4]^-$ complexes. They were also observed to be extremely sensitive to impurities. As such, it was much more difficult to deduce structural information from the IR with any degree of confidence. This proved to be quite problematic, particularly when attempting to distinguish between the isomeric products, as neither product had a clearly unique spectrum. The $[ClO_4]^-$ peak (characteristically strong and broad, at approximately 1100 cm^{-1}) did, however, simplify the identification of **4.3**.

4.2.4 Magnetic Properties

For complexes **4.1** and **4.3**, the temperature (T) dependence of the molar magnetic susceptibilities (χ_M) was measured from 2 to 300 K and the data examined for the

presence of magnetic interactions. For the 1-D chain of [{Cu(tmeda)(μ-OH)}$_2$Au(CN)$_4$][Au(CN)$_4$] (**4.1**), the Cu–O–Cu angle of 96.24(19)° is suggestive of ferromagnetic interactions. The observed $\chi_M T$ of 0.87 cm^3 K mol^{-1} at 300 K is slightly high for two magnetically isolated S = 1/2 centres. The $\chi_M T$ increases with decreasing temperature to a maximum of 1.01 cm^3 K mol^{-1}at 15 K and then decreases to 0.89 cm^3 K mol^{-1} at 2 K as depicted in Figure 4.5. The increase is characteristic of ferromagnetic intradimer interactions and the maximum corresponds to the expected $\chi_M T$ value of a fully ferromagnetically coupled S = 1 system. The decrease is likely a result of interdimer antiferromagnetic interactions or zero-field splitting of the ferromagnetically coupled S = 1 dimer.

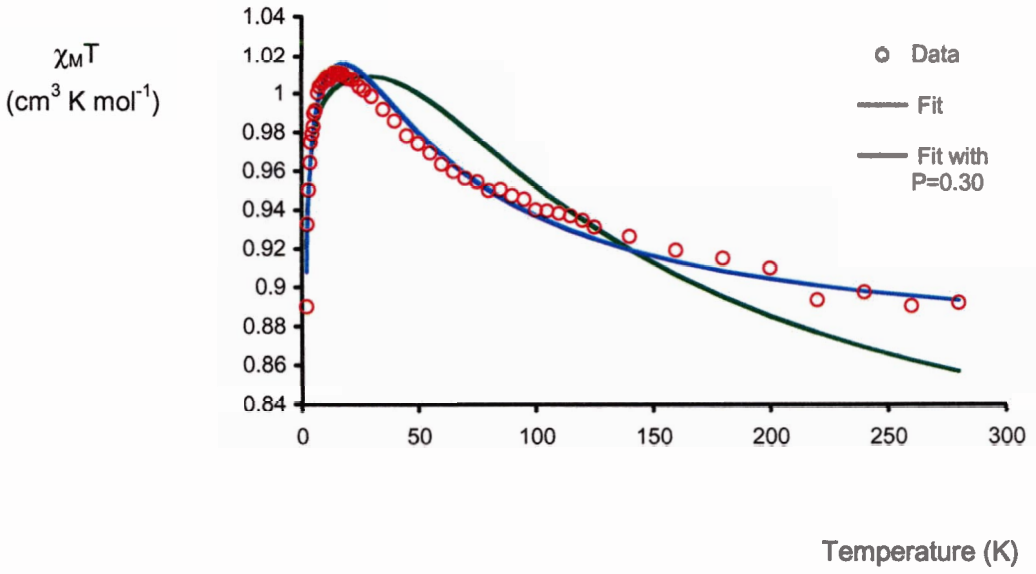

Figure 4.5 – Temperature dependence of the product $\chi_M T$ for **4.1**. Colored lines correspond to the fits using the Bleaney-Bowers model (with and without paramagnetic parameter; see text).

In previous examples of 1-D chains of Cu(II) dimers, the data was fit assuming that the intradimer interactions were much larger than the interdimer interactions in the chain [111,273]. Accordingly, the data was fit using the Bleaney-Bowers model for S = 1/2 dimers, with $\mathbf{H} = -2JS_1S_2$ and an additional molecular field parameter to account for the weak interdimer interactions [131,133]. This additional molecular field parameter is used under the assumption that the zJ′ (where z = the number of nearest metal centre

neighbors and J′ is the intradimer interaction parameter) is a much smaller value as compared to J. This fit (as depicted by the green line in Figure 4.5) results in the best-fit values of J = 56.2 ± 3.7 cm^{-1}, g = 2.017 ± 0.005 and zJ′ = –0.014 ± 0.002 cm^{-1}. A better fit, however, is obtained with the addition of a paramagnetic impurity parameter, as shown by the blue line in Figure 4.5. The paramagnetic impurity parameter reasonably assumes that the paramagnetic impurity follows the Curie Law (i.e. is magnetically dilute) and has the same molecular weight and g-value as the sample. This fit results in the best-fit values of J = 31.9 ± 2.1 cm^{-1}, g = 2.113 ± 0.009 and zJ′ = –0.016 ± 0.001 cm^{-1} with P = 0.30. This fit suggests that 30% of the sample is a spin-dilute Cu(II) monomer; the elemental analysis does not support this. The impurity present may, in fact, be the antiferromagnetic molecular isomer **4.2**, which would have the same elemental analysis. If this were the case, a far smaller percentage of impurity would produce the observed deviations from the fit. It is most likely, therefore, that the true J value of **4.1** is between the values with and without the impurity parameter.

For [{Cu(tmeda)OH}$_2$Au(CN)$_4$][ClO_4]•MeOH (**4.3**), $\chi_M T$ = 0.68 cm^3 K mol^{-1} at 300 K, which is slightly below the expected $\chi_M T$ value of 0.75 cm^3 K mol^{-1} for two independent S = 1/2 centres. The $\chi_M T$ is approximately temperature independent until 150 K, at which point $\chi_M T$ decreases to a minimum of 0.05 cm^3 K mol^{-1} at 10 K, as depicted in Figure 4.6(a). As expected from the average Cu–O–Cu angle of 98.4°, this decrease is characteristic of antiferromagnetic interactions. The plateau (rather than a fully coupled χT = 0) is likely the result of paramagnetic impurities, which is often observed for polymetallic compounds with singlet ground states [131]. The effect of this impurity is very apparent in the graph of the χ_M temperature dependence, shown in Figure 4.6(b). This graph shows a maximum at approximately 50 K, characteristic of the onset of antiferromagnetic interactions in a Cu(II) dimer, and also clearly displays the increase in χ at low temperatures, which results from the paramagnetic impurity (this effect is often referred to as a Curie tail, as the paramagnetic impurity follows the Curie Law).

The data can be fit using the Bleaney-Bowers model for S = 1/2 dimers, with **H** = $-2JS_1S_2$ (assuming no interdimer interactions) [131,133]. This fit (as depicted by the blue lines in Figure 4.6) results in the best-fit values of J = –59.5 ± 0.34 cm^{-1}, g = 2.04 ± 0.005 and P = 0.06 ± 5 x 10^{-5}.

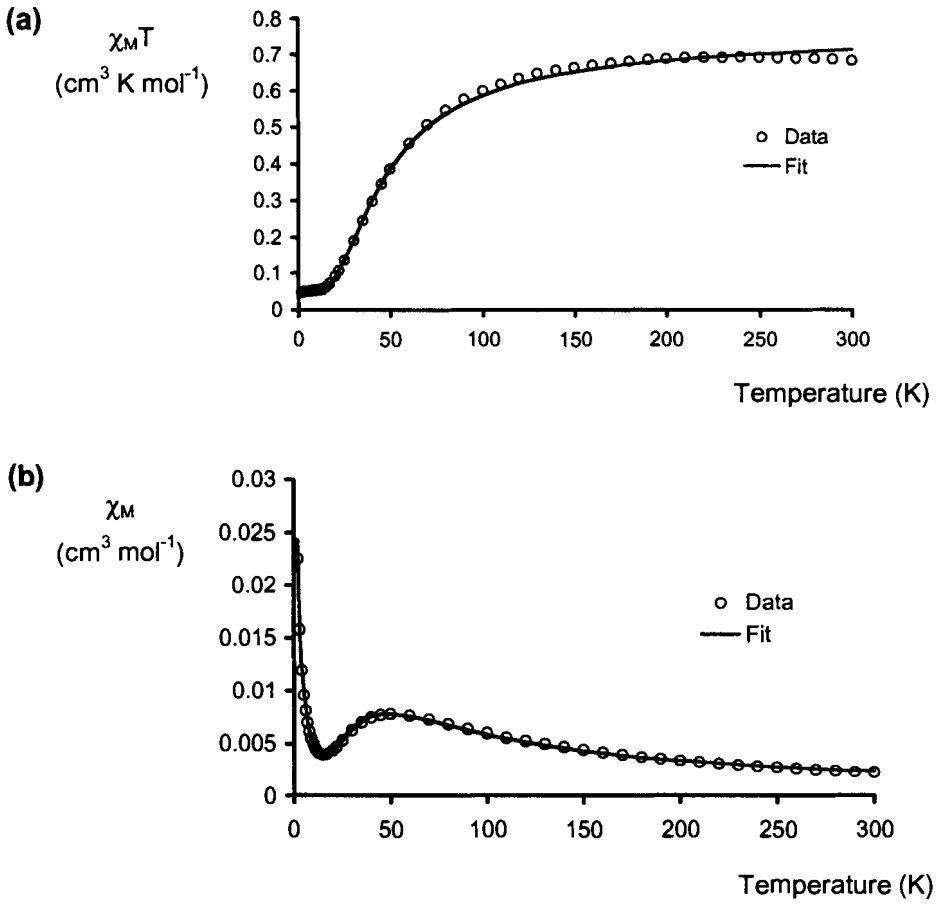

Figure 4.6 – (a) Temperature dependence of the product $\chi_M T$ for **4.3**.
(b) Temperature dependence of χ_M for **4.3**. Solid blue line (in both) corresponds to the fit using the Bleaney-Bowers model (see text).

4.3 DISCUSSION

4.3.1 Magnetostructural Correlations of $[Cu(tmeda)(\mu\text{-}OH)]_2^{2+}$ Dimers

Complexes **4.1** – **4.3** represent three new $[Cu(tmeda)(\mu\text{-}OH)]_2^{2+}$ dimers with a unique anionic unit. The magnetostructural correlation equation as proposed by Hodgson and Hatfield [262] can be applied to each complex, resulting in predicted J values of 97 cm^{-1}, –102.5 cm^{-1} and –63.75 cm^{-1} (based on the average Cu–O–Cu angle for **4.3**)

respectively. The observed J values of 31.9 – 56.2 cm^{-1} and –59.5 cm^{-1} for **4.1** and **4.3** deviate only slightly from the calculated values as can be observed in the graphical representation in Figure 4.7. This deviation is not uncommon for $[Cu(tmeda)(\mu\text{-}OH)]_2^{2+}$ dimers, as can also be observed in Figure 4.7, which illustrates the magnetostructural correlations of all such dimers. Similarly, the $[Cu(bipy)(\mu\text{-}OH)]_2(NO_3)_2$ complex has an observed J value of 172 cm^{-1} as compared to the predicted 107 cm^{-1} [270]. Recently, it has been suggested that these deviations are a result of the effect of the out of plane (oop) hydrogen atom angle's influence on magnetism [267-269]. However, the influence of the oop angle seems to be constrained to systems with Cu–O–Cu angles between 95° and 99° (suggesting that it serves only to perturb the magnetism in cases where the Cu–O–Cu angles predicts weaker magnetic interactions) [267]. Also, calculations have shown that, to some extent, this oop angle is actually correlated to the Cu–O–Cu angles [267-269]. Because only the oop hydrogen angle of **4.2** was determined and no magnetic data was obtained for this complex, no further comment can be made regarding the effect of this angle on the predicted magnetism of complexes **4.1** and **4.3**,

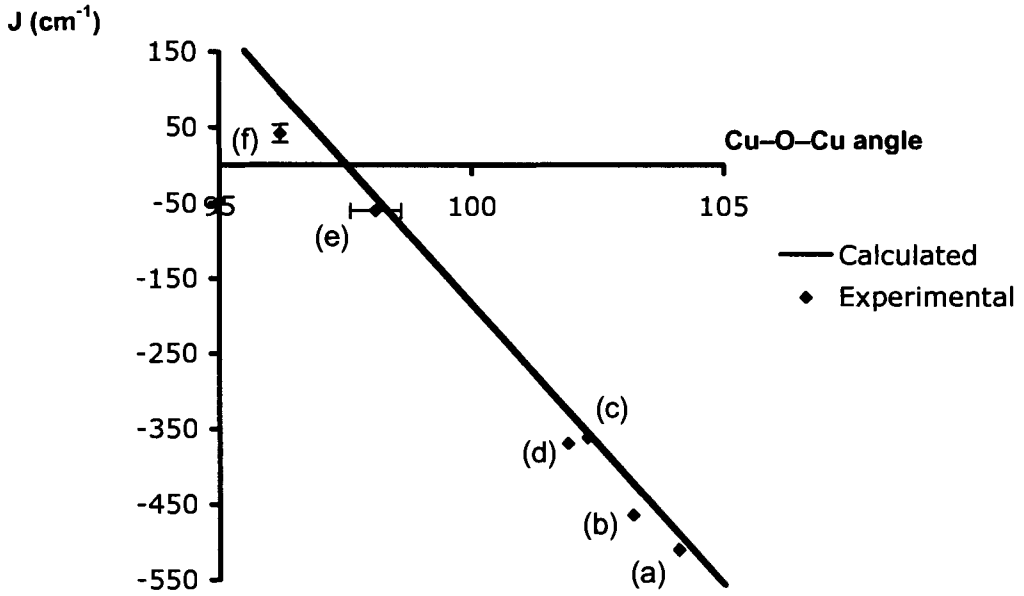

Figure 4.7 – Magnetostructural correlations of $[Cu(tmeda)(\mu\text{-}OH)]_2^{2+}$ dimers with various anions: (a) bromide [292-294]; (b) chloride [291]; (c) perchlorate [262,295]; (d) nitrate [251,288,289]; (e) **4.3**; (f) **4.1**. Solid blue line corresponds to the calculated correlation based on Hodgson and Hatfield's work [262].

except to reinforce that because the magnetostructural correlations as predicted by Hodgson and Hatfield [262] appear to be sufficient (as shown by Figure 4.7), the oop hydrogen angle likely has only a relatively minor effect on magnetism.

Other factors affecting magnetic results, such as the basicity of the ligand, Cu–O distances and hinge distortion of asymetric dimers have all been explored [268]. Also, the effect of anion choice has been shown to influence the magnetism only in cases where the anion is bound to the dimer [268]. For complexes **4.1** and **4.3**, which both contain coordinated anions, the anion would be expected to alter the observed magnetism. As has been discussed previously, the structure of **4.3** is similar to a published structure $[Cu(dmbipy)(\mu\text{-}OH)CF_3SO_3]_2$, which also contains anion coordination through two cis donors. In this example, the deviation from the predicted J value of 227 cm^{-1} of the observed value of 148 cm^{-1} is quite significant, and has been attributed to a combination of additional structural effects such as hydrogen bonding and non-planarity of the dimer [283]. Complex **4.1**, which forms a 1-D chain, would be expected to show further deviations from the calculated magnetism, as the dimer-bridging anion could further influence the structural parameters of the dimer, as well as increase potential magnetic pathways between dimers (although this interdimer pathway is likely very weak as can be concluded by the zJ′ value).

Significantly, complexes **4.1** – **4.3** represent the first $[Cu(tmeda)(\mu\text{-}OH)]_2^{2+}$ complexes with Cu–O–Cu angles below 100°. Furthermore, complex **4.1** is the first ferromagnetic $[Cu(tmeda)(\mu\text{-}OH)]_2^{2+}$ complex. This is also the first instance where a series of μ-bridged Cu(II) dimers with a specific capping ligand has exhibited both antiferromagnetic and ferromagnetic interactions. This suggests that the anion choice could be much more instrumental than previously thought. The implementation of various anions that possess coordination ability to Cu(II) dimers could thus be a magnetically interesting endeavor and another method with which to control magnetic properties of dimer complexes. This possibility has recently been expressed and calculations have predicted that for dimer systems with the en ligand (or multiple NH_3 ligands) changes in anion choice could produce this variety of interactions (both ferromagnetic and antiferromagnetic within a series of dimer complexes), although no such dimers have ever been successfully synthesized [268]. The tmeda ligand, which more readily forms Cu(II) dimers due to its steric bulk, is an excellent choice for a dimer

building block for use with a variety of coordinating anions, as has been illustrated in the examples of **4.1** and **4.3**.

4.3.2 Isomeric Products and Structural Parameters

Complexes **4.1** and **4.2** represent the first isomeric products whereby the Cu–O–Cu angle difference is such that one isomer is ferromagnetically coupled, whereas the other is predicted to be antiferromagnetic. The magnetism results of **4.3** also suggest that the predicted antiferromagnetic interactions for **4.2** are realistic. Although the experimental procedure was not reproducible to a reasonable purity or yield, the use of two different solvents (water and methanol) appears to have an impact on the isomer formed, whereby the 1-D chain results from a water solution, and the molecular system is one of many products formed in methanol.

The multiple coordination mode of the $[Au(CN)_4]^-$ unit has been previously discussed in Chapter 3, showing that it can be used to increase dimensionality [306]. Both cyanometallate bridging modes whereby bridging occurs through two cyano(N) atoms are observed in these complexes; the trans mode is observed in **4.1** and the cis mode in **4.3**. It is interesting to note, however that the multiple trans coordination of the anion has the ability to alter the structural parameters of the Cu(II) dimer and decrease the Cu–O–Cu angle. This suggests that the increased dimensionality may be achieved at the cost of some degree of flexibility of the Cu(II) cation.

The formation of multiple dimer products from a solution has been observed before. The same aqueous solution of Cu^{2+}, NO_3^-, bpm (2,2′-bipyrimidine), and sodium carbonate was shown to produce crystals of both $[Cu_2(bpm)(H_2O)_2(\mu\text{-}OH)_2](NO_3)_2$ and $[Cu_2(bpm)(H_2O)_2(\mu\text{-}OH)_2(NO_3)_2]\bullet 2H_2O$ with undefined yields, whereas very slight changes to the reactant concentrations yielded primarily $[Cu_2(bpm)_2(H_2O)_2(\mu\text{-}OH)_2(NO_3)_2]\bullet 4H_2O$ with undefined minimal yields (crystals were reportedly hand-picked) of $[Cu_2(bpm)(\mu\text{-}OH)_2(NO_3)_2]\bullet 2H_2O$ [296]. This delicate equilibrium was not thoroughly discussed in the publication, but it appears to be a common occurrence in the formation of the hydroxo-bridged Cu(II) dimer systems.

4.4 CONCLUSIONS

Two isomeric products of $[\{Cu(tmeda)(\mu\text{-}OH)\}_2Au(CN)_4][Au(CN)_4]$ (**4.1**) and $[Cu(tmeda)(\mu\text{-}OH)Au(CN)_4]$ (**4.2**) were synthesized and their X-ray structures

determined, showing that one (**4.1**) forms a 1-D chain through bridging $[Au(CN)_4]^-$ units, whereas the other remains molecular (**4.2**), with mono-coordinated anionic units. This structural difference changes the magnetostructural parameter of the Cu–O–Cu angle such that, according to the well-established magnetostructural equation, the 1-D chain, with an angle of 96.24(19)°, is predicted to be ferromagnetically coupled, whereas the molecular complex, with an angle of 98.92(17)°, is predicted to be antiferromagnetically coupled. The magnetism of **4.1** was examined and fit to produce a J value ranging between 31.9 and 56.2 cm^{-1}, as compared to the calculated expected value of 97 cm^{-1}. A similar Cu(II) dimer complex, $[\{Cu(tmeda)(\mu\text{-}OH)\}_2Au(CN)_4][ClO_4]\bullet MeOH$ (**4.3**) was also synthesized and characterized, showing a Cu–O–Cu angle average of 98.4°. This suggests antiferromagnetic interactions with a predicted J value of –63.75 cm^{-1}, which were confirmed through magnetic studies, with a J value of –59.5 cm^{-1}.

These examples represent the first complexes of $[Cu(tmeda)(\mu\text{-}OH)]_2^{2+}$ dimers where the Cu–O–Cu angles are lower than 100° and thus the first complex (**4.1**) that exhibits ferromagnetic coupling. This suggests that anionic coordination and particularly anionic bridging, can greatly influence the magnetic properties of hydroxo-bridged Cu(II) dimers.

4.5 EXPERIMENTAL

General experimental details were as indicated in Chapter 2, with the addition of the use of the amine ligand N,N,N′,N′-tetramethylethylenediamine (tmeda) and ammonium hydroxide (NH_4OH), which were also obtained from commercial sources and used as received.

4.5.1 Preparation of $[Cu(tmeda)(\mu\text{-}OH)]_2(ClO_4)_2$

The dimer starting material was prepared in a similar fashion to the published methods [262], although a larger amount of solvent was required for ease of filtration and to avoid emulsification. This excess of solvent resulted in a low yield (due to solubility of the product). To a 10 mL aqueous solution of $Cu(ClO_4)_2\bullet 6H_2O$ (2.445 grams, 6.6 mmol) was added a 1 mL neat solution (6.6 mmol) of tmeda. An immediate blue precipitate formed, which was separated by filtration, washed with 5 mL of ethanol and vacuum dried for 3 hours to produce a purple powder of $[Cu(tmeda)(\mu\text{-}OH)]_2(ClO_4)_2$. The product slowly takes up water, therefore it should be stored under nitrogen. Yield:

1.98 grams (17%). Anal. Calcd for $C_{12}H_{34}N_4Cu_2Cl_2O_{10}$: C, 24.33; H, 5.78; N, 9.46. Found: C, 24.03; H, 5.82; N, 9.34. IR (KBr): 3611, 3605, 1479, 1470, 1092 (s, br) 1019, 951, 807, 767, 624, 598, 516, 419 cm^{-1}.

4.5.2 Preparation of the 1-D Chain [{Cu(tmeda)(μ-OH)}$_2$Au(CN)$_4$][Au(CN)$_4$] (4.1)

Numerous reactions were attempted to produce maximum yield. The two most successful are outlined below. The crystallographic data was collected on a recrystallized sample of the second preparation method (as described in 4.5.2.2), whereas the magnetic data was collected on a sample of the first preparation method.

4.5.2.1 Preparation Using Dimer Starting Material

The starting material dimer [Cu(tmeda)(μ-OH)]$_2$(ClO$_4$)$_2$ (34 mg, 0.057 mmol) was added to 20 mL of water and stirred vigorously for 1 hour, then filtered to remove undissolved impurities. To the resulting blue solution was added a 5 mL aqueous solution of KAu(CN)$_4$ (48 mg, 0.14 mmol) drop-wise while stirring. This mixture was left to stir for 10 minutes, at which point a light blue precipitate was separated by filtration, washed with 1 mL of water, then air-dried overnight to yield a blue powder of [{Cu(tmeda)(μ-OH)}$_2$Au(CN)$_4$][Au(CN)$_4$] (**4.1**). Yield: 20 mg (37%). Anal. Calcd. for $C_{20}H_{34}N_{12}Au_2Cu_2O_2$: C, 24.13; H, 3.44; N, 16.88. Found: C, 24.28; H, 3.42; N, 16.73. IR (KBr): 2193 (νCN, w), 2181 (νCN, vw), 1469, 1283, 1245, 1124, 1045, 1021, 1001, 952, 807, 767, 482, 422, 415 cm^{-1}.

4.5.2.2 *In Situ* Preparation

To a 5 mL aqueous solution of Cu(ClO$_4$)$_2$•6H$_2$O (28 mg, 0.075 mmol) was added a 2 mL aqueous stock solution (0.150 mmol) of tmeda. While stirring, a 5 mL aqueous solution of KAu(CN)$_4$ (51 mg, 0.150 mmol) was added drop-wise to this dark blue solution. This mixture was left to stir for 10 minutes, at which point a light blue precipitate was separated by filtration, washed with 1 mL of water, then air-dried overnight to yield a blue powder of [{Cu(tmeda)(μ-OH)}$_2$Au(CN)$_4$][Au(CN)$_4$] (**4.1**). After several weeks of slow evaporation of the filtrate (covered in perforated parafilm), a crystalline solid was also collected by filtration, washed with 1 mL of water and air-dried overnight. Total yield: 30 mg (83% based on the Cu(II) limiting reagent). Anal. Calcd. for $C_{20}H_{34}N_{12}Au_2Cu_2O_2$: C, 24.13; H, 3.44; N, 16.88. Found: C, 24.40; H, 3.39; N, 16.81. IR (KBr): 2193 (νCN, w br), 1468, 1284, 1245, 1124, 1045, 1020, 1000, 952, 846, 806, 767, 490, 421, 414 cm^{-1}. The crystalline solid and initial powder samples had comparable IR spectra. To obtain an X-ray quality crystal, a 5 mg portion of the powder sample was

dissolved in 2 mL of NH_4OH and allowed to slowly evaporate (covered in perforated parafilm). After one week, large crystals and crystalline powder of **4.1** were obtained via filtration and washed with small amounts of water. Both the crystals (hand picked using a microscope and forceps) and powder had comparable EA and IR spectrum to that of the initial powder sample.

4.5.3 Preparation of $[\{Cu(tmeda)(\mu\text{-}OH)\}_2Au(CN)_4][ClO_4]\bullet MeOH$ (4.3)

Similar to the synthesis of **4.1**, numerous reactions were attempted to produce maximum yield and optimum purity. The two most successful are outlined below, but all X-ray and magnetic data was obtained using samples from the second method.

4.5.3.1 Preparation Using Dimer Starting Material

The starting material dimer $[Cu(tmeda)(\mu\text{-}OH)]_2(ClO_4)_2$ (44 mg, 0.075 mmol) was added to 40 mL of warm methanol and stirred vigorously for 1 hour. To the resulting green solution was added a 10 mL methanolic solution of $KAu(CN)_4$ (50 mg, 0.15 mmol), resulting in 6 mg of an immediate light blue precipitate, which was filtered, washed with 1 mL of methanol and air-dried for several hours. The IR spectrum of this product was consistent with primarily $KClO_4$ (main absorption peak at 1100 cm^{-1}). The resulting filtrate was left to slowly evaporate (covered in perforated parafilm), yielding X-ray quality blue crystals of $[\{Cu(tmeda)(\mu\text{-}OH)\}_2Au(CN)_4][ClO_4]\bullet MeOH$ (**4.3**) over several weeks. The crystals were separated from the solution (volume of solution decreased by approximately 1/2) after 3 weeks using a pipette, were washed with small amounts (< 1 mL) of methanol and air-dried overnight. Yield: 25 mg (40%). IR (KBr): 2187 (νCN, w), 1478, 1474, 1469, 1461, 1291, 1283, 1246, 1091, 1045, 1021, 1003, 951, 807, 767, 638, 625, 492, 441, 413 cm^{-1}.

4.5.3.2 *In Situ* Preparation

To a 10 mL methanolic solution of $Cu(ClO_4)_2\bullet 6H_2O$ (111 mg, 0.30 mmol) was added a 4 mL methanolic stock solution (0.130 mmol) of tmeda. Five drops of NH_4OH was added to the green solution. While stirring, a 10 mL methanolic solution of $KAu(CN)_4$ (102 mg, 0.30 mmol) was added drop-wise, resulting in 21 mg of an immediate light blue precipitate, which was filtered, washed with 1 mL of methanol and air-dried overnight. The IR spectrum of this product was consistent with $KClO_4$. The resulting filtrate was left to slowly evaporate, (covered in perforated parafilm) yielding X-ray quality blue crystals of $[\{Cu(tmeda)(\mu\text{-}OH)\}_2Au(CN)_4][ClO_4]\bullet MeOH$ (**4.3**) over several weeks. The crystals were separated from the solution (volume of solution decreased by approximately 3/4)

after 2 weeks using a pipette, were washed with 2 mL of methanol and air-dried overnight. Yield: 109 mg (44%). Anal. Calcd for $C_{16}H_{34}N_8Au_1Cu_2ClO_6 \bullet CH_3OH$: C, 24.72; H, 4.64; N, 13.57. Found: C, 23.92; H, 4.60; N, 13.40. IR (KBr): 2187 (νCN, w), 1475, 1470, 1462, 1283, 1248, 1100 (s, br), 1046, 1022, 1003, 952, 807, 768, 623, 493, 413 cm^{-1}.

CHAPTER 5

OTHER ENDEAVORS AND GLOBAL CONCLUSIONS

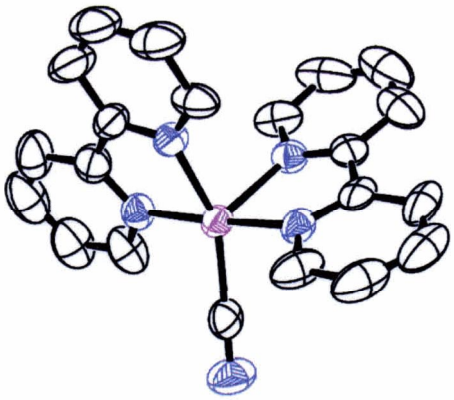

5.1 TETRAHEDRAL CYANOMETALLATES

5.1.1 Tetrahedral Cyanometallates in Coordination Polymers and Applications

Although four-coordinate cyanometallates have previously been discussed, all previous discussions have focused on square planar cyanometallates. Tetrahedral cyanometallates, such as $[Cd(CN)_4]^{2-}$ and $[Hg(CN)_4]^{2-}$ also exist and have been incorporated into coordination polymers [80,307-309]. The tetrahedral geometry of the cyanometallate increases the probability of a non-centrosymmetric product. This is of interest as acentricity is a requirement for the existence of second order non-linear optical (NLO) properties, as well as other interesting electrical phenomena [14]. Crystal structures of tetrahedral cyanometallates of the coinage metals Ag(I) and Cu(I) have been reported [310,311], but have never been used in coordination polymers with other transition metals. The use of the coinage metal cyanometallates is of interest due to the possibility of metal–metal interactions in the resulting product, thus pairing the acentricity with high-dimensionality and increased stability.

The structure of $K_3Ag(CN)_4$ was reported in 1956 [311] whereby the crystals were isolated from the evaporation of an aqueous solution containing potassium cyanide and silver cyanide in a molar ration of 3:1. This $[Ag(CN)_4]^{3-}$ unit has also been reported in recent crystal structures [312] and thus the potential of incorporating it into a supramolecular array is promising. Likewise, the structure of $K_3Cu(CN)_4$ has long been known [310] and has been successfully used in the formation of a supramolecular system, though the system has been studied only in terms of its porosity [313].

5.1.2 Reactions, Results and Analyses using $[Ag(CN)_4]^{3-}$

As has been detailed in early literature, the procedure to make $K_3Ag(CN)_4$ was performed by evaporating an aqueous solution of 3KCN and AgCN [311]. The resulting starting material had unreacted AgCN impurities in it, as observed from the IR spectrum and thus was reacted with an additional quantity of KCN (see Section 5.1.5). The final product had an IR spectrum similar to that published, but the elemental analysis showed impurities. The starting material was still used, assuming the main component of the material was the desired $K_3Ag(CN)_4$.

Over 20 reactions were conducted with combinations of the following components in either water or methanol solutions: Transition metals: Cu^{2+}, Ni^{2+}, Zn^{2+}, Mn^{2+}, Fe^{3+}, Cr^{3+}; Ligands (1 or 2 equiv.): bipy, en, dien, tren, phen, pyz; and the required amount of $K_3Ag(CN)_4$ to balance the transition metal charge. A representative experimental can be found in Section 5.1.5. The νCN stretches in the infrared spectra of the resulting products were compared to the experimental value (νCN = 2096 ± 2 cm^{-1}) of the $K_3Ag(CN)_4$ to determine whether the $[Ag(CN)_4]^{3-}$ moiety was present and possibly bound. The results of these examinations showed a surprising trend, as seen in Table 5.1. Depending on the time span elapsed from the mixing of the reactants and the extraction of the product, the νCN stretches show significant changes for most reactions. In most cases, the νCN stretches shifted to higher frequency in later products as compared to the earlier products. "Early" products were generally those that precipitated immediately, or crystallized out of the reactant mixture after one or two days, whereas the "later" products required weeks, sometimes months of slow evaporation for precipitation.

These IR changes suggest that the $[Ag(CN)_4]^{3-}$ moiety is likely in equilibrium. This has been the subject of numerous solution studies (both aqueous and ammonia solutions) of silver(I) cyanides, as was previously discussed in relation to the $[Ag(CN)_2]^-$ moiety in Chapter 2. In aqueous solutions, it has been shown that the ions $[Ag(CN)_2]^-$,

$[Ag(CN)_3]^{2-}$ and $[Ag(CN)_4]^{3-}$ all exist, with their CN stretches occuring at 2135, 2105 and 2092 cm^{-1} respectively [67,152]. It is thus not surprising, considering this equilibrium, that purifying the products was a challenge.

Table 5.1 – IR Results for Reactions with the $[Ag(CN)_4]^{3-}$ Moiety*

Transition Metal	Ligand	"Early" product νCN band (cm^{-1})	"Late" Product νCN band (cm^{-1})
Cu(II)	en	2098, 2118	2076, 2091
Cu(II)	2en	2078, 2090	2138
Cu(II)	tren	2088 (broad)	2069, 2099, 2125, 2130
Cu(II)	dien	2136, 2118	no change
Cu(II)	2bipy	2104, 2128, 2140	2133
Cu(II)	pyz	2125	N/A
Ni(II)	en	2121, 2149	2138, 2156
Ni(II)	tren	2127, 2147	2139, 2168
Ni(II)	dien	2132, 2160	2116, 2126, 2140
Mn(II)	phen	2116	N/A
Zn(II)	en	2218	N/A
Zn(II)	dien	N/A	2133
Fe(III)	bipy	2070	2060, 2086, 2140
Fe(III)	2bipy	2070, 2135	2059, 2140
Cr(III)	bipy	N/A	2132
Fe(III)	phen	2065, 2080	no change

* See Section 5.1.5 for a representative experimental description. "Early" products precipitated within 2 days of the mixing of the reactants, whereas "late" products precipitated after at least 3 days.

Many of the products showed visible impurities and thus it became very difficult to confidently suggest their composition. Futhermore, despite many attempts, the preparation of X-ray quality crystals was not successful in most cases. The only reactions with identifiable products (from crystal structures) are discussed briefly in the following sections, with the experimental procedure in Section 5.1.5.

5.1.2.1 Reaction of $3[Cu(en)_2]^{2+} + 2[Ag(CN)_4]^{3-}$

Very large, purple crystals were deposited from an aqueous solution of 3 equivalents of $[Cu(en)_2]^{2+}$ and 2 equivalents of $[Ag(CN)_4]^{3-}$ after several days. The IR spectrum

shows two νCN stretches at 2090 and 2078 cm^{-1}. The X-ray structure showed, however, that these bands were not attributable to the presence of $[Ag(CN)_4]^{3-}$, but to the presence of Cu(I) cyanides. The resulting formula, from X-ray analysis, was $Cu(en)_2Cu_2(CN)_4 \bullet H_2O$ – a previously published compound with identical unit cell parameters to the resulting product of this reaction [314]. This suggests that the free cyanide in solution has reacted with Cu(II) (as discussed in Chapter 2), thus forming the Cu(I) cyanide moieties. The versatility of the Cu(I) cyanide moiety to form $[Cu_x(CN)_y]^{n-}$ structural motifs to accommodate various geometric requirements has been previously discussed [315,316]. There are also a variety of research groups examining Cu(I) cyanide/Cu(II) mixed valent coordination polymers [315,317-319].

Later extractions from the same solution showed a significant shift of the νCN band to 2139 cm^{-1}, suggesting the presence of $[Ag(CN)_2]^-$ and accounting for the lack of observed Ag(I) in the crystal structure.

5.1.2.2 Reaction of $3[Cu(dien)]^{2+} + 2[Ag(CN)_4]^{3-}$

From the aqueous filtrate solution of 3 equivalents of $[Cu(dien)]^{2+}$ and 2 equivalents of $[Ag(CN)_4]^{3-}$, very small blue crystals were extracted after one month. The IR analysis showed two νCN stretches at 2136 and 2118 cm^{-1} that matched the initial precipitate. The X-ray structure showed that, again, there was no $[Ag(CN)_4]^{3-}$ present. Instead, the resulting formula from the X-ray analysis was $Cu(dien)Cu(CN)_3$, a previously published structure [319].

Although the IR of a salt of $[Cu(CN)_3]^{2-}$ has never been reported, the νCN stretch in aqueous solution has been reported as 2094 cm^{-1} [67] and other Cu(I) cyanide coordination complexes with the moiety have reported νCN bands between 2075 and 2143 cm^{-1} (usually seen as doublets) [89,315], which is consistent with the above IR observations.

5.1.2.3 Reaction of $3[Cu(bipy)_2]^{2+} + 2[Ag(CN)_4]^{3}$

After the removal of an initial precipitate from the reaction of 3 equivalents of $[Cu(bipy)_2]^{2+}$ with 2 equivalents of $[Ag(CN)_4]^{2-}$, the filtrate was allowed to stand undisturbed and yielded blue needle crystals after approximately 1 month. The IR spectrum showed one νCN stretch at 2133 cm^{-1}, which differed from the original precipitate, containing three νCN bands at 2104, 2128 and 2140 cm^{-1}. The X-ray analysis confirmed the suspicion arising from the IR data that the crystal did not contain any Ag(I) cyanide. The X-ray determined formula was $[Cu(bipy)_2CN][ClO_4]$, (**5.1**)

whereby an excess of free cyanide migrated to the Cu(II) centre and this cationic unit was not further coordinated. The two bound equivalents of bipy completed the five-coordinate Cu(II) cation. Although this is a new structure, the $[Cu(bipy)_2CN]^+$ cation with a nitrate anion has been reported and has similar structural parameters [320], and the phen equivalent $[Cu(phen)_2CN]NO_3$ has also been reported [321]. The cationic moiety is shown on page 100.

5.1.3 Reactions, Results and Analyses using $[Cu(CN)_4]^{3-}$

Similar to the procedure described for $[Ag(CN)_4]^{3-}$, the $K_3Cu(CN)_4$ starting material was prepared according to literature methods. Two such methods exist, one starting from CuCN [310] and the other from CuCl [322,323] and both were attempted and the experimental procedures can be found in Section 5.1.5. Neither literature method produced a high purity starting material (as observed from the IR spectra and elemental analyses), but the latter procedure was used as the starting material, assuming that the main component of the material was the desired $K_3Cu(CN)_4$, as it was less likely to contain free cyanide. It should also be noted that recent literature in which a coordination polymer was formed containing the $[Cu(CN)_4]^{3-}$ unit, difficulties in obtaining a starting material salt of $[Cu(CN)_4]^{3-}$ were also expressed [313], and thus the reaction was done with an *in situ* preparation of the $[Cu(CN)_4]^{3-}$ unit from an aqueous solution of CuCN and $3(Bu_4N)CN$.

As was done in the $[Ag(CN)_4]^{3-}$ study, dozens of reactions were conducted with combinations of the following components in either water or methanol solutions: Transition metals: Cu^{2+}, Ni^{2+}; Ligands (1 or 2 equiv.): bipy, en, dien, tmeda, tren, phen; and the required amount of $K_3Cu(CN)_4$ to balance the transition metal charge. A representative experimental for these reactions can be found in Section 5.1.5. The νCN stretches in the IR spectra of the resulting products were compared to the reported νCN stretches of $K_3Cu(CN)_4$ (2075, 2081 and 2094 cm^{-1}) [67,324] and the coordination polymer containing the $[Cu(CN)_4]^{3-}$ unit (2104 cm^{-1}, broad) [313] to determine whether the $[Cu(CN)_4]^{3-}$ moiety was present and possibly bound. The results of these examinations, as seen in Table 5.2, suggest the possibility of both bound $[Cu(CN)_4]^{3-}$ *and/or* the possibility of the presence of other Cu(I) cyanides (any combination of $[Cu_x(CN)_y]^{n-}$). Although there were variations in IR spectra depending on the time elapsed for product formation, the more interesting data obtained pertains to the elemental analyses data, as depicted in Table 5.2.

Table 5.2 – IR and EA Results for Reactions with the $[Cu(CN)_4]^{3-}$ Moiety

Cation (all 2+)	Product vCN band (cm^{-1})	Actual EA**	EA calc $[Cation]_3[Cu(CN)_4]_2$	EA calc $[Cation]Cu_2(CN)_4$
$Cu(en)_2$	2098, 2116 /* 2076, 2091			
Cu(dien)	2100, 2130	C: 24.81 H: 3.46 N: 24.41	C: 28.76 H: 4.71 N: 28.50	C: 24.15 H: 3.29 N: 24.64
$Ni(en)_2$	2106 / 2146, 2116	C: 23.53 H: 3.99 N: 26.17	C: 27.55 H: 5.55 N: 32.13	C: 23.43 H: 3.93 N: 27.33
Ni(en)	2143 (broad)	C: 20.58 H: 2.48 N: 23.72	C: 24.31 H: 3.47 N: 28.36	C: 20.58 H: 2.30 N: 24.01
Ni(tmeda)	2136	C: 28.93 H: 4.41 N: 19.25	C: 36.32 H: 5.63 N: 22.80	C: 28.32 H: 4.28 N: 19.82 (w/ 1 H_2O)
Ni(tren)	2100 / 2130, 2140	C: 27.49 H: 4.31 N: 25.58	C: 32.87 H: 5.69 N: 29.50	C: 27.54 H: 4.16 N: 25.70

* / ≡ divides earlier product vCN from later product vCN stretches (when applicable)
** EA always taken of first (earlier) product

The elemental analyses corresponded to the general formula $[TM(ligand)_n][Cu_2(CN)_4]$ rather than the expected coordination polymer containing the $[Cu(CN)_4]^{3-}$ unit. This general formula has been previously reported as the product in many reactions of transition metal cations (primarily Cu(II)) with Cu(I) cyanide [89,314,318,325].

To confirm this finding, X-ray data of a crystal formed from the aqueous reaction solution containing 3 equivalents of $[Cu(en)_2]^{2+}$ and 2 equivalents of the Cu(I) cyanide starting material was collected (experimental can be found in Section 5.1.5). The unit cell confirmed that the resulting product was actually the previously reported $[Cu(en)_2H_2O][Cu_2(CN)_4]$ [314]. This suggests that the elemental analyses trends in Table 5.2 are correct and the stable product formed in most cases is of the general formula $[TM(ligand)_n][Cu_2(CN)_4]$.

Because Cu(II)/Cu(I) mixed valent cyanide polymers have been well documented as compared to Ni(II)/Cu(I) cyanide polymers, a crystal structure was also obtained from a crystal formed from the aqueous reaction solution containing 3 equivalents of $[Ni(en)_2]^{2+}$ and 2 equivalents of the Cu(I) cyanide starting material. This crystal product formed after 2 months of elapsed time in solution and showed vCN stretches at 2146 and 2116 cm^{-1}. The X-ray structure showed that Cu(I) cyanide was not present in this final

product, but instead the very stable $[Ni(CN)_4]^{2-}$ anion accounted for the observed νCN stretch. The resulting structure of $Ni(en)_2Ni(CN)_4 \bullet xH_2O$ has been previously published [105]. Although the final product was not of interest, the process by which it was formed was. The formation of $[Ni(CN)_4]^{2-}$ with longer elapsed reaction times suggests the presence of an excess of free cyanide in the reactant solution that may have resulted from impurities in the starting material, or the dissociation of the starting material to the $[Cu_2(CN)_4]^{2-}$ unit that was observed in many of the elemental analyses (thus resulting in free cyanide).

5.1.4 Conclusions and Outlook for Tetrahedral d^{10} Cyanometallate Building Blocks

The results with $[Ag(CN)_4]^{3-}$ did not confirm the formation of any coordination polymers containing the $[Ag(CN)_4]^{3-}$ unit and were complicated by the formation of other side products due to the excess of cyanide used to make the starting material, paired with the equilibria in aqueous solution of the $[Ag(CN)_4]^{3-}$ unit. All reactions showed that the excess cyanide was problematic, reacting with Cu(II) to form Cu(I) cyanides, and binding through the carbon atom to Cu(II) atoms, thus occupying needed coordination sites for polymer formation. The *in situ* formation of $[Ag(CN)_4]^{3-}$ with stoichiometric amounts of CN^- may be a useful method in forming the desired complexes, as it would eliminate the substantial amount of excess cyanide that was required for the solid starting material.

The results of the reactions with $[Cu(CN)_4]^{3-}$ showed that the stable product formed in most cases was of the general formula $[TM(ligand)_n][Cu_2(CN)_4]$, rather than the expected $[TM(ligand)_n]_3[Cu(CN)_4]_2$. The crystal structure of $Ni(en)_2Ni(CN)_4$ suggests the presence of excess cyanide in the reactant solution. Because a coordination polymer containing the $[Cu(CN)_4]^{3-}$ unit does exist, despite the results presented in this thesis, the goal remains achievable. Most likely, the impurities present in the starting material contributed to the observed outcomes, and further attempts to use other starting materials (with other counter-ions, and preferably formed *in situ*) is still a promising endeavor. This is more promising than using the $[Ag(CN)_4]^{3-}$ unit, as Cu(I) cyanides have been shown to be more stable and undergo less equilibrium reactions in solution as compared to Ag(I) cyanides [67].

5.1.5 Experimental Descriptions for Tetracyanometallate Reactions

Many of the reactions performed with the tetracyanometallates resulted in impure products that could not be conclusively characterized. Due to such difficulties, only a representative experimental description for each series of reactions is reported, along with the experimental for any reactions that did produce characterizable products.

5.1.5.1 Preparation of $KAg(CN)_4$ Starting Material

To a round bottom flask covered in foil, containing 250 mL of water, was added 1.339 grams (10 mmol) of AgCN and 1.953 grams (30 mmol) of KCN. The suspension was stirred for 6 hours until all AgCN had fully dissolved. The water was then removed via rotovap and the flask was placed under vacuum to thoroughly dry the resulting white product. Yield: 3.161 grams (96%). At this point, the IR showed a peak at 2140 cm^{-1}, indicating the presence of $KAg(CN)_2$ and thus the product was redissolved in 100 mL of water, to which an additional 1.013 grams (15.6 mmol) of KCN was added, with stirring. This solution was stirred for an additional 1 hour, then all solvent was evaporated using a rotovap. The white product was dried thoroughly on a vacuum line for 2 hours. Anal. Calcd. for $K_3AgC_4N_4$: C, 14.59; H, 0.00; N, 17.02. Found: C, 13.29; H, 0.55; N, 14.53 (indicating the product is still slightly wet and impure). IR (KBr): 2096 cm^{-1} as expected from the literature value [67].

5.1.5.2 Representative Experimental Procedure for Reactions with $[Ag(CN)_4]^{3-}$

To a 4 mL aqueous solution of $Cu(ClO_4)_2 \bullet 6H_2O$ (279 mg, 0.75 mmol) was added a 1 mL aqueous stock solution of en (0.75 mmol). The resulting solution was stirred for 5 minutes. While stirring, a 3 mL aqueous solution of the prepared (see above) $K_3Ag(CN)_4$ (165 mg, 0.50 mmol) was added drop-wise to the dark purple solution. An immediate green precipitate was formed, which was filtered, washed with 2 mL of water and air-dried overnight. Yield of this "early" product: 77 mg (13%). Anal. Calcd. for $Cu_3C_6H_{24}N_6Ag_2C_8N_8$ (assuming $[Cu(en)]_3[Ag(CN)_4]_2$): C, 21.16; H, 3.04; N, 24.67. Found: C, 21.25; H, 3.02; N, 24.85. Ir (KBr): 3346, 3286, 2118 (νCN), 2098 (νCN), 1580, 1275, 1089, 1042, 1012, 657, 518 cm^{-1}.

The remaining purple filtrate was covered with parafilm and left undisturbed. After 6 weeks, several small purple crystals were deposited within the solution, with no apparent change in the volume of the solution. These crystals were extracted with a pipette, washed with 1 mL of water and air-dried overnight. Yield of this "later" product: 6 mg. Yield was not sufficient for elemental analysis. IR (KBr): 3308, 3232, 2091 (νCN), 2076

(νCN), 1122, 1089, 1036, 689, 518 cm^{-1}. The remaining solution was still purple in colour.

5.1.5.3 Reaction of $3[Cu(en)_2]^{2+} + 2[Ag(CN)_4]^{3-}$

To a 5 mL aqueous solution of $Cu(ClO_4)_2 \bullet 6H_2O$ (140 mg, 0.38 mmol) was added a 1 mL aqueous stock solution of en (0.75 mmol). The resulting solution was stirred for 5 minutes. While stirring, a 5 mL aqueous solution of the prepared $K_3Ag(CN)_4$ (83 mg, 0.25 mmol) was added drop-wise to the dark purple solution. No precipitate was formed, so the resulting purple solution was covered with parafilm and left undisturbed. After two days, purple crystals were deposited from the solution, which were removed from the solution with a pipette, washed with 1 mL of water and air-dried overnight, Yield of this "early" product: 25 mg (13%). The resulting formula, from X-ray analysis, was $Cu(en)_2Cu_2(CN)_4 \bullet H_2O$ – a previously published compound with identical unit cell parameters to the resulting product of this reaction [314]. IR (KBr): 3308, 3273, 3236, 2090 (νCN), 2078 (νCN), 1580, 1574, 1461, 1454, 1278, 1090, 1036, 1012, 684, 657 cm^{-1}.

The remaining purple filtrate was covered with perforated parafilm and left undisturbed. After 5 weeks, purple precipitate had formed within the solution (which had evaporated to approximately 3/4 volume). This precipitate was filtered, washed with 2 mL of water and air-dried overnight. Yield of this "later" product: 78 mg. Elemental analysis was not attempted due to visible impurities in the product (as observed by color difference) and the presence of the 2138 cm^{-1} νCN stretch, which would be indicative of rearrangement of the $[Ag(CN)_4]^{3-}$ moiety to $[Ag(CN)_2]^-$. IR (KBr): 3335, 3255, 2138 (νCN), 1581, 1574, 1268, 1084, 1024, 697, 626, 527 cm^{-1}. The remaining solution was still purple in colour.

5.1.5.4 Reaction of $3[Cu(dien)]^{2+} + 2[Ag(CN)_4]^{3-}$

To a 5 mL aqueous solution of $Cu(ClO_4)_2 \bullet 6H_2O$ (140 mg, 0.38 mmol) was added a 1 mL aqueous stock solution of en (0.38 mmol). The resulting solution was stirred for 5 minutes. While stirring, a 5 mL aqueous solution of the prepared $K_3Ag(CN)_4$ (83 mg, 0.25 mmol) was added drop-wise to the dark blue solution. No precipitate was formed, so the resulting purple solution was covered with parafilm and left undisturbed. After one day, blue precipitate was formed, which was filtered, washed with 1 mL of water and air-dried overnight. Yield of this "early" product: 10 mg. IR (KBr): 3326, 3270, 3155,

2975, 2925, 2873, 2136 (νCN), 2118 (νCN), 1580, 1446, 1461, 1454, 1322, 1147, 1075, 1055, 1031, 999, 529, 526 cm^{-1}.

From the aqueous filtrate, very small blue crystals were deposited after one month, extracted with a pipette, washed with 1 mL of water and air-dried. Yield of this later product: 4 mg (total yield = 8%). The IR analysis was identical to the earlier product. Due to the small size of the crystals, an H-tube was prepared of the same reaction (same reactant quantities) in methanol and after one month, several of the larger blue crystals (13 mg total) were extracted using a pipette. The crystals were washed with 1 mL of water and air-dried. The IR spectrum was identical to the early precipitate described above. The resulting formula from the X-ray analysis was $Cu(dien)Cu(CN)_3$, a previously published structure [319]. Anal. Calcd. for $CuC_4H_{13}N_3CuC_3N_3$: C, 27.11; H, 4.25; N, 27.26. Found: C, 27.11; H, 4.23; N, 27.05. The remaining solution was still blue in colour.

5.1.5.5 Preparation of $[Cu(bipy)_2CN][ClO_4]$ (5.1)

To a 10 mL aqueous solution of $Cu(ClO_4)_2 \bullet 6H_2O$ (111 mg, 0.30 mmol) was added a 10 mL methanolic stock solution of bipy (94 mg, 0.60 mmol). The resulting solution was stirred for 5 minutes. While stirring, a 8 mL mixed solution (50:50 $MeOH:H_2O$) of the prepared $K_3Ag(CN)_4$ (66 mg, 0.20 mmol) was added drop-wise to the dark blue solution. After several hours of stirring, a light purple precipitate was formed, which was filtered, washed with 2 mL of water and air-dried overnight. Yield of this "early" product: 28 mg (7%). Anal. Calcd. For $Cu_3C_{60}H_{48}N_{12}Ag_2C_8N_8$ (assuming product = $[Cu(bipy)_2]_3[Ag(CN)_4]_2$): C, 52.64; H, 3.12; N, 18.05. Found: C, 52.44; H, 3.06; N, 20.30. IR (KBr): 2140 (νCN), 2128 (νCN), 2104 (νCN), 1600, 1567, 1494, 1475, 1445, 1315, 1062, 1027, 769, 731 cm^{-1}.

The filtrate was allowed to stand undisturbed and began to yield blue needle crystals after several weeks (with no apparent change in solution volume). After 7 weeks, these crystals were extracted from the solution with a pipette, washed with 1 mL of water and air-dried. Yield of this "later" product: 22 mg (21%). The X-ray analysis confirmed the product to be $[Cu(bipy)_2CN][ClO_4]$ (**5.1**). IR (KBr): 2133 (νCN), 1605, 1599, 1567, 1494, 1475, 1442, 1318, 1251, 1176, 1161, 1092 (broad), 1027, 1013, 903, 764, 633, 624, 417 cm^{-1}.

5.1.5.6 Preparation of $K_3Cu(CN)_4$ Starting Material

From CuCN: To 175 mL of water in a round bottom flask was added 896 mg (10 mmol) of CuCN and 1.96 grams (30 mmol) of KCN. This solution was stirred for 3 days

and then the solution was boiled to dryness using an oil bath. The white powder product turned brown upon cooling. Yield: 2.475 grams (87%). The product was recrystallized from 75 mL of warm water and dried on a vacuum line for 3 hours to form a white powder. Anal. Calcd. for $K_3CuC_4N_4$: C, 16.86; H, 0.00; N, 19.66. Found: C, 15.76; H, 0.64; N, 15.54. IR (KBr): 2170 (νCN), 2082 (νCN), 1599, 1381 (broad) 803 cm^{-1}.

From CuCl: To 125 mL of water at 60 °C was added 6.5 grams of KCN (0.10 mol) and 3 grams (0.03 mol) of CuCl. The solution was stirred at 60 °C for 3 days until the volume had been reduced to half. The solution was then placed under vacuum until all the solvent had evaporated (several hours). Yield of the white solid: 9.160 grams (>100%). Anal. Calcd for $K_3CuC_4N_4$: C, 16.86; H, 0.00; N, 19.66. Found: C, 12.24; H, not reported; N, 13.18. IR (KBr): 2082 (νCN), 1392 (br) cm^{-1}.

5.1.5.7 Representative Experimental Procedure for Reactions with $[Cu(CN)_4]^{3-}$

To a 5 mL aqueous solution of $Cu(ClO_4)_2 \bullet 6H_2O$ (140 mg, 0.38 mmol) was added a 1 mL aqueous stock solution of dien (0.38 mmol). The resulting solution was stirred for 5 minutes. While stirring, a 5 mL aqueous solution of the prepared $K_3Cu(CN)_4$ (72 mg, 0.25 mmol) (from CuCl, see above) was added drop-wise to the dark blue solution. An immediate blue precipitate was formed, which was filtered, washed with 2 mL of water and air-dried overnight. Yield: 47 mg (47%). Anal. Calcd. for $CuC_4H_{13}N_3Cu_2C_4N_4$ (assuming $[Cu(dien)]Cu_2(CN)_4$): C, 24.15; H, 3.29; N, 24.64. Found: C, 24.81; H, 3.46; N, 24.41. IR (KBr): 3340, 3303, 3263, 3237, 2130 (νCN), 2100 (νCN), 1587, 1470, 1127, 1077, 1008, 953, 530 cm^{-1}.

5.1.5.8 Reaction of $3[Cu(en)_2]^{2+} + 2[Cu(CN)_4]^{3-}$

To a 5 mL aqueous solution of $Cu(ClO_4)_2 \bullet 6H_2O$ (68 mg, 0.19 mmol) was added a 5 mL aqueous stock solution of en (0.37 mmol). The resulting solution was stirred for 5 minutes. While stirring, a 5 mL aqueous solution of the prepared $K_3Cu(CN)_4$ (35 mg, 0.12 mmol) was added drop-wise to the dark purple solution. An immediate blue precipitate was formed, which was filtered, washed with 2 mL of water and air-dried overnight. Yield: 10 mg. IR (KBr): 3347, 3287, 2116 (νCN), 2098 (νCN), 1577, 1047, 1013, 660, 520 cm^{-1}.

The filtrate was covered with parafilm and left undisturbed for several days. After 1 week, several crystals were extracted from the solution with a pipette (with no apparent change of solution volume). The unit cell from X-ray data showed that the resulting product was the previously reported $[Cu(en)_2H_2O][Cu_2(CN)_4]$ [314]. Yield was not

sufficient for elemental analysis. IR (KBr): 3310, 3237, 2091, 2076, 1580, 1277, 1083, 1037, 665, 466, 420 cm^{-1}.

5.1.5.9 Reaction of $3[Ni(en)_2]^{2+}$ + $2[Cu(CN)_4]^{3-}$

To a 5 mL aqueous solution of $Ni(NO_3)_2 \bullet 6H_2O$ (53 mg, 0.19 mmol) was added a 5 mL aqueous stock solution of en (0.37 mmol). The resulting solution was stirred for 5 minutes. While stirring, a 5 mL aqueous solution of the prepared $K_3Cu(CN)_4$ (35 mg, 0.12 mmol) was added drop-wise to the purple solution. An immediate purple precipitate was formed, which was filtered, washed with 2 mL of water and air-dried overnight. Yield: 14 mg (29%). Anal. Calcd. for $NiC_4H_{16}N_4Cu_2C_4N_4$ (assuming product is $[Ni(en)_2]Cu_2C_4N_4$): C, 23.43; H, 3.93; N, 27.33. Found: C, 23.53; H, 3.99; N, 26.17. IR (KBr):.3334, 3283, 2106, 1573, 1020, 965, 662, 503 cm^{-1}.

The filtrate was covered with parafilm and left undisturbed for 1 month. After no change, holes were poked in the parafilm and the solution was left to slowly evaporate. After another 3 weeks, the solution had evaporated to approximately 2/3 volume and crystals had formed. These purple crystals were picked out of solution with a pipette, washed with 1 mL of water and air dried. Yield: 7 mg. The X-ray structure showed that this product was actually $Ni(en)_2Ni(CN)_4 \bullet xH_2O$, which has been previously published [105]. IR (KBr): 3334, 3287, 2146 (νCN), 2115 (νCN), 1611, 1585, 1276, 1029, 1004, 965, 685, 671, 520, 430, 419 cm^{-1}. Yield was not sufficient for an elemental analysis.

5.2 FE(II) IN CYANOMETALLATE COORDINATION POLYMERS

5.2.1 Fe(II) in Spin-Transition Compounds

Many sensors and memory devices depend on molecular bistability, such as can be obtained with spin-transition compounds. Iron(II) spin-transition compounds represent one of the best examples of this bistability, as the energy gap between the low-spin (LS) and excited high-spin (HS) state is close to the thermal energy and thus a conversion can be obtained by variation of temperature, pressure or light irradiation [326,327]. Furthermore, because this LS/HS transition also involves a change in bond lengths, supramolecular systems of Fe(II) spin-transition molecules also possess the potential to have large hysteresis properties [158].

It is thus of interest to develop Fe(II) supramolecular coordination polymers using cyanometallates. Concomitant with the research involved in the preparation of this

thesis, this goal was published with the method of using $[Ag(CN)_2]^-$ building blocks. The successful preparation of several Fe(II)/$Ag(CN)_2$ polymers with pyrazine, 4,4′-bipyridine and bispyridylethylene (bpe) as ancillary ligands was published and the study showed that the bpe complex underwent a spin-transition with a large hysteresis loop at 95 K [158]. Although the group has expressed an interest in other $[M^I(CN)_2]^-$ units (M = Cu, Au) as building blocks, they do not refer to metallophilic bonding as a goal with which to increase the dimensionality or strength of the resulting polymers. This has been, and continues to be a goal in this thesis, and thus the choice of building block was the $[Au(CN)_2]^-$ moiety. No Fe(II) spin-transition polymers with this building block have been reported to date, nor have any spin-transition polymers been reported with metallophilic bonding present.

5.2.2 Synthetic Challenges

A major preparation challenge in the formation of polymers with the general formula $[Fe(N\text{-}N)_2Au(CN)_2][Au(CN)_2]$ (where N-N is a chelating amine ligand) is the tendency of Fe(II) to form complexes of the *tris* chelate form $[Fe(N\text{-}N)_3]^{2+}$ [328]. It has been suggested that the bis form will only be stable when the counter-ion is of sufficiently high ligand field strength to affect the pairing of spins [328]. As such, an often employed technique is the formation of the tris complex and subsequent removal of an amine ligand via Soxhlet extraction. This is the procedure used to make $Fe(phen)_2(NCS)_2$ [329], which is known to exhibit an abrupt spin-transition from the S = 2 to the S = 0 spin state at T_c close to 176 K [330]. Due to the similarity of the $[Au(CN)_2]^-$ ligand to the thiocyanate ligand, this method was employed in the attempted formation of $[Fe(phen)_2Au(CN)_2][Au(CN)_2]$ from $[Fe(phen)_3][Au(CN)_2]_2$

Although a Soxhlet extraction using acetone as a solvent was successful in the transformation of $[Fe(phen)_3][SCN]_2$ to the bis form, the same procedure with the successfully synthesized and analyzed $[Fe(phen)_3][Au(CN)_2]_2$ produced no change. It is expected that differences in solubility were responsible for this synthetic difference. Subsequent attempts to form $[Fe(phen)_2Au(CN)_2][Au(CN)_2]$ or $[Fe(bipy)_2Au(CN)_2][Au(CN)_2]$ were also unsuccessful.

To form a bis chelating amine Fe(II) complex, the use of steric bulk was also examined, changing the amine ligand from phen to the methyl substituted 2,9-dimethyl-1,10-phenanthroline (dimphen).

5.2.3 Successful Reactions, Magnetism and Discussion

To react dimphen with Fe(II) without oxidation of Fe(II), an O_2-free solution of 50/50 water/methanol was made by bubbling N_2 through the solution. Under constant N_2 flow, 2 equivalents of dimphen and 1 equivalent of $(NH_4)_2Fe(SO_4)_2$ was dissolved in the solution and 2 equivalents of $KAu(CN)_2$ was subsequently added with constant stirring (experimental in Section 5.2.5). The resulting precipitate had νCN stretches at 2148 and 2173 cm^{-1}, indicating that the $[Au(CN)_2]^-$ had bound to the Fe(II) centre (as shifted from the literature νCN stretch of 2140 cm^{-1} for $KAu(CN)_2$ [67]). The elemental analysis confirmed the product to be $[Fe(dimphen)_2Au(CN)_2][Au(CN)_2]$ (**5.2**) with either one or two equivalents of water. A crystal, however, could not be obtained for X-ray diffraction studies to confirm the identity of the resulting product. Further attempts to obtain product and possible crystals could not produce the same IR or elemental analysis, suggesting possible equilibria in the reaction solution.

Regardless of synthetic difficulties, the magnetic properties of the initial product were studied to determine whether this product displayed spin-transition behavior. The temperature (T) dependence of the molar magnetic susceptibility (χ_M) was measured from 2 to 300 K. The product of the magnetic susceptibility with temperature, $\chi_M T$, was plotted against T, as seen in Figure 5.1. At room temperature the product of $\chi_M T$ was

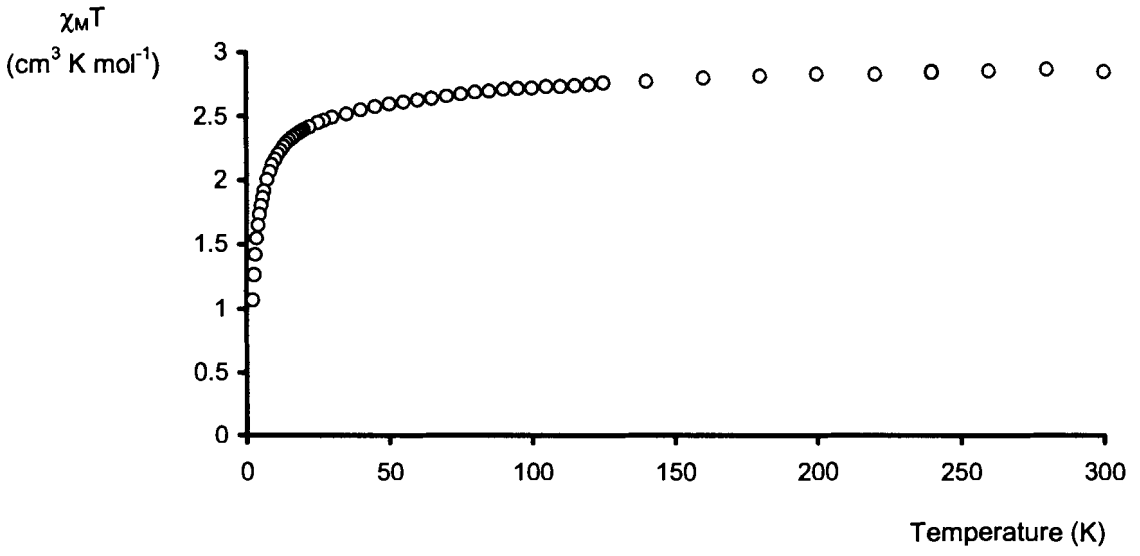

Figure 5.1 – Temperature dependence of the product $\chi_M T$ for $[Fe(dimphen)_2Au(CN)_2][Au(CN)_2]$ (**5.2**).

found to be 2.85 cm^3 K mol^{-1}, only slightly lower than the expected value of 3.00 cm^3 K mol^{-1} for high-spin Fe(II) (S = 2). The $\chi_M T$ value remains relatively constant until approximately 50 K, at which point it drops to 1.06 cm^3 K mol^{-1} at 2 K. This suggests either zero-field splitting, or weak antiferromagnetic interactions between Fe(II) centres.

The absence of an observed low-spin, S = 0 magnetic state suggests that the field strength of the ligands in **5.2** is significantly weaker than those in the spin-transition compound $Fe(phen)_2(SCN)_2$, thus it remains more stable in the high-spin state.

5.2.4 Conclusions and Outlook

The preparation of $[Fe(phen)_2Au(CN)_2][Au(CN)_2]$ was not possible via Soxhlet extraction from the $[Fe(phen)_3][Au(CN)_2]_2$ starting material due the solubility of the starting material. It remains possible, however, that the use of other solvents may produce the desired product, provided the phen ligand is soluble in the chosen solvent while the starting material remains insoluble. Other methods of preparing a bis phenanthroline Fe(II) complex could be attempted as well, as the $[Fe(phen)_2]^{2+}$ cation is likely to produce the molecular bistability needed for spin-transition behavior.

Although the dimphen ligand did not show the desired spin-transition behavior, the use of bulky ligands to prevent the formation of tris-chelate complexes of Fe(II) was successful and the $[Au(CN)_2]^-$ anion did successfully bind, as indicated by the change in νCN stretch of the IR. This suggests that the use of other bulky ligands with Fe(II) and $[Au(CN)_2]^-$ may prove promising for the development of highly dimensional spin-transition complexes.

5.2.5 Preparation of $[Fe(dimphen)_2Au(CN)_2][Au(CN)_2]$ (5.2)

In a round bottom flask, N_2 was bubbled through 14 mL of a 50:50 solution of water:methanol for 10 minutes. To this solution was added 39 mg (0.1 mmol) of $(NH_4)_2Fe(SO_4)_2$ with stirring, resulting in a colorless solution. While stirring, 42 mg (0.2 mmol) of dimephen (obtained from Aldrich) was added. Additional methanol (10 mL) was required for complete dissolution of the ligand (N_2 was bubbled through the methanol prior to addition to the reactant mixture), resulting in a light yellow solution which was allowed to stir for 10 minutes. Meanwhile, a 5 mL aqueous solution of $KAu(CN)_2$ (58 mg, 0.2 mmol) was prepared and N_2 was bubbled through the colorless solution for 10 minutes. This solution was added to the Fe/dimphen solution with stirring. After 15 minutes of stirring under an atmosphere of N_2 a yellow precipitate was

formed. This product was filtered, washed with 2 mL of water and air-dried overnight. Yield: 19 mg (20%). Anal Calcd. for $FeAu_2C_{32}N_8H_{24}\bullet H_2O$: C, 38.87; H, 2.65; N, 11.34. Found: C; 38.52, H; 2.73, N, 11.17. IR (KBr): 2175 (νCN), 2147 (νCN), 1625, 1592, 1510, 1502, 1421, 1357, 1148, 1032, 853, 729, 550, 490, 472 cm^{-1}. The remaining solution (still yellow in colour) was discarded due to potential oxidation of Fe(II).

5.3 GLOBAL CONCLUSIONS AND OUTLOOK

The general goal of this thesis has been to increase the database of interactions and mechanisms for increasing dimensionality of supramolecular heterobimetallic coordination polymers. Although, certainly, this database is far from complete, this thesis has contributed important new tools and trends that should assist in the eventual completion of such an endeavor.

Argentophilic interactions were shown to be capable of increasing dimensionality of heterobimetallic coordination systems, suggesting that the $[Ag(CN)_2]^-$ building block can be used as a tool in a similar fashion to the previously examined $[Au(CN)_2]^-$ building block. Interactions between silver and nitrogen were also observed, contributing another method of increasing dimensionality, although the ability to control and predict such an interaction remains a future goal. Similarly, the lability of the $[Ag(CN)_2]^-$ was shown to produce another building block: $[Ag_2(CN)_3]^-$, but an increased understanding of the factors influencing its formation is required before determining the architectural merit of this building block.

A new building block: $[Au(CN)_4]^-$ was also found to be useful in the preparation of coordination polymers, as it is capable of bridging heteroatom centres through multiple cyanide moieties. The number of cyanides observed to bridge proved to be difficult to predict, suggesting that the addition of more structures with this building block to the database is required to gain a better understanding of its bridging ability. Although no d^8 interactions were observed between Au(III) atoms, the possibility of such interactions remains high; their formation may have been hindered in the complexes studied here by other interactions. The goal, therefore, would be to decrease the number and possibility of other such interactions, thus increasing the possibility of metallophilic interactions.

The $[Au(CN)_4]^-$ building block was also shown to be capable, through coordination, to alter the structural parameters of a $[Cu(tmeda)(\mu\text{-}OH)]^{2+}$ dimer to produce ferromagnetic

interactions. With the aid of $[Au(CN)_4]^-$, this Cu(II) dimer, which has previously only exhibited antiferromagnetic interactions, could be used as a ferromagnetic building block. This example further illustrates the versatility of the $[Au(CN)_4]^-$ building block and the importance of further exploring its chemistry and coordination ability in supramolecular systems.

APPENDIX 1

METALLOPHILIC INTERACTIONS AND RELATIVISTIC EFFECTS

The theoretical evidence, based on a combination of ab initio calculations, semi-empirical calculations and density functional calculations, has suggested that the interactions between d^{10} metal centres originate from correlation effects and are strengthened by relativistic effects [40-48]. However, this thesis illustrates that Ag-Ag and Ag-Cu interactions occur with similar ease to the Au-Au interactions, suggesting that relativistic effects may not be a determining factor. In support of this experimental data, recent calculations have suggested that the relative contribution of each of these effects to the attraction between the Au(I) is 90% correlation effects and only 10% relativistic effects [45]; i.e. relativistic effects are not paramount in the formation of these interactions. Despite this recent suggestion, a large amount of literature pertaining to aurophilic interactions continues to focus on the contribution of relativistic effects [116,331-333], and thus a brief overview of this theory is given in this appendix.

By the most basic of definitions, a bond is considered to be any "strong link" between atoms in a molecule [334] which corresponds to an energy minimum related to the distance between the atoms. Covalent bonding is often expected from open-shell species when such an interaction results in more bonding MO's occupied than antibonding MO's [43]. Closed-shell species would be expected to form strong ionic bonds if they carry opposite charges. In contrast, *neutral* metals with d^{10} electronic configuration, which are formally closed-shell, would be expected to repel each other. There exist, however, many inorganic and organometallic complexes that show evidence of valid interactions between such species such that the interactions, though weaker than most "bonds", are stronger than other van der Waals forces and comparable in strength to hydrogen bonds [43]. It has thus been suggested that the idealized concepts of covalent, ionic and van der Waals bonding are far too simplistic [43]. A combination of attractions are involved, paired also with complications of Pauli repulsion, which together suggest that the most promising discussion of "bonding" requires a much more detailed mathematical investigation and methods. Indeed, such methods have been developed and investigated, most thoroughly perhaps by Pekka Pyykkö, who has published numerous accounts of his theoretical approaches and calculations regarding

these issues [40-48,335]. The details of these calculations, however, are well beyond the scope of this thesis.

Relativistic effects can be defined simply as effects that arise when velocities approach the finite speed of light (c) [331,332]. Because the velocity of electrons as they approach the nucleus increases as the nuclear charge (Z) increases, these effects are often present in atoms with high nuclear charge and account for many of the conspicuous chemical anomalies in the latter half of the periodic table. Relativistic effects cause contraction of atoms because the mass increases (as per the special theory of relativity) and thus, in accordance with Equation A.1, the Bohr radius decreases.

$$a_o = 4\pi\varepsilon_o\hbar^2 / mZe^2 \qquad \text{(Equation A1.1 – Bohr Radius)}$$

The relativistic average radius is expected to be approximately 20% smaller than the non-relativistic one [331]. This contraction is most prominent in the s orbitals, and to a lesser extent, the p orbitals [333].

Also, relativistic effects account for the expansion of d and f orbitals in atoms with high Z. These expansions occurs because the electrons in these orbitals are seldom close enough to the nucleus to reach high velocities, and thus become shielded from the nuclear attraction due to the contracted s and p atomic orbitals (AO's) [331]. Due to this weaker attraction, the d and f atomic AO's expand radially and are destabilized energetically.

The resulting impact of relativistic effects is many-fold and the importance of this effect for gold chemistry was noted over 20 years ago [331,336] and recently summarized [337]. For the purposes of gold(I)–gold(I) interactions, the important impact of relativistic effects comes from the concomitant contraction and expansion of orbitals, which results in an energy gap between the 5d, 6s and 6p orbitals [116].

APPENDIX 2

SUMMARY OF CRYSTALLOGRAPHIC DATA

The following pages contain summary tables of the crystallographic data and refinement details for all reported structures contained in this thesis. The complete list of fractional atomic coordinates and equivalent isotropic thermal parameters (U(iso) in $Å^2$) are collected in Appendix 3. Details regarding the collection data methods can be found in the experimental section of Chapter 2.

Table A2.1 – Summary of Crystallographic Data for Chapter 2

	2.1	2.2	2.3	2.5	2.6
Formula	$C_9H_{16}N_9Ag_3Cu$	$C_{17}H_{26}N_{15}Ag_5Cu_2$	$C_9H_{16}N_9Ag_3Ni$	$C_{10}H_{18}N_8Ag_2Ni$	$C_6H_8N_6AgCu_2$
Formula Weight	637.43	1106.92	632.59	524.75	399.13
R, R_w ($I>2.5\sigma(I)$)	0.021, 0.024	0.028, 0.021	0.025, 0.038	0.029, 0.037	0.022, 0.034*
Crystal Habit	Purple prism	Blue plate	Purple plate	Purple prism	Blue block
Crystal Dimensions (mm^3)	0.29 x 0.19 x 0.12	0.15 x 0.12 x 0.05	0.36 x 0.28 x 0.14	0.31 x 0.25 x 0.25	0.50 x 0.50 x 0.35
Space group	$P\bar{1}$ (No. 2)	$P2_1/n$ (No. 14)	$P\bar{1}$ (No. 2)	$P2_1/n$ (No. 14)	$P2_1/n$ (No. 14)
a, A	6.6945(10)	6.9921(7)	7.4948(11)	7.9841(7)	8.0393(5)
b, Å	8.2741(13)	17.6629(17)	8.1709(9)	16.4951(15)	12.7741(6)
c, Å	9.0411(12)	12.5504(15)	8.4004(12)	13.9185(19)	11.0643(5)
α, deg	69.739(12)	90	65.33(1)	90	90
β, deg	89.622(12)	90.714(8)	69.534(11)	104.106(8)	94.264(4)
γ, deg	70.226(12)	90	68.90(1)	90	90
Volume, $Å^3$	438.63(11)	1549.9(3)	423.9	1777.8(3)	1133.10(9)
Z	1	2	1	4	4
Calc. density, g/cm^3	2.413	2.372	2.478	1.961	2.339
Linear absorption correction, cm^{-1}	44.8	44.5	44.9	32.2	54.01
Data range	$4° \le 2\theta \le 55°$	$4° \le 2\theta \le 55°$	$4° \le 2\theta \le 67°$	$4° \le 2\theta \le 60°$	$6° \le 2\theta \le 60°$
Absorption Correction Transmission Range	0.4837 – 0.6533	0.6255 – 0.8192	0.3395 – 0.5885	0.4249 – 0.5568	0.5730 – 1.0000
Final Unit Cell Reflections: Range	40: $40° \le 2\theta \le 52°$	58: $40° \le 2\theta \le 46°$	32: $40° \le 2\theta \le 52°$	72: $44° \le 2\theta \le 54°$	7354: $6° \le 2\theta \le 60°$
Parameters/Observed Data	106 / 1690	185 / 1824	106 / 2840	196 / 3123	1 / 12.44 (ratio)

* For $I>3\sigma(I)$

Table A2.2 – Summary of Crystallographic Data for Chapter 3: Complexes **3.1** – **3.3**

	3.1	**3.2**	**3.3**
Formula	$C_{12}H_{18}N_{12}Au_2NiO$	$C_{12}H_{13}N_{11}Au_2Cu$	$C_{12}H_{16}N_{12}Au_2Cu$
Formula Weight	798.98	768.79	785.82
R, R_w ($I>2.5\sigma(I)$)	0.022, 0.029	0.034, 0.033	0.030, 0.037
Crystal Habit	Purple needle	Purple block	Purple block
Crystal Dimensions (mm^3)	0.40 x 0.10 x 0.10	0.23 x 0.16 x 0.16	0.36 x 0.24 x 0.24
Space group	$P\bar{1}$ (No. 2)	$P2_1/n$ (No. 14)	$P2_1/c$ (No. 14)
a, A	8.372(1)	7.5489(9)	6.688(1)
b, Å	9.844(1)	15.3231(19)	7.6961(9)
c, Å	14.819(3)	17.7943(19)	20.273(3)
α, deg	73.00(2)	90	90
β, deg	77.16(2)	95.474(8)	97.044(14)
γ, deg	68.90(1)	90	90
Volume, $Å^3$	1080.26	2048.9	1038.80
Z	2	4	2
Calc. density, g/cm^3	2.456	2.492	2.520
Linear absorption correction, cm^{-1}	144	153	151
Data range	$4° \leq 2\theta \leq 53°$	$4° \leq 2\theta \leq 53°$	$4° \leq 2\theta \leq 50°$
Absorption Correction Transmission Range	0.0439 – 0.1101	0.0999 – 0.1405	0.0292 – 0.0707
Final Unit Cell Reflections: Range	32: $48° \leq 2\theta \leq 53°$	56: $40° \leq 2\theta \leq 48°$	32: $40° \leq 2\theta \leq 44°$
Parameters/Observed Data	260 / 3655	238 / 2148	127 / 1472

Table A2.3 – Summary of Crystallographic Data for Chapter 3: Complexes **3.4 – 3.6**

	3.4	**3.5**	**3.6**
Formula	$C_{16}H_{24}N_{12}Au_2Cu$	$C_{12}H_{13}N_{11}Au_2Ni$	$C_{18}H_{12}N_{10}Au_2CuO_2$
Formula Weight	841.95	763.94	857.84
R, R_W (I>2.5σ(I))	0.035, 0.044	0.041, 0.047	0.024, 0.027
Crystal Habit	Purple block	Purple prism	Blue needle
Crystal Dimensions (mm^3)	**0.36 x 0.32 x 0.27**	**0.30 x 0.15 x 0.15**	**0.30 x 0.30 x 0.20**
Space group	*Pnam* (No. 62)	$P2_1/n$ (No. 14)	$P\bar{1}$ (No. 2)
a, A	8.9325(12)	9.9807(14)	7.5006(9)
b, Å	15.7920(21)	19.811(2))	12.0252(18)
c, Å	18.362(4)	10.300(2)	14.2116(17)
α, deg	90	90	73.878(11)
β, deg	90	100.364(11))	89.642(11)
γ, deg	90	90	73.102(11)
Volume, $Å^3$	2590.1	2003.4	1174.39
Z	4	4	2
Calc. density, g/cm^3	2.159	2.533	2.426
Linear absorption correction, cm^{-1}	121	155	134
Data range	$4° \leq 2\theta \leq 52°$	$4° \leq 2\theta \leq 48°$	$4° \leq 2\theta \leq 48°$
Absorption Correction Transmission Range	0.0625 – 0.1820	0.0410 – 0.0466	0.0358 – 0.0889
Final Unit Cell Reflections: Range	**24: $30° \leq 2\theta \leq 37°$**	**42: $40° \leq 2\theta \leq 45°$**	**26: $44° \leq 2\theta \leq 48°$**
Parameters/Observed Data	155 / 1829	237 / 1933	304 / 3015

Table A2.4 – Summary of Crystallographic Data for Chapter 4

	4.1	4.2	4.3
Formula	$C_{20}H_{34}N_{12}Au_2Cu_2O_2$	$C_{20}H_{34}N_{12}Au_2Cu_2O_2$	$C_{17}H_{38}N_8AuCu_2O_7Cl$
Formula Weight	995.60	995.60	826.05
R, R_W (I>2.5σ(I))	0.023, 0.025	0.027, 0.035	0.030, 0.033
Crystal Habit	Blue plate	Blue plate	Blue plate
Crystal Dimensions (mm^3)	0.40 x 0.15 x 0.10	0.35 x 0.35 x 0.10	0.40 x 0.21 x 0.06
Space group	$P\bar{1}$ (No. 2)	$P\bar{1}$ (No. 2)	$P2_1/n$ (No. 14)
a, A	9.7135(17)	8.465(2)	8.4529(13)
b, Å	10.5792(19)	10.274(2)	15.7403(15)
c, Å	17.429(2)	10.468(2)	11.307(1)
α, deg	76.411(13)	64.35(2)	90
β, deg	82.953(13)	76.27(2)	95.03(1)
γ, deg	64.964(14)	79.26(2)	90
Volume, $Å^3$	1576.8	793.6	1498.6
Z	2	1	2
Calc. density, g/cm^3	2.093	2.083	1.822
Linear absorption correction, cm^{-1}	106	106	64.3
Data range	$4° \leq 2\theta \leq 50°$	$4° \leq 2\theta \leq 57°$	$4° \leq 2\theta \leq 54°$
Absorption Correction Transmission Range	0.3053 – 0.5618	0.0355 – 0.1395	0.1406 – 0.2691
Final Unit Cell Reflections: Range	26: $40° \leq 2\theta \leq 44°$	26: $33° \leq 2\theta \leq 36°$	42: $28° \leq 2\theta \leq 30°$
Parameters/Observed Data	349 / 4006	179 / 3343	183 / 2408

APPENDIX 3

Note: Unless otherwise stated, the occupancies for all atoms in the tables contained in this appendix are 1.0.

A3.1 Fractional Atomic Coordinates and Equivalent Isotropic Thermal Parameters (U(iso) in $Å^2$) for $[Cu(en)_2][Ag_2(CN)_3][Ag(CN)_2]$ (**2.1**)

Atom	X	y	z	U(iso) ($Å^2$)	Occ
Ag1	0.00000	0.00000	0.00000	0.05052(23)	1.0
Ag2	0.10146(5)	0.34066(4)	-0.21246(3)	0.05883(20)	1.0
Cu1	0.50000	0.00000	-0.50000	0.0334(3)	1.0
N1	0.6104(4)	0.1871(3)	-0.4765(3)	0.0390(15)	1.0
N4	0.4437(4)	0.1582(3)	-0.7332(3)	0.0425(16)	1.0
N11	0.4916(5)	-0.2171(4)	0.1325(3)	0.0555(20)	1.0
N20	0.0196(5)	0.4668(5)	-0.0459(3)	0.0575(21)	0.5
N21	0.0941(5)	0.1898(4)	-0.4907(4)	0.0631(24)	1.0
C2	0.5410(6)	0.3523(4)	-0.6218(3)	0.0497(21)	1.0
C3	0.5562(6)	0.2898(5)	-0.7605(4)	0.0544(23)	1.0
C11	0.3182(5)	-0.1394(4)	0.0828(3)	0.0439(20)	1.0
C20	0.0196(5)	0.4668(5)	-0.0459(3)	0.0575(21)	0.5
C21	0.0888(5)	0.2458(4)	-0.3949(4)	0.0438(19)	1.0
H11	0.7592(4)	0.1386(3)	-0.4598(3)	0.063(6)	1.0
H12	0.5584(4)	0.2175(3)	-0.3903(3)	0.063(6)	1.0
H41	0.4934(4)	0.0841(3)	-0.7927(3)	0.064(6)	1.0
H42	0.2976(4)	0.2229(3)	-0.7625(3)	0.064(6)	1.0
H21	0.6289(6)	0.4232(4)	-0.6285(3)	0.070(6)	1.0
H22	0.3966(6)	0.4249(4)	-0.6217(3)	0.070(6)	1.0
H31	0.4925(6)	0.3925(5)	-0.8561(4)	0.073(6)	1.0
H32	0.7025(6)	0.2305(5)	-0.7681(4)	0.073(6)	1.0

A3.2 Fractional Atomic Coordinates and Equivalent Isotropic Thermal Parameters (U(iso) in $Å^2$) for $[Cu(dien)Ag(CN)_2]_2[Ag_2(CN)_3][Ag(CN)_2]$ (**2.2**)

Atom	x	y	z	U(iso) ($Å^2$)	Occ
Ag1	0.19532(8)	0.41825(2)	0.21016(4)	0.0505	1.0
Ag2	0.64071(8)	0.43981(3)	0.17602(4)	0.0534	1.0
Ag3	0.0000	0.5000	0.0000	0.0547	1.0
Cu1	0.6152(1)	0.18294(3)	0.18777(5)	0.0337	1.0
N1	0.6556(7)	0.1708(3)	0.0306(4)	0.0467	1.0
N4	0.8680(7)	0.1286(3)	0.2005(4)	0.0429	1.0
N7	0.6727(7)	0.2142(2)	0.3389(4)	0.0442	1.0
N11	0.4141(7)	0.2618(2)	0.1755(4)	0.0429	1.0
N12	0.0517(7)	0.5825(3)	0.2794(4)	0.0445	1.0
N21	0.8121(8)	0.3823(3)	0.3965(5)	0.0652	1.0
N22	0.5275(8)	0.4887(3)	0.0398(4)	0.0484	0.5
N31	-0.1345(8)	0.3273(3)	0.0157(5)	0.0678	1.0
C2	0.806(1)	0.1149(4)	0.0137(5)	0.0635	1.0
C3	0.9610(9)	0.1278(4)	0.0957(5)	0.0596	1.0
C5	0.9763(9)	0.1616(4)	0.2895(5)	0.0594	1.0
C6	0.8404(9)	0.1729(4)	0.3791(5)	0.0573	1.0
C11	0.3244(8)	0.3156(3)	0.1858(5)	0.0420	1.0
C12	0.1064(8)	0.5252(3)	0.2548(5)	0.0407	1.0
C21	0.7477(9)	0.4060(3)	0.3204(5)	0.0471	1.0
C22	0.5275(8)	0.4887(3)	0.0398(4)	0.0484	0.5
C31	-0.0809(9)	0.3880(4)	0.0139(5)	0.0517	1.0
H11	0.6918(7)	0.2169(3)	0.0014(4)	0.065(15)	1.0
H12	0.5428(7)	0.1544(3)	-0.0020(4)	0.065(15)	1.0
H41	0.8559(7)	0.0776(3)	0.2177(4)	0.06(2)	1.0
H71	0.6973(7)	0.2659(2)	0.3410(4)	0.066(15)	1.0
H72	0.5681(7)	0.2033(2)	0.3812(4)	0.066(15)	1.0
H21	0.857(1)	0.1206(4)	-0.0556(5)	0.075(16)	1.0
H22	0.756(1)	0.0653(4)	0.0212(5)	0.075(16)	1.0
H31	1.0226(9)	0.1748(4)	0.0832(5)	0.069(15)	1.0
H32	1.0524(9)	0.0880(4)	0.0930(5)	0.069(15)	1.0
H51	1.0761(9)	0.1283(4)	0.3110(5)	0.080(17)	1.0
H52	1.0293(9)	0.2088(4)	0.2689(5)	0.080(17)	1.0
H61	0.9010(9)	0.2013(4)	0.4343(5)	0.078(16)	1.0
H62	0.8019(9)	0.1252(4)	0.4062(5)	0.078(16)	1.0

A3.3 Fractional Atomic Coordinates and Equivalent Isotropic Thermal Parameters (U(iso) in Å^2) for $[Ni(en)_2Ag_2(CN)_3][Ag(CN)_2]$ (**2.3**)

Atom	x	y	z	U(iso) (Å^2)	Occ
Ag1	0.46088(3)	0.86125(3)	0.28916(3)	0.04562(13)	1.0.
Ag2	0.00000	1.00000	0.50000	0.04414(19)	1.0.
Ni1	0.00000	1.50000	0.00000	0.02561(19)	1.0.
N1	-0.2317(3)	1.3684(3)	0.0997(3)	0.0384(12)	1.0.
N4	0.0024(3)	1.4818(3)	-0.2439(3)	0.0350(11)	1.0.
N11	0.2015(3)	1.2419(3)	0.0622(3)	0.0350(10)	1.0
N21	0.2608(4)	1.1078(4)	0.6543(4)	0.0493(16)	1.0
N12	0.4900(4)	0.5753(3)	0.4542(4)	0.0444(15)	0.5
C2	-0.2268(5)	1.3000(4)	-0.0402(5)	0.0511(19)	1.0.
C3	-0.1810(4)	1.4412(5)	-0.2222(4)	0.0476(18)	1.0.
C11	0.2987(3)	1.1048(3)	0.1340(3)	0.0318(11)	1.0.
C12	0.4900(4)	0.5753(3)	0.4542(4)	0.0444(15)	0.5
C21	0.1650(4)	1.0741(4)	0.5976(4)	0.0388(14)	1.0
H11	-0.3515(3)	1.4529(3)	0.1227(3)	0.066(6)	1.0
H12	-0.2148(3)	1.2691(3)	0.2053(3)	0.066(6)	1.0.
H21	-0.3513(5)	1.2801(4)	-0.0202(5)	0.045(4)	1.0.
H22	-0.1284(5)	1.1864(4)	-0.0343(5)	0.045(4)	1.0.
H31	-0.2846(4)	1.5516(5)	-0.2319(4)	0.045(4)	1.0.
H32	-0.1664(4)	1.3933(5)	-0.3127(4)	0.045(4)	1.0.
H41	0.0116(3)	1.5944(3)	-0.3362(3)	0.066(6)	1.0.
H42	0.1090(3)	1.3876(3)	-0.2722(3)	0.066(6)	1.0.

A3.4 Fractional Atomic Coordinates and Equivalent Isotropic Thermal Parameters (U(iso) in $Å^2$) for $[Ni(tren)Ag(CN)_2][Ag(CN)_2]$ (**2.5**)

Atom	x	y	z	U(iso) ($Å^2$)
Ag1	0.50000	0.50000	1.00000	0.05537(24)
Ag2	0.25638(4)	0.456360(20)	0.75522(3)	0.05425(18)
Ag3	0.00000	0.50000	0.50000	0.0593(3)
Ni1	0.66390(5)	0.710850(20)	0.78354(3)	0.03306(20)
N1	0.7134(4)	0.69426(18)	0.93920(23)	0.0484(16)
N4	0.8780(4)	0.63284(18)	0.80051(22)	0.0429(15)
N7	0.6483(4)	0.69436(16)	0.63252(20)	0.0413(14)
N10	0.8550(4)	0.80171(17)	0.79950(23)	0.0476(17)
N21	0.4870(4)	0.61524(17)	0.77301(22)	0.0429(15)
N22	0.0228(4)	0.29779(17)	0.7345(3)	0.0505(18)
N11	0.3247(5)	0.65432(24)	1.0708(3)	0.077(3)
N31	-0.3067(5)	0.3778(3)	0.4996(3)	0.079(3)
C2	0.8532(5)	0.6361(3)	0.9726(3)	0.0575(23)
C3	0.8792(5)	0.58326(22)	0.8885(3)	0.0533(21)
C5	0.8396(6)	0.58344(24)	0.7082(3)	0.0597(23)
C6	0.7807(6)	0.6368(3)	0.6179(3)	0.0605(23)
C8	1.0373(5)	0.6819(3)	0.8095(3)	0.0591(24)
C9	1.0209(5)	0.7658(3)	0.8479(3)	0.062(3)
C21	0.4017(4)	0.55959(21)	0.7657(3)	0.0446(18)
C22	0.1087(5)	0.35359(22)	0.7433(3)	0.0533(22)
C11	0.3894(6)	0.60047(24)	1.0450(3)	0.0553(22)
C31	-0.2008(6)	0.4218(3)	0.4995(3)	0.062(3)
H11	0.7448(4)	0.74365(18)	0.97068(23)	0.081(6)
H12	0.6140(4)	0.67507(18)	0.95517(23)	0.081(6)
H21	0.9570(5)	0.6648(3)	0.9998(3)	0.066(4)
H22	0.8260(5)	0.6024(3)	1.0221(3)	0.066(4)
H31	0.9870(5)	0.55610(22)	0.9086(3)	0.062(4)
H32	0.7887(5)	0.54444(22)	0.8725(3)	0.062(4)
H51	0.9409(6)	0.55509(24)	0.7036(3)	0.069(4)

Continued on next page...

Atom	x	y	z	U(iso) (Å^2)
H52	0.7509(6)	0.54564(24)	0.7105(3)	0.069(4)
H61	0.8768(6)	0.6661(3)	0.6070(3)	0.071(4)
H62	0.7338(6)	0.6038(3)	0.5618(3)	0.071(4)
H71	0.6648(4)	0.74395(16)	0.60440(20)	0.072(6)
H72	0.5397(4)	0.67420(16)	0.60184(20)	0.072(6)
H81	1.1306(5)	0.6552(3)	0.8535(3)	0.067(4)
H82	1.0608(5)	0.6862(3)	0.7459(3)	0.067(4)
H91	1.0301(5)	0.7630(3)	0.9172(3)	0.071(4)
H92	1.1111(5)	0.7988(3)	0.8358(3)	0.071(4)
H101	0.8296(4)	0.84392(17)	0.83792(23)	0.079(6)
H102	0.8591(4)	0.82144(17)	0.73752(23)	0.079(6)

A3.5 Fractional Atomic Coordinates and Equivalent Isotropic Thermal Parameters (U(iso) in $Å^2$) for $[Cu(en)Cu(CN)_2Ag(CN)_2]$ (**2.6**)

Atom	x	y	z	U(iso) ($Å^2$)
Ag(1)	1.22887(2)	0.13789(2)	0.14153(2)	0.02702(6)
Cu(1)	0.79315(3)	0.04630(2)	0.40650(2)	0.01344(6)
Cu(2)	1.22717(3)	0.31850(2)	0.32860(2)	0.01807(7)
N(1)	0.8578(2)	-0.0208(2)	0.2505(2)	0.0211(4)
N(2)	0.6820(2)	-0.0942(1)	0.4319(2)	0.0175(4)
N(3)	0.7612(3)	0.0888(2)	0.5756(2)	0.0220(5)
N(4)	0.5682(3)	0.1155(2)	0.3108(2)	0.0252(5)
N(6)	1.4008(3)	0.3533(2)	0.4581(2)	0.0259(5)
N(7)	0.9618(3)	0.1580(2)	0.3894(2)	0.0209(4)
C(1)	0.7502(3)	-0.1139(2)	0.2249(2)	0.0228(5)
C(2)	0.7377(3)	-0.1701(2)	0.3430(2)	0.0227(5)
C(3)	0.7468(3)	0.1195(2)	0.6718(2)	0.0196(5)
C(4)	0.4495(3)	0.1244(2)	0.2484(2)	0.0229(5)
C(6)	1.0139(3)	0.1395(2)	0.0258(2)	0.0213(5)
C(7)	1.0591(3)	0.2198(2)	0.3702(2)	0.0190(5)
H(1)	0.8409	0.0294	0.1835	0.026
H(2)	0.9750	-0.0420	0.2592	0.026
H(3)	0.7138	-0.1196	0.5141	0.021
H(4)	0.5610	-0.0864	0.4211	0.021
H(5)	0.6395	-0.0922	0.1917	0.028
H(6)	0.8009	-0.1599	0.1668	0.028
H(7)	0.8470	-0.1987	0.3712	0.027
H(8)	0.6568	-0.2273	0.3322	0.027

A3.6 Fractional Atomic Coordinates and Equivalent Isotropic Thermal Parameters (U(iso) in $Å^2$) for $Ni(en)_2[Au(CN)_4]_2 \bullet H_2O$ (**3.1**)

Atom	x	y	z	U(iso) ($Å^2$)
Au1	0.36465(3)	0.00482(2)	0.189351(15)	0.0324
Au2	0.71240(3)	0.06343(2)	0.380168(16)	0.0345
Ni1	0.5000	0.5000	0.0000	0.0311
Ni2	0.0000	0.5000	0.5000	0.0295
O1	0.1841(6)	-0.0468(6)	0.0508(4)	0.0665
N5	0.3102(6)	0.6019(6)	0.0987(4)	0.0424
N6	0.2865(6)	0.5426(6)	-0.0681(4)	0.0450
N7	-0.2547(6)	0.5116(6)	0.5028(4)	0.0402
N8	0.0106(6)	0.5171(6)	0.3549(3)	0.0388
N11	0.4716(6)	0.2896(5)	0.0792(4)	0.0421
N12	0.6836(7)	-0.2155(7)	0.0944(5)	0.0596
N13	0.2459(9)	-0.2726(7)	0.2971(5)	0.0654
N14	0.0386(9)	0.2158(8)	0.2863(6)	0.0820
N21	0.9236(6)	-0.2637(5)	0.4722(4)	0.0425
N22	0.5438(8)	0.1334(7)	0.5790(4)	0.0610
N23	0.464(1)	0.3719(7)	0.2864(5)	0.0776
N24	0.8594(8)	-0.0070(7)	0.1798(4)	0.0585
C1	0.1420(8)	0.6029(8)	0.0823(5)	0.0554
C2	0.1346(9)	0.6439(8)	-0.0231(5)	0.0551
C3	-0.2678(8)	0.4835(8)	0.4132(5)	0.0504
C4	-0.1635(9)	0.5628(8)	0.3325(5)	0.0509
C11	0.4379(7)	0.1815(6)	0.1190(4)	0.0381
C12	0.5706(8)	-0.1322(7)	0.1271(5)	0.0412
C13	0.2895(8)	-0.1714(7)	0.2606(5)	0.0428
C14	0.1584(9)	0.1386(7)	0.2531(5)	0.0477
C21	0.8546(7)	-0.1416(6)	0.4416(4)	0.0384
C22	0.6125(7)	0.1087(6)	0.5080(5)	0.0393
C23	0.5575(8)	0.2621(7)	0.3196(5)	0.0462

Continued on next page...

Atom	x	y	z	U(iso) (Å^2)
C24	0.8052(8)	0.0190(7)	0.2509(5)	0.0438
H11	0.0516(8)	0.6743(8)	0.1115(5)	0.071(8)
H12	0.1302(8)	0.5063(8)	0.1093(5)	0.071(8)
H21	0.1336(9)	0.7445(8)	-0.0493(5)	0.069(8)
H22	0.0324(9)	0.6333(8)	-0.0337(5)	0.069(8)
H31	-0.3853(8)	0.5191(8)	0.4029(5)	0.072(8)
H32	-0.2226(8)	0.3790(8)	0.4165(5)	0.072(8)
H41	-0.2135(9)	0.6679(8)	0.3261(5)	0.071(8)
H42	-0.1626(9)	0.5388(8)	0.2747(5)	0.071(8)
H51	0.3095(6)	0.6996(6)	0.0903(4)	0.050(7)
H52	0.3321(6)	0.5484(6)	0.1602(4)	0.050(7)
H61	0.3083(6)	0.5869(6)	-0.1323(4)	0.057(7)
H62	0.2669(6)	0.4530(6)	-0.0621(4)	0.057(7)
H71	-0.3281(6)	0.6064(6)	0.5081(4)	0.048(7)
H72	-0.2844(6)	0.4401(6)	0.5542(4)	0.048(7)
H81	0.0656(6)	0.5865(6)	0.3192(3)	0.048(7)
H82	0.0715(6)	0.4243(6)	0.3410(3)	0.048(7)
H1	0.2070(6)	0.0359(6)	0.0133(4)	0.16(4)
H2	0.0814(6)	-0.0203(6)	0.0870(4)	0.16(4)

A3.7 Fractional Atomic Coordinates and Equivalent Isotropic Thermal Parameters (U(iso) in $Å^2$) for $Cu(dien)[Au(CN)_4]_2$ (**3.2**)

Atom	x	y	z	U(iso) ($Å^2$)
Au1	1.39472(8)	0.12684(5)	0.50015(3)	0.0356
Au2	1.39782(9)	0.13030(5)	0.98970(3)	0.0378
Cu1	1.0465(3)	0.05393(13)	0.72271(9)	0.0370
N11	1.2098(17)	0.0883(9)	0.6474(6)	0.0481
N12	1.213(2)	-0.033(1)	0.4215(9)	0.0688
N13	1.568(2)	0.1684(12)	0.3510(8)	0.0836
N14	1.610(2)	0.2812(12)	0.5805(8)	0.0774
N21	1.2172(17)	0.0878(9)	0.8275(7)	0.0496
N22	1.566(2)	0.2945(12)	0.9191(9)	0.0771
N23	1.599(2)	0.1656(11)	1.1490(7)	0.0767
N24	1.236(2)	-0.0336(11)	1.0547(8)	0.0715
C11	1.282(2)	0.1030(9)	0.5949(8)	0.0378
C12	1.280(2)	0.0227(11)	0.4496(8)	0.0451
C13	1.505(2)	0.1482(11)	0.4058(8)	0.0501
C14	1.531(2)	0.2289(13)	0.5474(8)	0.0513
C21	1.2745(18)	0.1044(9)	0.8879(8)	0.0342
C22	1.503(2)	0.2336(12)	0.9470(9)	0.0506
C23	1.528(2)	0.1571(12)	1.0919(9)	0.0547
C24	1.292(2)	0.0254(11)	1.0290(9)	0.0485
N5	1.1095(15)	-0.0723(7)	0.7189(7)	0.0410
N6	0.9108(19)	0.1649(9)	0.7157(7)	0.0617
N7	0.8485(15)	0.0118(8)	0.7790(6)	0.0353
C1	1.009(3)	-0.1200(11)	0.768(1)	0.0661
C2	0.813(2)	-0.0794(12)	0.765(1)	0.0655
C3	0.684(2)	0.0668(11)	0.760(1)	0.0586
C4	0.753(3)	0.1559(12)	0.762(1)	0.0785
H51	1.2300(15)	-0.0793(7)	0.7340(7)	0.12(2)
H52	1.0853(15)	-0.0926(7)	0.6697(7)	0.12(2)

Continued on next page...

Atom	x	y	z	U(iso) (Å^2)
H61	0.9832(19)	0.2105(9)	0.7347(7)	0.03(2)
H62	0.8710(19)	0.1762(9)	0.6656(7)	0.03(2)
H71	0.8835(15)	0.0180(8)	0.8302(6)	0.01(2)
H11	1.065(3)	-0.1176(11)	0.818(1)	0.040(16)
H12	1.000(3)	-0.1790(11)	0.752(1)	0.040(16)
H21	0.748(2)	-0.1037(12)	0.804(1)	0.043(16)
H22	0.748(2)	-0.0881(12)	0.718(1)	0.043(16)
H31	0.601(2)	0.0590(11)	0.796(1)	0.036(16)
H32	0.629(2)	0.0528(11)	0.711(1)	0.036(16)
H41	0.790(3)	0.1709(12)	0.813(1)	0.061(16)
H42	0.662(3)	0.1945(12)	0.742(1)	0.061(16)

A3.8 Fractional Atomic Coordinates and Equivalent Isotropic Thermal Parameters (U(iso) in $Å^2$) for $Cu(en)_2[Au(CN)_4]_2$ (**3.3**)

Atom	x	y	z	U(iso) ($Å^2$)
Au1	0.17613(5)	-0.34090(4)	1.199069(15)	0.0357
Cu1	0.5000	-1.0000	1.0000	0.0395
N11	0.3038(13)	-0.2125(11)	1.0639(4)	0.0553
N12	0.5550(16)	-0.1564(12)	1.2723(5)	0.0724
N13	0.0465(14)	-0.4646(12)	1.3341(4)	0.0611
N14	-0.1898(16)	-0.5211(14)	1.1163(5)	0.0734
C11	0.2579(14)	-0.2603(12)	1.1128(4)	0.0404
C12	0.4132(15)	-0.2221(13)	1.2465(5)	0.0461
C13	0.0932(15)	-0.4154(12)	1.2855(4)	0.0438
C14	-0.0588(15)	-0.4578(13)	1.1477(4)	0.0469
N3	0.2527(11)	-0.865(1)	0.9647(4)	0.0448
N4	0.5098(12)	-0.8362(9)	1.0779(4)	0.0452
C1	0.1800(16)	-0.7713(15)	1.0202(5)	0.0604
C2	0.3593(18)	-0.6991(14)	1.0616(6)	0.0659
H31	0.1547(11)	-0.941(1)	0.9453(4)	0.058(15)
H32	0.2852(11)	-0.786(1)	0.9330(4)	0.058(15)
H41	0.4848(12)	-0.8962(9)	1.1158(4)	0.062(15)
H42	0.6371(12)	-0.7859(9)	1.0850(4)	0.062(15)
H11	0.1114(16)	-0.8496(15)	1.0459(5)	0.08(2)
H12	0.0905(16)	-0.6816(15)	1.0034(5)	0.08(2)
H21	0.3197(18)	-0.6568(14)	1.1021(6)	0.08(2)
H22	0.4136(18)	-0.6065(14)	1.0385(6)	0.08(2)

A3.9 Fractional Atomic Coordinates and Equivalent Isotropic Thermal Parameters (U(iso) in $Å^2$) for $[Cu(dmeda)_2Au(CN)_4][Au(CN)_4]$ (**3.4**)

Atom	x	y	z	U(iso) ($Å^2$)
Au1	0.10597(5)	0.37771(3)	0.75000	0.0357(3)
Au2	0.22587(6)	0.65658(3)	0.75000	0.0468(3)
Cu1	0.00000	1.00000	0.50000	0.0441(8)
N1	0.1095(8)	1.0930(5)	0.5620(5)	0.050(4)
N2	0.1653(9)	0.9252(5)	0.5328(4)	0.046(4)
N11	0.1007(10)	0.3766(7)	0.5806(5)	0.069(6)
N12	0.3259(15)	0.2228(10)	0.75000	0.068(8)
N13	-0.0768(14)	0.5451(9)	0.75000	0.060(8)
N21	0.3587(10)	0.5427(6)	0.6263(6)	0.068(6)
N22	0.0935(16)	0.7696(9)	0.6303(7)	0.109(9)
C1	0.1976(17)	1.1522(9)	0.5166(8)	0.094(11)
C2	0.0071(14)	1.1465(7)	0.6038(8)	0.079(8)
C3	0.2053(13)	1.0435(8)	0.6134(7)	0.070(7)
C4	0.2775(12)	0.9732(8)	0.5764(7)	0.072(7)
C11	0.1042(10)	0.3790(6)	0.6411(6)	0.046(5)
C12	0.2408(15)	0.2765(10)	0.75000	0.053(8)
C13	-0.0159(14)	0.4841(8)	0.75000	0.042(7)
C21	0.3109(12)	0.5820(6)	0.6718(6)	0.056(6)
C22	0.1398(14)	0.7304(7)	0.6752(7)	0.072(7)
H1	0.1259	0.8820	0.5614	0.057(22)
H2	0.2122	0.9019	0.4922	0.057(22)
H11	0.2668	1.1211	0.4878	0.15(3)
H12	0.2505	1.1903	0.5472	0.15(3)
H13	0.1323	1.1832	0.4856	0.15(3)
H21	-0.0534	1.1119	0.6342	0.14(3)
H22	0.0632	1.1847	0.6330	0.14(3)
H23	-0.0550	1.1776	0.5714	0.14(3)
H31	0.2799	1.0797	0.6332	0.11(3)
H32	0.1445	1.0220	0.6516	0.11(3)
H41	0.3529	0.9945	0.5449	0.11(3)
H42	0.3215	0.9366	0.6114	0.11(3)

A3.10 Fractional Atomic Coordinates and Equivalent Isotropic Thermal Parameters (U(iso) in $Å^2$) for $Ni(dien)[Au(CN)_4]_2$ (**3.5**)

Atom	x	y	z	U(iso) ($Å^2$)
Au1	1.36469(6)	0.02112(3)	0.64653(6)	0.0313
Au2	1.07781(6)	-0.02731(3)	1.18045(7)	0.0352
Ni1	1.3853(2)	0.16806(11)	1.0685(2)	0.0325
N1	1.5356(16)	0.2293(7)	1.0177(15)	0.0462
N4	1.2583(15)	0.2340(7)	0.9490(16)	0.0441
N7	1.3332(16)	0.2290(8)	1.2157(15)	0.0497
C2	1.474(2)	0.2718(12)	0.902(2)	0.0718
C3	1.340(3)	0.2788(16)	0.882(4)	0.1579
C5	1.172(4)	0.2659(18)	1.036(3)	0.1523
C6	1.218(3)	0.2716(13)	1.166(2)	0.0781
N11	1.4014(15)	0.1051(7)	0.9047(15)	0.0394
N12	1.289(2)	0.1534(9)	0.4855(18)	0.0752
N13	1.3249(16)	-0.0561(9)	0.3789(17)	0.0516
N14	1.4807(15)	-0.1065(8)	0.8032(14)	0.0414
N21	1.2298(15)	0.1010(7)	1.0997(15)	0.0424
N22	1.222(2)	-0.1248(11)	1.006(2)	0.0888
N23	0.9335(16)	-0.1557(9)	1.2650(16)	0.0545
N24	0.915(2)	0.0563(11)	1.358(2)	0.0788
C11	1.3894(17)	0.0731(9)	0.8134(17)	0.0349
C12	1.3100(19)	0.1062(9)	0.5436(18)	0.0449
C13	1.3374(15)	-0.0309(8)	0.4764(17)	0.0310
C14	1.4321(18)	-0.0621(8)	0.7466(15)	0.0292
C21	1.172(2)	0.056(1)	1.1289(18)	0.0465
C22	1.175(2)	-0.086(1)	1.068(2)	0.0524
C23	0.9847(19)	-0.109(1)	1.2291(19)	0.0452
C24	0.974(2)	0.030(1)	1.292(2)	0.0478
H11	1.5730(16)	0.2560(7)	1.0894(15)	0.06(3)
H12	1.6033(16)	0.2026(7)	0.9930(15)	0.06(3)

Continued on next page...

Atom	x	y	z	U(iso) (Å^2)
H41	1.2023(15)	0.2134(7)	0.8782(16)	0.05(3)
H71	1.4067(16)	0.2562(8)	1.2508(15)	0.07(3)
H72	1.3109(16)	0.2014(8)	1.2817(15)	0.07(3)
H21	1.512(2)	0.3155(12)	0.917(2)	0.10(4)
H22	1.496(2)	0.2533(12)	0.824(2)	0.10(4)
H31	1.322(3)	0.3226(16)	0.912(4)	0.15(4)
H32	1.308(3)	0.2759(16)	0.790(4)	0.15(4)
H51	1.150(4)	0.3102(18)	1.004(3)	0.17(4)
H52	1.091(4)	0.2397(18)	1.025(3)	0.17(4)
H61	1.244(3)	0.3173(13)	1.184(2)	0.10(4)
H62	1.146(3)	0.2601(13)	1.211(2)	0.10(4)

A3.11 Fractional Atomic Coordinates and Equivalent Isotropic Thermal Parameters (U(iso) in Å^2) for $[Cu(bipy)(H_2O)_2(Au(CN)_4)_{0.5}][Au(CN)_4]_{1.5}$ (**3.6**)

Atom	x	y	z	U(iso) (Å^2)
Au1	0.0000	0.0000	0.0000	0.0334
Au2	0.03007(4)	-0.35480(2)	0.27849(2)	0.0437
Au3	0.5000	-0.5000	0.0000	0.0488
Cu1	-0.58342(11)	0.10870(7)	0.21454(6)	0.0373
O1	-0.7073(7)	0.2769(4)	0.1231(4)	0.0459
O2	-0.8601(8)	0.1184(5)	0.3113(4)	0.0546
N1	-0.4581(8)	0.1631(5)	0.3078(4)	0.0390
N2	-0.4642(8)	-0.0533(5)	0.3114(4)	0.0385
N11	-0.3391(9)	0.1067(6)	0.1091(5)	0.0543
N12	0.2834(8)	0.0453(5)	0.1324(4)	0.0415
N21	-0.2005(12)	-0.2730(7)	0.0757(5)	0.0773
N22	0.0210(9)	-0.0942(6)	0.2833(5)	0.0591
N23	0.2436(13)	-0.4471(6)	0.4851(6)	0.0821
N24	0.0552(11)	-0.6234(6)	0.2998(6)	0.0705
N31	0.8972(11)	-0.6483(9)	0.1043(7)	0.0980
N32	0.6127(12)	-0.6154(8)	-0.1717(7)	0.0848
C1	-0.4600(11)	0.2775(6)	0.2976(6)	0.0446
C2	-0.3631(12)	0.3057(7)	0.3652(6)	0.0546
C3	-0.2625(11)	0.2138(8)	0.4452(7)	0.0565
C4	-0.2627(11)	0.0967(7)	0.4560(6)	0.0470
C5	-0.3611(9)	0.0736(6)	0.3869(5)	0.0369
C6	-0.3693(9)	-0.0484(6)	0.3888(5)	0.0363
C7	-0.2853(11)	-0.1516(7)	0.4658(6)	0.0476
C8	-0.2992(11)	-0.2614(7)	0.4604(6)	0.0547
C9	-0.3970(12)	-0.2658(7)	0.3797(6)	0.0545
C10	-0.4762(11)	-0.1602(7)	0.3063(6)	0.0488
C11	-0.215(1)	0.0714(6)	0.0701(5)	0.0425
C12	0.181(1)	0.0280(6)	0.0858(5)	0.0400

Continued on next page...

Atom	x	y	z	U(iso) (Å^2)
C21	-0.1162(12)	-0.3000(7)	0.1484(6)	0.0553
C22	0.0218(11)	-0.1854(7)	0.2781(6)	0.0513
C23	0.1698(12)	-0.4138(6)	0.4098(6)	0.0546
C24	0.0413(11)	-0.5243(7)	0.2890(6)	0.0539
C31	0.7516(13)	-0.5954(8)	0.0683(7)	0.0662
C32	0.5702(11)	-0.5772(8)	-0.1079(7)	0.0586
H1	-0.7451	0.2875	0.0675	0.070(14)
H2	-0.8561	0.3118	0.1303	0.070(14)
H3	-0.9459	0.0879	0.2901	0.070(14)
H4	-0.9172	0.1556	0.3145	0.033(14)
H11	-0.56(1)	0.333(6)	0.241(5)	0.051(8)
H21	-0.37(1)	0.396(7)	0.349(5)	0.051(8)
H31	-0.20(1)	0.223(6)	0.497(6)	0.051(8)
H41	-0.19(1)	0.035(6)	0.507(6)	0.051(8)
H71	-0.22(1)	-0.149(6)	0.520(6)	0.051(8)
H81	-0.25(1)	-0.334(6)	0.512(6)	0.051(8)
H91	-0.43(1)	-0.338(6)	0.371(5)	0.051(8)
H101	-0.55(1)	-0.162(6)	0.253(6)	0.051(8)

A3.12 Fractional Atomic Coordinates and Equivalent Isotropic Thermal Parameters (U(iso) in $Å^2$) for $[\{Cu(tmeda)(\mu\text{-}OH)\}_2Au(CN)_4][Au(CN)_4]$ (**4.1**)

Atom	x	y	z	U(iso) ($Å^2$)
Au1	0.5000	0.5000	0.5000	0.0468
Au2	0.0000	0.0000	0.0000	0.0418
Au3	0.00793(3)	0.17808(3)	0.738798(14)	0.0451
Cu1	0.60749(9)	0.91504(8)	0.56247(4)	0.0442
Cu2	-0.40873(9)	0.53882(8)	0.04178(4)	0.0474
O1	0.3935(5)	1.0443(5)	0.5528(2)	0.0689
O2	-0.5392(6)	0.4380(5)	0.0670(3)	0.0691
N11	0.5326(8)	0.7219(8)	0.5776(5)	0.0965
N12	0.7364(9)	0.551(1)	0.3714(5)	0.0982
N21	-0.1738(8)	0.3171(6)	0.0192(4)	0.0756
N22	0.2204(8)	-0.0528(7)	0.1325(4)	0.0793
N31	-0.130(1)	0.4582(8)	0.8051(4)	0.0979
N32	0.2580(7)	0.0355(8)	0.8670(4)	0.0751
N33	0.1443(8)	-0.0979(7)	0.6691(4)	0.0803
N34	-0.2400(8)	0.3040(8)	0.6119(4)	0.0943
C11	0.5162(8)	0.6430(8)	0.5502(5)	0.0655
C12	0.649(1)	0.530(1)	0.4181(5)	0.0743
C21	-0.1116(8)	0.2032(8)	0.0114(4)	0.0556
C22	0.1416(9)	-0.0327(7)	0.0842(4)	0.0547
C31	-0.0783(9)	0.3555(9)	0.7806(4)	0.0665
C32	0.1675(8)	0.0888(8)	0.8190(4)	0.0533
C33	0.0935(8)	0.0012(8)	0.6956(4)	0.0538
C34	-0.1500(8)	0.2616(8)	0.6582(4)	0.0610
N1	0.8335(6)	0.7933(6)	0.5687(3)	0.0468
N2	0.6151(6)	0.9231(6)	0.6782(3)	0.0460
N3	-0.3733(6)	0.5321(6)	0.1563(3)	0.0505
N4	-0.3089(6)	0.6763(5)	0.0118(3)	0.0444
C1	0.8650(8)	0.7426(9)	0.6537(4)	0.0747
C2	0.7782(9)	0.861(1)	0.6969(4)	0.0785
C3	-0.3099(11)	0.638(1)	0.1549(4)	0.0845
C4	-0.223(1)	0.652(1)	0.0823(4)	0.0847

Continued on next page...

Atom	x	y	z	U(iso) (Å^2)
C5	0.9180(9)	0.8811(9)	0.5317(5)	0.0755
C6	0.8837(9)	0.6739(9)	0.5284(5)	0.0913
C7	0.5419(11)	1.0695(9)	0.6916(5)	0.0925
C8	0.5370(9)	0.8413(9)	0.7296(4)	0.0742
C9	-0.516(1)	0.5681(9)	0.2046(5)	0.0868
C10	-0.273(1)	0.3871(8)	0.1941(4)	0.0841
C13	-0.423(1)	0.8188(8)	-0.0089(6)	0.1007
C14	-0.1993(8)	0.6499(7)	-0.0551(4)	0.0573
H11	0.9709(8)	0.7075(9)	0.6616(4)	0.097(12)
H12	0.8318(8)	0.6682(9)	0.6736(4)	0.097(12)
H21	0.8155(9)	0.933(1)	0.6794(4)	0.106(12)
H22	0.7904(9)	0.827(1)	0.7522(4)	0.106(12)
H31	-0.3911(11)	0.728(1)	0.1565(4)	0.138(12)
H32	-0.2480(11)	0.609(1)	0.1993(4)	0.138(12)
H41	-0.135(1)	0.566(1)	0.0842(4)	0.136(12)
H42	-0.193(1)	0.729(1)	0.0780(4)	0.136(12)
H51	0.8965(9)	0.9145(9)	0.4771(5)	0.101(6)
H52	0.8873(9)	0.9601(9)	0.5565(5)	0.101(6)
H53	1.0240(9)	0.8257(9)	0.5378(5)	0.101(6)
H61	0.8635(9)	0.7089(9)	0.4737(5)	0.118(6)
H62	0.9895(9)	0.6181(9)	0.5351(5)	0.118(6)
H63	0.8293(9)	0.6169(9)	0.5507(5)	0.118(6)
H71	0.4373(11)	1.1080(9)	0.6797(5)	0.125(6)
H72	0.5515(11)	1.0699(9)	0.7451(5)	0.125(6)
H73	0.5889(11)	1.1255(9)	0.6580(5)	0.125(6)
H81	0.4331(9)	0.8812(9)	0.7162(4)	0.092(6)
H82	0.5439(9)	0.8438(9)	0.7831(4)	0.092(6)
H83	0.5841(9)	0.7454(9)	0.7228(4)	0.092(6)
H91	-0.557(1)	0.5007(9)	0.2060(5)	0.103(6)
H92	-0.586(1)	0.6606(9)	0.1818(5)	0.103(6)
H93	-0.495(1)	0.5668(9)	0.2568(5)	0.103(6)
H101	-0.319(1)	0.3243(8)	0.1930(4)	0.095(6)
H102	-0.178(1)	0.3585(8)	0.1660(4)	0.095(6)
H103	-0.257(1)	0.3843(8)	0.2473(4)	0.095(6)
H131	-0.474(1)	0.8271(8)	-0.0541(6)	0.114(6)

Continued on next page...

Atom	x	y	z	U(iso) (Å^2)
H132	-0.376(1)	0.8842(8)	-0.0203(6)	0.114(6)
H13	-0.493(1)	0.8393(8)	0.0339(6)	0.114(6)
H1	-0.2525(8)	0.6659(7)	-0.1011(4)	0.075(6)
H142	-0.1254(8)	0.5543(7)	-0.0446(4)	0.075(6)
H143	-0.1503(8)	0.7131(7)	-0.0633(4)	0.075(6)

A3.13 Fractional Atomic Coordinates and Equivalent Isotropic Thermal Parameters (U(iso) in Å^2) for [Cu(tmeda)(μ-OH)Au(CN)$_4$]$_2$ (**4.2**)

Atom	x	y	z	U(iso) (Å^2)
Au1	0.27905(3)	0.42341(2)	0.03364(2)	0.0417
Cu1	0.01673(7)	0.34083(6)	0.56980(7)	0.0389
O1	0.1513(5)	0.4999(4)	0.4873(5)	0.0523
N11	0.0801(8)	0.3077(7)	0.3457(6)	0.0740
N12	0.0514(9)	0.7133(6)	-0.0270(8)	0.0760
N13	0.4972(9)	0.5365(7)	-0.2714(7)	0.0805
N14	0.4910(9)	0.1250(7)	0.1148(8)	0.0867
C11	0.1489(8)	0.3488(7)	0.2316(7)	0.0558
C12	0.1389(8)	0.6102(6)	-0.0085(7)	0.0543
C13	0.4149(8)	0.4976(6)	-0.1628(7)	0.0566
C14	0.4144(8)	0.2330(6)	0.0836(7)	0.0573
N1	-0.1374(5)	0.1815(4)	0.6691(5)	0.0417
N2	0.1940(5)	0.1868(4)	0.6671(5)	0.0454
C3	-0.0286(8)	0.0449(6)	0.7121(8)	0.0608
C4	0.1058(8)	0.0596(6)	0.7722(8)	0.0678
C5	-0.2453(9)	0.1953(8)	0.7962(8)	0.0702
C6	-0.2413(8)	0.1821(8)	0.5739(8)	0.0653
C7	0.3198(8)	0.1456(7)	0.5657(8)	0.0626
C8	0.2733(9)	0.2399(8)	0.7444(9)	0.0699
H1	0.2486	0.4850	0.4128	0.11(3)
H31	-0.0897(8)	-0.0327(6)	0.7809(8)	0.10(2)
H32	0.0183(8)	0.0257(6)	0.6293(8)	0.10(2)
H41	0.0592(8)	0.0751(6)	0.8570(8)	0.084(18)
H42	0.1797(8)	-0.0257(6)	0.7951(8)	0.084(18)
H51	-0.3133(9)	0.2840(8)	0.7668(8)	0.090(16)
H52	-0.1800(9)	0.1948(8)	0.8587(8)	0.090(16)
H53	-0.3113(9)	0.1165(8)	0.8454(8)	0.090(16)
H61	-0.3113(8)	0.2697(8)	0.5469(8)	0.081(14)

Continued on next page...

Atom	x	y	z	U(iso) (Å^2)
H62	-0.3053(8)	0.1019(8)	0.6226(8)	0.081(14)
H63	-0.1736(8)	0.1751(8)	0.4901(8)	0.081(14)
H71	0.3744(8)	0.2278(7)	0.4980(8)	0.088(15)
H72	0.3965(8)	0.0718(7)	0.6153(8)	0.088(15)
H73	0.2688(8)	0.1104(7)	0.5167(8)	0.088(15)
H81	0.3303(9)	0.3210(8)	0.6773(9)	0.087(15)
H82	0.1915(9)	0.2682(8)	0.8096(9)	0.087(15)
H83	0.3478(9)	0.1653(8)	0.7963(9)	0.087(15)

A3.14 Fractional Atomic Coordinates and Equivalent Isotropic Thermal Parameters (U(iso) in $Å^2$) for $[\{Cu(tmeda)(\mu\text{-}OH)\}_2Au(CN)_4][ClO_4]\bullet MeOH$ (**4.3**)

Atom	x	y	z	U(iso) ($Å^2$)
Au1	0.26675(7)	-0.2500	0.20682(5)	0.0402
Cu1	0.71003(13)	0.15709(7)	0.2071(1)	0.0369
Cl1	0.8257(5)	0.7500	0.0491(4)	0.0637
O1	0.5583(11)	0.2500	0.1994(9)	0.0441
O2	0.8582(11)	0.2500	0.1997(9)	0.0434
O3	0.619(3)	-0.2500	0.317(2)	0.166(8)
O11	0.666(3)	0.7500	0.052(2)	0.177(9)
O12	0.846(3)	0.7500	-0.075(2)	0.178(9)
O13	0.888(3)	0.8196(14)	0.1017(19)	0.237(9)
N1	0.879(1)	0.0657(6)	0.2528(7)	0.047(2)
N4	0.548(1)	0.0696(6)	0.2521(7)	0.046(2)
N11	0.2092(13)	-0.1067(7)	0.390(1)	0.075(3)
N12	0.3220(11)	-0.3792(6)	0.0055(8)	0.060(3)
C2	0.7962(15)	-0.0046(9)	0.3123(11)	0.069(4)
C3	0.6308(16)	-0.0133(9)	0.2536(12)	0.073(4)
C4	1.0043(14)	0.1010(8)	0.3432(11)	0.065(3)
C5	0.9562(14)	0.0343(8)	0.1477(11)	0.064(3)
C6	0.4929(14)	0.0941(8)	0.3683(11)	0.065(3)
C7	0.4072(14)	0.0632(8)	0.165(1)	0.062(3)
C8	0.733(4)	-0.2500	0.411(3)	0.14(1)
C11	0.2303(13)	-0.1596(7)	0.325(1)	0.052(3)
C12	0.3031(13)	-0.3358(7)	0.085(1)	0.049(3)

REFERENCES

(1) Lehn, J. M. *Supramolecular Chemistry*; VCH: New York, 1995.

(2) Lehn, J. M. *Pure Appl. Chem.* **1978**, *60*, 871.

(3) Steed, J. W.; Atwood, J. L. *Supramolecular Chemistry*; Wiley: New York, 2000.

(4) Mirkin, C. A.; Holliday, B. J. *Angew. Chem. Int. Ed.* **2001**, *40*, 2022.

(5) Ouahab, L. *Chem. Mater.* **1997**, *9*, 1909 and references therein.

(6) *Crystal Engineering: From Molecules and Crystals to Materials*; Braga, D., Grepioni, F., Orpen, A. G. Eds.; Kluwer Academic Publishers: Dordrecht, 1999.

(7) Moulton, B.; Zaworotko, M. J. *Chem. Rev.* **2001**, *101*, 1629.

(8) Braga, D. *J. Chem. Soc., Dalton Trans.* **2000**, 3705.

(9) Braga, D.; Grepioni, F.; Desiraju, G. R. *Chem. Rev.* **1998**, *98*, 1375.

(10) Miller, J. S. *Inorg. Chem.* **2000**, *39*, 4392.

(11) *Magnetism: A Supramolecular Function*; Kahn, O. Eds.; Kluwer Academic Publishers: Dordrecht, 1996.

(12) Decurtins, S.; Pellaux, R.; Antorrena, G.; Palacio, F. *Coord. Chem. Rev.* **1999**, *190-192*, 841.

(13) *Optoelectronic Properties of Inorganic Compounds*; Roundhill, D. M., Fackler, J. P., Jr. Eds.; Plenum Press: New York, 1999.

(14) Marks, T. J.; Ratner, M. A. *Angew. Chem. Int. Ed.* **1995**, *34*, 155.

(15) Coe, B. J. *Chem. Eur. J.* **1999**, *5*, 2464.

(16) *Handbook of Conducting Polymers*; Skotheim, T. A., Elsenbaumer, R. L., Reynolds, J. R. Eds.; 2nd ed.; M. Dekker: New York, 1998.

(17) Marguerettaz, X.; Redmond, G.; Rao, S. N.; Fitzmaurice, D. *Chem. Eur. J.* **1996**, *2*, 420.

(18) Cassoux, P.; Valade, L.; Kobayashi, H.; Kobayashi, A.; Clark, R. A.; Underhill, A. E. *Coord. Chem. Rev.* **1991**, *110*, 115.

(19) Imakubo, T.; Tajima, N.; Tamura, M.; Kato, R.; Nishio, Y.; Kajita, K. *J. Mater. Chem.* **2002**, *12*, 159.

(20) Eddaoudi, M.; Moler, D. B.; Li, H.; Chen, B.; Reineke, T. M.; O'Keeffe, M.; Yaghi, O. M. *Acc. Chem. Res.* **2001**, *34*, 319.

(21) Iwamoto, T. In *Inclusion Compounds*; Atwood, J. L., Davies, J. E. D., MacNicol, D. D., Eds.; Oxford University Press: London, 1984; Vol. 5, p 177.

(22) Zaworotko, M. J. *Angew. Chem. Int. Ed.* **2000**, *39*, 3052.

(23) Schmidbaur, H. *Gold Bull.* **1990**, *23*, 11.

(24) Schmidbaur, H. *Chem. Rev.* **1995**, *24*, 391.

(25) Scherbaum, F.; Grohmann, A.; Huber, B.; Krüger, C.; Schmidbaur, H. *Angew. Chem. Int. Ed.* **1988**, *27*, 1544.

(26) Scherbaum, F.; Grohmann, A.; Müller, G.; Schmidbaur, H. *Angew. Chem. Int. Ed.* **1989**, *28*, 463.

(27) Schmidbaur, H.; Scherbaum, F.; Hubert, B.; Müller, G. *Angew. Chem. Int. Ed.* **1988**, *27*, 419.

(28) Schmidbaur, H. *Gold Bull.* **2000**, *33*, 3.

(29) Hollatz, C.; Schier, A.; Schmidbaur, H. *J. Am. Chem. Soc.* **1997**, *119*, 8115.

(30) Zank, J.; Schier, A.; Schmidbaur, H. *J. Chem. Soc., Dalton Trans.* **1998**, 323.

(31) Schmidbaur, H.; Kolb, A.; Bissinger, P. *Inorg. Chem.* **1992**, *31*, 4370.

(32) Schmidbaur, H.; Graf, W.; Müller, G. *Helv. Chim. Acta* **1986**, *69*, 1748.

(33) Harwell, D. E.; Mortimer, M. D.; Knobler, C. B.; Anet, F. A. L.; Hawthorne, M. F. *J. Am. Chem. Soc.* **1996**, *118*, 2679.

(34) Narajanaswnay, R.; Young, M. A.; Parkhurst, E.; Ouelette, M.; Kerr, M. E.; Ho, D. M.; Elder, R. C.; Bruce, A. E.; Bruce, M. R. M. *Inorg. Chem.* **1993**, *32*, 2506.

(35) Schmidbaur, H.; Graf, W.; Müller, G. *Angew. Chem.* **1988**, *27*, 417.

(36) Schmidbaur, H.; Dziwok, K.; Grohmann, A.; Müller, G. *Chem. Ber.* **1989**, *122*, 893.

(37) Dziwok, K.; Lachmann, J.; Wilkinson, D. L.; Müller, G.; Schmidbaur, H. *Chem. Ber.* **1990**, *123*, 423.

(38) Mansour, M. A.; Connick, W. B.; Lachicotte, R. J.; Gyoling, H. J.; Eisenberg, R. *J. Am. Chem. Soc.* **1998**, *120*, 1329.

(39) Vickery, J. C.; Olmstead, M. M.; Fung, E. Y.; Balch, A. L. *Angew. Chem. Int. Ed.* **1997**, *36*, 1179.

(40) Pyykkö P.; Runeberg, N.; Mendizabal, F. *Chem. Eur. J.* **1997**, *3*, 1451.

(41) Pyykkö, P.; Zhao, Y.-F. *Angew. Chem.* **1991**, *103*, 622.

(42) Pyykkö, P.; Li, L.; Runenberg, N. *Chem. Phys. Lett.* **1994**, *218*, 133.

(43) Pyykkö, P. *Chem. Rev.* **1997**, *97*, 597.

(44) Pyykkö, P.; Mendizabal, F. *Inorg. Chem.* **1998**, *110*, 7210.

(45) Runenberg, N.; Schütz, M.; Werner, H.-J. *Chem. Phys.* **1999**, *110*, 7210.

(46) Li, J.; Pyykkö, P. *Chem. Phys. Lett.* **1992**, *197*, 586.

(47) Schwerdtfeger, P.; Li, J.; Pyykkö, P. *Theor. Chim. Acta* **1994**, *87*, 313.

(48) Klinkhammer, K. W.; Pyykkö, P. *Inorg. Chem.* **1995**, *34*, 4134.

(49) Novoa, J. J.; Aullon, G.; Alemany, P.; Alvarez, S. *J. Am. Chem. Soc.* **1995**, *117*, 7169.

(50) Crespo, O.; Laguna, A.; Fernández, E. J.; López-de-Luzuriaga, J. M.; Jones, P. G.; Teichert, M.; Monge, M.; Pykkö, P.; Runeberg, N.; Shütz, M.; Werner, H.-J. *Inorg. Chem.* **2000**, *39*, 4786 and references therein.

(51) Bennett, M. A.; Welling, L. L.; Willis, A. C. *Inorg. Chem.* **1997**, *36*, 5670.

(52) Pathaneni, S. R.; Desiraju, G. R. *J. Chem. Soc., Dalton Trans.* **1993**, 319.

(53) Leznoff, D. B.; Xue, B.-Y.; Batchelor, R. J.; Einstein, F. W. B.; Patrick, B. O., *Inorg. Chem.* **2001**, *40*, 6026.

(54) Leznoff, D. B.; Xue, B.-Y.; Stevens, C. L.; Storr, A.; Thompson, R. C.; Patrick, B. O. *Polyhedron* **2001**, *20*, 1247.

(55) Leznoff, D. B.; Xue, B.-Y.; Stevens, C. L.; Storr, A.; Thompson, R. C.; Patrick, B. O. *Chem. Commun.* **2001**, 259.

(56) Dunbar, K. R.; Heintz, R. A. *Prog. Inorg. Chem.* **1997**, *45*, 283 and references therein.

(57) Chadwick, B. M.; Sharpe, A. G. In *Advances in Inorganic Chemsitry and Radiochemistry*; Emeleus, H. J., Sharpe, A. G., Eds.; Academic: New York, 1966; Vol. 8, pp 83-176.

(58) Britton, D. In *Perspectives in Structural Chemistry*; Dunitz, J. D., Ibers, J. A., Eds.; Wiley: New York, 1967; Vol. 1, pp 109-171.

(59) Ludi, A.; Gudel, H. U. *Structure Bonding* **1973**, *14*, 1.

(60) Griffith, W. P. In *Comprehensive Inorganic Chemistry*; Bailar, J. C., Jr., Emeleus, H. J., Nyholm, R., Trotman-Dickenson, A. F., Eds.; Pergamon: Oxford, UK, 1973; Vol. 4, pp 105-180.

(61) Griffith, W. P. *Coord. Chem. Rev.* **1975**, *17*, 177.

(62) Rigo, P.; Turco, A. *Coord. Chem. Rev.* **1974**, *17*, 177.

(63) Jones, L. H.; Swanson, B. I. *Acc. Chem. Res.* **1976**, *9*, 128.

(64) Gill, J. B.; Gans, P.; Dougal, J. C.; Johnson, L. H. *Rev. Inorg. Chem.* **1991**, *11*, 155.

(65) Hanusa, T. P.; Burkey, D. J. In *Encyclopedia of Inorganic Chemistry*; King, R. B., Ed.; Wiley: New York; Vol. 2, pp 558-949.

(66) Leipoldt, J. G.; Basson, S. S.; Roodt, A. In *Advances in Inorganic Chemistry*; Sykes, G., Ed.; Academic: New York, 1994; Vol. 40, pp 241-322.

(67) Sharpe, A. G. *The Chemistry of Cyano Complexes of Transition Metals*; Academic Press: London, 1976.

(68) Sharpe, A. G. In *Comprehensive Coordination Chemistry*; Wilkinson, G., Gillard, R. D., McCleverty, J. A., Eds.; Pergamon: New York, 1987; Vol. 2, pp 7-14.

(69) Nakamoto, K. *Infrared and Raman Spectra of Inorganic and Coordination Compounds*; 3rd Ed.; Wiley: New York, 1978, pp. 259-270.

(70) Rosenzweig, A.; Cromer, D. T. *Acta Cryst.* **1959**, *12*, 709.

(71) Hoard, J. L. *Z. Kristallogr.* **1933**, *84*, 231.

(72) Ruegg, M.; Ludi, A. *Theor. Chim. Acta* **1971**, *20*, 147.

(73) Krogmann, K.; Stephan, D. *Z. Anorg. Allg. Chem.* **1968**, *362*, 290.

(74) Bertonotti, C.; Bertinotti, A. *Acta Cryst.* **1970**, *B26*, 422.

(75) Ohba, M.; Maruono, N.; Ōkawa, H.; Tenoki, T.; Latour, J. *J. Am. Chem. Soc.* **1994**, *116*, 11566.

(76) Entley, W. R.; Girolami, G. S. *Science* **1995**, *268*, 397.

(77) Sato, O.; Iyoda, T.; Fujishima, A.; Hashimoto, K. *Science* **1996**, *271*, 49.

(78) Miyasaka, H.; Matsumoto, N.; Ōkawa, H.; Gallo, E.; Floriana, C. *J. Am. Chem. Soc.* **1996**, *118*, 981.

(79) Mallah, T.; Thiebaut, S.; Verdaguer, M.; Veillet, P. *Science* **1993**, *262*, 1554.

(80) Iwamoto, T. In *Comprehensive Supramolecular Chemistry*; Lehn, J. M., Atwood, J. L., Davies, J. E. D., MacNicol, D. D., Vogtle, F., Alberti, G. T. B., Eds.; Pergagon Press: Oxford, 1996; Vol. 7, pp 643-690 and references thereinm

(81) Back, S.; Lang, H. *Organometallics* **2000**, *19*, 749.

(82) Ohba, M.; Ōkawa, H. *Coord. Chem. Rev.* **2000**, *198*, 313.

(83) Ohba, M.; Ōkawa, H.; Ito, T.; Ohto, A. *Chem. Commun.* **1995**, 1545.

(84) Soma, T.; Yuge, H.; Iwamoto, T. *Angew. Chem. Int. Ed.* **1994**, *33*, 1665.

(85) Knoeppel, D. W.; Shore, S. G. *Inorg. Chem.* **1996**, *35*, 1747.

(86) Zhang, H.-X.; Tong, Y.-X.; Chen, Z.-N.; Yu, K.-B.; Kang, B.-S. *J. Organomet. Chem.* **2000**, *598*, 63.

(87) Černák, J.; Orendáč, M.; Potočňák, I.; Chomič, J.; Orendáčová, A.; Skoršepa, J.; Feher, A. *Coord. Chem. Rev.* **2002**, *224*, 51.

(88) Vahrenkamp, H.; Geib, A.; Richardson, G. N. *J. Chem. Soc., Dalton Trans.* **1997**, 3643.

(89) Colacio, E.; Lloret, F.; Kivekäs, R.; Ruiz, F.; Suárez-Valera, J.; Sundberg, M. R. *Chem. Commun.* **2002**, 592.

(90) Colacio, E.; Lloret, F.; Kivekäs, R.; Suárez-Valera, J.; Sundberg, M. R.; Uggla, R. *Inorg. Chem.* **2003**, *42*, 560.

(91) Yeung, W.-F.; Wong, W.-T.; Zuo, J.-L.; Lau, T.-C. *J. Chem. Soc., Dalton Trans.* **2000**, 629.

(92) Stier, A.; Range, K.-J. *Z. Kristallogr.* **1997**, *212*, 51.

(93) Assefa, Z.; Shankle, G.; Patterson, H. H.; Reynolds, R. *Inorg. Chem.* **1994**, *33*, 2187.

(94) Assefa, Z.; Staples, R. J.; Fackler, J. P., Jr.; Patterson, H. H.; Shankle, G. *Acta Cryst.* **1995**, *C51*, 2527.

(95) Hoskins, B. F.; Robson, R.; Scarlett, N. V. Y. *Angew. Chem. Int. Ed.* **1995**, *34*, 1203.

(96) Chu, I. K.; Shek, I. P. Y.; Siu, K. W. M.; Wong, W.-T.; Zuo, J.-L.; Lau, T.-C. *New J. Chem.* **2000**, *24*, 765.

(97) Abrahams, S. C.; Zyontz, L. E.; Bernstein, J. L. *J. Chem. Phys.* **1982**, *76*, 5458.

(98) Abrahams, S. C.; Bernstein, J. L.; Liminga, R.; Eisenmann, E. T. *J. Chem. Phys.* **1980**, *73*, 4585.

(99) Stier, A.; Range, K.-J. *Z. Naturforsch.* **1996**, *51B*, 698.

(100) Cramer, R. E.; Smith, D. W.; VanDoorne, W. *Inorg. Chem.* **1998**, *37*, 5895.

(101) Che, C.-M.; Yip, H.-K.; Wong, W.-T.; Lai, T.-F. *Inorg. Chim. Acta* **1992**, *197*, 177.

(102) Hussain, M. S.; Al-Arfaj, A. R.; Akhtar, M. N.; Isab, A. A. *Polyhedron* **1996**, *15*, 2781.

(103) Chomič, J.; Černák, J. *Therm. Acta* **1985**, *93*, 93.

(104) Kappenstein, C.; Ouali, A.; Guerin, M.; Černák, J.; Chomič, J. *Inorg. Chim. Acta* **1988**, *147*, 189.

(105) Černák, J.; Chomič, J. *Acta Cryst.* **1990**, *C46*, 2103.

(106) Černák, J.; Gerard, F.; Chomič, J. *Acta Cryst.* **1993**, *C94*, 1294.

(107) Černák, J.; Kaňuchová, M.; Chomič, J.; Potočňák, I.; Kameníček, J.; Zdirad, Z. *Acta Cryst.* **1994**, *C50*, 1563.

(108) Černák, J.; Chomič, J.; Gravereau, P.; Orendáčová, A.; Orendáč, M.; Kováč, J.; Feher, A.; Kappenstein, C. *Inorg. Chim. Acta* **1998**, *281*, 134.

(109) Černák, J.; Abboud, K. A.; Chomič, J.; Meisel, M. W.; Orendáč, M.; Orendáčová, A.; Feher, A. *Inorg. Chim. Acta* **2000**, *311*, 126.

(110) Draper, N. D.; Batchelor, R. J.; Sih, B. C.; Ye, Z.-G.; Leznoff, D. B. *Chem. Mater.* **2003**, *15*, 1612.

(111) Leznoff, D. B.; Draper, N. D.; Batchelor, R. J. *Polyhedron,* **2003**, *22*, 1735.

(112) *Gold Progress in Chemistry, Biochemistry and Technology*; Schmidbaur, H. Eds.; Wiley: New York, 1999.

(113) Puddephatt, R. J. *The Chemistry of Gold*; Elsevier: Amsterdam, 1978.

(114) Puddephatt, R. J. In *Comprehensive Coordination Chemistry*; Wilkinson, G., Gillard, R. D., McCleverty, J. A., Eds.; Pergamon: Oxford, 1987, pp 861-923 and references therein.

(115) Laguna, A.; Laguna, M. *Coord. Chem. Rev.* **1999**, *193-195*, 837.

(116) Bardaji, M.; Laguna, A. *J. Chem. Ed.* **1999**, *76*, 201.

(117) Schmidbaur, H.; Dash, K. C. *Adv. Inorg. Chem. Radiochem.* **1982**, *25*, 239.

(118) Tzeng, B.-C.; Schier, A.; Schmidbaur, H. *Inorg. Chem.* **1999**, *38*, 3978.

(119) Bondi, A. *J. Phys. Chem.* **1964**, *68*, 441.

(120) Lancashire, R. J. In *Comprehensive Coordination Chemistry*; Wilkinson, G., Gillard, R. D., McCleverty, J. A., Eds.; Pergamon: Oxford, 1987, pp 775-859.

(121) Bayler, A.; Schier, A.; Bowmaker, G. A.; Schmidbaur, H. *J. Am. Chem. Soc.* **1996**, *118*, 7006.

(122) Singh, K.; Long, J. R.; Stavropoulos, P. *J. Am. Chem. Soc.* **1997**, *119*, 2942.

(123) Lang, J.-P.; Kawaguchi, H.; Tatsumi, K. *Chem. Commun.* **1999**, 2315.

(124) Černák, J.; Abboud, K. A. *Acta Cryst.* **2000**, *C56*, 783.

(125) Dows, D. A.; Haim, A.; Wilmarth, W. K. *J. Inorg. Nucl. Chem.* **1961**, *21*, 33.

(126) Shriver, D. F.; Shriver, A.; Anderson, S. E. *Inorg. Chem.* **1965**, *4*, 725.

(127) Swanson, B. I. *Inorg. Chem.* **1976**, *15*, 253.

(128) Swanson, B. I.; Rafalko, J. J. *Inorg. Chem.* **1976**, *15*, 249.

(129) West, A. R. *Basic Solid State Chemistry*; 2nd ed.; Wiley: New York, 1999.

(130) Carlin, R. L. *Magnetochemistry*; Springer-Verlag: Dusseldorf, Germany, 1986.

(131) Kahn, O. *Molecular Magnetism*; VCH: Weinheim, 1993.

(132) Van Vleck, J. H. *The Theory of Electric and Magnetic Suscpetibilities*; Oxford University Press: Oxford, 1932.

(133) Bleaney, B.; Bowers, K. D. *Proc. R. Soc. London, Ser. A* **1952**, *214*, 451.

(134) Estes, W. E.; Gavel, D. P.; Hatfield, W. E.; Hodgson, D. *Inorg. Chem.* **1978**, *17*, 1415.

(135) Bonner, J. C.; Fisher, M. E. *Phys. Rev. A.* **1964**, *135*, 646.

(136) Hall, J. W.; Marsch, W. E.; Weller, R. R.; Hatfield, W. E. *Inorg. Chem.* **1981**, *20*, 1033.

(137) Fernández, E. J.; López-de-luzuriaga, J. M.; Monge, M.; Rodríguez, M. A.; Crespo, O.; Gimeno, M. C.; Laguna, A.; Jones, P. G. *Inorg. Chem.* **1998**, *37*, 6002.

(138) Wang, Q.-M.; Mak, T. C. W. *J. Am. Chem. Soc.* **2000**, *122*, 7608.

(139) Wang, Q.-M.; Mak, T. C. W. *J. Am. Chem. Soc.* **2001**, *123*, 7594.

(140) Wang, Q.-M.; Mak, T. C. W. *J. Am. Chem. Soc.* **2001**, *123*, 1501.

(141) Nomiya, K.; Takahashi, S.; Noguchi, R.; Nemoto, S.; Takayama, T.; Oda, M. *Inorg. Chem.* **2000**, *39*, 3301 and references therein.

(142) Tong, M.-L.; Chen, X.-M.; Ye, B.-H.; Ji, L.-N. *Angew. Chem. Int. Ed.* **1999**, *38*, 2237.

(143) Kristiansson, O. *Inorg. Chem.* **2001**, *40*, 5058.

(144) Brandys, M.-C.; Puddephatt, R. J. *Chem. Commun.* **2001**, 1508.

(145) Guo, G.-C.; Zhou, G.-D.; Mak, T. C. W. *J. Am. Chem. Soc.* **1999**, *121*, 3136.

(146) Che, C.-M.; Tse, M.-C.; Chan, M. C. W.; Cheung, K.-K.; Phillips, D. L.; Leung, K.-H. *J. Am. Chem. Soc.* **2000**, *122*, 2464.

(147) Kim, Y.; Seff, K. J. *J. Am. Chem. Soc.* **1978**, *100*, 175.

(148) Eastland, G. W.; Mazid, M. A.; Russell, D. R.; Symons, M. C. R. *J. Chem. Soc., Dalton Trans.* **1980**, 1682.

(149) Quíros, M. *Acta Cryst.* **1994**, *C50*, 1236.

(150) Omary, M. A.; Webb, T. R.; Assefa, Z.; Shankle, G.; Patterson, H. H. *Inorg. Chem.* **1998**, *37*, 1380.

(151) Izatt, R. M.; Johnston, M. D.; Watt, G. D.; Christensen, J. J. *Inorg. Chem.* **1967**, *6*, 132.

(152) Jones, L. H.; Penneman, R. A. *J. Chem. Phys.* **1954**, *22*, 965.

(153) Gans, P.; Gill, J. B.; Griffin, M.; Cahill, P. C. *J. Chem. Soc., Dalton Trans.* **1981**, 968.

(154) Range, K.-J.; Kuhnel, S.; Zabel, M. *Acta Crysta* **1989**, *C45*, 1419.

(155) Sakaguchi, U.; Tomioka, K.; Yoneda, H. *Inorg. Chim. Acta* **1985**, *101*, 23.

(156) Hoskins, B. F.; Robson, R.; Scarlett, N. V. Y. *Chem. Commun.* **1994**, 2025.

(157) Dasna, I.; Golhen, S.; Ouahab, L.; Daro, N.; Sutter, J.-P. *Polyhedron* **2001**, *20*, 1371.

(158) Niel, V.; Muñoz, M. C.; Gaspar, A. B.; Galet, A.; Levchenko, G.; Real, J. A. *Chem. Eur. J.* **2002**, *8*, 2446.

(159) Soma, T.; Iwamoto, T. *Chem. Lett.* **1994**, 821.

(160) Soma, T.; Iwamoto, T. *Inorg. Chem.* **1996**, *35*, 1849.

(161) Shek, I. P. Y.; Wong, W.-Y.; Lau, T.-C. *New J. Chem.* **2000**, *24*, 733.

(162) Zhang, H.-X.; Chen, Z.-N.; Su, C.-Y.; Ren, C.; Kang, B.-S. *J. Chem. Crystallog.* **1999**, *29*, 1239.

(163) Jansen, M. *Angew. Chem. Int. Ed.* **1987**, *26*, 1098.

(164) Batten, S. R.; Hoskins, B. F.; Robson, R. *New J. Chem.* **1998**, 173.

(165) Wu, H.-P.; Janiak, C.; Rheinwald, G.; Lang, H. *J. Chem. Soc., Dalton Trans.* **1998**, 183.

(166) Janiak, C.; Uehlin, L.; Wu, H.-P.; Klüfers, P.; Piotrowski, H.; Scharmann, T. G. *J. Chem. Soc., Dalton Trans.* **1999**, 3121.

(167) Carlucci, L.; Ciani, G.; Macchi, P.; Proserpio, D. M.; Rizzato, S. *Chem. Eur. J.* **1999**, *5*, 237.

(168) Fortin, D.; Drouin, M.; Harvey, P. D.; Herring, F. G.; Summers, D. A.; Thompson, R. C. *Inorg. Chem.* **1999**, *38*, 1253.

(169) Bessler, K. E.; Romualdo, L. L.; Deflon, V. M.; Hagenbach, A. *Z. Anorg. Allg. Chem.* **2000**, *626*, 1942.

(170) Kleina, C.; Graf, E.; Hosseini, M. W.; De Cian, A.; Fischer, J. *Chem. Commun.* **2000**, 239.

(171) Konnert, J.; Britton, D. *Inorg. Chem.* **1966**, *5*, 1193.

(172) Withersby, M. A.; Blake, A. J.; Champness, N. R.; Hubbersty, P.; Li, W.-S.; Schroder, M. *Angew. Chem. Int. Ed.* **1997**, *36*, 2327.

(173) Nilsson, K.; Oskarsson, Å. *Acta Chem. Scand.* **1984**, *A38*, 79.

(174) Barnhart, D. M.; Caughlan, C. N.; Ul-Haque, M. *Inorg. Chem.* **1969**, *8*, 2768.

(175) Bowmaker, G. A.; Effendy; Junk, P. C.; White, A. H. *J. Chem. Soc., Dalton Trans.* **1998**, 2131.

(176) Bowmaker, G. A.; Effendy; Reid, J. C.; Rickard, C. E. F.; Skelton, B. W.; White, A. H. *J. Chem. Soc., Dalton Trans.* **1998**, 2139.

(177) Hathaway, B. J. In *Comprehensive Coordination Chemistry*; Wilkinson, G., Gillard, R. D., McCleverty, J. A., Eds.; Permagon: Oxford, 1987; Vol. 5, p 533.

(178) Kou, H. Z.; Wang, H.-M.; Liao, D.-Z.; Cheng, P.; Jiang, Z.-H.; Yan, S.-P.; Huang, X.-Y.; Wang, G.-L. *Aust. J. Chem.* **1998**, *51*, 661.

(179) Yuge, H.; Iwamoto, T. *J. Chem. Soc., Dalton Trans.* **1994**, 1237.

(180) Batten, S. R.; Robson, R. *Angew. Chem. Int. Ed.* **1998**, *37*, 1460.

(181) Freeman, M. J.; Orpen, A. G. *J. Chem. Soc., Dalton Trans.* **1987**, 1001.

(182) Freeman, M. J.; Green, M.; Orpen, A. G.; Salter, I. D.; Stone, F. G. A. *Chem. Commun.* **1983**, 1332.

(183) Abu-Salah, O. M.; Hussain, M. S.; Schlemper, E. O. *Chem. Commun.* **1988**, 212.

(184) Fackler, J. P., Jr.; Lopez, C. R.; Staples, R. J.; Wang, S.; Winpenny, R. E. P.; Lattimer, R. P. *Chem. Commun.* **1992**, 146.

(185) Hussain, M. S.; Abu-Salah, O. M. *J. Organomet. Chem.* **1987**, *445*, 295.

(186) Schwarten, M.; Chomič, J.; Černák, J.; Babel, R. *Z. Anorg. Allg. Chem.* **1996**, *622*, 1449.

(187) Oshio, H.; Watanabe, T.; Ohto, A.; Ito, T.; Ikoma, T.; Tero-Kubota, S. *Inorg. Chem.* **1997**, *36*, 3014.

(188) Oshio, H.; Watanabe, T.; Ohto, A.; Ito, T.; Ikoma, T.; Tero-Kubota, S. *Mol. Cryst. Liq. Cryst.* **1995**, *273*, 47.

(189) Vicente, R.; Escuer, A.; Peñalba, E.; Solans, X.; Font-Bardía, M. *Inorg. Chim. Acta* **1997**, *255*, 77.

(190) White, C. A.; Yap, G. P. A.; Greedan, J. E.; Crutchley, R. J. *Inorg. Chem.* **1999**, *38*, 2548.

(191) Oshio, H.; Watanabe, T.; Ohto, A.; Ito, T.; Nagashima, U. *Angew. Chem. Int. Ed.* **1994**, *33*, 670.

(192) Comte, V.; Chen, Z.-N.; Flay, M.-L.; Vahrenkamp, H. *J. Organomet. Chem.* **2000**, *614-615*, 131.

(193) Brunner, H.; Hollman, A.; Nuber, B.; Zabel, M. *J. Organomet. Chem.* **2001**, *633*, 1.

(194) Geiser, U.; Wang, H.-H.; Gerdom, L. E.; Firestone, M. A.; Sowa, L. M.; Williams, J. M.; Whangbo, M.-H. *J. Am. Chem. Soc.* **1985**, *107*, 8305.

(195) Beno, M. A.; Firestone, M. A.; Leung, P. C. W.; Sowa, L. M.; Wang, H.-H.; Williams, J. M.; Whangbo, M.-H. *Solid State Commun.* **1986**, *57*, 735.

(196) Zhan, S.-z.; Guo, D.; Zhang, X.-y.; Du, C.-x.; Zhu, Y.; Yang, R.-n. *Inorg. Chim. Acta* **2000**, *298*, 57.

(197) Mukherjee, P. S.; Maji, T. K.; Mallah, T.; Zangrando, E.; Randaccio, L.; Chaudhuri, N. R. *Inorg. Chim. Acta* **2001**, *315*, 249.

(198) Maji, T. K.; Mukherjee, P. S.; Mostafa, G.; Zangrando, E.; Chaudhuri, N. R. *Chem. Commun.* **2001**, 1368.

(199) Cotton, F. A.; Wilkinson, G.; Murillo, C. A.; Bochmann, M. *Advanced Inorganic Chemistry*; 6th ed.; Wiley: New York, 1999.

(200) Gabe, E. J.; White, P. S.; Enright, G. D. *DIFRAC A Fortran 77 Control Routine for 4-Circle Diffractometers*; N. R. C.: Ottawa, 1995.

(201) Gabe, E. J.; LePage, Y.; Charland, J.-P.; Lee, F. L.; White, P. S. *J. Appl. Cryst.* **1989**, *22*, 384.

(202) Watkin, D. J.; Prout, C. K.; Carruthers, J. R.; Betteridge, P. W.; Cooper, R. I. *CRYSTALS Issue 11, Chemical Crystallography Laboratory*; University of Oxford: Oxford, 1999.

(203) Farrugia, L. J. *J. Appl. Cryst.* **1997**, *30*, 565.

(204) *International Tables for X-ray Crystallography*; Kynoch Press: Birmingham, U. K. (present distributor Kluwer Academic Publishers: Boston, MA); Vol. IV, p.99.

(205) d*TREK: *Area Detector Software*; Version 4.13. Molecular Structure Corporation: The Woodlands, TX (1996-1998).

(206) Beurskens, P. T.; Admiraal, G.; Beurskens, G.; Bosman, W. P.; Garcia-Granda, S.; Gould, R. O.; Smits, J. M. M.; Smykalla, C. The DIRDIF program system, Technical Report of the Crystallography Laboratory, University of Nijmegen, 1992.

(207) Knoeppel, D. W.; Shore, S. G. *Inorg. Chem.* **1996**, *35*, 5328.

(208) Gable, R. W.; Hoskins, B. F.; Robson, R. *Chem. Commun.* **1990**, 762.

(209) Falvello, L. R.; Garde, R.; Tomás, M. *J. Cluster Sc.* **2000**, *11*, 125.

(210) Kou, H. Z.; Liao, D.-Z.; Jiang, Z.-H.; Yan, S.-P.; Wu, Q. J.; Gao, S.; Wang, G.-L. *Inorg. Chem. Commun.* **2000**, *3*, 151.

(211) Hofmann, K. A.; Kuspert, F. A. *Z. Anorg. Allg. Chem.* **1897**, *15*, 204.

(212) Powell, H. M.; Rayner, J. H. *Nature* **1949**, *163*, 566.

(213) Rayner, J. H.; Powell, H. M. *J. Chem. Soc.* **1952**, 319.

(214) Jones, P. G. *Gold Bull.* **1983**, *16*, 114.

(215) Jones, P. G. *Gold Bull.* **1981**, *14*, 103.

(216) Penneman, R. A.; Ryan, R. R. *Acta Cryst.* **1972**, *B28*, 1629.

(217) Jones, P. G.; Thone, C. *Acta Cryst.* **1989**, *C45*, 11.

(218) Smith, J. M.; Jones, L. H.; Kressin, I. K.; Penneman, R. A. *Inorg. Chem.* **1965**, *4*, 369.

(219) Krogmann, K. *Angew. Chem. Int. Ed.* **1969**, *8*, 35 and references therein.

(220) Miller, J. S.; Epstein, A. J. *Prog. Inorg. Chem.* **1976**, *20*, 1.

(221) Osborn, R. J.; Rogers, D. *J. Chem. Soc., Dalton Trans.* **1974**, 1002.

(222) Yamada, S. *Bull. Chem. Soc. Japan* **1951**, *24*, 125.

(223) Rundle, R. E. *J. Phys. Chem.* **1957**, *61*, 45.

(224) Miller, J. S. *J. Chem. Soc.* **1965**, 713.

(225) McQuarrie, D. A. *Quantum Chemistry*; University Science Books: Sausalito, CA, 1983.

(226) Oshio, H.; Tamada, O.; Onodera, H.; Ito, T.; Ikoma, T.; Tero-Kubota, S. *Inorg. Chem.* **1999**, *38*, 5686.

(227) Oshio, H.; Yamamoto, M.; Ito, T. *Inorg. Chem.* **2002**, *41*, 5817.

(228) Falvello, L. R.; Tomás, M. *Chem. Commun.* **1999**, 273.

(229) Ginsberg, A. P.; Martin, R. L.; Brookes, R. W.; Sherwood, R. C. *Inorg. Chem.* **1972**, *11*, 2884.

(230) Shorrock, C. J.; Xue, B.-Y.; Kim, P. B.; Batchelor, R. J.; Patrick, B. O.; Leznoff, D. B. *Inorg. Chem.* **2002**, *41*, 6743.

(231) Escorihuela, I.; Falvello, L. R.; Tomás, M. *Inorg. Chem.* **2001**, *40*, 636.

(232) Iwamoto, T.; Nalkano, T.; Morita, M.; Miyoshi, T.; Miyamoto, T.; Sasaki, Y. *Inorg. Chim. Acta* **1968**, *2-3*, 313.

(233) Timkovich, R.; Tulinsky, A. *Inorg. Chem.* **1977**, *16*, 962.

(234) Sommerer, S. O.; MacBeth, C. E.; Jircitano, A. J.; Abboud, K. A. *Acta Cryst.* **1997**, *C53*, 1551.

(235) Micklitz, W.; Lippert, B.; Müller, G.; Mikulcik, P.; Riede, J. *Inorg. Chim. Acta* **1989**, *165*, 57.

(236) Elder, R. C.; Watkins, J. W., II *Inorg. Chem.* **1986**, *25*, 223.

(237) Shimanski, A.; Freisinger, E.; Erxleben, A.; Lippert, B. *Inorg. Chim. Acta* **1998**, *283*, 223.

(238) Charlton, R. J.; Harris, C. M.; Patil, H.; Stephenson, N. C. *Inorg. Nucl. Chem. Lett.* **1966**, *2*, 409.

(239) Robinson, W. T.; Sinn, E. *J. Chem. Soc., Dalton Trans.* **1975**.

(240) O'Connor, C. J.; Sinn, E. *Inorg. Chem.* **1978**, *17*, 2067.

(241) Marangoni, G.; Pitteri, B.; Bertolasi, V.; Gilli, G.; Ferretti, V. *J. Chem. Soc., Dalton Trans.* **1986**, 1941.

(242) Ferretti, V.; Gilli, P.; Bertolasi, V.; Marangoni, G.; Pitteri, B.; Chessa, G. *Acta Cryst.* **1992**, *C48*, 814.

(243) Vicente, J.; Chicote, M. T.; Bermúdez, M. D.; Jones, P. G.; Fittschen, C.; Sheldrick, G. M. *J. Chem. Soc., Dalton Trans.* **1986**, 2361.

(244) Richardson, G. N.; Brand, U.; Vahrenkamp, H. *Inorg. Chem.* **1999**, *38*, 3070.

(245) Shek, I. P. Y.; Lau, T.-C.; Wong, W.-T.; Zuo, J.-L. *New J. Chem.* **1999**, *23*, 1049.

(246) Munakata, M.; Zhong, J. C.; Ino, I.; Kuroda-Sowa, T.; Maekawa, M.; Suenaga, Y.; Oiji, N. *Inorg. Chim. Acta* **2001**, *317*, 268.

(247) Gatteschi, D.; Kahn, O.; Miller, J. R.; Palacio, F. *Magnetic Molecular Materials*; Kluwer Academic: Dordrecht, The Netherlands, 1991.

(248) Hay, P. J.; Thibeault, J. C.; Hoffmann, R. *J. Am. Chem. Soc.* **1975**, *97*, 4884.

(249) Hodgson, D. J. *Prog. Inorg. Chem.* **1974**, *19*, 173.

(250) Estes, E. D.; Hatfield, W. E.; Hodgson, D. J. *Inorg. Chem.* **1974**, *13*, 1654.

(251) Hatfield, W. E. In *Magneto-Structural Correlations in Exchange Coupled Systems*; Willett, R. D., Gatteschi, D., Kahn, O., Eds.; Reidel: Dordrecht, The Netherlands, 1984, p 555 and references therein.

(252) Rojo, T.; Arriortua, M. I.; Ruiz, J.; Darriet, J.; Villeneuve, G.; Betlran-Porter, D. *J. Chem. Soc., Dalton Trans.* **1987**, 285.

(253) Rodriguez, M.; Llobet, A.; Corbella, M. *Polyhedron* **2000**, *19*, 2483 and references therein.

(254) Geetha, K.; Nethaji, M.; Vasanthacharya, N. Y.; Chakravarty, A. R. *J. Coord. Chem.* **1999**, *47*, 77 and references therein.

(255) Tadsanaprasittipol, A.; Kraatz, H.-B.; Enright, G. D. *Inorg. Chim. Acta* **1998**, *278*, 143.

(256) Mahadevan, V.; Hou, Z.; Cole, A. P.; Root, D. E.; Lal, T. K.; Solomon, E. I.; Stack, T. D. P. *J. Am. Chem. Soc.* **1997**, *119*, 11996.

(257) Thompson, J. S. *J. Am. Chem. Soc.* **1984**, *106*, 8308.

(258) Simpson, G. D.; Carlisle, G. O.; Hatfield, W. E. *J. Inorg. Nucl. Chem.* **1974**, *36*, 2257.

(259) Merz, L.; Haase, W. *J. Chem. Soc., Dalton Trans.* **1980**, 875.

(260) McGregor, K. T.; Watkins, N. T.; Lewis, D. L.; Drake, R. F.; Hodgson, D. J.; Hatfield, W. E. *Inorg. Nucl. Chem. Lett.* **1973**, *9*, 423.

(261) McGregor, K. T.; Hodgson, D. J.; Hatfield, W. E. *Inorg. Chem.* **1976**, *15*, 421.

(262) Crawford, V. H.; Richardson, H. W.; Wasson, J. R.; Hodgson, D. J.; Hatfield, W. E. *Inorg. Chem.* **1976**, *15*, 2107.

(263) Barnes, J. A.; Hatfield, W. E.; Hodgson, D. J. *Chem. Commun.* **1970**, 1593.

(264) Bencini, A.; Gatteschi, D. *Inorg. Chim. Acta* **1978**, *31*, 11.

(265) Kahn, O.; Charlot, M. F. *Nouv. J. Chim.* **1980**, *4*, 567.

(266) Astheimer, H.; Haase, W. *J. Chem. Phys.* **1986**, *85*, 1427.

(267) Ruiz, E.; Alemany, P.; Alvarez, S.; Cano, J. *J. Am. Chem. Soc.* **1997**, *119*, 1297.

(268) Ruiz, E.; Alemany, P.; Alvarez, S.; Cano, J. *Inorg. Chem.* **1997**, *36*, 3683.

(269) Ruiz, E.; Alvarez, S.; Alemany, P. *Chem. Commun.* **1998**, 2767.

(270) Majeste, R. J.; Meyers, E. A. *J. Phys. Chem.* **1970**, *74*, 3497.

(271) Casey, A. T.; Hoskins, B. F.; Whillans, F. D. *Chem. Commun.* **1970**, 904.

(272) Casey, A. T. *Aust. J. Chem.* **1972**, *25*, 2311.

(273) Castro, I.; Faus, J.; Julve, M.; Verdaguer, M.; Monge, A.; Gutierrez-Puebla, E. *Inorg. Chim. Acta* **1990**, *170*, 251.

(274) Castro, I.; Faus, J.; Julve, M.; Bois, C.; Real, J. A.; Lloret, F. *J. Chem. Soc., Dalton Trans.* **1992**, 47.

(275) Hoskins, B. F.; Whillans, F. D. *J. Chem. Soc., Dalton Trans.* **1975**, 1267.

(276) Jeter, D. Y.; Lewis, D. L.; Hempel, J. C.; Hodgson, D. J.; Hatfield, W. E. *Inorg. Chem.* **1972**, *11*, 1958.

(277) Krahmer, P.; Masser, M.; Staiger, K.; Uhlig, E. *Z. Anorg. Allg. Chem.* **1967**, *354*, 242.

(278) Lewis, D. L.; Hatfield, W. E.; Hodgson, D. J. *Inorg. Chem.* **1972**, *11*, 2216.

(279) Lewis, D. L.; McGregor, K. T.; Hatfield, W. E.; Hodgson, D. J. *Inorg. Chem.* **1974**, *13*, 1013.

(280) Lewis, D. L.; Hatfield, W. E.; Hodgson, D. J. *Inorg. Chem.* **1974**, *13*, 147.

(281) Sletten, J.; Sorensen, A.; Julve, M.; Journaux, Y. *Inorg. Chem.* **1990**, *29*, 5054.

(282) Toofan, M.; Boushehri, A.; Ul-Haque, M. *J. Chem. Soc., Dalton Trans.* **1976**, 217.

(283) van Albada, G. A.; Mutikainen, I.; Turpeinen, U.; Reedijk, J. *Inorg. Chim. Acta* **2001**, *324*, 273.

(284) Barnes, J. A.; Hodgson, D. J.; Hatfield, W. E. *Inorg. Chem.* **1972**, *11*, 144.

(285) McGregor, K. T.; Hodgson, D. J.; Hatfield, W. E. *Inorg. Chem.* **1973**, *12*, 731.

(286) Ivarsson, G. J. M. *Acta Chem. Scand.* **1979**, *A33*, 323.

(287) Reedijk, J.; Kentsch, D.; Nieuwenhuijse, G. *Inorg. Chim. Acta* **1971**, *5*, 568.

(288) Nasakkala, M. *Ann. Acad. Sci. Fenn., Ser. A2* **1977**, 15.

(289) Nasakkala, M. *Ann. Acad. Sci. Fenn., Ser. A2* **1977**, 54.

(290) Hatfield, W. E.; Piper, T. S.; Klabunde, U. *Inorg. Chem.* **1963**, *2*, 629.

(291) Meinders, H. C.; Van Bolhuis, F.; Challa, G. *J. Mol. Cat.* **1979**, *5*, 225.

(292) Mitchell, T. P.; Bernard, W. H. *Acta Cryst.* **1970**, *B26*, 2096.

(293) Wasson, J. R.; Mitchell, T. P.; Bernard, W. H. *J. Inorg. Nucl. Chem.* **1968**, *30*, 2865.

(294) Cole, B. J.; Brumage, W. H. *J. Chem. Phys.* **1970**, *53*, 4718.

(295) Arcus, C.; Fivizzani, K. P.; Pavkovic, S. F. *J. Inorg. Nucl. Chem.* **1977**, *39*, 285.

(296) de Munno, G.; Julve, M.; Lloret, F.; Faus, J.; Verdaguer, M.; Caneschi, A. *Inorg. Chem.* **1995**, *34*, 157.

(297) Chiari, B.; Hatfield, W. E.; Piovesana, O.; Tarantelli, T.; Ter Haar, L. W.; Zanazzi, P. F. *Inorg. Chem.* **1983**, *22*, 1468.

(298) Basolo, F.; Murmann, R. K. *J. Am. Chem. Soc.* **1952**, *74*, 5343.

(299) Basolo, F.; Murmann, R. K. *J. Am. Chem. Soc.* **1954**, *76*, 211.

(300) Mann, F. G.; Watson, H. R. *J. Chem. Soc.* **1958**, 2772.

(301) Barclay, G. A.; Kennard, C. H. L. *J. Chem. Soc.* **1961**, 5244.

(302) Hanic, F.; Stempelova, D.; Hanicova, K. *Acta Cryst.* **1964**, *17*, 633.

(303) van Niekerk, J. N.; Schoening, F. R. L. *Acta Cryst.* **1973**, *B29*, 29.

(304) Manaka, H.; Yamada, I.; Yamaguchi, K. *J. Phys. Soc. Jpn.* **1997**, *66*, 564.

(305) Brown, D. S.; Lee, J. D.; Melsom, B. G. A.; Hathaway, B. J.; Procter, I. M.; Tomlinson, A. A. G. *Chem. Commun.* **1967**, 369.

(306) Shorrock, C. J.; Jong, H.; Batchelor, R. J.; Leznoff, D. B. *Inorg. Chem.* **2003**, *42*, 3917.

(307) Kim, J.; Whang, D.; Lee, J. I.; Kim, K. *Chem. Commun.* **1993**, 1400.

(308) Kitazawa, T.; Nishikiori, S.; Yamagishi, R.; Kuroda, T.; Iwamoto, T. *Chem. Commun.* **1992**, 413.

(309) Abrahams, B. F.; Hoskins, B. F.; Robson, R. *Chem. Commun.* **1990**, 60.

(310) Roof, R. B. J.; Larson, A. C.; Cromer, D. T. *Acta Cryst.* **1968**, *B24*, 269.

(311) Staritzky, E.; Ellinger, F. H. *Anal. Chem.* **1956**, *28*, 423.

(312) Stein, T; Lang, H. *Chem. Commun.* **2001**, 1502.

(313) Brimah, A. K.; Siebel, E.; Fischer, R. D.; Davies, N. A.; Apperly, D. C.; Harris, R. K. *J. Organomet. Chem.* **1994**, *475*, 85.

(314) Williams, R. J.; Larson, A. C.; Cromer, D. T. *Acta Cryst.* **1972**, *B28*, 858.

(315) Stocker, F. B.; Staeva, T. P.; Rienstra, C. M.; Britton, D. *Inorg. Chem.* **1999**, *38*, 984.

(316) Chestnut, D. J.; Kusnetzow, A.; Birge, B. W.; Zubieta, J. *Inorg. Chem.* **1999**, *38*, 2663.

(317) Colacio, E.; Kivekäs, R.; Lloret, F.; Sundberg, M. R.; Sarez-Valera, J.; Bardaji, M.; Laguna, A. *Inorg. Chem.* **2002**, *41*, 5141.

(318) Williams, R. J.; Cromer, D. T.; Larson, A. C. *Acta Cryst.* **1971**, *B27*, 1701.

(319) Huang, S. F.; Wei, H. H.; Wang, Y. *Polyhedron* **1997**, *16*, 1747.

(320) Tyagi, S.; Hathaway,B. J. *J. Chem. Soc., Dalton Trans.* **1983**, 199.

(321) Anderson, O. *Inorg. Chem.* **1975**, *14*, 730.

(322) Eastes, J. W.; Burgess, W. M. *J. Am. Chem. Soc.* **1942**, *64*, 2715.

(323) Ibraham, A. M. A.; Siebel, E.; Fischer, R. D. *Inorg. Chem.* **1998**, *37*, 3521.

(324) Jones, L. H. *J. Chem. Phys.* **1958**, *29*, 463.

(325) Cooper, D.; Plane, R. A. *Inorg. Chem.* **1966**, *5*, 1677.

(326) Gutlich, P.; Hauser, A.; Spiering, H. *Angew. Chem. Int. Ed.* **1994**, *33*, 2024.

(327) Kahn, O.; Martinez, C. J. *Science* **1998**, *279*, 44.

(328) König, E. *Coord. Chem. Rev.* **1968**, *3*, 471.

(329) Madeja, V. K.; Wilke, W.; Schmidt, S. *Z. Anorg. Allg. Chem.* **1966**, *346*, 306.

(330) Gallois, B.; Real, J. A.; Hauw, C.; Zarembowitch, J. *Inorg. Chem.* **1990**, *29*, 1152 and references therein.

(331) Pyykkö, P.; Desclaux, J.-P. *Acc. Chem. Res.* **1979**, *12*, 276.

(332) Pyykkö, P. *Chem. Rev.* **1988**, *88*, 563.

(333) Bartlett, N. *Gold Bull.* **1998**, *31*, 22.

(334) Radel, S. R.; Navidi, M. H. *Chemistry*; 2nd ed.; West Publishing Company: St. Paul, 1994.

(335) Pyykkö, P.; Angermaier, B.; Assmann, H.; Schmidbaur, H. *Chem. Commun.* **1995**, 1889.

(336) Pitzer, K. *Acc. Chem. Res.* **1979**, *12*, 271.

(337) Kaltsoyannis, N. *J. Chem. Soc., Dalton Trans.* **1997**, 1.